ENERGY LABORATORY

MASSACHUSETTS INSTITUTE
OF TECHNOLOGY

THE SELECTIVE USE OF THORIUM AND HETEROGENEITY IN URANIUM-EFFICIENT PRESSURIZED WATER REACTORS

by

A. KAMAL, M. J. DRISCOLL and D. D. LANNING

DOE Contract No. DE-AC02-79ET34022
Energy Laboratory Report No. MIT-EL-82-033
August 1982

DOE/ET/34022-4
MITNE-253
MIT-EL-82-033

THE SELECTIVE USE OF THORIUM AND HETEROGENEITY IN URANIUM-EFFICIENT PRESSURIZED WATER REACTORS

by

A. KAMAL, M. J. DRISCOLL and D. D. LANNING

DOE Contract No. DE-AC02-79ET34022
Energy Laboratory Report No. MIT-EL-82-033
August 1982

THE SELECTIVE USE OF THORIUM AND HETEROGENEITY IN URANIUM-EFFICIENT PRESSURIZED WATER REACTORS

by

A. KAMAL, M. J. DRISCOLL and D. D. LANNING

August 1982

Department of Nuclear Engineering

and

Energy Laboratory

Massachusetts Institute of Technology

Cambridge, Massachusetts 02139

Sponsored by:

U.S. Department of Energy

Division of Energy Technology

under

Contract No. DE-AC02-79ET34022

"THE SELECTIVE USE OF THORIUM AND HETEROGENEITY IN URANIUM-EFFICIENT PRESSURIZED WATER REACTORS"

by

Altamash Kamal

ABSTRACT

Systematic procedures have been developed and applied to assess the uranium utilization potential of a broad range of options involving the selective use of thorium in Pressurized Water Reactors (PWRs) operating on the once-through cycle. The methods used rely on state-of-the-art physics methods coupled with batch-wise core depletion models based on the "group-and-one-half" theory.

The possible roles for thorium that were investigated are: as internal and radial blanket material, as thorium pins dispersed within uranium fuel assemblies, its use in PWRs operating on spectral shift control, and its reconstitution and reinsertion as radial blanket assemblies. The use of smaller assemblies in PWRs (for cores with and without thorium) was also investigated, as well as options which can be regarded as reasonable substitutes for employing thorium. The analyses were performed for both current (3-batch, discharge burnup $\sim$ 30 GWD/MT) and high-burnup (5-batch, discharge burnup $\sim$ 50 GWD/MT) PWR cores in their steady-state.

It was found that except for special circumstances (dry lattices and/or high burnup), the use of thorium does not save uranium compared to the conventional all-uranium PWRs. When savings are achieved (typically 1-3%, but as high as 9% in special circumstances), they can be, for the most part, equalled or exceeded by easier means: in particular, by the re-use of spent fuel. On the other hand, up to 15 or 20% thorium could be added into PWRs without significant losses in uranium utilization, if policies called for the build up of a U-233 inventory for later use in the recycle mode.

It was also found that, regardless of the deployment of thorium, the use of smaller fuel assemblies with the concurrent deployment of radial blankets is an effective uranium conservation strategy, with accompanying power-shaping advantages.

ACKNOWLEDGEMENTS

The work presented in this report has been performed primarily by the principal author, Altamash Kamal, who has submitted substantially the same report in partial fulfillment of the requirements for the Sc.D. degree in Nuclear Engineering at MIT.

The principal author wishes to thank Wee Tee Loh for his help and friendship over the past several years. He also greatefully acknowledges the financial support provided by the U.S. Department of Energy.

The help of Rachel Morton in the computer-related aspects of the analysis is much appreciated, as is the assistance of the staff at MIT's Information Processing Center, where the computations were performed and the bulk of this document prepared. We also wish to thank Wynter Snow for her skillful typing.

The authors would also like to express their appreciation for the cooperation of Dr. Edward Pilat of the Yankee Atomic Electric Company in facilitating the acquisition of descriptive data from publicly available documentation on the Maine Yankee Reactor. Although the information in this report is referred to as deriving from "Maine Yankee," it should not be considered as representing that actual system in its present or projected operating configuration, but as an idealization thereof. It should be noted that the results in this report have not been either reviewed or approved by the Yankee Organization.

NOTICE

TABLE OF CONTENTS

TABLE OF CONTENTS (Continued)

TABLE OF CONTENTS (Continued-3)

TABLE OF CONTENTS (Continued-4)

TABLE OF CONTENTS (Continued-5)

LIST OF FIGURES

LIST OF FIGURES (Continued)

LIST OF FIGURES (Continued-3)

LIST OF TABLES

LIST OF TABLES (Continued)

LIST OF TABLES (Continued-3)

LIST OF TABLES (Continued-4)

LIST OF TABLES (Continued-5)

CHAPTER 1

BACKGROUND AND RESEARCH OBJECTIVES

1.1 Introduction

In recent years, increased emphasis has been placed on the more efficient use of the world's natural uranium resources in Light Water Reactors (LWRs) operating on the once-through fuel cycle. Several incentives have contributed towards this consensus: the conviction of some to defer reprocessing because of concern over the resulting commerce in weapons-usable material, the slower than originally planned progress towards the deployment of commercial breeder reactors, and a re-assessment of the cost-effectiveness of fuel recycle restricted to thermal reactors. These motives are also compatible with the desire of utilities to extend their reactors' burnup cycle and to improve fuel reliability. The work described here is a part of this effort and was done under the sponsorship of the LWR Technology Assessment Program for Improved Uranium Utilization of the U.S. Department of Energy.

The general purpose of this investigation was to assess the potential of using small quantities of thorium in pressurized water reactors (PWRs) on the once-through fuel cycle. The criterion of merit employed was uranium utilization: the energy extracted from a reactor per unit mass of natural uranium required to fuel the reactor. The rationale for restricting the study to PWRs is that they account for nearly two-thirds of the nuclear power reactors in the United States, and for just more than half world-wide (N-1). Moreover this reactor type is now the choice of many countries which initially focused on other types of reactors, or which have only recently committed to a system preference (e.g. the Soviet Union, the United Kingdom, Pakistan and the Peoples Republic of China). Finally, the boiling water reactor (BWR), which accounts for most of the remaining market has many points of similarity with the PWR.

Current PWR core designs originated in an era of cheap yellowcake, a firm commitment to reprocessing and the anticipated wide-spread deployment of Fast Breeder Reactors (FBRs). The design and fuel management strategies of the PWR are not necessarily best suited to the present/future environment when uranium may be more expensive, the introduction of FBRs may be delayed far into the future, and the once through cycle prevails.

The PWR is, therefore, the ideal candidate to focus on as far as conserving uranium ore is concerned. Moreover, the use of thorium, which could be a relatively inexpensive substitute for at least part of the uranium, would also appear to be potentially attractive. The concept of using thorium in LWRs is not new, but as indicated in the following pages, thorium has not been looked at very closely with the aim of using it in small quantities to conserve uranium on the once-through fuel cycle. At the conceptual level the ways in which thorium can be used have also increased, both in number and complexity, requiring an analysis of the present genus.

1.2 Background

Thorium has been looked at several times in many different contexts. The same is true for uranium conservation in PWRs. This review will be confined to the more germane work in both areas. It is assumed that the reader is familiar with the uranium based nuclear fuel cycle, especially in relation to PWRs. Knowledge of LWR physics and fuel management strategies currently in use will also be taken for granted.

1.2.1 The Thorium-232 / Uranium-233 cycle:

Thorium is potentially an abundant and relatively cheap energy resource, if certain problems associated with it can be overcome. Table 1.1 compares the assured and probable reserves for thorium and uranium in the non-communist world. The exploration effort for thorium has been minimal due to low economic incentives. It is therefore believed that, contrary to the quantities shown, thorium reserves at least equal those of uranium, and may well exceed them (N-2). In any event, since uranium is really mined for its U-235 content, roughly five times more uranium is mined than is loaded into the reactor; conversely, thorium requirements should at most amount to one-fifth that for uranium. Before going further into the use of thorium in LWRs it is neccessary to review the basics of the thorium fuel cycle.

Thorium-232 is the only thorium isotope found in nature. Figure 1.1 shows the main transmutation mechanisms for thorium under neutron irradiation, with Fig. 1.2 providing the same information for uranium-238, the predominant uranium isotope. The similarities between the two chains are obvious. Among the more important differences is the presence of protactinium-233 (Pa-233) in the thorium chain, as the precursor to the fissile U-233.

TABLE 1.1

Non-Communist World Uranium and Thorium Resources[a]

	URANIUM[b] (MT U)		THORIUM[c] (MT Th)	
	Reserves (Reasonably Assured)	Estimated Additional (Probable Potential)	Reserves (Reasonably Assured)	Estimated Additional (Probable Potential)
Australia	250,000	60,000	5,000	10,000
Brazil	n.a.[d]	n.a.	10,000	15,000
Canada	130,000	470,000	80,000	100,000
India	n.a.	n.a.	240,000	200,000
Malaysia	n.a.	n.a.	15,000	n.a.
Sweden	230,000	n.a.	n.a.	n.a.
South Africa (including Namibia)	215,000	n.a.	n.a.	n.a.
United States	380,000	630,000	50,000	270,000
Other	225,000	240,000	15,000	340,000
Total	1,430,000	1,400,000	415,000	935,000

[a]Data from Reference (N-2).

[b]Economic at 30 $/lb U_3O_8.

[c]Economic at 15 $/lb ThO_2.

[d]Reliable data not available or included in "Other" category.

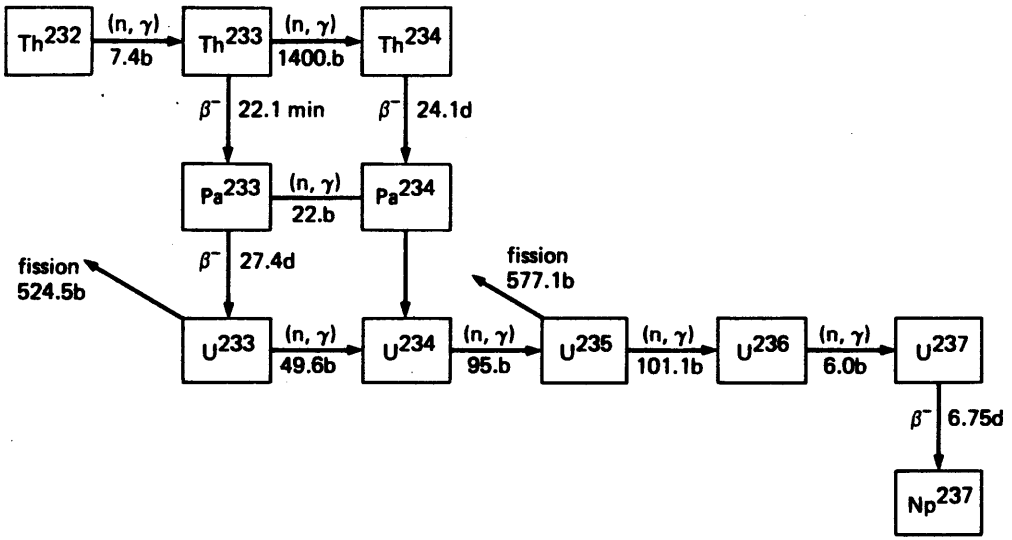

Fig. 1.1 The Chain of Isotopes Created by the Neutron Irradiation of Th-232 (H-1).

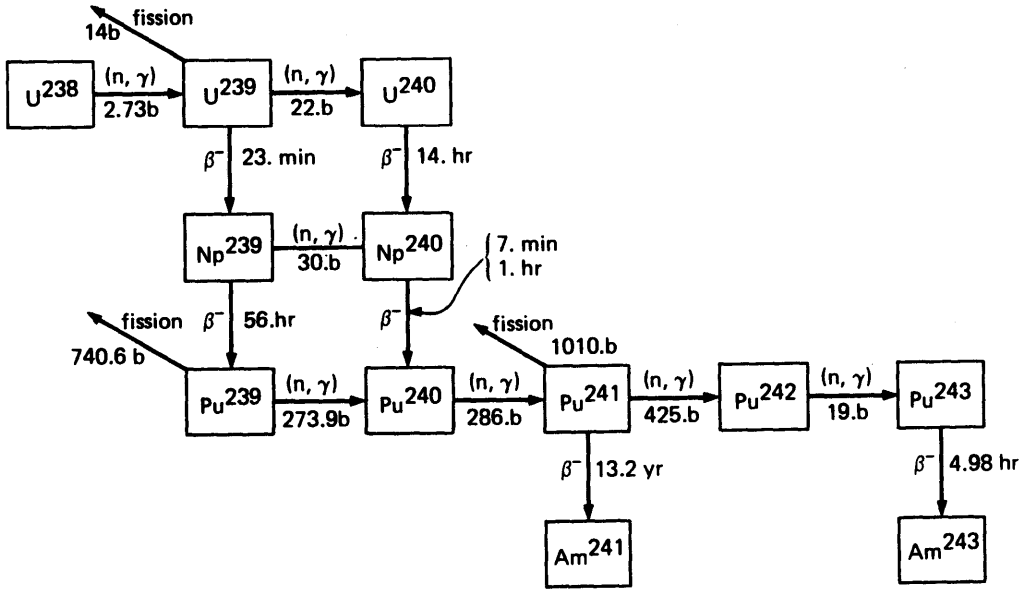

Fig. 1.2 The Chain of Isotopes Created by the Neutron Irradiation of U-238 (H-1).

Pa-233 has a significant neutron absorption cross-section and a half-life of about 27 days. This combination causes a substantial reduction in the production of U-233. However as Fig. 1.1 shows, the product of a neutron absorption in Pa-233 is Pa-234 which decays to the fertile U-234, making Pa-233 less harmful to the neutron economy and fissile production than it would otherwise be.

U-233 is often regarded as the most useful fissile material for LWRs. This is due primarily to its favorable properties at thermal energies. For example, U-233 has the highest thermal eta (ratio of the number of neutrons produced to the number of neutrons absorbed) of all the fissile isotopes. At epithermal neutron energies the U-233 eta is still large and second only to that of Pu-241, a plutonium isotope present only in small quantities in the LWR uranium cycle.

The high U-233 eta arises from a very low capture-to-fission ratio, which more than compensates for the low neutron yield per fission. This and other relevant information is shown in Table 1.2 for the various fissile and fertile isotopes.

U-232 is an important nuclide in irradiated thorium fuels, primarily because of the radioactivity of its decay products. Although present in minute quantities, U-232 is nonetheless a

Table 1.2

CROSS SECTIONS FOR PRINCIPAL NUCLIDES IN THE THORIUM AND URANIUM CHAINS [C-4]

	ISOTOPE											
	Th-232	Pa-233	U-233	U-234	U-235	U-236	U-238	Np-239	Pu-239	Pu-240	Pu-241	Pu-242
THERMAL DATA												
σ_a(0.025 eV)	7.40	41.46	571.01	95.77	678.40	6.00	2.73	80.00	1013.04	290.08	1375.37	30.00
σ_c(0.025 eV)	7.40	41.46	45.99	95.77	101.30	6.00	2.73	80.00	271.19	290.02	367.81	30.00
σ_f(0.025 eV)	0.00	0.00	525.11	0.00	577.10	0.00	0.00	0.00	741.85	0.06	1007.56	0.00
α	--	--	0.0874	--	0.1755	--	--	--	0.3656	--	0.3651	--
ν	--	--	2.498	--	2.442	--	--	--	2.880	--	2.936	--
η	--	--	2.300	--	2.077	--	--	--	2.109	--	2.151	--
INFINITELY DILUTE RI (barns) 0.625 eV-10 MeV												
ABSORPTION	85.78	858.83	883.73	632.16	380.13	348.82	273.57	0.00	445.15	8494.02	686.76	1118.65
CAPTURE	85.20	857.00	135.10	627.96	130.22	346.55	272.37	0.00	168.58	8486.17	112.41	1115.00
FISSION	0.58	1.83	748.63	4.20	249.91	2.27	1.20	0.00	276.57	7.85	574.35	3.65
α	--	--	0.1805	--	0.5210	--	--	--	0.6096	--	0.1957	--

prominent actor in the handling of irradiated thorium fuels. The alpha activity from U-232 is important, but the greater problem is posed by the energetic and penetrating gamma rays from the other isotopes in the decay chain, mainly Bi-212 and Tl-208. The gamma rays from these isotopes result in a high dose rate, making the diversion and processing of U-232 containing fuel more complicated than it is for U-238 based fuels.

It was the presence of U-232 in recycled U-233 fuel, and the possibility of "denaturing" it with U-238 (as a safeguard against proliferation) that prompted the study of the thorium based cycle as a possible alternative to the currently employed uranium cycle in the NASAP (A-1,U-1) and INFCE (I-2) efforts, and their tributary studies.

Thorium can be used as a nuclear fuel in its metallic or oxide forms. The use of thorium metal has some advantages over the oxide. For example, the metal has a higher density and thermal conductivity. On the other hand the metallic form has a lower melting point than the oxide. The use of metallic thorium has been investigated and references (P-1) and (Z-1) are good information sources on the subject. In this study only the use of thorium oxide has been examined. This choice was made because oxide fuel fabrication technology is well established , both in the U.S. and elsewhere, and because the

oxides of thorium and uranium are very similar compounds as illustrated in Table 1.3. Both have a face-centered cubic crystal structure, with comparable densities, melting points, thermal conductivities and heat capacities. This similarity, and the resulting compatability, is particularly useful when homogeneous mixtures of thorium oxide and uranium oxide fuels are of interest.

1.2.2 Thorium in Light Water Reactors: Previous Work

A great deal has been published on the use of thorium in LWRs, starting with the early 1960's. However almost all of the research has concentrated on the recycle mode. Large parts of the Shippingport Light Water Breeder Reactor (LWBR) program and the Advanced Water Breeder Application (ABWA) program in the United States were devoted to thorium (B-1). The DOE's Nonproliferation Alternative System Assessment Program (NASAP) also examined the thorium cycle with particular attention to its nonproliferation aspects (U-1). Studies done by the Oak Ridge National Laboratory for the DOE assessed the economics and utilization of thorium in nuclear reactors in general (O-1,K-1), and also for BWRs in particular (W-1).

Combustion Engineering subsequently performed an assessment of thorium fuel cycles in PWRs for the Electric Power Research

TABLE 1.3

Physical Properties of Thorium and Uranium Oxides*

	UO_2	ThO_2
Crystal Structure	Face-Centered Cubic (CaF_2 type)	Face-Centered Cubic (CaF_2 type)
Theoretical Density (gm/cm^3)	10.96	10.00
Melting Point (°C)	2760	3300
Thermal Conductivity at 600°C (W/cm °C)	0.045	0.044
Heat Capacity at 600°C (Joule/gm °C)	0.30	0.28

*From Reference (P-1).

Institute (M-1,M-2). Again the focus was on a complete recycle mode with high or medium enrichment U-235 to satisfy the initial fissile requirements. While all of these studies made substantial contributions to the understanding of thorium, they are largely of peripheral relevance to the present work.

Work on the use of thorium in small quantities on a once-through cycle in LWRs is of recent origin. The bulk of this has been done on BWRs by the General Electric Corporation (T-1,C-2). Uranium savings of between 4 and 10 percent have been reported possible, by using reconstituted thorium (with its bred-in U-233) as radial blankets in existing BWR cores. Another desirable effect associated with the selective use of thorium fuel pins in BWRs (reported by GE) is a reduced void reactivity coefficient, leading to flatter axial power shapes and reduced power mismatches between adjacent assemblies. A reduction in burnable poison requirements is also reported, which contributes to the improved uranium utilization.

An analysis done at M.I.T. concluded that uniform thorium lattices in PWRs would only worsen uranium utilization on the once-through cycle (D-1,G-2).

A recent study by the Pacific Northwest Laboratory of the Battle Memorial Institute is undoubtedly the most germane (E-1). Done under DOE sponsorship, the research was part of

the same effort as the present work. The use of thorium in PWRs on the once-through cycle was analyzed. Options studied included thorium as a replacement for burnable poisons, spectral shift, reconstitution and lattice optimization. Thoria-urania in both homogenized and duplex pellets were investigated. All calculations were performed at two levels of sophistication, for both currently employed and high-burnup cores. In all cases the all-uranium cores were found to be more uranium efficient than those containing any amount of thorium.

The PNL study explains these apparently anomalous results as being caused by the relatively lower end-of-cycle reactivity contribution of the U-233, compared to that of the Pu-239 (which the U-233 effectively replaces). On a per nucleus basis, reactivity worth is proportional to $(\eta - 1)\overline{\sigma}_a$, and while Pu-239 has a lower spectrum-averaged value of η, it has a compensatorily larger value of $\overline{\sigma}_a$. This end-of-cycle reactivity loss is more detrimental to the uranium utilization than the benefit from the U-233 burnup during the cycle. The study concludes that "the nuclear power industry appears properly launched with uranium fuels, whether spent fuel is reprocessed or not."

1.2.3 Uranium Conservation in Light Water Reactors:

Although LWR fuel burnup has increased steadily over the past twenty years uranium conservation in LWRs began to be looked at seriously mostly as a result of the U.S. administration decision in 1977 to defer commercial reprocessing and deployment of the FBR. It was given added impetus by the rising cost of uranium ore in the United States and on the world market. At the present time the situation is somewhat different. The Reagan administration has announced plans to proceed with commercial reprocessing and breeder development, and the price of uranium has fallen from a high of about $40/lb. in 1978 to a current price of about $20/lb..

It is widely believed that the decrease in uranium price is temporary and that it will rise once substantial numbers of the newer plants come on-line. Commercial reprocessing is also not expected to make a significant contribution to the nuclear fuel cycle till at least the mid 1990's, and the pricing of this service is uncertain. Non-proliferation concerns may also have a bearing on the extent to which it is deployed. For these reasons it is important that research, development and implementation of improved uranium utilization options continue in the immediate future. In any event, many of these options will also benefit recycle mode operation, and help

fulfill utility desires for longer burnup cycles and higher fuel integrity.

Many strategies for improving uranium utilization in LWRs have been identified and investigated. These include: extended burnup, increased number of batches, lattice reoptimization, low-leakage fuel management, bundle reconstitution and reinsertion, spectral shift control, use of radial and axial blankets, annular fuel, and the utilization of improved burnable poisons. Loh (L-2) has tabulated the potential uranium savings from each of the options, as reported by various investigators. Table 1.4 has been adapted from his list, with some additions.

The biggest improvements are possible from increased discharged burnup. The savings from reconstitution and spectral shift control are also large, but considerably more difficult to implement. It is worth noting that the savings reported are sensitive to the base-case used in each study. Furthermore the savings from a composite core, employing some combination of strategies, would in general be less than the algebraic sum of the savings from each individual innovation.

TABLE 1.4

Possible Strategies to Improve Uranium Utilization in PWRs on the Once-Through Cycle

Strategy	Uranium Savings	References	Comments
1. Extended Burnup and Increased Number of Batches	∿15%	F-1,M-3, M-4,S-2	For a 5-batch core with ∿55 GWD/MT discharge burnup.
2. Low-Leakage Fuel Management/Radial Blankets	∿3%	M-3,S-2, S-3	Increased radial power peaking.
3. Axial Blankets	∿2%	K-2,M-3, M-5,S-2	Increased axial power peaking.
4. Lattice Re-optimization	2 - 3%	R-1,S-4	Improvement is design specific.
5. Continuous Mechanical Spectral Shift	10 - 15%	S-4	Possibly severe engineering problems.
6. Mid-Cycle Bundle Reconstitution	∿10%	R-1,S-4	Potential thermal-hydraulic problems. Lower plant capacity factors.
7. D_2O Spectral Shift	10 - 15%	C-3,G-1, S-4	Lower control poison requirements. Added expense of D_2O.
8. Routine Pre-Planned Coastdown	∿7%	D-2,F-1, M-3,M-4, S-4	Savings depend on economically acceptable coastdown duration.
9. Burnable Poisons	∿1%	L-2	Also facilitates other options.

1.3 Research Objectives

The main objective of this study is to identify and analyze options to improve uranium utilization in PWRs on the once-through fuel cycle, by judiciously employing small quantities of thorium.

One of the earliest problems encountered in the course of this work was the need to develop a consistent methodology to evaluate thorium. A model based on the "advanced linear reactivity model" (S-4) has been developed for this purpose and used in conjunction with detailed physics calculations to assess the many possible roles for thorium in PWRs.

The options studied include: mixed thorium and uranium assemblies, internal and radial blankets of thorium, reconstitution and reinsertion of thorium assemblies, and the use of thorium in PWRs with spectral shift control. Smaller sized assemblies for both thorium containing and uranium-only cores have also been analyzed.

1.4 Organization of this Report

The work reported here is arranged as follows:

Chapter two provides a background to the analytical models developed for this study. These include modifications to the "advanced linear reactivity model" of Sefcik (S-4). Descriptions of the computer codes (LEOPARD and PDQ-7) used in the course of this work are also included.

Chapter three deals with details of the uranium utilization model used in this work. These include a power sharing algorithm, which has been used extensively in this work. The algorithm is derived from basic principles and then applied to a variety of fuel bundle arrays and core configurations, in order to test its validity and quantify its accuracy.

In Chapter four thorium is analyzed as a uranium saving material for PWRs in options which are relatively easy to retrofit. These are : assembly-sized thorium inserts as internal and external blankets, and thorium pins in uranium assemblies. Both current and high burnup PWR cores are examined.

In Chapter five those options which are more difficult to implement, at least retrofittably, are analyzed. These are :

reconstitution and reinsertion of thorium assemblies and using thorium in a spectral shift mode of operation. Smaller fuel assemblies for PWRs are also assessed, and the uranium utilization advantages of their deployment are quantified.

Chapter six concludes this study by summarizing the methods used and the results obtained for the various options studied. It also identifies areas where future effort in this regard should be directed.

Chapter six is followed by a series of appendices and a list of references, which provide detail and support to the information in the main text.

CHAPTER 2

DESCRIPTION OF METHODS AND MODELS

2.1 Introduction

A methodology based on the Linear Reactivity Model of Sefcik (S-4) was used to assess the use of thorium in PWRs on the once-through cycle, and to quantify the uranium utilization improvement potential of the other schemes examined in the present work. This methodology relies on the use of input from detailed neutron physics calculations of pincells, assembly clusters and core configurations. The availability of computer codes which employ thoroughly tested physics models and well established numerical methods have made the acquisition of such information relatively simple. The programs used in this work are currently state-of-the-art, and will be discussed briefly in this chapter, with references to more detailed descriptions.

The high cost of using these programs on problems in their most general form necessitates the development of simpler and more cost efficient models based on analytical, empirical and numerical methods. If carefuly formulated, these simple

models can be used as low cost substitutes for the more expensive codes, while retaining sufficient accuracy to substantiate confidence in the final results. These models also facilitate making comparisons on a consistent and well defined basis. The theoretical base for the models of this type used in the present work will also be described here.

The broader task can be divided into two distinct parts. The first involves calculation of an infinite medium neutron spectrum, and its use for the generation of few-group cross-sections as a function of burnup. The second subtask is concerned with the space and burnup dependent behavior of the power in a reactor core. This division is also motivated by the high cost of performing a multi-group, fine-mesh analysis in three dimensions, and is widely employed in the nuclear power industry.

2.2 The LEOPARD Code (B-2)

The "Lifetime Evaluating Operations Pertinent to the Analysis of Reactor Designs" program, or LEOPARD, is one of the most widely used neutronics codes in the nuclear power industry. It is a zero-dimensional, spectrum-dependent depletion program, and is used to generate few-group cross-sections for

square or hexagonal lattices, as a function of discrete burnup steps.

The calculation at epithermal energies is done using a modified MUFT scheme (B-3), while the SOFOCATE program (A-2) handles the thermal calculation. The version of LEOPARD used in the present analysis was that provided by the Electric Power Research Institute (EPRI). Its cross-section set is derived from the ENDF/B-IV cross-section library using the SPOTS program (B-2).

The basic LEOPARD methodology is well documented (C-4,G-2,K-2,L-2,S-4). Only the more pertinent points will be addressed here. One important aspect is the applicability of LEOPARD to thorium-based fuels. Previous workers at MIT have explored this problem: in particular Correa (C-4) and Garel (G-2) have benchmarked the MIT version of LEOPARD against published results of critical and exponential experiments.

Correa benchmarked LEOPARD against critical experiments for U-233/ThO_2 and U-235/UO_2 lattices over a wide range of fuel-to-moderator volume ratios (V_F/V_M), enrichments and heavy-water (D_2O) content. Garel performed benchmarks for both critical and exponential experiments. Most of these were for U-235/UO_2 lattices, with five cases for U-233/ThO_2. A summary of their results is presented in Table 2.1 . The average k_{eff}

TABLE 2.1

Summary of LEOPARD Benchmark Comparisons

Fuel	UO_2-ThO_2 [a]	UO_2-ThO_2 [a]	UO_2 [a]	UO_2 [b]	PuO_2-UO_2 [b]	ThO_2-UO_2 [b]
ε (w/o)	3.00	3.78-6.33	3.00-4.02	1.3-4.1	1.5-6.6	2.63
F/M	0.01-1.00	0.11-0.78	0.23-2.32	0.1-1.3	0.1-0.9	0.33-1.00
D_2O(%)	0.0-99.34	0.0-81.96	0.0-89.14	—	—	—
Boron (PPM)	—	—	—	0.0-3400.	—	—
$\bar{k}$	1.003	1.009	0.998	1.003	1.018	1.0103
$\overline{\lvert\Delta k\rvert}$	0.012	0.016	0.006	0.012	0.014	0.010
# of cases	16	16	26	63	42	5

[a] Reference (C-4).

[b] Reference (G-2).

for the U-233/ThO_2 criticals reported by Correa is 1.003, and for Garel's five cases it is 1.010. For U-235/UO_2 lattices the results are in even better agreement with the experiments.

Two points need particular emphasis. First, the error associated with using LEOPARD for thorium-based fuels is small enough to be acceptable, second, these results show a small, but consistent positive bias in LEOPARD when applied to U-233/ThO_2 lattices. The bias is however not significant enough to affect the results of the present work.

While LEOPARD has been superseded in rigor and complexity, in a recent evaluation against newer programs (EPRI-CELL and LASER) it still more than held its own (L-3).

2.3 The PDQ-7 Program (C-5)

PDQ-7 is a state-of-the-art diffusion-depletion code. It is designed to be used at at various levels of sophistication and can be applied to essentially any reactor type, provided that few-group cross-sections (as a function of burnup, for fuel depletion studies) can be provided by the user (e.g. from separate LEOPARD calculations). PDQ-7 can solve diffusion-depletion problems in up to three spatial dimensions, with a maximum of five neutron energy groups, in

rectangular, spherical, cylindrical or hexagonal geometries. The code can perform eigenvalue, boundary-value, adjoint (perturbation) and fixed-source calculations.

Reference (H-2) provides a good description of the numerical solution schemes employed by the code, and references (K-2,L-2 and S-4) provide details on the ways in which it is applied for the analysis of PWR cores.

2.4 The Linear Reactivity Model: A Review

In nuclear fuel management the reactivity, ρ, of a region is commonly defined in terms of its infinite medium neutron multiplication factor, k_∞, as follows :

$$\rho = 1 - \frac{1}{k_\infty} \qquad (2.1)$$

While, strictly speaking, this definition holds only for a region of infinite extent, (i.e. the material is bathed in a self-generated neutron spectrum) it has been found acceptable for present purposes to use the same value for assemblies in a PWR core.

It is now well established that the unpoisoned reactivity, ρ, of a PWR assembly, defined by Eq. (2.1), varies linearly with burnup (G-1,K-2,S-4). This variation is mathematically represented as :

$$\rho = \rho_0 - AB \tag{2.2}$$

where,

ρ_0 = the extrapolated Beginning-of-Life (BOL) reactivity,

B = the assembly Burnup, MWD/MT,

A = the slope of the ρ versus B linear fit, MT/MWD.

One such fit, for a 3 w/o Maine Yankee PWR assembly, is shown as Fig. 2.1. Both ρ_0 and A are functions of BOL enrichment, fuel-to-moderator ratio, fuel pellet radius, etc. (see Appendix B). Equation (2.2) is true for U-235 enrichments between 2 w/o and 5 w/o as shown in Fig. 2.2 and for a similar range of U-235 enrichments in ThO_2, as shown in Fig. 2.3. The reason why Eq. (2.2) holds so well has been investigated by Loh (L-2) who attributes it to the "fortunate convergence of several complicated adjustments in lattice neutronics."

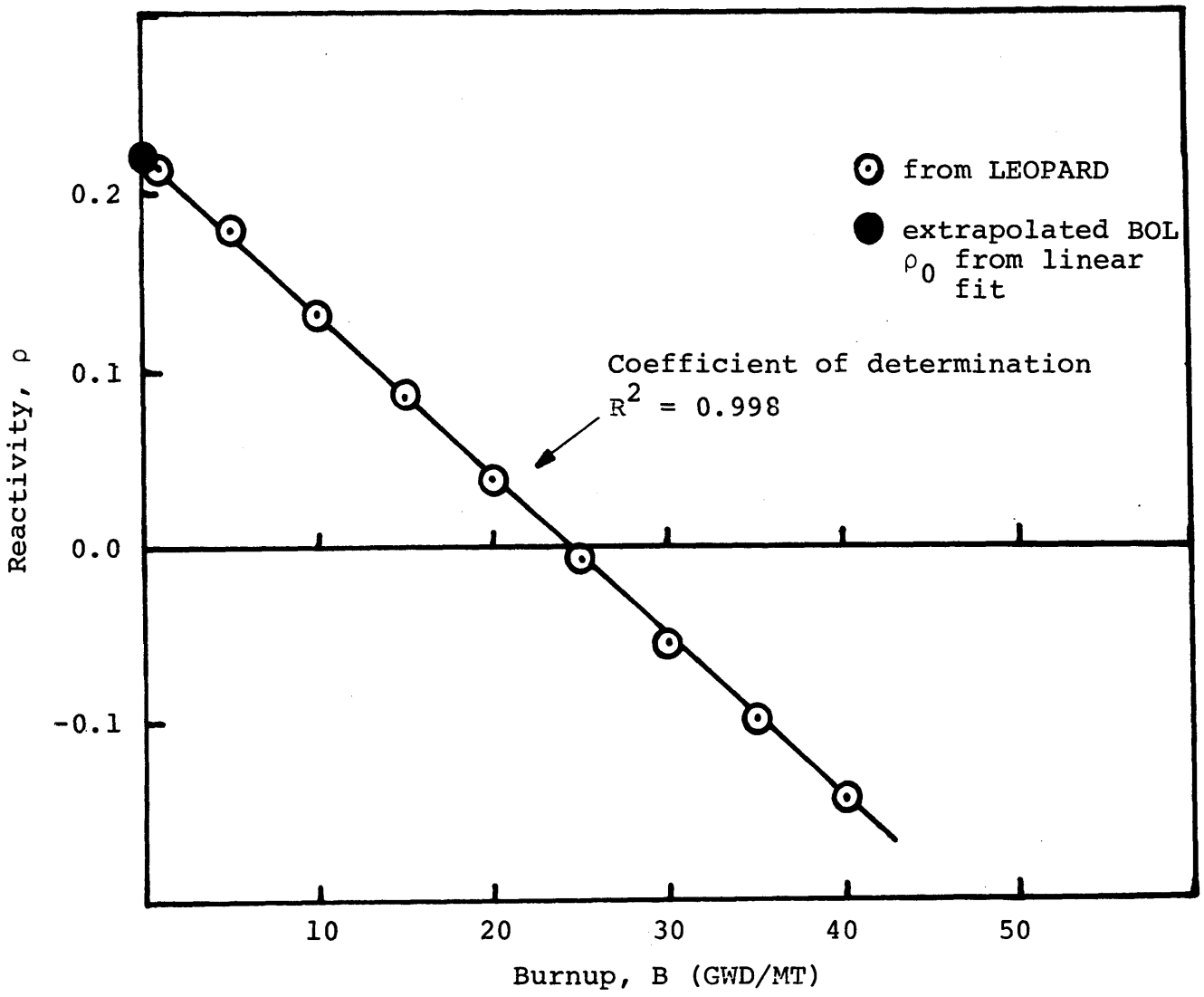

Fig. 2.1 Reactivity versus Burnup for a Maine Yankee Supercell with 3 w/o U-235 in UO_2.

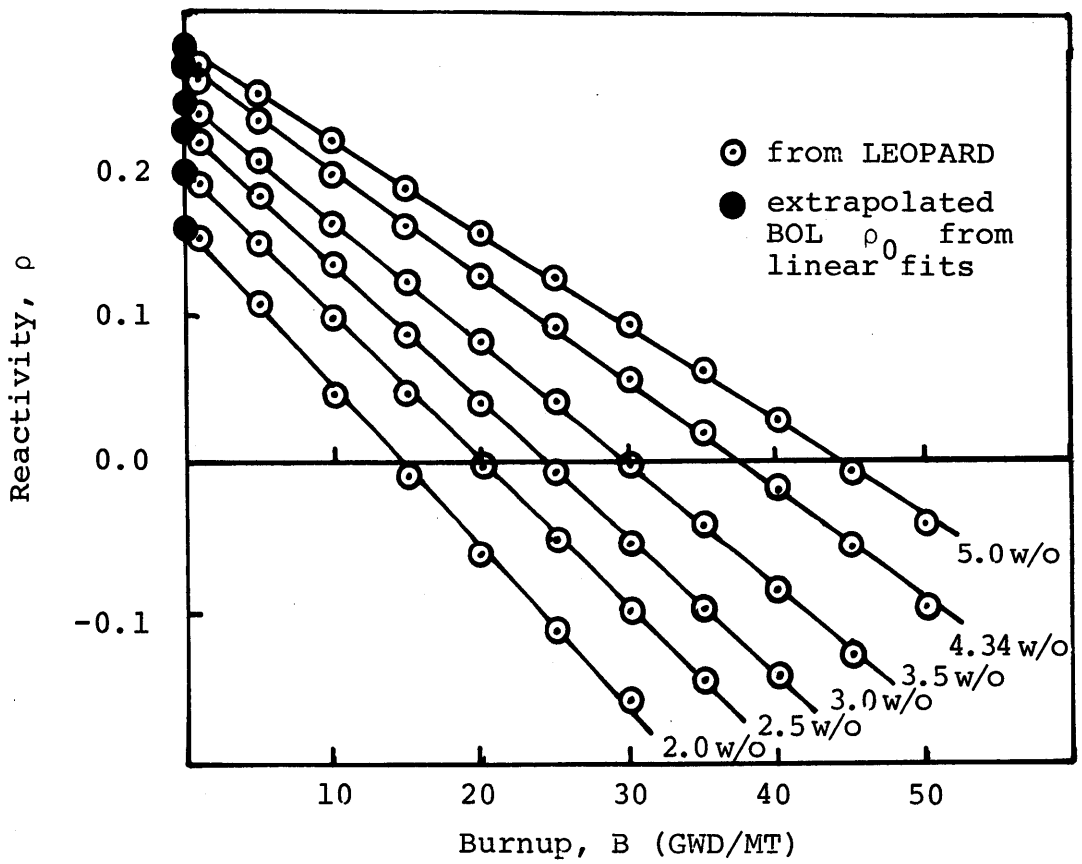

Fig. 2.2 Reactivity versus Burnup for the Maine Yankee Supercell for Different Fuel Enrichments of U-235 in UO_2.

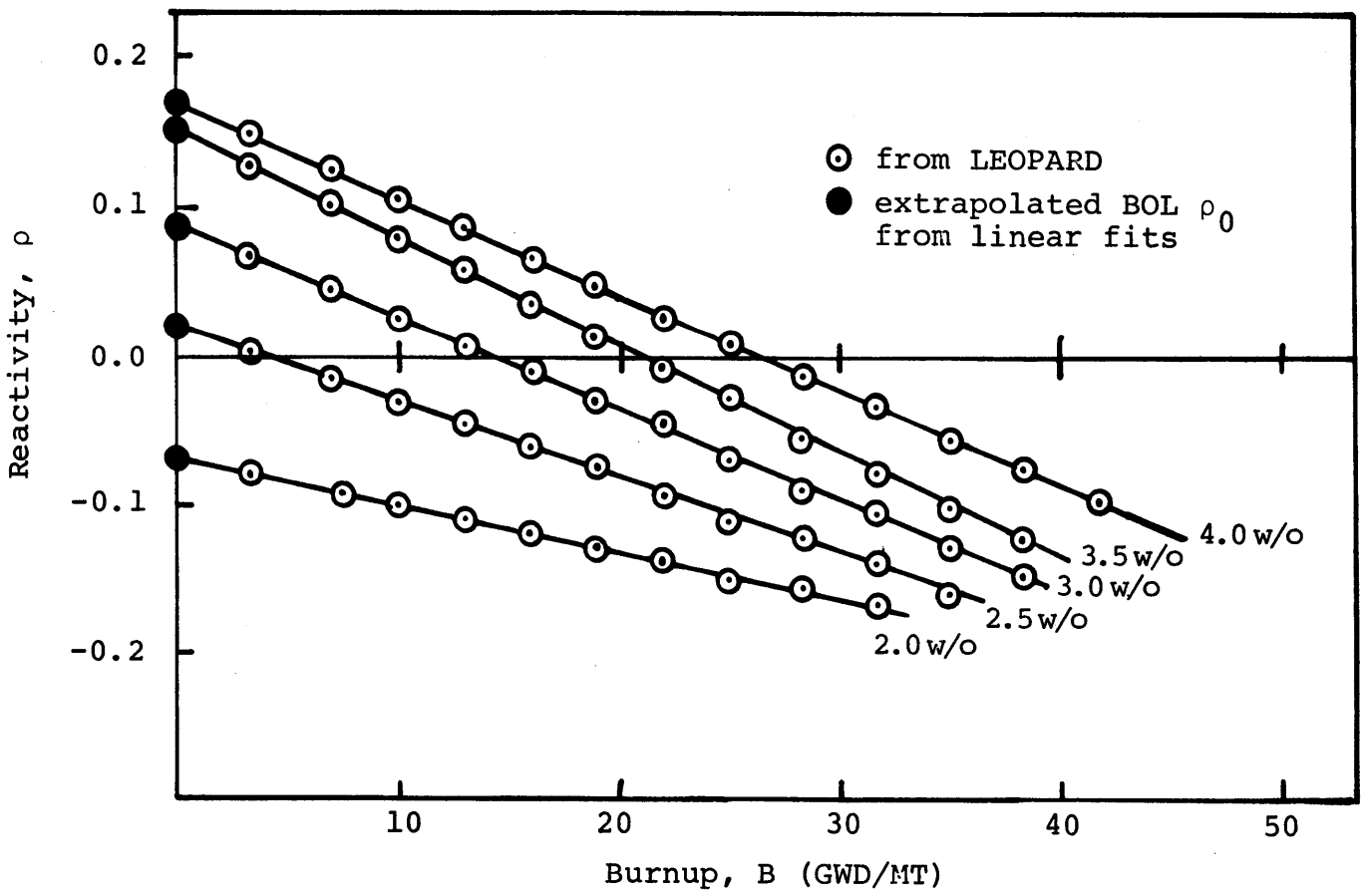

Fig. 2.3 Reactivity versus Burnup for the Maine Yankee Supercell for Different Fuel Enrichments of U-235 in ThO_2.

This linearity has been exploited to develop simple and surprisingly accurate models for assessing various fuel-management strategies. In its simplest form, the linear reactivity model can be used to compute the discharge burnup of a core at steady-state.

If B_d denotes the average discharge burnup of the fuel in the core and $\bar{f}_k$ the averaged power fraction of the k^{th} fuel batch, then their product gives the average burnup accumulated by that batch over the cycle. Hence, for the fresh fuel (k=1) at end-of-cycle, the burnup incurred is $\bar{f}_1 B_d$. For batch-2 the burnup over the cycle is $\bar{f}_2 B_d$, and the cumulative burnup (since beginning-of-life) is $\bar{f}_1 B_d + \bar{f}_2 B_d$, and so on for each batch. With this, Eq. 2.2 can now be written successively for each batch in the n-batch core as follows:

$$\rho_1 = \rho_0 - AB_d\bar{f}_1 \tag{2.3}$$

$$\rho_2 = \rho_0 - AB_d(\bar{f}_1 + \bar{f}_2)$$

$$\vdots$$

$$\rho_k = \rho_0 - AB_d \sum_{i=1}^{k} \bar{f}_i \tag{2.4}$$

$$\vdots$$

$$\rho_n = \rho_0 - AB_d \sum_{i=1}^{n} \bar{f}_i \tag{2.5}$$

Note that by definition, the sum of the power fractions of all the batches in the core is unity, i.e.

$$\sum_{i=1}^{n} \bar{f}_i = 1.0 \tag{2.6}$$

The next task is to determine the system reactivity, for which a prescription for the system-averaged reactivity is required.

A definition of reactivity entirely equivalent to that used in Eq. (2.1) is

$$\rho_i = \frac{\nu F_i - A_i}{\nu F_i} \tag{2.7}$$

where,

ρ_i = the reactivity of fuel region i.

ν = the average neutron yield per fission.

F_i = the total fission rate in region i.

A_i = the total neutron absorption rate in region i.

The reactivity of the entire core fuel region, ρ_{sys}, can be similarly defined in terms of the fission and absorption rates of each batch

$$\rho_{sys} = \frac{\sum_{i=1}^{n} (\nu F_i - A_i)}{\sum_{i=1}^{n} \nu F_i} \tag{2.8}$$

Using Eq. (2.7) to eliminate A_i in Eq. (2.8) yields:

$$\rho_{sys} = \frac{\sum_{i=1}^{n} \nu F_i \rho_i}{\sum_{i=1}^{n} \nu F_i} \tag{2.9}$$

For a given fuel composition, the neutron production rate, νF_i, is directly proportional to the thermal energy generation rate, κF_i. If it is assumed that the ratio κ/ν is constant for all fuel types examined, at all burnups, then the power fraction of batch i (f_i), defined as

$$f_i = \frac{\kappa F_i}{\sum_{i=1}^{n} \kappa F_i} \tag{2.10}$$

can be written in the form

$$f_i = \frac{\nu F_i}{\sum_{i=1}^{n} \nu F_i} \tag{2.11}$$

Substitution for νF_i from Eq.(2.11) in Eq. (2.9) yields

$$\rho_{sys} = \sum_{i=1}^{n} f_i \rho_i \tag{2.12}$$

The only approximation employed thus far is that κ/ν is a constant for all fuel types and burnups of interest. Figure (2.4) shows the variation of κ/ν with burnup for U-235/UO_2 and U-233/ThO_2 fuels in a typical PWR lattice. The plot has been generated using LEOPARD. The maximum variation in κ/ν, from the mean value of 79.8 MeV/neutron, is less than one percent, making the approximation a very good one indeed. It is also worth noting that this approximation is not essential but merely a convenient simplification.

The usefulness of Eq. (2.12) is that given assembly, region or batch reactivities and power-fractions, the system reactivity can be computed.

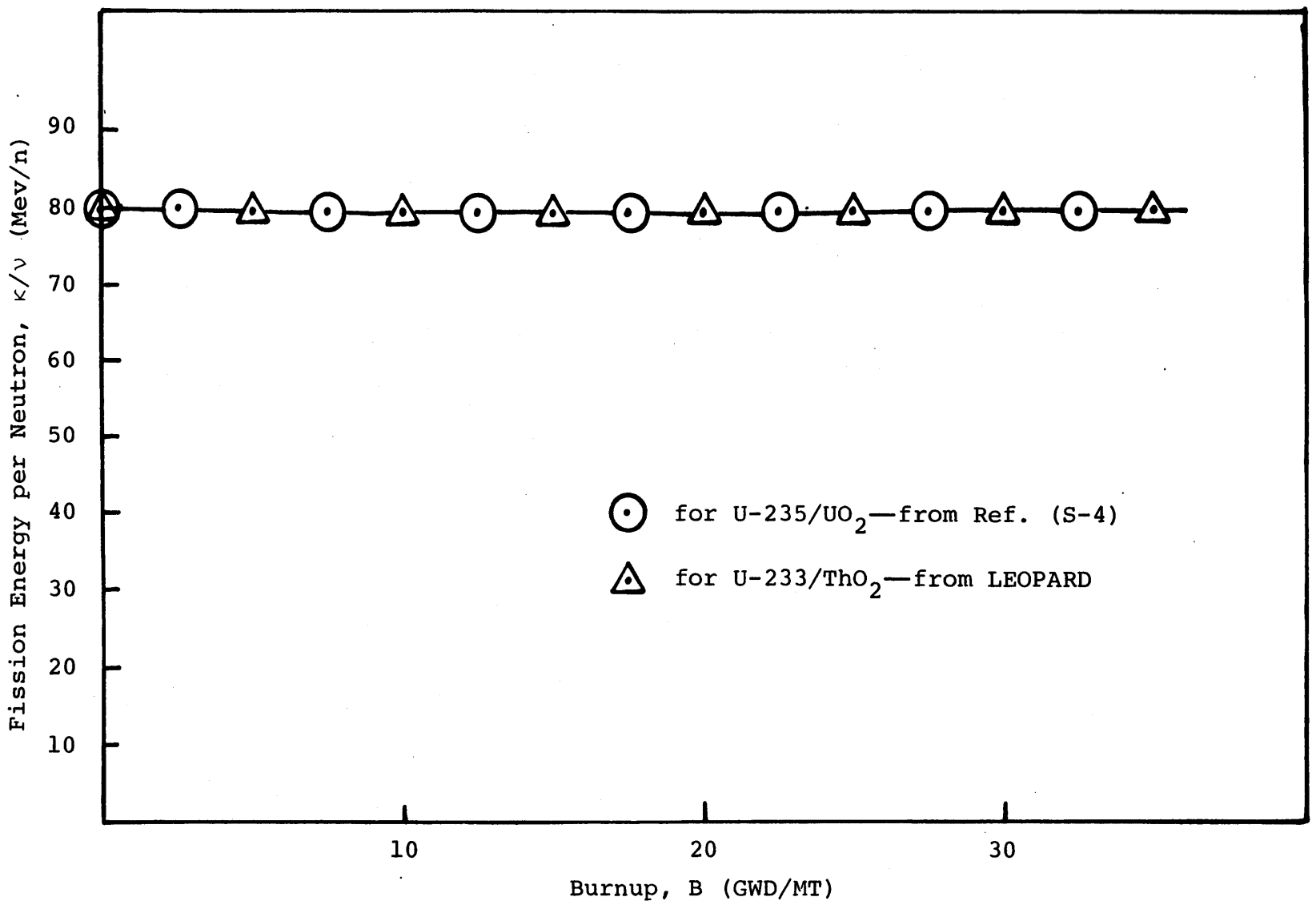

Fig. 2.4 Average Energy Release per Fission Neutron (κ/ν) as a Function of Fuel Burnup.

A reactor must remain critical at all times during normal operation, so that the system reactivity, ρ_{sys}, must equal the reactivity lost to leakage, ρ_L, i.e,

$$\rho_{sys} = \rho_L = \sum_{i=1}^{n} f_i \rho_i \tag{2.13}$$

with ρ_L defined as the fraction of the total neutron production in the core that is absorbed in the ex-core (non-fuelled) regions:

$$\rho_L = \frac{A_R}{\sum_{i=1}^{n} \nu F_i} \tag{2.14}$$

where,

A_R = the total neutron absorption rate in the non-fuel, (ex-core) region.

Combining Eqs. (2.11), (2.12) and (2.13) yields, after some algebra:

$$\rho_{sys} = \rho_L = \rho_0 - AB_d \left\{ \sum_{i=1}^{n} \sum_{k=1}^{i} f_i \bar{f}_k \right\} \tag{2.15}$$

or

$$B_d = \frac{\rho_0 - \rho_L}{A \left\{ \sum_{i=1}^{n} \sum_{k=1}^{i} f_i \bar{f}_k \right\}} \qquad (2.16)$$

where,

f_i = the end-of-cycle power fraction of batch i.

The term in the denominator with the double summation was designated the "Cycle Schedule Index" by Sefcik (S-4), who originally developed this approach.

The remaining problem that must be solved before Eq. (2.16) can be used is the determination of the end-of-cycle and cycle-averaged power fractions for each batch, and the reactivity loss to leakage at end-of-cycle. The task is a formidable one, since in order to determine these quantities the end-of-cycle points must be known a priori. Moreover, the power fractions depend on the fuel type, the core loading pattern, the control poison employed and the number of batches. The development of a methodology for the estimation of batch powers is presented in the next chapter.

One convenient approximation that is often very useful is "Equal Power Sharing" (EPS), according to which it is assumed that at all points during the cycle, all batches share power

(and therefore incremental burnup) equally, i.e. the cycle-averaged and end-of-cycle power fractions are equal to 1/n , for an n-batch core. Mathematically

$$f_i = \bar{f}_k = \frac{1}{n} \tag{2.17}$$

Substituting this limiting case into Eq. (2.16) yields:

$$B_{d,EPS} = \left(\frac{2n}{n+1}\right)\left(\frac{\rho_0 - \rho_L}{A}\right) \tag{2.18}$$

where,

$B_{d,EPS}$ = the average core discharge burnup, under the EPS approximation.

The EPS treatment gives good agreement with more exact results, through a fortunate cancellation of effects. For example, in a 3 batch core, the difference between the discharge burnup obtained using the EPS power fractions (1/3,1/3,1/3) and that from the set of batch powers as extreme as (1/2, 1/3, 1/6) is only 4 percent, with EPS predicting the higher value.

There are two main uses of this limiting case treatment. The first is in developing quick analytical solutions to

screen different fuel management strategies and the second is in providing a first guess for the discharge and cycle burnups in accurate numerical methods where the power-weighted solutions are arrived at iteratively. Both of these aspects are discussed and applied in the next chapter.

2.5 Chapter Summary

In this chapter the state-of-the-art computer codes used in this analysis, namely LEOPARD and PDQ-7, have been described. In particular, results of the benchmark comparisons performed by other researchers have been presented which show that the LEOPARD code provides sufficient accuracy when applied to U-233/ThO_2 and U-235/UO_2 lattices.

The basic methodology of the power-weighted linear reactivity model has been presented, and the Equal Power Sharing version of this model has been introduced.

CHAPTER 3

POWER SHARING AMONG BATCHES AND SUB-BATCHES

3.1 Introduction

The Linear Reactivity Model described in the preceding chapter was developed for use on current PWR cores and derived under simple assumptions, such as equal power sharing among batches, linear behavior of reactivity with burnup, and for only one type of fuel in the reload batch. The assessment of cores with "split" batches (e.g. batches containing thorium, or more than one reload enrichment) requires a more sophisticated treatment. The power sharing among fuel assemblies during the cycle and at the end of cycle, the effects arising from neutron leakage, and those from soluble poison, all need to be incorporated into the model.

In this chapter these problems are addressed. First an algorithm is derived to predict power sharing among fuel assembly clusters and fuel batches. The algorithm is then tested using PDQ-7 calculations and published results for the Combustion Engineering System-80^{TM} reactor and the Maine Yankee reactor. The same sources are also used to verify an

algorithm to model neutron leakage from the core periphery. Finally, the general methodology for evaluating various fuel management options is presented, with applications deferred till later chapters.

3.2 The Power Sharing Algorithm

In this section, starting from the two-group diffusion equation, the "group-and-one-half" theory approximation will be made and used to derive the basic power sharing relations. These relations have been used extensively in this work to calculate end-of-cycle and cycle-averaged power sharing among assembly clusters and fuel batches. The details of the derivations appear in Appendix C.

The diffusion equation for the fast group (subscript 1) can be written in the form :

$$- D_1\nabla^2\phi_1 + \Sigma_{a1}\phi_1 + \Sigma_{12}\phi_1 - \frac{1}{k}(\nu\Sigma_{f1}\phi_1 + \nu\Sigma_{f2}\phi_2) = 0 \tag{3.1}$$

and for the thermal group (subscript 2)

$$- D_2\nabla^2\phi_2 + \Sigma_{a2}\phi_2 - \Sigma_{12}\phi_1 = 0 \tag{3.2}$$

Here "k" is the neutron multiplication factor, and the other symbols have their usual meaning. The essence of the group-and-one-half model is the approximation that thermal neutrons are absorbed at the point of their removal from the fast group. Stated differently, in the group-and-one-half model the thermal leakage is neglected by setting $\nabla^2\phi_2 = 0$, which reduces Eq. (3.2) to

$$\Sigma_{a2}\phi_2 = \Sigma_{12}\phi_1$$

or
$$\phi_2 = \frac{\Sigma_{12}\phi_1}{\Sigma_{a2}} \tag{3.3}$$

The local reactivity, ρ, defined by Eq. (2.1), can be written in the form

$$\rho = \frac{(\nu\Sigma_{f1}\phi_1 + \nu\Sigma_{f2}\phi_2) - (\Sigma_{a1}\phi_1 + \Sigma_{a2}\phi_2)}{(\nu\Sigma_{f1}\phi_1 + \nu\Sigma_{f2}\phi_2)} \tag{3.4}$$

Using Eq. (3.3) for the thermal group flux, ϕ_2, in terms of the fast flux, ϕ_1, in Eqs. (3.1) and (3.4), yields for a critical system (k=1.0):

$$\nabla^2\phi_1 + \frac{1}{M^2}\left(\frac{\rho}{1-\rho}\right)\phi_1 = 0 \tag{3.5}$$

where M^2 is the migration area, defined here as

$$M^2 = \frac{D_1}{\Sigma_{12} + \Sigma_{a1}} \tag{3.6}$$

The fast flux can also be related to the local power density, q, since

$$q = \kappa(\Sigma_{f1}\phi_1 + \Sigma_{f2}\phi_2) \tag{3.7}$$

or using Eq.(3.3) for ϕ_2,

$$q = \kappa(\Sigma_{f1} + \Sigma_{f2}\frac{\Sigma_{12}}{\Sigma_{a2}})\phi_1 \tag{3.8}$$

where,

κ = the average energy released per fission.

Combining Eqs. (3.4), (3.5) and (3.8) yields, after some manipulation,

$$\nabla^2\{q(1-\rho)\} + \frac{\rho q}{M^2} = 0 \tag{3.9}$$

The remaining problem is to approximate the Laplacian in Eq. (3.9) in terms of the difference between local and neighboring values of the bracketed function. Various situations have

been investigated and the more interesting of these are included in Appendix C. Only the final results are presented here.

For a fuel assembly in a reactor

$$q_i = \frac{q_s(1 - \theta_s\rho_s)}{(1 - \theta_i\rho_i)} \tag{3.10}$$

where,

q_i, q_s = the power density of the assembly, and the average power density of its 8 immediate neighbors, respectively.

ρ_i, ρ_s = the reactivity of the assembly, and the average (power-weighted) reactivity of its 8 neighbors.

θ_i = the "reactivity-power coupling factor" (RPCF); this is a function of the migration area and the size of the assemblies.

θ_s = a (properly modified) RPCF for the 8 surrounding assemblies; for example, $\theta_s \approx \frac{1}{2}(3 - \theta_i)$ for a 3x3 assembly cluster in a critical core, and $\theta_s \approx \theta_i$ for an isolated 3x3 cluster.

Very often it is more important to correctly predict the batch-wise power sharing in a core. Indeed, in studies involv-

ing the assessment of uranium utilization the main quantity of interest is the discharge burnup of the batches in the core. Since the reactor is always held critical, the average surroundings of an assembly in the core are very close to critical at any time during the cycle. Therefore in order to calculate the batch-averaged power split we can use Eq. (3.10) with $\rho_s=0$, and with the power densities replaced by the batch-averaged power fractions, f_i, i.e.

$$f_i = \frac{\bar{f}}{1 - \theta_i \rho_i} \qquad i = 1,n \tag{3.11}$$

where

f_i = the fraction of core power provided by batch i.

$\bar{f}$ = 1/n, the fraction of core power delivered by the core-averaged batch.

ρ_i = the average reactivity of batch i.

θ_i = the RPCF for the batches in the core.

n = the number of batches in the core.

The reader is referred to Appendix C for the derivation of Eq. (3.11).

3.3 Power Sharing Among Isolated Fuel Bundles

The significance of the power sharing algorithms given in Eqs. (3.10) and (3.11) lies in the fact that given information on the reactivity of an assembly and that of its surroundings, their relative power levels can be predicted with little additional information. In this section the power sharing prescription for "isolated" 3x3 clusters of fuel assemblies will be verified using detailed neutronic calculations from PDQ-7.

Figure 3.1 shows the configuration modelled on PDQ-7 to verify Eq. (3.10). This configuration is termed "isolated" because, due to the zero net-current boundary condition, the assemblies are effectively embedded in an infinite array and there is no net transfer of neutrons from the 3x3 array to the surroundings. Furthermore, in general, the 3x3 clusters, and therefore the infinite array, will not be critical. Both of these factors (no leakage and non-criticality) make this situation of limited practical relevance. It is however a very good check on the theoretical basis of the group-and-one-half model and on the approximations made in the course of deriving Eq. (3.10). It is also an important step in extending the model to cases of greater practical interest where the reactor is always held critical and, in general, there is a net trans-

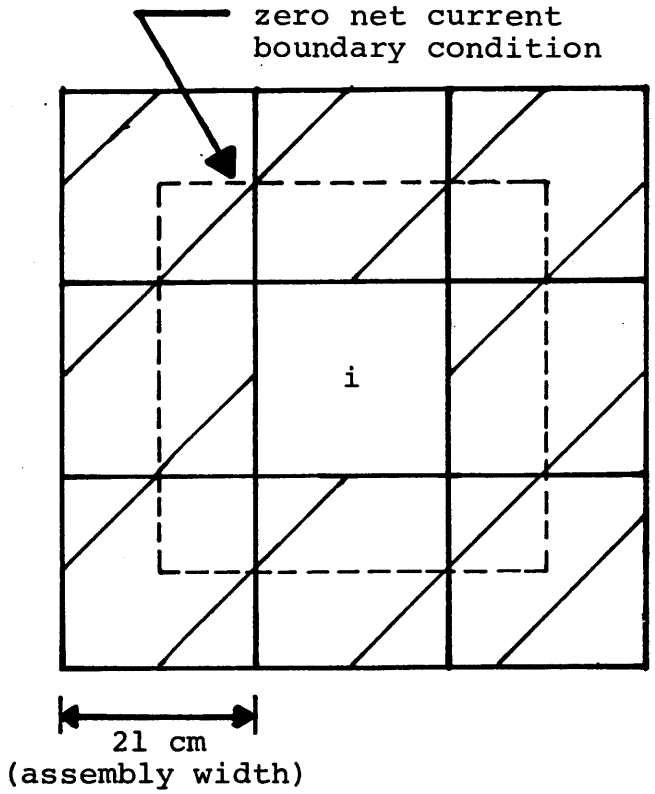

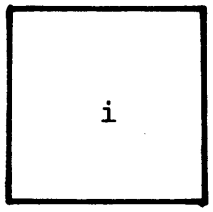

INTERIOR ASSEMBLY

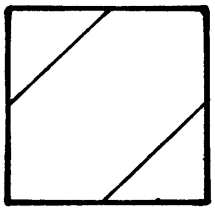

SURROUNDING ASSEMBLY

Fig. 3.1 'Isolated' 3 x 3 Assembly Clusters

fer of neutrons between any cluster of fuel assemblies and those surrounding it.

To verify Eq. (3.10) a total of 51 3x3 assembly clusters were modelled on PDQ-7. The cross-sections for the interior and exterior regions of the clusters were generated using a LEOPARD supercell burnup calculation for a 3.0 w/o enriched U-235/UO_2 lattice. The lattice and assembly dimensions, composition, temperatures etc., were obtained from publicly available information on the Maine Yankee reactor (see Appendix A).

As shown in Appendix C, for the case of isolated 3x3 clusters, theory predicts $\theta_s \approx \theta_i \approx 1.6$. A multiple linear regression, fit to the data obtained from PDQ-7 for q_i/q_s versus ρ_i and ρ_s gave $\theta_i=\theta_s=1.46$. The difference between the theoretically predicted and actual values of theta is due to the approximations made in the course of obtaining the theoretical estimates.

Equation (3.10) can be rearranged in the form:

$$\frac{q_s}{q_i}(1 - \theta_s\rho_s) = 1 - \theta_i\rho_i \qquad (3.12)$$

The results of the aforesaid data fit are shown in Fig. (3.2). The data points are documented in Appendix C. The value of θ_i (the slope of the fit) is 1.46, and the goodness of fit criteria, R^2, is 0.997. The maximum error in q_i/q_s is 2.8% and the average error only 0.7%.

This result confirms the theoretical basis of the analysis, since not only is $\theta_i = \theta_s$, as predicted on theoretical grounds, but the actual values obtained from state-of-the-art methods are close to those obtained from theory. Furthermore, the error associated with using the algorithm is very small.

3.4 Power Sharing Among Assemblies in a Core

If the power sharing algorithm is to be applied to fuel assemblies in a core, or on a batch-wise basis, then it must work in situations where neutrons are leaking to and from the cluster. In such situations theory predicts that Eq. (3.10) still holds but with different values for θ_i and θ_s. As shown in Appendix C, these values of theta are $\theta_i \approx 2.4$ and $\theta_s \approx 0.3$.

In order to test the validity of Eq. (3.10) in an actual core environment the following approach was used. One quarter of a PWR core, on a three batch refueling scheme, was modelled on PDQ-7. Each assembly was simulated using 36 mesh points.

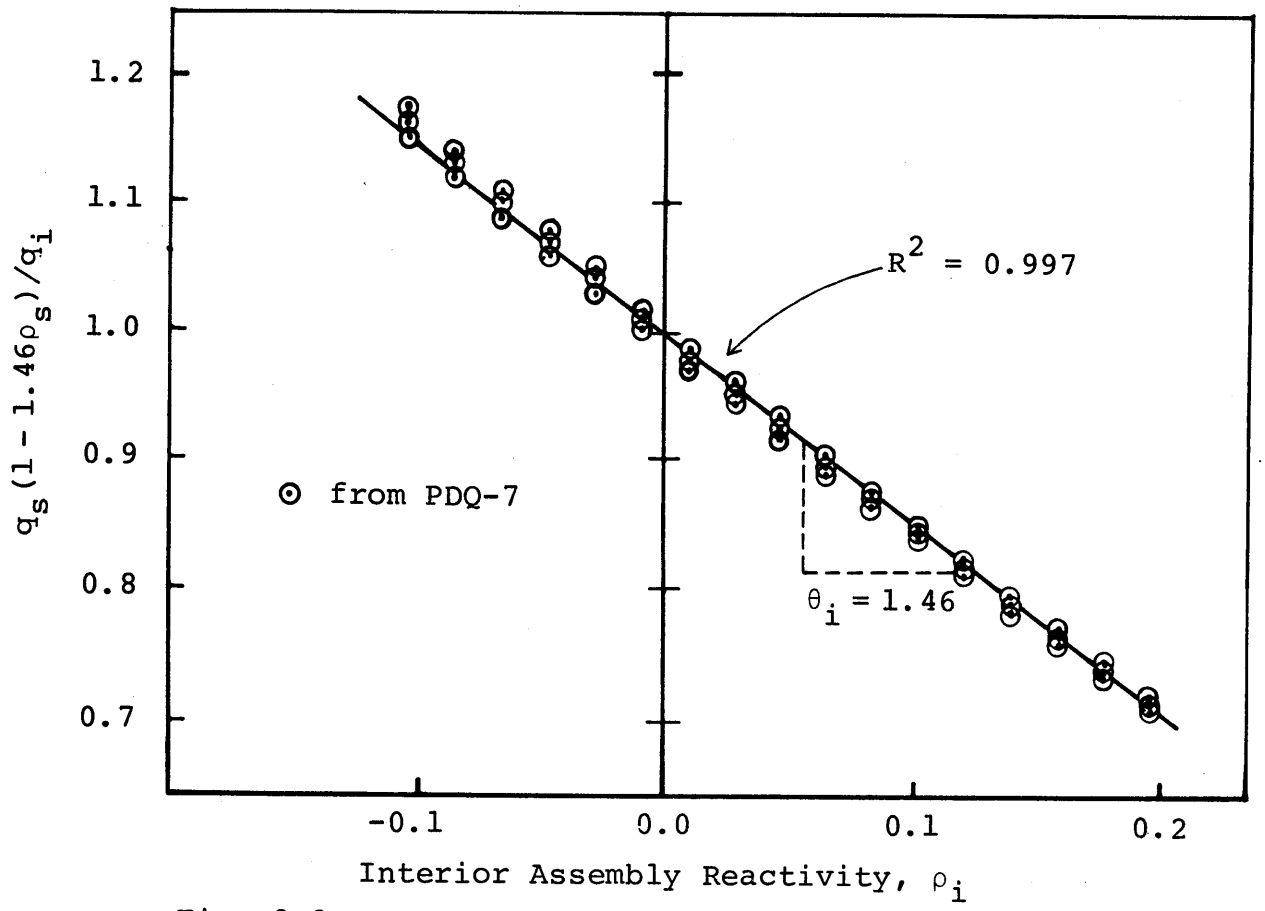

Fig. 3.2 Least-Squares Fit to Power Sharing Relation for 'Isolated' 3 x 3 Assembly Clusters

The cross-sections for each of the three batches were obtained from the same LEOPARD calculation cited in the previous section. Since it was of interest to examine the end-of-cycle (EOC) conditions, and a variety of fuel management strategies, the EOC burnups predicted by the equal power sharing approximation were used to assign the LEOPARD generated cross-sections to each batch. The core modelled on PDQ-7 is shown in Fig. 3.3.

A total of seven core-maps were generated, with an average k_{eff} of 1.02. The core-maps were used to analyze 3x3 assembly clusters, by applying the power sharing algorithm to 36 sets of clusters from the interior of the subject cores. The algorithm for assembly clusters in the core interior, Eq. 3.10, was tested against the PDQ-7 generated results for these 36 clusters. The interior assembly reactivity, ρ_i, the surrounding 8 assemblies' power-weighted reactivity, ρ_s, and the ratio of the power densities in the interior and surrounding regions, q_s/q_i, obtained from PDQ-7 are shown in Table 3.1.

A rearrangement and linearization of Eq. (3.10) yields

$$\frac{q_s}{q_i} = 1 - \theta_i\rho_i + \theta_s\rho_s \qquad (3.13)$$

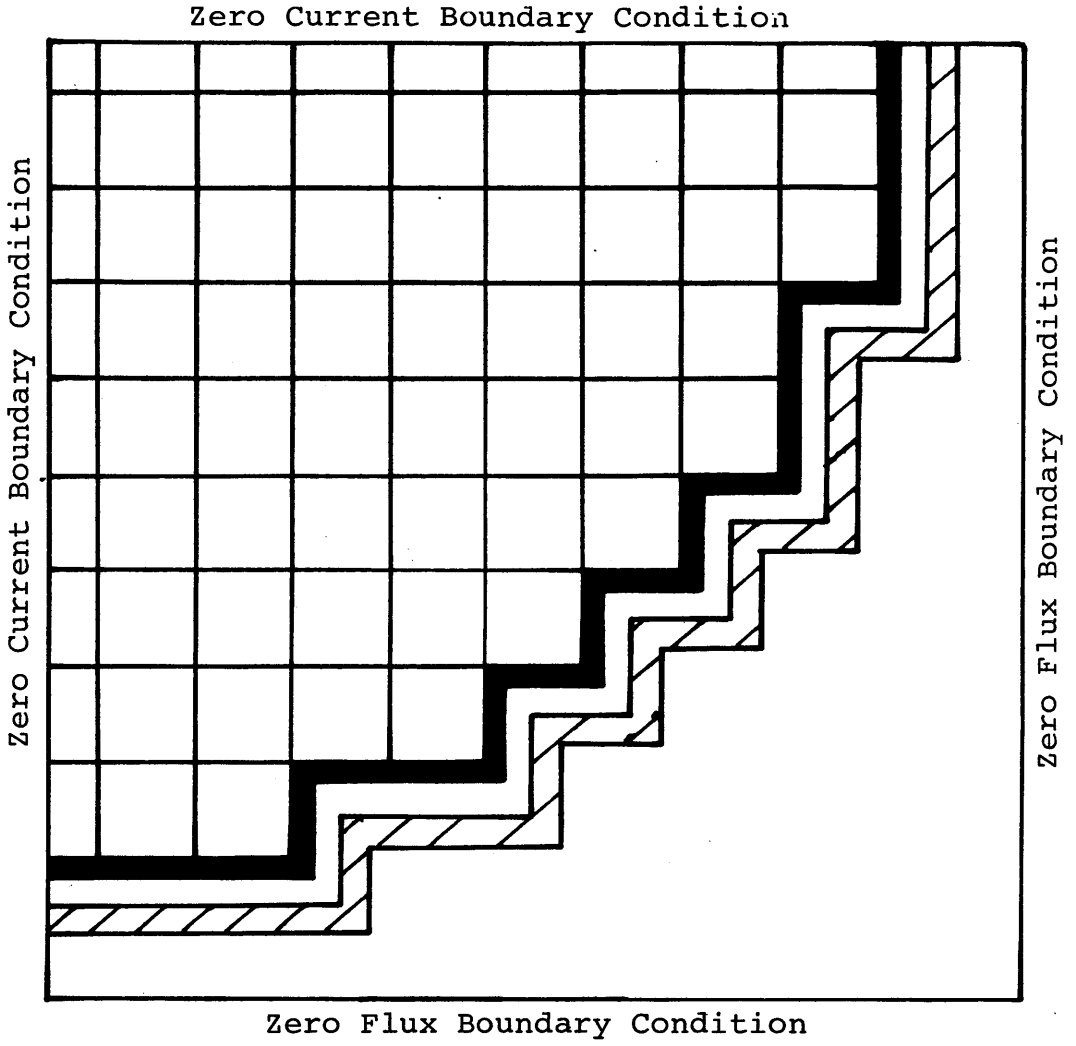

Fig. 3.3 PWR Core Configuration Modelled on PDQ-7

TABLE 3.1

Data on 3 x 3 Assembly Clusters from PDQ-7 Generated Core-Maps

	q_s/q_i	ρ_i	ρ_s		q_s/q_i	ρ_i	ρ_s
1.	0.9687	0.0428	0.0228	19.	0.7961	0.1327	0.0254
2.	1.0894	-0.0474	0.0240	20.	0.8113	0.1327	-0.0031
3.	1.1228	-0.0474	0.0202	21.	0.7855	0.1327	0.0146
4.	0.7805	0.1327	0.0131	22.	0.7769	0.1327	0.0026
5.	0.7602	0.1327	-0.0407	23.	0.9890	0.0428	-0.0214
6.	0.7830	0.1327	0.0138	24.	0.9357	0.0428	0.0006
7.	0.8124	0.1327	0.0267	25.	0.9239	0.0428	-0.0196
8.	0.8080	0.1327	0.0187	26.	0.9517	0.0428	-0.0081
9.	0.7817	0.1327	-0.0409	27.	0.9326	0.0428	0.0154
10.	0.9399	0.0428	0.0209	28.	0.9950	0.0428	0.0352
11.	1.0982	-0.0474	0.0393	29.	0.9399	0.0428	0.0209
12.	0.9728	0.0428	0.0249	30.	1.1228	-0.0474	0.0202
13.	0.9357	0.0428	0.0006	31.	1.1628	-0.0474	0.0237
14.	0.9846	0.0428	0.0057	32.	1.1505	-0.0474	0.0202
15.	1.1107	-0.0474	0.0291	33.	1.0673	-0.0474	0.0397
16.	1.1190	-0.0474	0.0257	34.	1.1190	-0.0474	0.0257
17.	0.8060	0.1327	0.0079	35.	1.1505	-0.0474	0.0279
18.	0.8037	0.1327	0.0277	36.	1.1453	-0.0474	0.0382

where only the first order terms in the binomial expansion of $1/(1-\theta_s\rho_s)$ have been retained.

A least-squares fit, using the data in Table 3.1 gave θ_i=1.78 and θ_s=0.21. The R^2 goodness-of-fit criterion was 0.98. The maximum difference between the predicted and actual (PDQ-7) values was 4%, with an average difference of under 2%. Without the linearization of Eq. (3.13) the results should be even more accurate.

Again the results from the PDQ-7 calculations are in acceptable agreement with those from group-one-and-a-half theory. The differences are more pronounced here than for the "isolated" bundles reported in the previous section. This was to be expected since the actual core environment is very much more heterogeneous and thus more difficult to model, and the criticality condition on the 3x3 clusters is not exactly satisfied. Furthermore, in any 3x3 cluster of assembly-sized nodes, the corner assemblies are neutronically less strongly coupled to the central assembly, than those sharing a common face with it. The present approach weights all 8 surrounding assemblies equally. Izenson has used the power sharing prescription with corner assemblies weighted less strongly than facing assemblies, in the SONUFA/B program (I-1). His results indicate that such a treatment further improves agree-

ment between the results from codes like PDQ-7 and those using the group-and-one-half model.

3.5 Power Sharing on a Batch-Wise Basis

In fuel management studies involving the assessment of different fuel designs, core loading patterns and operating strategies, it is of the utmost importance to predict how batches share power production at each point in the cycle. Indeed, this is one of the main reasons for expensive core depletion studies, using codes like PDQ-7. The instantaneous power sharing determines the instantaneous burnup of each batch, the cumulative power fractions determine where, and how, the end-of-cycle points are reached, and what burnup is accumulated by each batch.

The group-and-one-half model results embodied in Eq. (3.11) can be used to calculate batch-averaged power fractions. In this section the power split relation will be verified and its accuracy quantified against state-of-the-art calculations. For this purpose Eq. (3.11) will be benchmarked using published information on the Maine Yankee cycle 4 redesign and the Combustion Engineering System-80^{TM} cores.

Figures 3.4 and 3.5 show the core-maps for the two reactors, with each box representing an assembly. The power density (fraction of core average) and the reactivity, ρ, of each assembly are also included.

The inverse of the batch averaged power densities $(q/\bar{q})^{-1}$, as a function of the (power-weighted) average batch reactivities, for the two cores are shown in Figs. 3.6 and 3.7. For the Maine Yankee cycle 4 core the best fit is obtained with

$$\left[\frac{q_{batch}}{q_{average}}\right]^{-1} = \left[\frac{f_{batch}}{\bar{f}}\right]^{-1} = 0.98 - 1.42\,\bar{\rho}_{batch} \qquad (3.14)$$

The linear regression fit gave an R^2 of 0.988. Equation 3.14 can be rearranged to yield (with $0.98 \approx 1.00$):

$$f_{batch} \simeq \frac{\bar{f}}{1 - 1.42\,\rho_{batch}} \qquad (3.15)$$

which is in the form suggested by Eq. (3.11).

A similar analysis on the System-80^{TM} core yielded a θ value of 1.81, with an R^2 of 0.972. The theoretical estimate for θ, for both of these cores was 1.9.

ρ / $q/\bar{q}$							
					0.163 0.689	0.163 0.949	
			0.163 0.698	0.163 0.927	0.163 1.101	-0.100 0.952	0.118 1.324
		0.163 0.843	0.121 1.153	-0.071 0.891	-0.078 0.943	0.122 1.280	-0.070 1.062
	0.163 0.840	0.121 1.284	-0.068 0.987	0.081 1.148	0.003 0.986	-0.104 0.937	0.035 1.080
0.163 0.696	0.121 1.152	-0.068 0.991	0.070 1.200	0.016 1.040	-0.091 0.935	0.093 1.179	0.011 1.097
0.163 0.920	-0.071 0.833	0.082 1.150	0.016 1.045	-0.073 0.916	0.098 1.161	-0.096 0.896	0.070 1.152
0.163 1.087	-0.078 0.931	0.003 0.972	-0.091 0.929	0.099 1.161	-0.101 0.914	0.076 1.090	0.006 1.010
0.163 0.680	-0.100 0.936	0.123 1.251	-0.116 0.791	0.093 1.158	-0.096 0.889	0.076 1.090	-0.099 0.832	0.036 0.907
0.163 0.934	0.122 1.300	-0.070 1.039	0.035 1.049	0.011 1.078	0.070 1.041	0.006 1.005	0.035 0.905	-0.101 0.734

Fig. 3.4 Core-Map for the Maine Yankee Cycle 4 Redesign [S-4].

k $q/\bar{q}$								
						0.148 0.694	0.145 0.958	
				0.147 0.772	0.145 0.995	0.144 1.123	0.121 0.878	0.120 1.338
			0.145 0.923	0.119 1.278	-0.026 1.038	-0.110 0.856	0.111 1.295	0.111 0.966
		0.145 0.923	0.119 1.306	-0.046 1.064	0.120 1.280	-0.088 0.816	-0.105 0.839	0.122 1.267
	0.147 0.771	0.119 1.277	-0.046 1.063	-0.031 0.956	-0.110 0.819	-0.080 0.817	-0.014 0.923	-0.101 0.830
	0.145 0.994	-0.026 1.037	0.120 1.279	-0.110 0.819	0.039 1.071	0.107 1.133	0.024 1.067	0.012 1.043
	0.144 1.121	-0.110 0.854	-0.088 0.815	-0.080 0.816	0.052 1.132	0.038 1.120	-0.110 0.860	0.065 1.158
0.148 0.694	-0.111 0.875	0.121 1.292	-0.105 0.837	-0.012 0.922	0.024 1.063	-0.110 0.852	0.051 1.138	0.012 1.085
0.145 0.956	0.120 1.334	-0.111 0.963	0.122 1.264	-0.104 0.828	0.023 1.053	0.038 1.095	0.023 1.102	-0.116 0.877

Fig. 3.5 Core-Map for a Representative Combustion Engineering System-80™ Core [S-4].

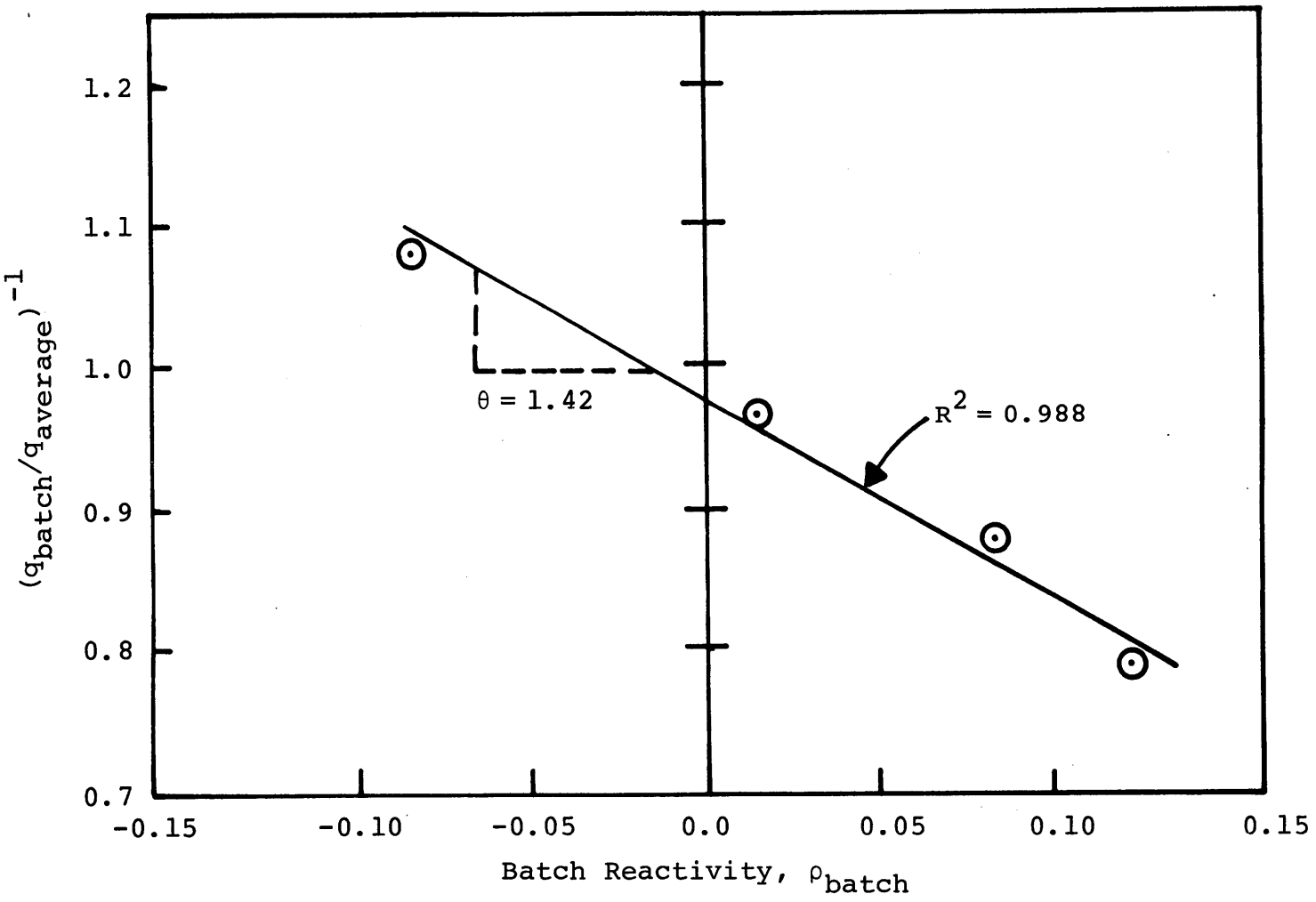

Fig. 3.6 Verification of the Batch Power Sharing Algorithm for the Maine Yankee Cycle 4 Redesign.

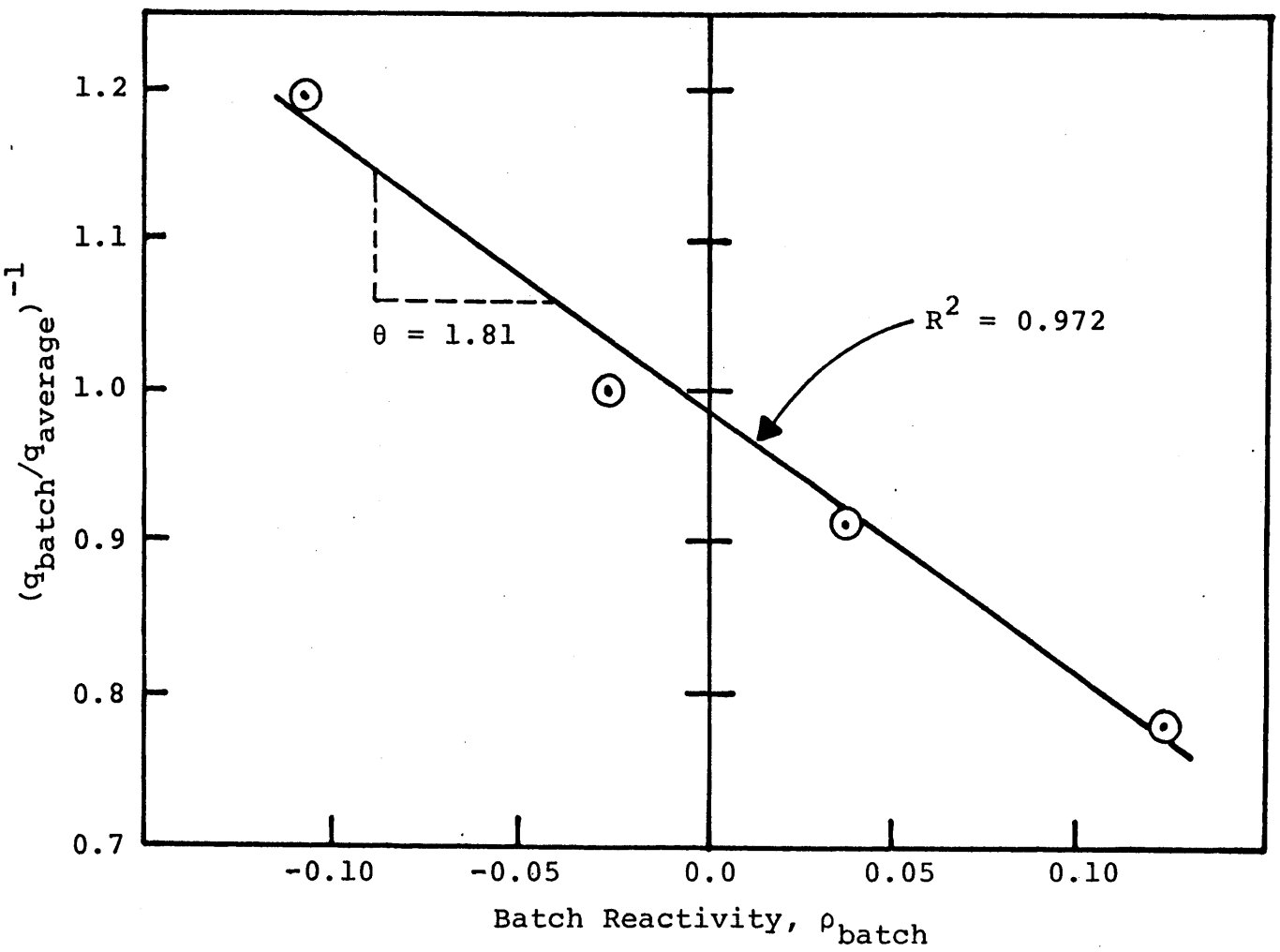

Fig. 3.7 Verification of the Batch Power Sharing Algorithm for the Combustion Engineering System-80™ Core.

The θ constant is design specific, as mentioned earlier, since it depends on the fuel-to-moderator ratio, the assembly size, and the materials in the core. Thus, strictly speaking, a particular θ value can only be used for a particular reactor design. Fortunately, as will be shown later, the final results are not very sensitive to small variations in theta, making this power sharing algorithm quite acceptable for use in studies of the present type.

3.6 Peripheral Assemblies, Radial Leakage and Poison Management

The algorithms presented thus far deal exclusively with assemblies in the core interior. In a typical PWR about 20% of the assemblies are on the core periphery. As such, at least a part of each batch spends one or more cycles on the edge of the core.

In this section the model will be extended to include peripheral assemblies and radial leakage. Both play important roles in many fuel management schemes of interest, e.g. the low-leakage schemes, and those with radial blankets of either fertile material (depleted uranium or thorium) or of spent fuel. The effects arising from the addition of soluble poison in the core will also be addressed.

The leakage of neutrons from the core periphery is dominated by fast neutrons. Therefore, the fast neutron production rate at the core periphery plays an important role in determining radial leakage. It has been shown that the leakage reactivity, ρ_L, defined by Eq. (2.14), is a linear function of the peripheral power, f_{per} (L-2,S-4). Hence for the incorporation of radial leakage we will verify the relation

$$\rho_L = \alpha f_{per} \tag{3.16}$$

where α is a "core leakage constant".

The PDQ-7 core-maps that were previously used to verify the power split relation in the core interior, will be employed here to assess the applicability of Eq. (3.16) to neutron leakage from the core periphery. The radial leakage reactivity, ρ_L, as a function of the peripheral power fraction, f_{per}, from these core-maps is shown in Fig. 3.8 and the data is documented in Appendix C. A linear fit to this data yields an excellent fit with

$$\rho_L = 0.0983\, f_{per} \tag{3.17}$$

The maximum difference between the PDQ-7 results and those from Eq. (3.17) is under 4%, and R^2 has a value of 0.984.

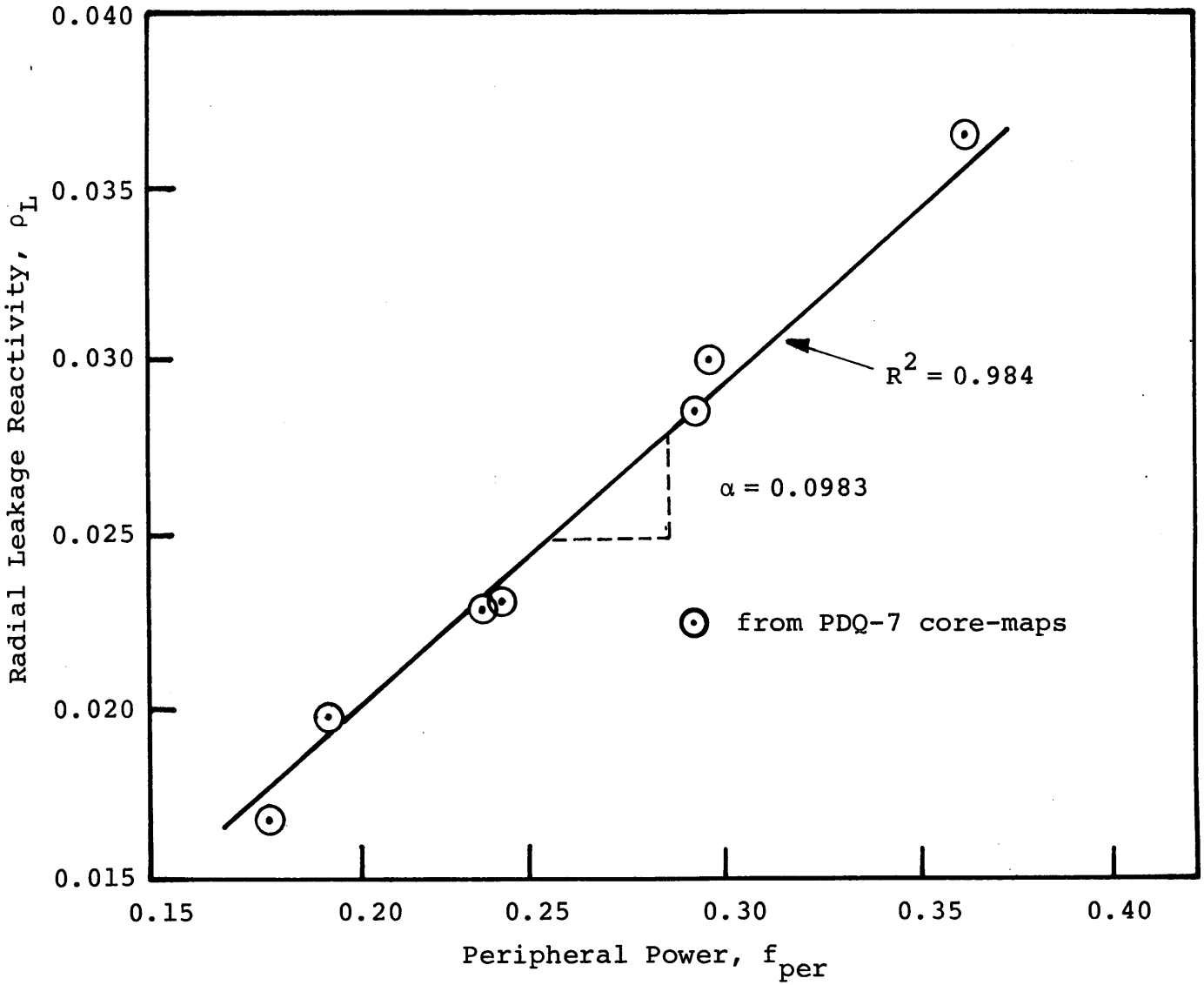

Fig. 3.8 Radial Reactivity as a Function of the Power Generated on the Core Periphery.

As with θ, the constant α is also reactor specific. It is a function of the physical size of the core, the material composition of the assemblies, the core and the shroud, the water gap beyond the shroud, etc. However, for a given reactor design the value of α does not vary with the particular fuel management scheme being employed, and an empirical value for α can be obtained from the analysis of core maps for that reactor.

Having established the applicability of Eq. (3.16) to model neutron leakage from the core periphery, it can now be incorporated in the power sharing algorithm. The peripheral power fraction f_{per}, can be written as a sum over the individual power fractions of the batches on the periphery, i.e.

$$f_{per} = \sum_{i=1}^{m} f_i \tag{3.18}$$

where 'm' is the number of batches on the core periphery. Substituting for f_{per} in Eq. (3.16) yields:

$$\rho_L = \alpha \sum_{i=1}^{m} f_i \tag{3.19}$$

At all points during the cycle the condition for criticality requires that the core reactivity, ρ_L, equal the leakage reactivity, ρ_{sys}. Combining the previously derived expression for ρ_{sys}, Eq. (2.13), with Eq. (3.19) yields

$$\sum_{i=1}^{n} f_i \rho_i = \alpha \sum_{i=1}^{m} f_i \tag{3.20}$$

where,

ρ_i = the batch averaged reactivity of the i^{th} batch in the n-batch core.

Rearranging Eq.(3.20) gives

$$\sum_{i=1}^{n-m} f_i \rho_i + \sum_{i=1}^{m} f_i \rho_i = \alpha \sum_{i=1}^{m} f_i \tag{3.21}$$

or

$$\sum_{i=1}^{n-m} f_i \rho_i + \sum_{i=1}^{m} f_i (\rho_i - \alpha) = 0 \tag{3.22}$$

In Eqs. (3.21) and (3.22) the summation in the first term (i=1,n-m) is over interior batches, while the second summation (i=1,m) is over peripheral batches. Equation (3.22) shows that

placing batches on the core periphery effectively results in a constant decrement in their unpoisoned reactivity. Qualitatively, the effect is identical to introducing a poison shim in the batches such that the shim reactivity penalty with respect to the batch is invariant with burnup. It should be recognized that the leakage (or shim) reactivity contribution to the core reactivity will, in general, be burnup dependent through Eq. (3.19), since the power fractions are a function of burnup.

During the cycle the excess core reactivity is controlled primarily through the introduction of poison uniformly distributed in the moderator. The derivation so far has assumed that the reactor is critical. To explicitly include poisoning, Eq. (3.22) can be written for a reactor with excess reactivity, ρ_x, in the form

$$\sum_{i=1}^{n-m} f_i \rho_i + \sum_{i=1}^{m} f_i (\rho_i - \alpha) = \rho_x \qquad (3.23)$$

and the normalization condition on the power fractions from Eq. (2.6) is

$$\sum_{i=1}^{n} f_i = 1.0$$

Hence Eq. (3.23) can be written as

$$\sum_{i=1}^{n-m} f_i \rho_i + \sum_{i=1}^{m} f_i (\rho_i - \alpha) = \sum_{i=1}^{n} f_i \rho_x \tag{3.24}$$

or

$$\sum_{i=1}^{n-m} f_i (\rho_i - \rho_x) + \sum_{i=1}^{m} f_i (\rho_i - \alpha - \rho_x) = 0 \tag{3.25}$$

The power fractions for each batch are now to be calculated using Eq. (3.15) with $\rho_{batch} = \rho_i - \alpha_i - \rho_x$, or

$$f_i = \frac{\bar{f}}{1 - \theta \rho_{batch}} = \frac{\bar{f}}{1 - \theta(\rho_i - \rho_x - \alpha_i)} \tag{3.26}$$

where,

ρ_i = the unpoisoned batch averaged reactivity.

α_i = 0, for interior batches, or
= α, the core leakage constant, for peripheral batches.

The determination of ρ_x is more problematic since it can only be known once the correct power fractions (i.e. those with the power flattening effect of the poison already

included in them) have been calculated. Thus the process of determining a consistent set of f_i's and ρ_x must be an iterative one, using Eqs. (3.25) and (3.26) in tandem to converge to the correct solution.

The addition of poison in this manner is equivalent to adding a one-group model poison uniformly in the core, since spectral effects (a spectrum-hardening in the case of boron) are not included. The error associated with this approach is small, since all end-of-cycle points are poison free and during the cycle the spectrum effects can be taken into account by using cycle-averaged poison concentrations in the supercell calculations. Furthermore, the effect of the poison on the batch power fractions is small in power-flattened cores.

3.7 The Algorithm for Split Batches: The SPILBAC Code

The general methodology presented so far will now be extended to applications where the reload batch is composed of two or more sub-batches of different fuel types. Such situations arise when fertile materials are included for use as radial or internal blankets, or in refueling schemes like that in the Soviet WWER, where two sub-batches with different enrichments are introduced into the core at each refueling.

Implicit in the derivations of the power split relations and reactivity averaging has been the use of only one type of fuel in a reload batch. The methodology presented in Chapter 2 was based on the linearity of the functional dependence between the reactivity, ρ, and the burnup, B. Both these constraints will now be relaxed and the general algorithm for split-batches will be derived. Finally the SPILBAC computer program will be described in which this methodology has been incorporated.

The core that will be considered has 'n' batches, with each batch split into two sub-batches such that a fraction M_A of the assemblies in the batch are of one fuel type, and a fraction M_B of the other fuel type. The methodology can be easily extended to any number of sub-batches.

As stated above

$$M_A + M_B = 1 \tag{3.27}$$

Writing Eq. (3.11) for the power fraction of sub-batch A in its i^{th} cycle yields:

$$f_{i,A} = \frac{M_A \bar{f}}{1 - \theta_A(\rho_{i,A} - \rho_x - \alpha_{i,A})} \tag{3.28}$$

where,

$f_{i,A}$ = the power fraction of sub-batch A, at a point in its i^{th} cycle.

θ_A = the theta constant for sub-batch A.

$\bar{f}$ = the power normalization coefficient.

$\rho_{i,A}$ = the unpoisoned reactivity of sub-batch A.

ρ_x = the excess core reactivity being supressed with soluble poison.

$\alpha_{i,A}$ = 0, if sub-batch A is in the core interior in its i^{th} cycle, or

= α, the core leakage constant, if sub-batch A is on the core periphery in its i^{th} cycle.

The power fraction of the batch (i.e. the two sub-batches taken together) is therefore:

$$f_i = f_{i,A} + f_{i,B} = \bar{f}\left[\frac{M_A}{1-\theta_A(\rho_{i,A}-\rho_x-\alpha_{i,A})} + \frac{M_B}{1-\theta_B(\rho_{i,B}-\rho_x-\alpha_{i,B})}\right] \qquad (3.29)$$

The system reactivity is always zero, so that using the expression given for ρ_{sys} in Eq. (3.25) in tandem with Eq. (3.29) a consistent set of $f_{i,A}$ and $f_{i,B}$ and ρ_x can be computed at each point in the cycle.

In order to do this, the reactivity as a function of burnup must also be known. If this functional dependence is simple (as is often the case) analytical solutions can be easily derived. If the $\rho(B)$ curve is analytically cumbersome, interpolation techniques may be employed to calculate the reactivity, given the burnup.

In order to start the process, beginning-of-cycle points for each sub-batch must be known. This, in effect, means knowing the burnups at the end of the previous cycle. In practice none of the end-of-cycle points are known a priori. Indeed, that is the problem to be solved ! Therefore a second set of iterations must be performed to converge to the correct end-of-cycle points for all the sub-batches (which are also the beginning of cycle points of the subsequent cycle). The beginning-of-life (BOC 1) points are always known, since the fuel has not incurred any burnup.

This, then, is the general methodology that is employed to analyze cores in a steady state. Start-up cores can be handled similarly; in fact they are simpler in many respects but have not be addressed here because, being transitional in nature, they lie beyond the scope of this work. For the same reason "change-over" cycles (e.g. from a three batch to a five batch refueling scheme) have not been examined.

The methodology for sub-batches described above has been incorporated into a computer code - SPILBAC. The basic structure of the program is similar to the ALARM code of Sefcik (S-4) and the DISBURN code of Loh (L-2).

The input to the SPILBAC code consists of the number of batches in the core, the reactivity as a function of burnup for each of the two sub-batches within the reload batch, the fraction of each sub-batch in the reload batch, the theta constants for each sub-batch, the core leakage constant (α), a specification of which sub-batches are on the core periphery, and over which cycles. The user also specifies the burnup step size (after which the sub-batch power fractions are to be recalculated and the core power renormalized), as well as the convergence criterion applied to the sub-batch cycle and discharge burnups.

Figure 3.9 shows the flow chart of the SPILBAC code. A brief description of the code and the order of calculation follows:

1. Using the reactivity as a function of burnup, $\rho(B)$, input data and the equal power sharing approximation (Eq. 2.18), the initial guess for the BOC points of the two sub-batches, $B_{BOC,i,A}$ and $B_{BOC,i,B}$, are calculated.

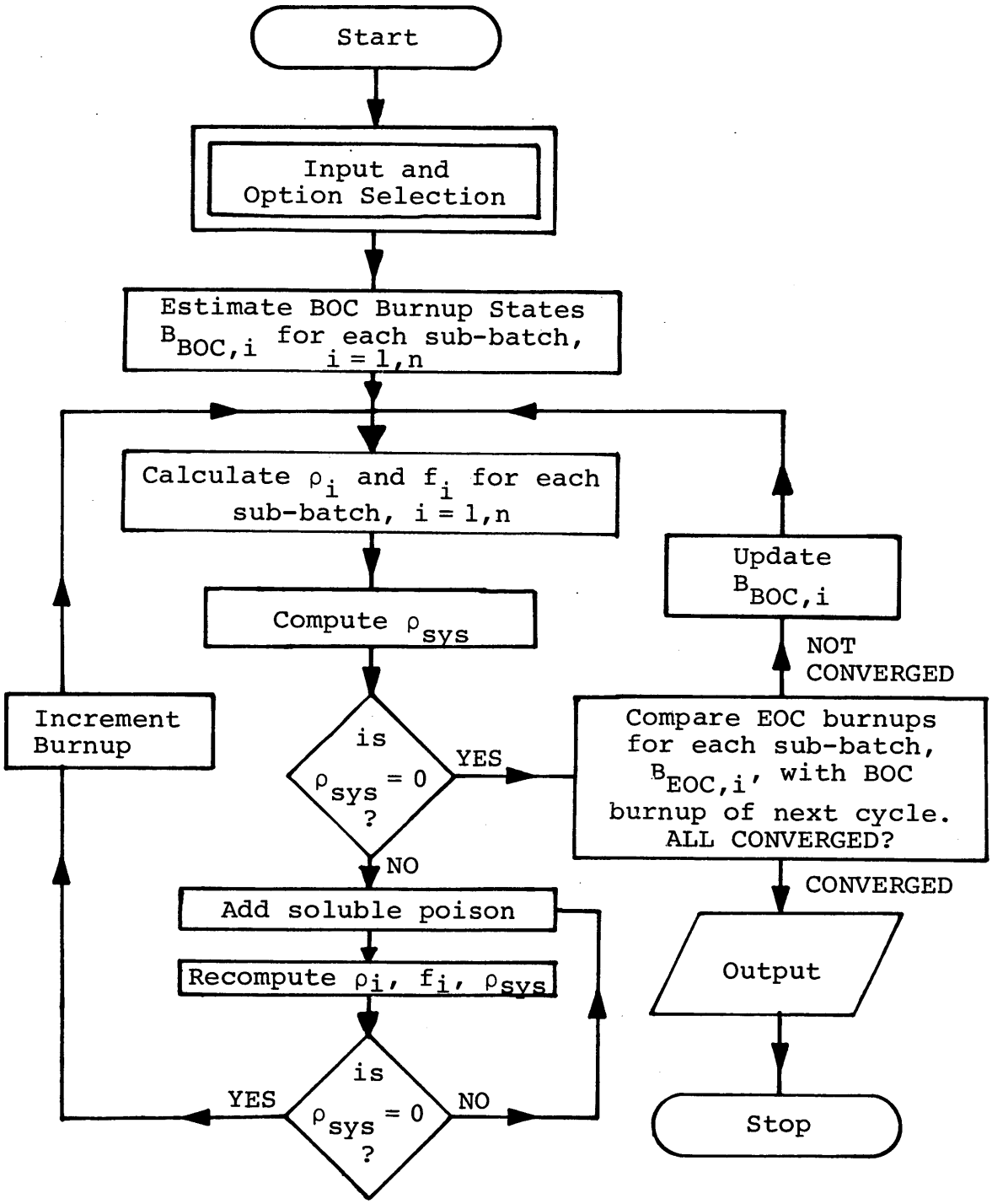

Fig. 3.9 A Flow chart for the SPILBAC Code.

2. At these burnup points the reactivity, ρ, of each sub-batch is calculated from the $\rho(B)$ data. The sub-batch power fractions, f_i's, are then calculated using the power split relation, without poison being added. If the system reactivity, ρ_{sys}, is positive, poison is added and the f_i's and ρ_{sys} recalculated until criticality is reached. If the ρ_{sys} is zero, without the addition of any poison, then the EOC point has been reached.

3. If the EOC point has not been reached, the poisoned (critical) core is depleted, over a small burnup step. The burnup increment for each sub-batch is the product of the $f_i/\overline{f}$ and the core burnup step. It is assumed that the power fractions do not change, and that the power normalization is valid over this depletion step. The depletion step, being an input variable, can be chosen to be small enough so that these conditions are almost exactly satisfied. The f_i's and ρ_{sys} are recalculated, and if the EOC point has not been reached, poison is again added until the converged set of f_i's and ρ_{sys} are obtained. This depletion and normalization process is repeated till the EOC point is reached.

4. The EOC point for cycle i is compared to the the BOC point for cycle i+1 for each sub-batch. If all of them in turn, satisfy the convergence criterion, the solution has

converged. If the absolute difference ($B_{EOC,i} - B_{BOC,i+1}$) is greater than the convergence criterion for any cycle and either sub-batch, then ($B_{EOC,i} + B_{BOC,i+1}$)/2 is used as the guess for the BOC burnups for the next iteration.

5. The inner iterations before each depletion step (for obtaining a consistent set of f_i's and ρ_x), and the outer iterations (for predicting and correcting the BOC burnups), are repeated till global convergence is obtained. This process is unconditionally convergent and requires about 10 outer iterations if the burnup convergence criterion is 200 MWD/MT for a five batch core with two sub-batches in each batch.

The output from the code includes the sub-batch BOC, EOC and cycle-averaged power fractions, and the cumulative EOC burnups. The discharge burnups of the two sub-batches are the key parameters used in the evaluation of uranium utilization.

The flexibility of the SPILBAC code allows the modelling of many different fuel management strategies. For example one of the sub-batches can be enriched uranium and the other thorium or depleted uranium (as a radial or internal blanket). The WWER concept mentioned earlier can also be modelled.

Appendix D provides further information on the SPILBAC code. A listing of the program, input data specification and instructions, a sample problem, and a sensitivity study on the input parameters are included. The application of the code to assess a variety of strategies is reported in the following chapters.

3.8 Chapter Summary

This chapter addressed the calculation of power sharing among assemblies, on individual and batch-averaged bases in a PWR core. Power sharing prescriptions were derived using the "group-and-one-half" model for isolated assembly clusters, for assembly clusters in the core interior and for groups of assemblies constituting a batch. The theoretically predicted results were verified using state-of-the-art PDQ-7 calculations, and published results for the Combustion Engineering System-80^{TM} and the Maine Yankee reactors. The agreement was found to be quite satisfactory for present purposes.

Neutron leakage from the core was successfully modelled in terms of the power produced at the core periphery. This prescription was also verified using the PDQ-7 code.

The algorithm was extended to accomodate sub-batches within each reload batch. Finally, the complete model was incorporated into a computer program, named SPILBAC, designed to assess various fuel management strategies of interest to the present work.

CHAPTER 4

THE USE OF THORIUM IN A RETROFITTABLE MODE

4.1 Introduction

The algorithms developed in the preceding chapters can be applied to a wide variety of fuel management schemes. The first set of applications involving the use of thorium in PWRs on the once-through cycle in a retrofittable mode will be presented here. The strategies considered are: thorium assemblies as radial and internal blankets, and thorium pins within low-enrichment uranium assemblies. Options involving thorium which require extensive redesign of existing PWR cores will be deferred until the next chapter.

The rationale for examining these roles for thorium arises from many different considerations. Foremost among them is the potential benefit of productively utilizing the excess reactivity in a PWR during the burnup cycle. While excess reactivity is not particular to PWRs, being a phenomenon associated with all reactors having a discrete (rather than a continuous) refueling scheme, the large excess of neutrons in PWRs leaves substantial room for improvement. The current practice of

using soluble boron to control excess reactivity not only wastes neutrons, but introduces the additional complication of reducing the moderator temperature coefficient. The only advantage of using boron, from a neutronic point of view, is the hardening of the neutron spectrum, which leads to some extra breeding of fissile isotopes during the cycle. Furthermore, the soluble poison acts globally, rather than locally, a feature which makes it less attractive for some of the newer fuel management schemes being employed (e.g. low leakage reload configurations).

These considerations have led to investigation of other reactivity control options - burnable poisons in particular. However, these schemes produce the same wasteful neutron economy as the soluble poisons.

The selective use of thorium in PWRs offers, in principle, advantages both as a reactivity control option and as a uranium saver. During the intial period of its residence in the core it can be used to control the neutron population in the core through fertile absorptions, breeding fissile uranium-233 to provide energy and neutrons later in the cycle. The major question regarding the introduction of thorium is whether these features can compensate for the uranium it is displacing.

Simply stated, this problem is addressed here. A variety of thorium lattices are examined, with different fuel-to-moderator ratios and fuel pin radii, to identify the more promising among them. To aid in this analysis, a simple model is developed to perform the screening for subsequent detailed analysis using the SPILBAC code. The evaluations are performed for both current and high-burnup PWR cores.

4.2 Thorium Lattices Investigated

A total of 12 thorium oxide lattices were investigated, encompassing different fuel-to-moderator ratios and fuel pin diameters. The cell calculations were performed using LEOPARD.

Table 4.1 shows the important dimensions of the lattices. The fuel-to-moderator volume ratios (V_F/V_M) considered were: 1.0, 0.6, and 0.2. The first is a dry lattice, the second is representative of current PWR fuel designs, and the third is a wet lattice. Even drier lattices of thorium were not considered since it is problematic that they could satisfy thermal constraints. All V_F/V_M values refer to the pincell volume ratios (rather than the assembly ratios, which will be lower).

The four fuel pellet diameters considered were: 0.025 cm. (simulating a hypothetical homogeneous assembly), 0.5 cm., 1.0

Table 4.1

The Thorium Lattices Investigated

Thorium Fuel-Pin Diameters	Fuel-to-Moderator Volume Ratio (Pincell)		
	Dry Lattice $V_F/V_M = 1$	Standard Lattice $V_F/V_M = 0.60$	Wet Lattice $V_F/V_M = 0.2$
0.025 cm ('homogeneous')	d-h*	s-h	w-h
0.50 cm ('thin')	d-t	s-t	w-t
1.00 cm ('standard')	d-s	s-s	w-s
2.00 cm ('fat')	d-f	s-f	w-f

*These two-letter designators are used to identify the lattice. See text for details.

cm., and 2.0 cm.. For comparison, note that current PWR fuel pellets have diameters of about 1.0 cm.. All combinations of the above mentioned V_F/V_M and fuel pellet diameters were investigated.

To aid in the identification of these lattices a two index reference system is used in the present work. The first of the two indices refers to the fuel-to-moderator ratio, and the second to the fuel pin diameter, as follows;

-For the fuel-to-moderator volume ratios:

d = 'dry', (V_F/V_M = 1.0)
s = 'standard', (V_F/V_M = 0.6), current PWR design
w = 'wet', (V_F/V_M = 0.2)

-For the fuel pellet diameters:

h = 'homogeneous', (pellet diameter = 0.025 cm.)
t = 'thin', (pellet diameter = 0.50 cm.)
s = 'standard', (pellet diameter= 1.00 cm.)
f = 'fat', (pellet diameter = 2.00 cm.)

Hence, "lattice d-s" refers to the lattice with a fuel-to-moderator ratio of 1.0, and a fuel pin diameter of 1.0 cm.. Similarly, "lattice w-f" refers to the lattice with a V_F/V_M of 0.2 and a pellet diameter of 2.00 cm.. For easy reference, these lattice labels are mapped out in Table 4.1.

4.2.1 Modelling Thorium in LEOPARD

The suitability of the LEOPARD code for thorium fuels has been discussed in Chapter 2. The particular parameters used to model thorium lattices will be described here.

In LEOPARD the absorption cross-section of the lumped fission products can be adjusted for different fuel types by varying the 'fission product scale factor', an input variable, to match experimental data or the results of more sophisticated calculations. Following Correa's lead, the value of 0.84 was used for U-233 fission products (C-4).

The 'non-lattice peaking factor' is used by LEOPARD to simulate thermal flux peaking in the water holes and other non-lattice regions in the assembly. This factor is obtained iteratively by performing LEOPARD and PDQ-7 calculations in tandem, while adjusting this factor until the k_{eff} values from the two codes match. The converged value for a typical PWR

lattice is 1.16. In the present work this value was also used for the thorium lattices. Since the non-lattice fraction of an assembly is only 10 % of the assembly volume, the choice of the non-lattice peaking factor has a negligible effect on the reactivity of the bundle.

For all thorium lattices Zy-4 was used as the clad material. The fuel, 'resonance', clad, and moderator temperatures were the same as those in the reference PWR (see Appendix A).

4.2.2 Characteristics of Thorium Lattices

In this section the results from the LEOPARD analyses of the 12 thorium lattices will be presented. The main quantities of interest are the reactivity as a function of burnup, and the peak reactivity reached by the thorium insert. The latter is important because it can be used to screen the lattices and select those worthy of more detailed analysis.

Figure 4.1 shows the variation of reactivity as a function of burnup for thorium lattices d-s, s-s, and w-s. The figure illustrates the variation in $\rho(B)$ when the fuel-to-moderator ratio is varied for a fixed fuel pin diameter. Other thorium lattices have the same general characteristics. The reactivity

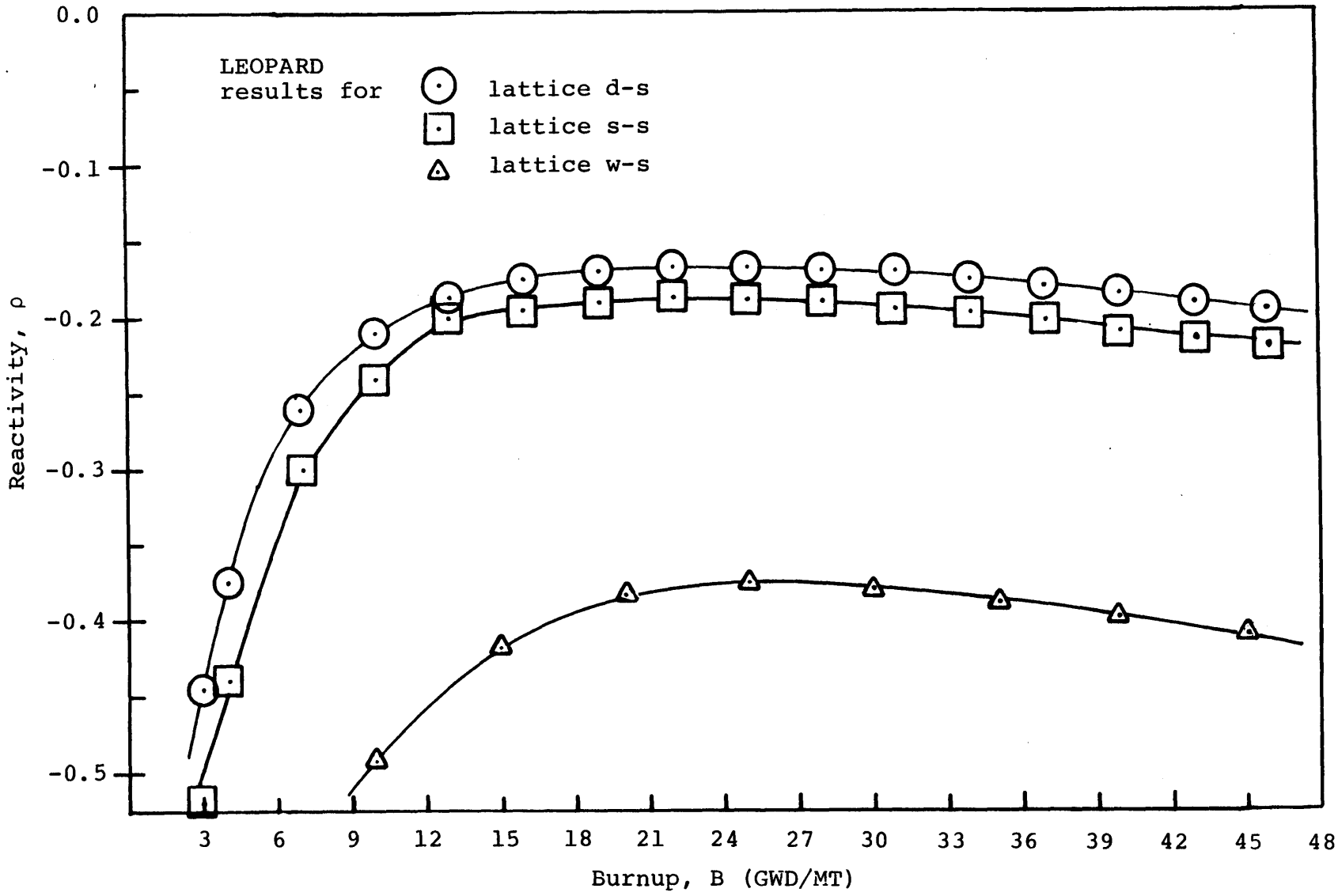

Fig. 4.1 The Variation of Reactivity as a Function of Burnup for Three Thorium Lattices.

as a function of burnup data for all 12 lattices is included in Appendix B. In all cases the peak reactivity is reached before a fuel burnup of 25 GWD/MT. A very desirable feature of thorium lattices is the relatively flat reactivity profile once the initial buildup has occurred.

Table 4.2 lists the peak reactivity, the peak U-233 enrichment and the burnup at which the peak reactivity is reached, for each of the 12 thorium lattices. The peak reactivity can be used as an initial indicator of the potential usefulness of a particular thorium lattice. The peak enrichment is useful in evaluating options such as reconstitution.

As shown in Table 4.2 the highest reactivity is reached by "dry" thorium lattices: i.e. d-f, d-s, d-t and d-h. The highest U-233 buildup is in the "homogeneous" lattices (d-h, s-h and w-h), due to their reduced self-shielding.

4.3 A Simple Model for Thorium Evaluation

4.3.1 Derivation of the Model

A simple model was developed to provide a preliminary screening mechanism for the thorium lattices being investi-

TABLE 4.2

Important Characteristics of Thorium Lattices Analyzed Using LEOPARD

Thorium Fuel Pin Diameters, D_f	Fuel-to-Moderator Volume Ratio		
	$V_F/V_M = 1.0$	$V_F/V_M = 0.60$	$V_F/V_M = 0.20$
$D_f = 0.025$ cm			
Lattice[a]	d-h	s-h	w-h
$\hat{\rho}$[b]	-0.1653	-0.1715	-0.3044
$\hat{X}$[c]	2.07	1.81	1.53
$B_{\hat{\rho}}$[d]	25.0	25.0	30.0
$D_f = 0.5$ cm			
Lattice	d-t	s-t	w-t
$\hat{\rho}$	-0.1567	-0.1702	-0.3292
$\hat{X}$	1.69	1.53	1.33
$B_{\hat{\rho}}$	25.0	25.0	25.0
$D_f = 1.0$ cm			
Lattice	d-s	s-s	w-s
$\hat{\rho}$	-0.1676	-0.1874	-0.3761
$\hat{X}$	1.65	1.45	1.28
$B_{\hat{\rho}}$	20.0	20.0	25.0
$D_f = 2.0$ cm			
Lattice	d-f	s-f	w-f
$\hat{\rho}$	-0.1607	-0.1814	-0.4509
$\hat{X}$	1.46	1.34	1.23
$B_{\hat{\rho}}$	15.0	15.0	25.0

[a]The two-letter index for identifying lattices adopted in Section 4.2—see Table 4.1.

[b]Peak reactivity, $\rho = 1 - 1/k_\infty$.

[c]Peak U-233 enrichment (at. %).

[d]Burnup at which peak reactivity occurs, GWD/MT.

gated, such that detailed analyses could be concentrated on the more promising variations. Here this model will be developed and applied.

The basic (unadjusted) index for uranium utilization, I_0, comparing the uranium utilization of a test case to a reference case, is defined as the ratio:

$$I_0 = \frac{U}{U_R} = \frac{B_R}{(M_U B_U + M_{Th} B_{Th})/M_U} \tag{4.1}$$

where,

U, U_R = the uranium usage (STU_3O_8/MWD) for the test and the reference cores respectively. It is assumed that the two have the same uranium enrichment.

M_U, M_{Th} = the fraction of uranium and thorium (as sub-batches) in the test core. Note that $M_U + M_{Th} = 1.0$.

B_R = the average discharge burnup of the reference (all-uranium) core, GWD/MT.

B_U, B_{Th} = the uranium and thorium average discharge burnups in the test core, GWD/MT.

If I_0 is 0.98, for example, this indicates a uranium saving in the test core over the reference core of 2 percent; Conversely, an I_0 value of 1.03 indicates a 3 percent loss in uranium utilization. As shown in Appendix E, the unadjusted

index can be adjusted to give the uranium saving (or loss) for cases when the test and the reference cores are required to have the same U-235 loadings (and therefore natural uranium requirements) or when comparisons need to be made under conditions of equal effective full power hours delivered by the test and the reference cores.

In order to determine the discharge burnups of the uranium and thorium sub-batches in the simple model an end-of-cycle reactivity balance is performed. This treatment closely follows the treatment developed in Chapter 2. Since all thorium lattices with uranium saving potential need to be identified, two thorium-favoring assumptions are made. The first is that at all points during the cycle the thorium sub-batches contribute their peak reactivity to the core. The second is that within each sub-batch there is equal power sharing during all cycles of its residence in the core. For the thorium sub-batch the initial reactivity and burnup penalties that it would actually incur are disregarded in this model. As before, the uranium sub-batch reactivity is a linear function of burnup.

With these characteristics the test core end-of-cycle (EOC) reactivity is the power-weighted sum of the following expressions for the individual sub-batch reactivities:

$$\left.\begin{aligned} \rho_{U,1} &= \rho_0 - AB_C \\ \rho_{U,2} &= \rho_0 - 2AB_C \\ &\vdots \\ \rho_{U,n} &= \rho_0 - nAB_C \end{aligned}\right\}$$ For the uranium sub-batches. (Assumes equal power sharing among uranium sub-batches.) (4.2) (4.3)

$$\left.\begin{aligned} \rho_{Th,1} &= \hat{\rho}_{Th} \\ \rho_{Th,2} &= \hat{\rho}_{Th} \\ &\vdots \\ \rho_{Th,n} &= \hat{\rho}_{Th} \end{aligned}\right\}$$ For the thorium sub-batches. (Assumes peak thorium reactivity at all EOC points.) (4.4)

where,

$\rho_{U,i}, \rho_{Th,i}$ = the EOC reactivity of the uranium or thorium sub-batch in its i^{th} cycle (i = 1,n).

B_C = the average cycle burnup of the uranium sub-batch.

$\hat{\rho}_{Th}$ = the peak thorium reactivity (assumed to occur at all EOC points).

The power-weighted sum of the above sub-batch reactivities yields after some algebra

$$\rho_{sys} = 0 = \frac{q_U M_U}{n}\left\{n\rho_0 - \frac{n(n+1)}{2}AB_C\right\} + q_{Th}M_{Th}\hat{\rho}_{Th} \tag{4.5}$$

where,

ρ_{sys} = the system (test core) reactivity at EOC,

q_U, q_{Th} = the uranium and thorium sub-batch power densities (fraction of core-average), at EOC.

Rearranging Eq. (4.5) to solve for the uranium sub-batch cycle burnup, B_C, gives

$$B_U = nB_C = \left(\frac{2n}{n+1} \cdot \frac{\rho_0}{A} \right) \left(1 + \frac{q_{Th} M_{Th} \hat{\rho}_{Th}}{q_U M_U \rho_0} \right) \tag{4.6}$$

where,

B_U = the uranium sub-batch discharge burnup in the test core.

For the reference (all-uranium) core, with the same uranium fuel enrichment as in the test case, the discharge burnup, B_R, is given by Eq. (2.18) in Chapter 2 as

$$B_R = \frac{2n}{n+1} \cdot \frac{\rho_0}{A} \tag{4.7}$$

where the leakage reactivity is assumed to be zero. Substituting for ρ_0/A in Eq. (4.6) yields

$$B_U = B_R \left(1 + \frac{q_{Th} M_{Th} \hat{\rho}_{Th}}{q_U M_U \rho_0} \right) \tag{4.8}$$

Equation (3.10) of Chapter 3 can be used to calculate the ratio of the power densities of the thorium and uranium sub-batches under the assumption that they are immersed in critical surroundings. For the thorium sub-batches

$$q_{Th} = \frac{\bar{q}}{1 - \theta_{Th}\rho_{Th}} \tag{4.9}$$

and for the uranium sub-batches

$$q_{U} = \frac{\bar{q}}{1 - \theta_{U}\rho_{U}} \tag{4.10}$$

Dividing Eq. (4.9) by Eq. (4.10) yields

$$\frac{q_{Th}}{q_{U}} = \frac{1 - \theta_{U}\rho_{U}}{1 - \theta_{Th}\rho_{Th}} \tag{4.11}$$

If it is assumed that the EOC power-weighted reactivity of the uranium sub-batches is zero, while for thorium it is the (previously assumed) peak reactivity, $\hat{\rho}_{Th}$, Eq. (4.11) gives

$$\frac{q_{Th}}{q_{U}} \approx 1 + \theta_{Th}\hat{\rho}_{Th} \tag{4.12}$$

where only the first order term of the expansion has been retained.

To calculate the cycle-averaged power fractions, Eq. (4.11) can be used with cycle-averaged values for ρ_{U} and ρ_{Th}. In an

n-batch core neglecting the effect of soluble poison, the cycle averaged ρ_U is

$$\rho_U \approx \frac{\rho_0}{n+1} \tag{4.13}$$

With thorium contributing its peak reactivity at all points during the cycle, the cycle-averaged power split is given by the relation

$$\left(\frac{q_{Th}}{q_U}\right)_{CA} = \frac{1 - \frac{\theta_U \rho_0}{n+1}}{1 - \theta_{Th}\hat{\rho}_{Th}} \tag{4.14}$$

Since all uranium sub-batches are assumed to share power equally (among themselves) and the same is assumed true for the thorium sub-batches, the ratio of the cycle-averaged power split in Eq. (4.14) is also the ratio of their discharge burnups. i.e.

$$\frac{B_{Th}}{B_U} = \left(\frac{q_{Th}}{q_U}\right)_{CA} = 1 - \frac{\theta_U \rho_0}{n+1} + \theta_{Th}\hat{\rho}_{Th} \tag{4.15}$$

Again only the first order term in the binomial expansion of $(1+\theta_{Th}\hat{\rho}_{Th})^{-1}$ has been retained. Combining Eqs. (4.1), (4.8), (4.12) and (4.15) yields, after some algebra:

$$I_0 = \left\{ \left[1 + \frac{M_{Th}\hat{\rho}_{Th}}{M_U\rho_0} (1 + \theta_{Th}\hat{\rho}_{Th}) \right] \cdot \left[1 + \frac{M_{Th}}{M_U} (1 - \frac{\theta_U\rho_0}{n+1} + \theta_{Th}\hat{\rho}_{Th}) \right] \right\}^{-1} \quad (4.16)$$

Equation (4.16) can be used for the preliminary assessment of thorium-containing PWR cores. As mentioned previously, it has been derived under thorium favoring assumptions to permit its use for identifying potentially advantageous thorium lattices for detailed analysis using the SPILBAC code.

4.4 Thorium Evaluation Using the Simple Model

The simple model derived above will now be applied to PWRs on the once-through cycle, for both current and high burnup cores. In both cases infinite reactors will be considered. Both assembly-sized thorium internal blankets and thorium pins dispersed within uranium fuel assemblies will be evaluated.

Equation (4.16) can be used to calculate the uranium utilization as a function of thorium in the test core. From the definition of the unadjusted uranium utilization index in Eq. (4.1), a value of I_0 of less than unity indicates an improve-

ment in uranium utilization (uranium saving) relative to the reference core. The key parameters used in Eq. (4.16) are shown in Table 4.3.

In evaluating thorium pins in uranium assemblies, in a fertile poison mode, a value of θ_{Th} equal to zero was used. This is the equal power sharing approximation, and assumes that the thorium pins produce as much power, and incur as much burnup, as the core average. Clearly, given the low reactivities attained by the thorium lattices, this approximation is again generous to thorium.

Calculations were done using Eq. (4.16) with the data listed in Tables 4.2 and 4.3, for thorium assembly fractions in the core of between zero and 40%, in increments of 2%. The results are reported below.

4.4.1 Assembly-Sized Thorium Inserts in Current PWR Cores

For current PWR cores on a 3-batch annual refueling scheme (with a discharge burnup of 36 GWD/MT in the reference core), the maximum improvement in uranium utilization was 1.3%, using the unadjusted uranium utilization index, I_0. This was for lattice d-t, at 16% thorium in the core. Lattice d-f was the

TABLE 4.3

Parameters Used in the Simple Model for Thorium Evaluations

	Current PWR Core		High Burnup PWR	
	Thorium as Assemblies	Thorium as Pincells	Thorium as Assemblies	Thorium as Pincells
ρ_0	0.220	0.220	0.266	0.266
n	3	3	5	5
θ_U	1.5	1.5	1.5	1.5
θ_{Th}	1.5	0.0[a]	1.5	0.0
Lattices Examined[b]	All	s-s[c]	All	s-s

[a]Equal power sharing approximation.

[b]Data for $\hat{\rho}_{Th}$ from Table 4.2.

[c]See Table 4.1 and accompanying text for an explanation of the lattice reference index.

next best lattice, with a maximum of 1.1% improvement in uranium utilization at 14% thorium in the core. The remaining lattices showed either negative or negligible (< 1.0%) savings in uranium utilization.

Figure 4.2 shows the variation of the unadjusted uranium index, I_0, as a function of the amount of thorium in the core for the best thorium lattice, namely lattice d-t. Lattice s-s which has the dimensions of current PWR lattices is also included for comparison. Figure 4.3 shows the same results for thorium lattice d-f.

Considering the thorium-favoring nature of the model under which these results were obtained, the prospects for thorium as a uranium saver in current burnup PWRs do not look very good.

4.4.2 Assembly-Sized Thorium Inserts in High Burnup Cores

With a high burnup PWR on a five batch refueling scheme and a discharge burnup of 60 GWD/MT as the reference core, the maximum improvement in uranium utilization achieved by including thorium in the core was 4.6%. This was, as above, for lattice d-t; in this case at 28% thorium in the core.

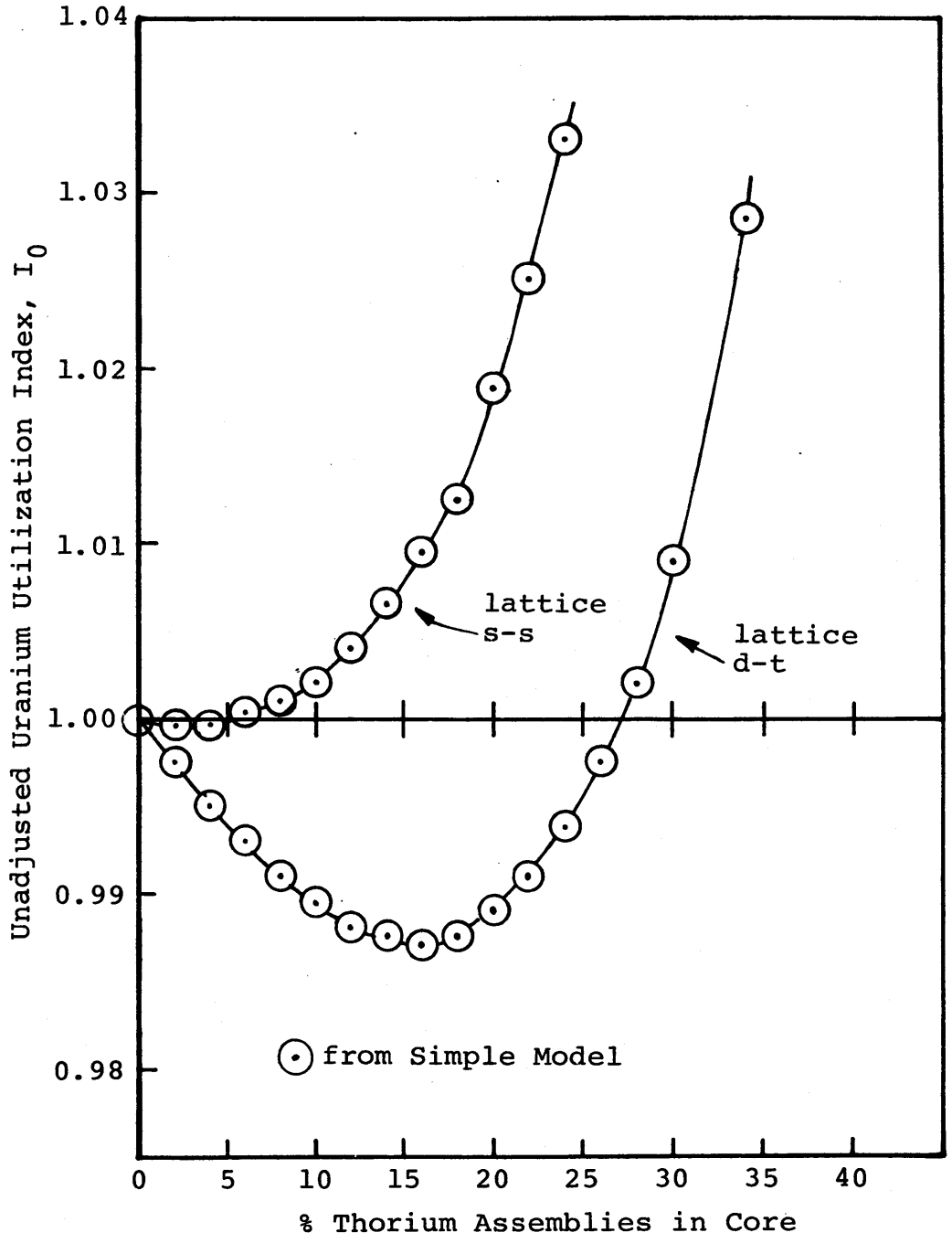

Fig. 4.2 Uranium Utilization Results for Thorium d-t and s-s Assemblies in Current PWR Cores.

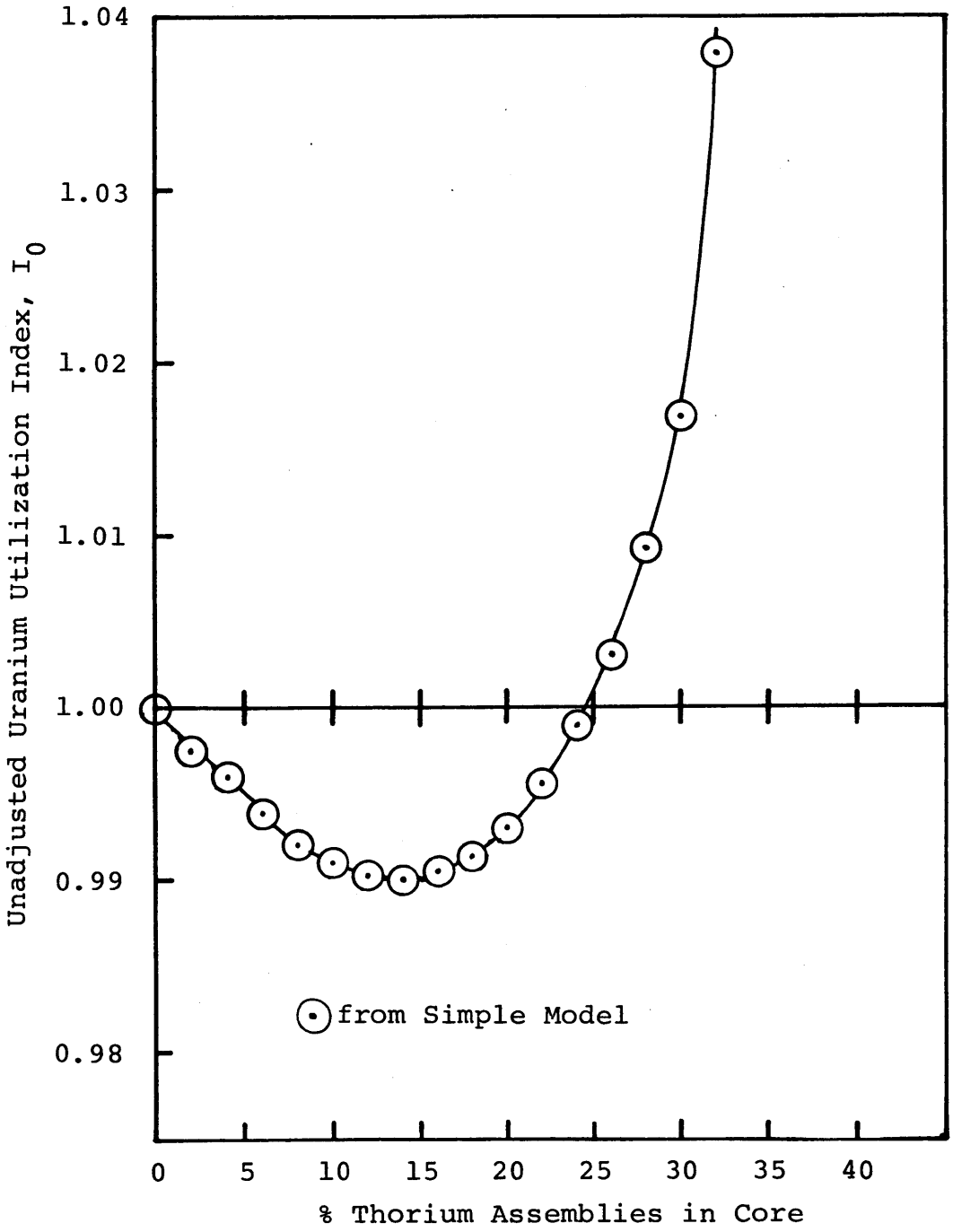

Fig. 4.3 Uranium Utilization Results for Thorium Lattice d-f Assemblies in Current Burnup PWR Cores.

A comparison of this result with that for current PWR cores illustrates some important differences. Not only is the uranium saving higher for the high burnup core but the thorium fraction in the core at which the maximum saving occurs is also higher. The higher excess reactivity of the uranium fuel in the high burnup cores favors thorium, by providing neutrons and thereby enabling thorium to incur higher burnups before the end-of-cycle is reached.

Other lattices which exhibited improved uranium utilization in the high burnup cores (according to the simple model) are: lattice d-f with a maximum improvement of 4.2% (at 26% thorium in the core), lattice d-s with 3.3% improvement (at 24% thorium), and lattice s-t with 3.1% improvement (at 24% thorium), as measured by the unadjusted index I_0.

Figures 4.4, 4.5 and 4.6 show the unadjusted uranium utilization for the three best lattices (d-t,d-f and d-s) in the high burnup PWRs.

4.4.3 Thorium Pins in Uranium Fuel Assemblies

The thorium pincell which has the same fuel-to-moderator volume ratio and fuel pin diameter as the uranium pincells of

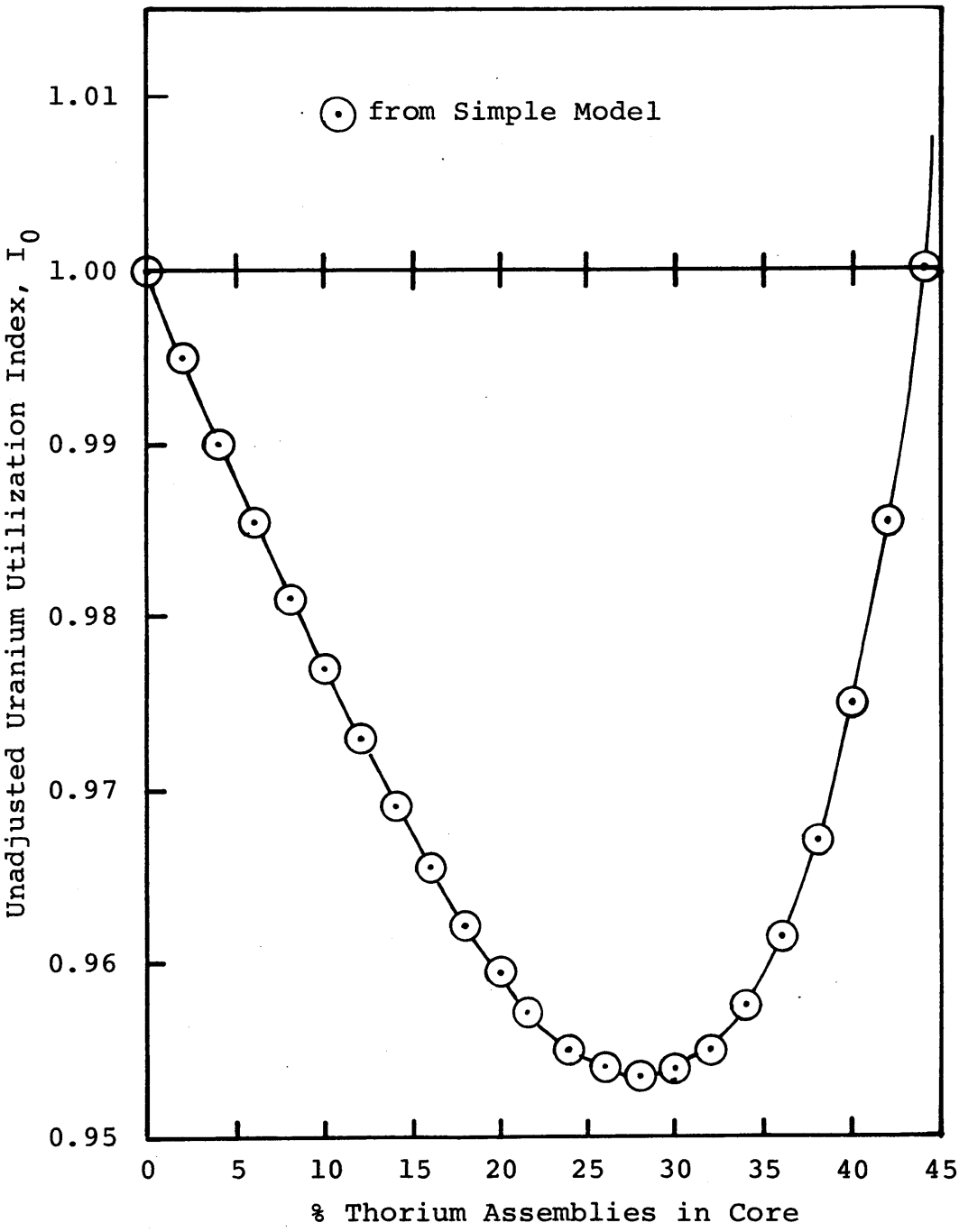

Fig. 4.4 Uranium Utilization Results for Thorium Lattice d-t Assemblies in High Burnup PWR Cores.

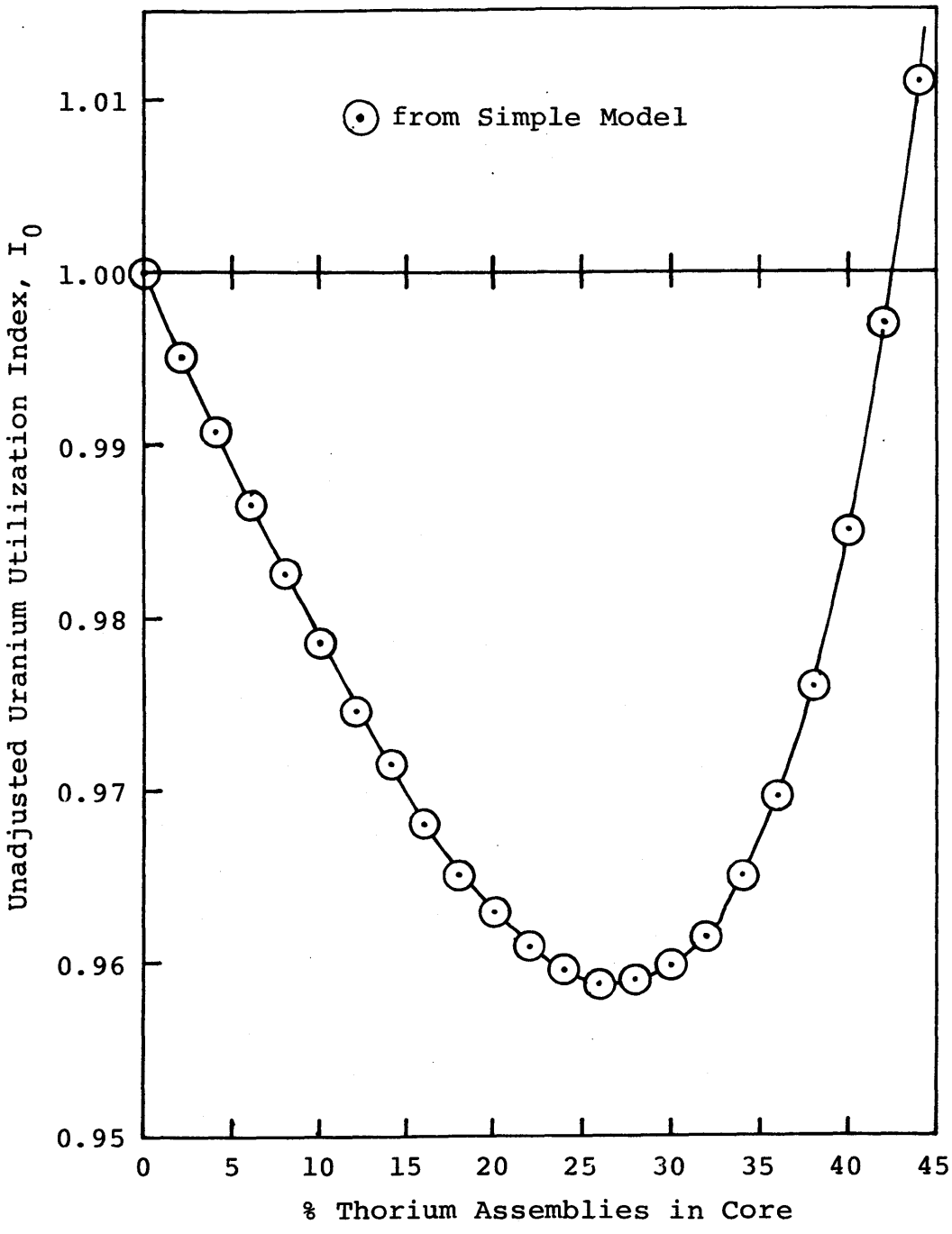

Fig. 4.5 Uranium Utilization Results for Thorium Lattice d-f Assemblies in High Burnup PWR Cores.

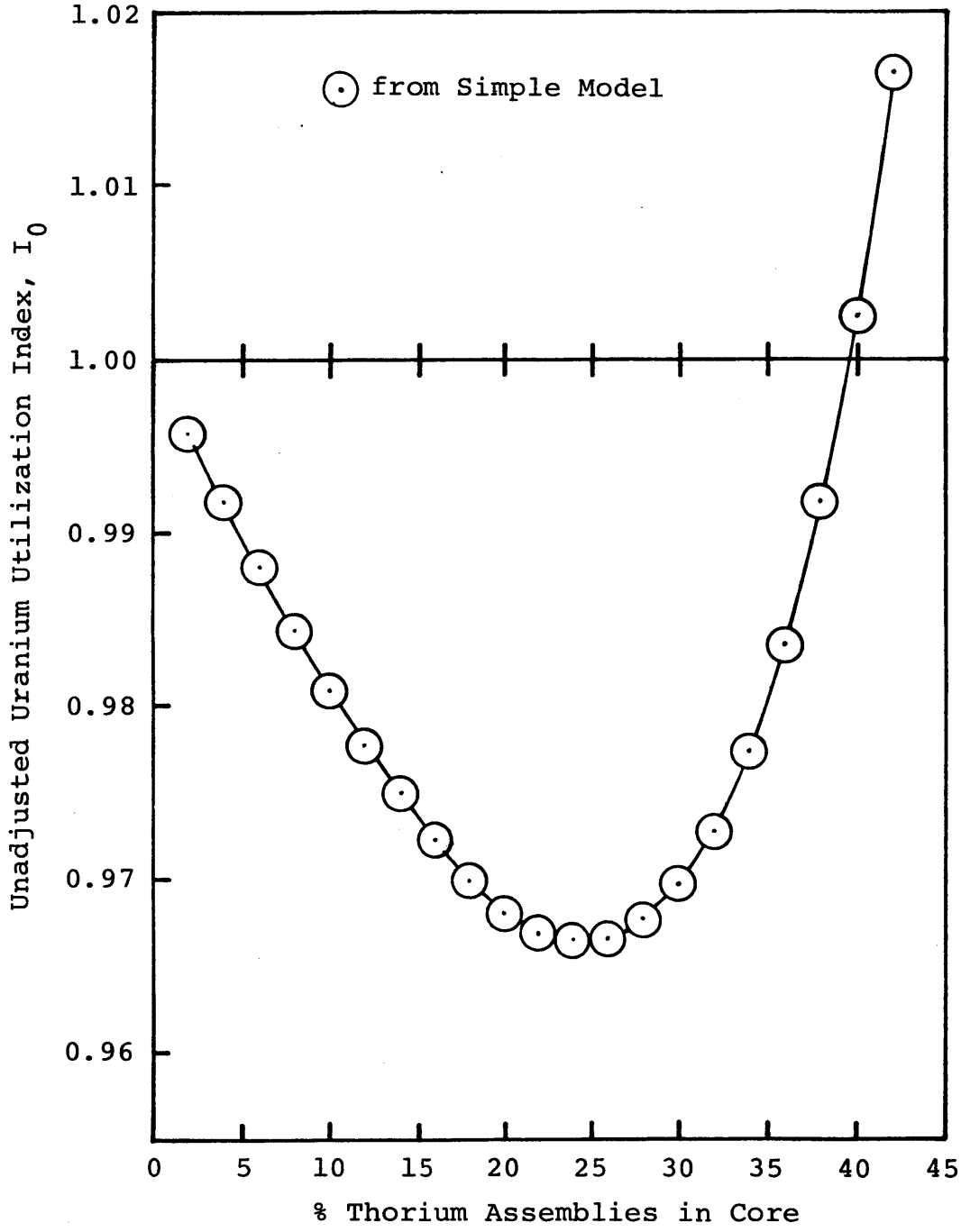

Fig. 4.6 Uranium Utilization Results for Thorium Lattice d-s Assemblies in High Burnup PWR Cores.

the reference core, i.e thorium lattice s-s, was modelled as if it were dispersed among uranium fuel pincells within an assembly. Only lattice s-s was examined in this mode since other thorium pincells have significantly different neutron spectra than a conventional host lattice, and mixing pincell sizes within a single assembly is a problematical undertaking on many grounds.

Including thorium in the standard PWR as pincells within uranium assemblies resulted in a maximum increase in uranium utilization of less than a tenth of one percent, relative to the all-uranium reference core. For the high burnup core the maximum uranium saving was about 2.0% (at 14% thorium). Figure 4.7 shows the variation of the unadjusted uranium utilization index as a function of thorium in the uranium fuel assemblies for both the current and the high burnup PWR cores.

4.4.4 Concluding Remarks on the Simple Model Evaluations

The evaluations presented here using the simple model show that even under the most generous thorium-favoring assumptions, the potential for thorium as a uranium saver in PWRs is fairly limited. The maximum savings predicted by the simple model for assembly-sized thorium internal blankets were about 1.5% for current PWRs, and about 5% for high burnup PWR

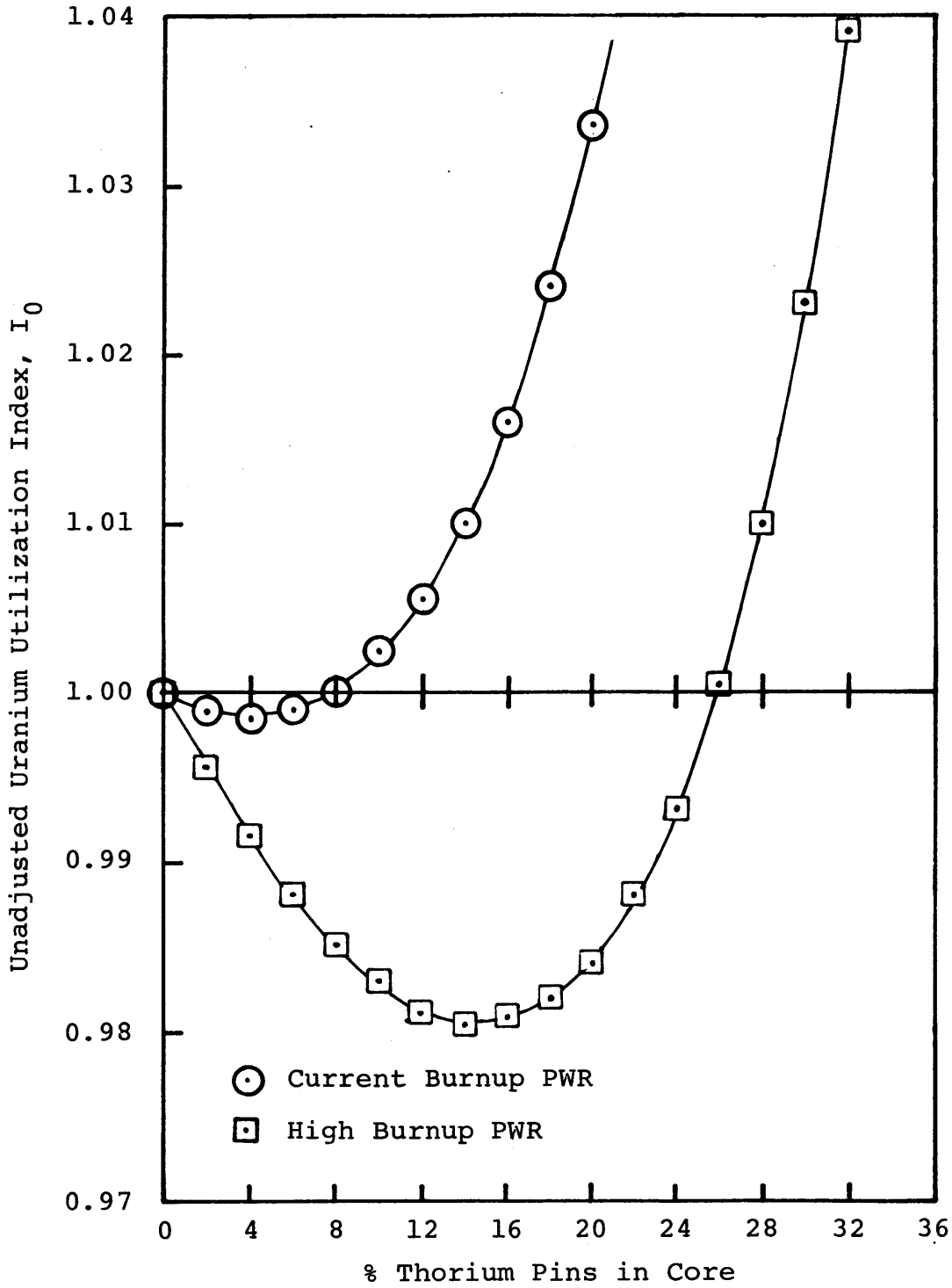

Fig. 4.7 Uranium Utilization Results for Thorium Pins Dispersed Among Uranium Fuel Assemblies.

cores. In all comparisons the unadjusted index for uranium utilization (see Appendix E) was used.

Thorium pins dispersed among uranium fuel pins, again evaluated under thorium-favoring assumptions, gave even smaller savings. For current PWR cores the uranium savings by employing thorium were negligible while for high burnup cores thorium pins were evaluated as improving uranium utilization by about 2%.

In summary: The simple model has identified lattices which should be analyzed using more detailed methods, while ruling out others as being totally unsuitable from the point of view of uranium utilization. Because of its deliberate thorium-favoring nature it has also provided an upper envelope on the uranium savings that the use of thorium may provide.

4.5 Thorium Assemblies as Internal Blankets

In this section the efficacy of thorium as an internal blanket will be evaluated in detail using the SPILBAC code. The thorium lattices identified as being potentially the most useful by the simple model will be investigated.

The reactor considered in this assessment is infinite (i.e. neutron leakage from the core periphery has been neglected). The focus will therefore be on the usefulness of thorium assembly internal blankets in the core interior, so that the potential advantages of such a scheme can be evaluated separately from the option of using thorium assemblies as radial blankets (which is addressed later in this chapter). This division also facilitates comparisons on a consistent basis.

The parameters used in the SPILBAC code in this assessment are listed in Table 4.4. In all cases, including those which serve as the reference cases (with uranium fuel only), the cores were burned to their reactivity limited lifetimes.

4.5.1. Internal Thorium Blankets in Current PWR Cores

Assembly-sized internal blankets of thorium lattices d-t, d-s, d-f and s-s were evaluated over a range of thorium mass fractions in the core. Lattices d-t and d-f, identified as being potentially the most useful by the simple model calculations, also performed better than the others in the detailed analysis using SPILBAC. However, none of the lattices showed any uranium saving as measured by the unadjusted uranium utilization index, I_0. Judging by this index the introduction

Table 4.4

Key Parameters Used in the SPILBAC Code for

Evaluating Thorium as an Internal Blanket

	Current PWR Cores		High Burnup	
	Thorium as Assemblies	Thorium as Pincells	Thorium as Assemblies	Thorium as Pincells
ρ_o	0.2200	0.2200	0.2661	0.2661
A, (MT/GWD)	0.009120	0.009120	0.007154	0.007154
n	3	3	5	5
θ_U	1.50	1.50	1.50	1.50
θ_{Th}	1.50	0.00	1.50	0.00
Lattices Examined	d-t, d-s d-f, s-s	s-s	d-t, d-s d-f, s-s	s-s
B_R, (GWD/MT)[a]	35.852	35.852	61.295	61.295

(a) Reference (all uranium) core discharge burnup (from SPILBAC).

of any quantity of thorium in the core increases uranium consumption in PWR cores.

Table 4.5 lists the thorium and uranium sub-batch discharge burnups, the unadjusted uranium utilization index I_0, and the two adjusted indices I_{235} and I_{efph}, as a function of the fraction of lattice d-t assemblies in the core. The adjusted indices have been derived in Appendix E. The first, I_{235}, measures the uranium utilization of the test core relative to the reference core after adjusting the results for differences in the U-235 loading (and therefore the natural uranium requirement) of the test and reference cores. The second, I_{efph}, gives the relative uranium utilization after adjusting the results such that the test and the reference cores deliver the same effective full power hours (efph). Figure 4.8 shows the variation of the uranium utilization indices I_0 and I_{235} with thorium (lattice d-t) content in the core.

The adjusted index for U-235 commitment, I_{235}, shows a small uranium saving. The saving is however less than half of one percent. There is little difference in the index I_0 and the adjusted index I_{efph}. The use of other thorium lattices showed no savings using any of the three indices as a guide.

Table 4.5

Key Results from the Evaluation of Thorium Lattice d-t as Internal Blanket Assemblies in a High Burnup PWR

M_{Th} [a] %	B_U [b] GWD/MT	B_{Th} [c] GWD/MT	I_o [d]	I_{235} [e]	I_{efph} [f]
0.0 [g]	35.852	0.0	1.0000	1.0000	1.0000
4.0	34.854	23.619	1.0004	0.9968	1.0004
8.0	33.746	22.533	1.0041	0.9965	1.0038
12.0	32.508	21.343	1.0122	1.0002	1.0113
16.0	31.139	20.052	1.0265	1.0084	1.0236
20.0	29.602	18.637	1.0465	1.0235	1.0429
24.0	27.840	17.060	1.0790	1.0489	1.0727
28.0	25.761	15.266	1.1131	1.0747	1.1038
32.0	23.231	13.179	1.2180	1.1668	1.1985

(a) The fraction of the total assemblies in the core that are thorium assemblies.

(b) Uranium sub-batch discharge burnup (from SPILBAC).

(c) Thorium sub-batch discharge burnup (from SPILBAC).

(d) Unadjusted uranium utilization index. Uranium savings = (1.0 - I) x 100 %.

(e) and (f) Adjusted uranium indices. See accompanying text and Appendix E.

(g) Reference (no thorium) core.

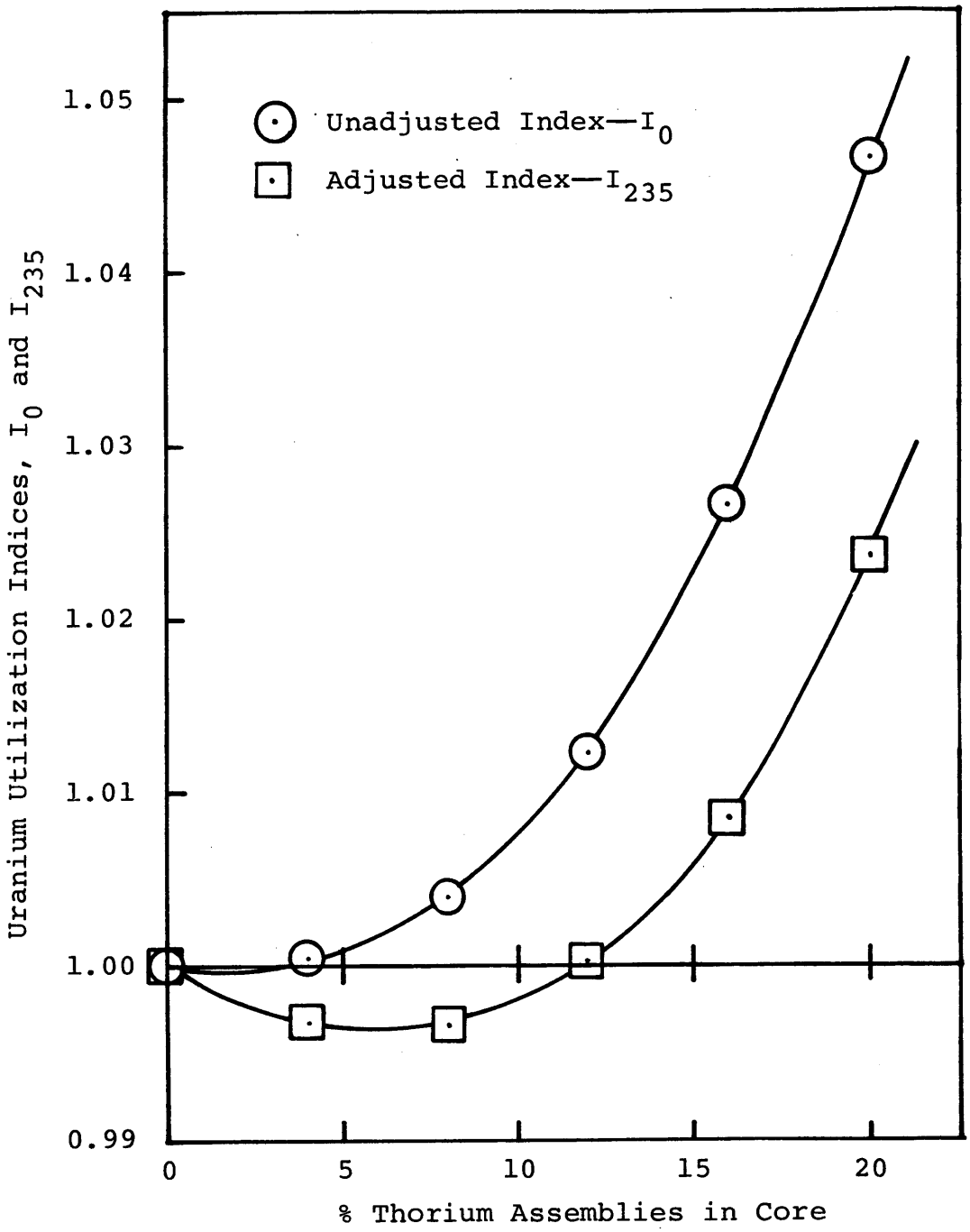

Fig. 4.8 Variation in Uranium Utilization with Fraction of Thorium d-t Assemblies as Internal Blankets in Current Burnup PWR Cores.

To conclude, the use of even small quantities of thorium as assembly-sized internal blankets is not advantageous, from the uranium utilization stand-point, in current burnup PWRs.

Depleted uranium blankets in the core interior were also evaluated, to compare with the thorium internal blankets. These performed worse than any of the thorium lattices examined in this evaluation. However, the depleted uranium inserts were at the same fuel-to-moderator ratio and fuel pin diameter as the uranium fuel. A proper optimization of depleted uranium lattices as internal blankets would improve their performance; but even then they will be inferior to the best thorium lattices, since they never equal the relatively high reactivities of the thorium lattices.

4.5.2 Internal Blankets of Thorium in High Burnup PWRs

Given the results of the simple model and the observation, previously made, about the relatively flat reactivity as a function of burnup (after the initial buildup period) for thorium lattices, thorium internal blankets should perform better in high burnup PWR cores than they did in current burnup PWRs.

The key parameters used in SPILBAC for this analysis are shown in Table 4.4. The thorium lattices examined as assembly sized inserts were: d-t, d-s, d-f, and s-s. These were evaluated at thorium fractions between zero and 30%. The use of lattices d-s and s-s resulted in a monotonic increase in uranium consumption (decrease in uranium utilization) as the fraction of thorium assemblies in the core increased. The assemblies composed of thorium lattices d-t and d-f resulted in some uranium savings: The results are presented below.

For lattice d-t, the uranium savings increased as the fraction of thorium in the core was increased, and peaked at 1.7% savings at 15% thorium in the core, using the unadjusted index I_0. When the results are adjusted for the U-235 differences in the reference and the test cores (index I_{235}), the savings rise to 3.0% at 20% thorium in the core. As explained earlier, this difference is due to the fact that the addition of thorium at fixed uranium sub-batch enrichment penalizes the test core since the reference core has a higher U-235 content. A comparison adjusted in this manner also assures the same natural uranium requirement for the two cores, making I_{235} an important index which can be used to assess the efficacy of a particular option.

The key results for lattice d-t thorium assemblies as internal blankets are shown in Table 4.6. The indices I_0 and

Table 4.6

Key Results from the Evaluation of Thorium Lattice d-t as Internal Blanket Assemblies in a High Burnup PWR

M_{Th} %	B_U GWD/MT	B_{Th} GWD/MT	I_o	I_{235}	I_{efph}
0.0*	61.295	0.0	1.000	1.000	1.000
5.0	59.548	42.455	0.9921	0.9895	0.9925
10.0	57.669	40.539	0.9859	0.9801	0.9866
15.0	55.595	38.457	0.9826	0.9732	0.9835
20.0	53.293	36.187	0.9832	0.9696	0.9840
25.0	50.683	33.666	0.9901	0.9717	0.9906
30.0	47.689	30.850	1.0063	0.9821	1.0060

*Reference (no thorium) core.

I_{235} are shown as functions of the fraction of thorium assemblies in the core, in Fig. 4.9.

The second thorium lattice which produced savings in uranium was lattice d-f. In this case the uranium savings peaked at 1.9% relative to the reference case, at 20% thorium in the core, using index I_0. The maximum savings using the adjusted index I_{235} was 3.3% at 25% thorium in the core. These and other key results from this assessment are included in Table 4.7, and Fig. 4.10 shows the variation of the indices I_0 and I_{235} with thorium fraction. The adjusted index I_{efph} has not been included because it is essentially identical to the unadjusted index I_0.

The use of internal blankets of depleted uranium was also examined. They were found to be worse, in terms of uranium utilization, than any of the thorium lattices. Again it should be pointed out that optimization of the depleted uranium lattices would improve their performance.

One option that is easily retrofittable is the use of spent fuel as "internal blankets". In a steady state this corresponds to increasing the number of reload batches from 5 (in the reference case) to 6, and using the last batch in the core interior as a "blanket". The discharge burnup in this case increased to 63.140 GWD/MT, an increase of 3.0% over the

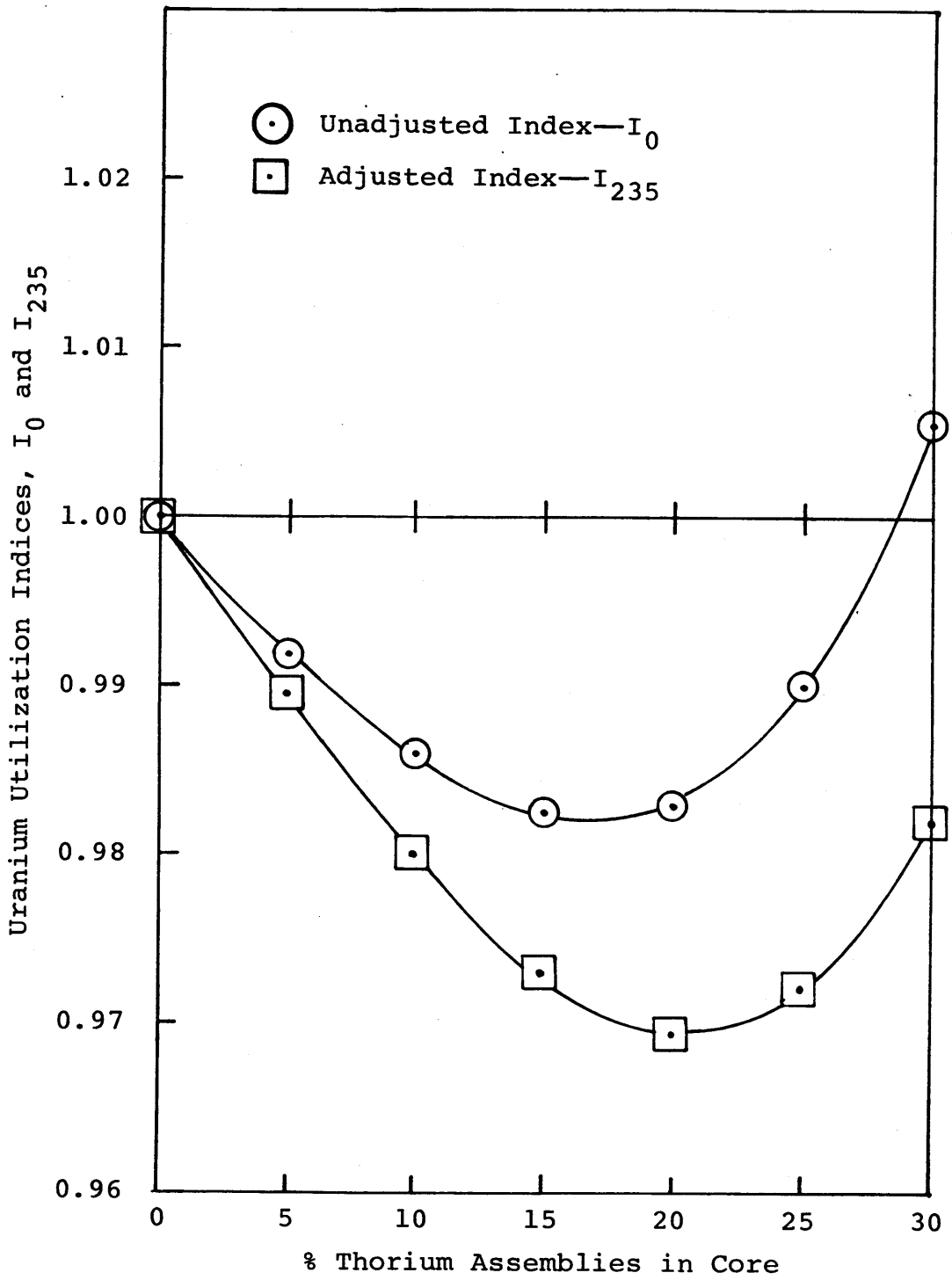

Fig. 4.9 Variation of Uranium Utilization with Fraction of Thorium d-t Assemblies as Internal Blankets in High Burnup PWR Cores.

TABLE 4.7

Key Results from the Evaluation of Thorium Lattice d-f as Internal Blanket Assemblies in a High Burnup PWR

%	B_U GWD/MT	B_{Th} GWD/MT	Uranium Utilization Indices		
			I_0	I_{235}	I_{efph}
0.0*	61.295	0.0	1.0000	1.0000	1.0000
5.0	59.539	42.580	0.9922	0.9895	0.9926
10.0	57.656	40.703	0.9858	0.9799	0.9865
15.0	55.611	38.692	0.9816	0.9721	0.9825
20.0	53.344	36.498	0.9812	0.9676	0.9821
25.0	50.830	34.111	0.9854	0.9671	0.9861
30.0	47.986	31.496	0.9971	0.9731	0.9972
35.0	44.691	28.493	1.0210	0.9898	1.0199

*Reference (no thorium) core.

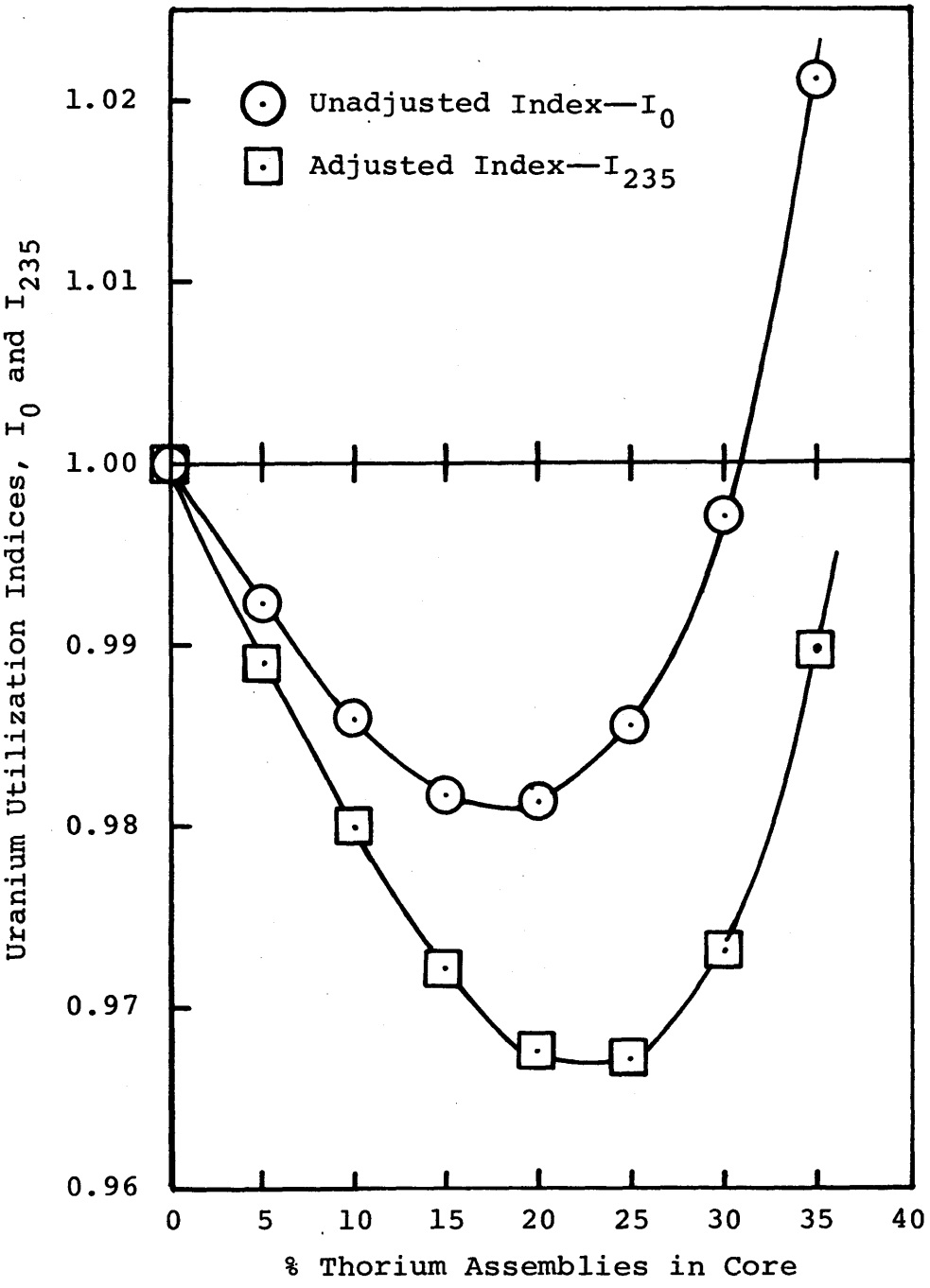

Fig. 4.10 Variation of Uranium Utilization with Fraction of Thorium d-f Assemblies as Internal Blankets in High Burnup PWR Cores.

reference core. This increased burnup translates directly, in this case, to an increase in uranium utilization of 3.0% as measured by the indices I_0 and I_{235}.

The evaluation of spent fuel internal blankets (really no more than going to one more batch in the core) shows that the benefit in terms of uranium utilization from this strategy is comparable to the maximum benefit that employing thorium would provide. Furthermore, given the difficulties in introducing a parallel thorium fuel cycle, the spent fuel blankets would be more attractive assuming that shorter cycle lengths are tolerable.

In going from the current PWR reference core to the high burnup PWR reference core the number of batches is increased from 3 to 5 and the reload enrichment from 3.0 to 4.32 w/o U-235. In order to isolate the effect of each of these variables separately on the performance of thorium internal blankets two additional cases were modelled on SPILBAC. The first was a three batch core with a reference (no thorium) discharge burnup of about 60 GWD/MT (i.e comparable to that of a 5-batch high burnup core). This required a uranium enrichment of 4.75 w/o U-235. The second was a 4-batch core with the same reload enrichment as the (5-batch) high burnup PWR reference core, i.e. 4.32 w/o U-235.

Using the SPILBAC code, the additions of thorium lattice d-t as assembly sized internal blankets in these reactors was examined. In the case of the 4.75 w/o enriched 3-batch core the maximum (unadjusted) savings of uranium were 2.7% (at 20% thorium in the core). This saving is higher than the 1.7% obtained for the high burnup 5-batch case (also at 20% thorium in the core).

By changing the number of batches in the high burnup cores from 5 to 4, the reference (no thorium) discharge burnup decreased by 4.1%. Additions of thorium lattice d-t as assembly-sized inserts resulted in a maximum (unadjusted) uranium saving of 1.9% (at 15% thorium in the core), whereas the saving in the 5-batch core was 1.7%.

This analysis points out trends that are also (more transparently) visible in the simple model. Namely, that high excess core reactivity favors the addition of thorium. This can be accomplished by increasing the uranium sub-batch enrichment. Increasing the number of reload batches, while increasing the discharge burnup, worsens the uranium saving potential of thorium unless accompanied by an increase in the reload enrichment which is sufficient to offset its effects.

To conclude, properly optimized lattices of thorium as assembly-sized internal blankets have the potential of

increasing uranium utilization by about 3%. Higher burnups and reload enrichments favor the use of thorium. The evaluation of spent fuel blankets (which in the present context are equivalent to using one more batch in the core) showed that this scheme offers comparable uranium savings to those possible by using thorium.

4.6 Thorium Assemblies as Radial Blankets

Radial blankets in PWRs offer the advantages of improved neutron economy (leading to better uranium utilization) and reduced irradiation of the core shroud, barrel and reactor vessel. The current interest in low-leakage loading patterns stems from these considerations. Employing radial blankets of fertile or burned fuel has the disadvantage of increasing the power peaking in the core interior to an extent that almost always necessitates the concurrent deployment of burnable poisons with low-leakage fuel management.

In this respect using blankets of purely fertile materials leads to more severe power peaking than using once or twice-burned fuel as radial blankets. In the analysis which follows the complete range of such schemes have been evaluated, for both current and high burnup PWRs. In the evaluation of high burnup cores, for example, the reference

case employs the conventional "out-in/scatter" fuel loading scheme with fresh fuel on the periphery. This case is then compared with low-leakage schemes in the steady-state, with any one of the four "burned batches" loaded on the core periphery, to quantify the uranium utilization advantages of these schemes. The reference and the low-leakage cores are then compared to steady-state cores with thorium, depleted uranium, natural uranium or spent fuel as the radial blanket material.

While burnable poisons were not modelled in these analyses, it is assumed that power peaking in the core interior can be controlled through the use of burnable poisons without affecting the discharge burnups of the subject cores. While the use of burnable poisons affects cycle burnups, Loh (L-2) found that discharge burnups do not change significantly because of the compensating effects of power history levelling and residual poison.

4.6.1 Radial Blankets in Current PWR Cores

The parameters used in the SPILBAC code for evaluating current PWR cores are shown in Table 4.8. These are the same as those used in the internal blanket assessments, except that now leakage from the core is explicitly included through the

Table 4.8

Key Parameters Used in SPILBAC for the Analysis of Radial Blankets and Low-Leakage Schemes

	Current PWR Cores	High Burnup PWR Cores
ρ_o	0.2200	0.2661
A, (MT/GWD)	0.009120	0.007154
n	3	5
θ_U	1.50	1.50
θ_{Th}	1.50	1.50
α	0.285	0.285

core leakage constant, α. The value for the constant α used in all cases was 0.285. This was obtained by Loh (L-2) from analyzing published data on the Combustion Engineering System-80^{TM} core for a variety of fuel loading patterns.

In a typical PWR about 20% of the assemblies are on the core periphery. This fraction is 19.9% for the System-80^{TM} core (48 out of 241). In a three batch core at steady state about 33% of the total number of the assemblies in the core are from each of the three batches. Therefore only part of any batch can be placed on the periphery, with the rest in the interior. In a five batch core exactly 20% belong to each batch so that all of one batch can serve one cycle on the core periphery.

In the reference core for this case the out-in/scatter scheme was employed, i.e. 66% of the fresh batch was modelled on the core periphery with the remaining 33% in the interior. The discharge burnup for this core was 28.198 GWD/MT.

With once-burned (cycle 2) fuel on the periphery in the first of the low-leakage schemes, the discharge burnup was 28.880 GWD/MT, an increase of 2.4% compared to the reference core. With twice-burned (oldest batch) fuel on the periphery the discharge burnup was 29.430 GWD/MT, an increase of 4.4%

over the reference case. The key results from this assessment are shown in Table 4.9.

Since the reload enrichment and the quantity of uranium heavy metal is equal in all cases, the percentage increase in the discharge burnup is also the percent saving in uranium requirements as measured by the uranium utilization indices I_0 and I_{235}.

The option of using spent fuel as a radial blanket was also evaluated. In the steady-state this effectively requires increasing the number of batches to four, and placing the oldest batch on the core periphery as a radial balnket. The discharge burnup for this case was 31.626 GWD/MT, which is 9.5% higher than the reference case and a 5% gain on the best case with three batches (i.e. twice burned fuel on the periphery). It is important to recognize that part of this gain in discharge burnup (and hence uranium utilization) is derived from the increase in the number of batches.

Fuel assemblies of thorium (lattices d-t and d-s), which performed best in the simple model evaluation and in the detailed analysis of internal blankets, were also evaluated as radial blankets. The thorium assemblies were modelled as occupying the entire core periphery (20% of the total number of assemblies in the core), for the three cycles they were in the

TABLE 4.9

Comparison of the Reference Core with Low-Leakage Cores in a Current Burnup PWR

Peripheral Batch	End-of-Cycle Batch Burnups (GWD/MT)			Uranium Utilization Indices (savings)	
	CYCLE 1	CYCLE 2	CYCLE 3[b]	I_0, I_{235}[c]	I_{efph}
1 (Fresh Fuel)[a]	9.247	19.327	28.198	1.0000	1.0000
2	11.733	19.908	28.880	0.9764 (2.4%)	0.9781 (2.2%)
3 (Oldest Fuel)	11.920	21.914	29.430	0.9581 (4.2%)	0.9611 (3.9%)

[a]Reference case (Out-In/Scatter).

[b]Discharge.

[c]Since the U-235 content is the same in the three cores, $I_0 = I_{235}$.

reactor. For comparison, radial blankets of depleted and natural uranium (at reference PWR lattice dimensions) were evaluated in the same mode of operation as the thorium radial blankets. The key results from these comparisons are included in Table 4.10.

These results indicate that, by any of the indices, radial blankets of thorium show only small uranium savings (<1%) in current PWR cores. Blankets of natural uranium improve uranium utilization by about 2%, relative to the reference core after adjusting for the U-235 differences in the reference and test cores. These should be compared to the previously mentioned savings of 4% from using the oldest batch as a radial blanket, and the 9% savings from radial blankets of spent fuel.

In conclusion, radial blankets of thorium, depleted uranium or natural uranium, do not effectively compete with low-leakage schemes or with radial blankets of spent fuel, in current PWR cores.

4.6.2 Radial Blankets in High Burnup PWRs

In the five batch core the out-in/scatter reference core depletion gave a steady-state discharge burnup of 49.961

TABLE 4.10

Key Results from the Assessment of Radial Blankets for Current PWR Cores

	CYCLE	Average EOC Burnups GWD/MT		Uranium Utilization Indices		
		Uranium Fuel	Blanket	I_0	I_{235}	I_{efph}
Reference Case[a]	1	9.247				
	2	19.327	—	1.0000[b] (0.0%)	1.0000 (0.0%)	1.0000 (0.0%)
	3	28.198[c]				
Reference Case with Radial Blanket of Thorium (d-t)	1	9.337	3.180			
	2	17.442	6.903	1.0274 (-2.7%)	1.0048 (0.5%)	1.0253 (-2.5%)
	3	24.703	10.972			
Reference Case with Radial Blanket of Thorium (d-f)	1	9.449	3.317			
	2	17.641	7.204	1.0135 (-1.4%)	0.9912 (0.9%)	1.0125 (-1.3%)
	3	24.975	11.396			
Reference Case with Depleted Uranium Radial Blanket	1	9.431	3.664			
	2	17.608	7.567	1.0136 (-1.4%)	0.9913 (0.9%)	1.0126 (-1.3%)
	3	24.928	11.561			
Reference Case with Natural Uranium Radial Blanket	1	9.868	4.706			
	2	18.389	9.302	1.0015 (-0.2%)	0.9795 (2.1%)	1.0014 (-0.1%)
	3	25.995	13.782			

[a]Out-In/Scatter fuel management. Fresh fuel on core periphery.

[b]Numbers in parentheses indicate percent uranium savings.

[c]Since steady-state cores are evaluated, EOC3 burnups are also the discharge burnups for all cases.

GWD/MT. The key parameters used in SPILBAC for this analysis are shown in Table 4.8.

Steady state cores with batch 2, 3, 4, or 5 on the periphery were evaluated to quantify the advantages of low leakage fuel management schemes. The key results from these low-leakage cores are presented in Table 4.11. Discharge burnups and uranium savings increase monotonically as older batches are placed on the periphery. With the oldest batch (batch 5) on the periphery the discharge burnup is 5.6% higher than the reference case. As explained earlier, this also translates into a 5.6% uranium saving, as measured by the indices I_0 and I_{235}.

A six batch core, with the same reload enrichment as the five batch reference and low-leakage cores, was analyzed with the oldest batch on the core periphery (as a spent fuel radial blanket). The discharge burnup in this case was 54.451 GWD/MT. This increased discharge burnup amounts to a 9.1% saving in uranium requirements, compared to the reference core and a 3.5% saving compared to the best low-leakage core (batch 5 on the periphery).

Radial blankets of fertile thorium assemblies of lattices d-f and d-t were also analyzed, as were radial blankets of

TABLE 4.11

Comparison of Reference Core with Low-Leakage Cores in High Burnup PWRs

Peripheral Batch	End-of-Cycle Batch Burnup GWD/MT					Uranium Utilization Indices	
	CYCLE 1	CYCLE 2	CYCLE 3	CYCLE 4	CYCLE 5	I_0, I_{235} [b]	I_{efph}
1 (Fresh Fuel)[a]	8.832	21.072	31.716	41.227	49.912	1.0000 (0.0%)[c]	1.0000 (0.0%)
2	13.846	21.811	32.535	42.150	50.898	0.9806 (1.9%)	0.9816 (1.8%)
3	14.012	25.815	33.181	42.878	51.704	0.9653 (3.5%)	0.9670 (3.3%)
4	14.152	26.063	36.556	43.460	52.328	0.9538 (4.6%)	0.9560 (4.4%)
5 (Oldest Fuel)	14.273	26.269	36.828	46.361	52.845	0.9445 (5.6%)	0.9472 (5.3%)

[a] Reference case (Out-In/Scatter)

[b] Since the U-235 content in all five cores is identical, $I_0 = I_{235}$.

[c] Numbers in parentheses indicate percent improvement in uranium utilization.

depleted and natural uranium. The key results from these assessments are presented in Table 4.12.

In the high burnup cores radial blankets of thorium, natural uranium and depleted uranium all result in substantial uranium savings relative to the out-in/scatter reference core. The savings, adjusted for U-235 content, range from 6% for thorium (lattice d-f) to 4% for depleted uranium radial blankets. A small advantage for thorium (0.5%) persists when the comparison is made between the best 5 batch low-leakage core (batch 5 on the core periphery) and the core blanketed with thorium d-f assemblies. As in the current burnup PWR cores, the best radial blanket material is still spent fuel, which gives a 9% increase in uranium utilization over the reference core, corresponding to a 3% improvement compared to the best thorium radial blanket. When the thorium (d-f) radial blanket is modelled as spending 10 cycles in the core (instead of the 5 cycles in the other cases) the advantage of the spent fuel blanket is reduced to 1.6%.

In conclusion, of the options considered, spent fuel was evaluated as being the most effective radial blanket from the point of view of uranium utilization, providing uranium savings of about 9% compared to the out-in/scatter reference core. It is important to recognize that, in the steady-state, a spent fuel radial blanket scheme is equivalent to

TABLE 4.12

Key Results from the Assessment of Radial Blankets in High Burnup PWRs

	CYCLE	Average EOC Burnups GWD/MT		Uranium Utilization Indices		
		Uranium Fuel	Blanket	I_0	I_{235}	I_{efph}
Reference Case[a]	1	8.832				
	2	21.072				
	3	31.716	—	1.0000 (0.0%)[b]	1.0000 (0.0%)	1.0000 (0.0%)
	4	41.227				
	5	49.912[c]				
Reference Case with Radial Blanket of Thorium (d-t)	1	11.732	3.674			
	2	21.804	8.014			
	3	30.767	12.689	0.9586 (4.1%)	0.9453 (5.5%)	0.9606 (3.9%)
	4	38.926	17.506			
	5	46.467	22.406			
Reference Case with Radial Blanket of Thorium (d-f)	1	11.791	3.805			
	2	21.910	8.284			
	3	30.914	13.051	0.9527 (4.7%)	0.9395 (6.1%)	0.9550 (4.5%)
	4	39.108	17.922			
	5	46.678	22.846			
Reference Case with Depleted Uranium as Radial Blanket	1	11.511	4.078			
	2	21.421	8.397			
	3	30.256	12.775	0.9759 (2.4%)	0.9624 (3.8%)	0.9771 (2.3%)
	4	38.308	17.168			
	5	45.752	21.574			
Reference Case with Natural Uranium as Radial Blanket	1	11.828	5.092			
	2	21.983	10.041			
	3	31.021	14.833	0.9721 (2.8%)	0.9586 (4.1%)	0.9735 (2.7%)
	4	39.249	19.526			
	5	46.850	24.169			

[a] Out-In/Scatter fuel management.
[b] Numbers in parentheses indicate percent uranium savings over reference case.
[c] Since steady-state cores are evaluated, EOC5 burnups are also the discharge burnup for all cases.

low-leakage fuel management with one more reload batch in the core. Thorium radial blankets performed better in high burnup cores than in current burnup PWRs, a trend previously noted in the assessment of internal blankets. The maximum saving from using thorium blankets was about 6%.

4.7 Thorium Pins in Enriched Uranium Assemblies

Following up on the simple model results of section 4.4.3, the introduction of thorium pins among uranium assemblies was evaluated as a uranium conservation measure for current and high burnup PWRs. In these evaluations an infinite reactor was considered.

The analysis for the current burnup PWR cores showed that the inclusion of thorium pins in uranium assemblies worsens uranium utilization, and this deterioration increases monotonically as the fraction of thorium in the assemblies is increased.

For the five batch high burnup cores, a maximum (unadjusted) saving in uranium requirements of 1.2% was obtained at 11% thorium. The uranium saving using the adjusted index I_{235} was 1.9% at 13% thorium. Table 4.13 records the key results of this analysis, and Fig. 4.11 shows

TABLE 4.13

Key Results from the Assessment of Thorium Pins Dispersed Among Uranium Fueled Assemblies in High Burnup PWRs

M_{Th}[a]	B_U	B_{Th}	Uranium Utilization Indices		
%	GWD/MT	MWD/MT	I_0	I_{235}	I_{efph}
0.0[b]	61.295	—	1.0000	1.0000	1.0000
5.0	58.777	57.459	0.9918	0.9892	0.9922
7.0	57.709	55.891	0.9900	0.9861	0.9905
9.0	56.617	54.312	0.9888	0.9836	0.9894
11.0	55.491	52.713	0.9885	0.9819	0.9891
13.0	54.322	51.087	0.9893	0.9813	0.9898
15.0	53.127	49.452	0.9910	0.9815	0.9915
20.0	49.959	45.260	1.0003	0.9865	1.0003
25.0	46.461	40.870	1.0201	1.0012	1.0191

[a]Fraction of thorium pins in the core.

[b]Reference (no thorium case).

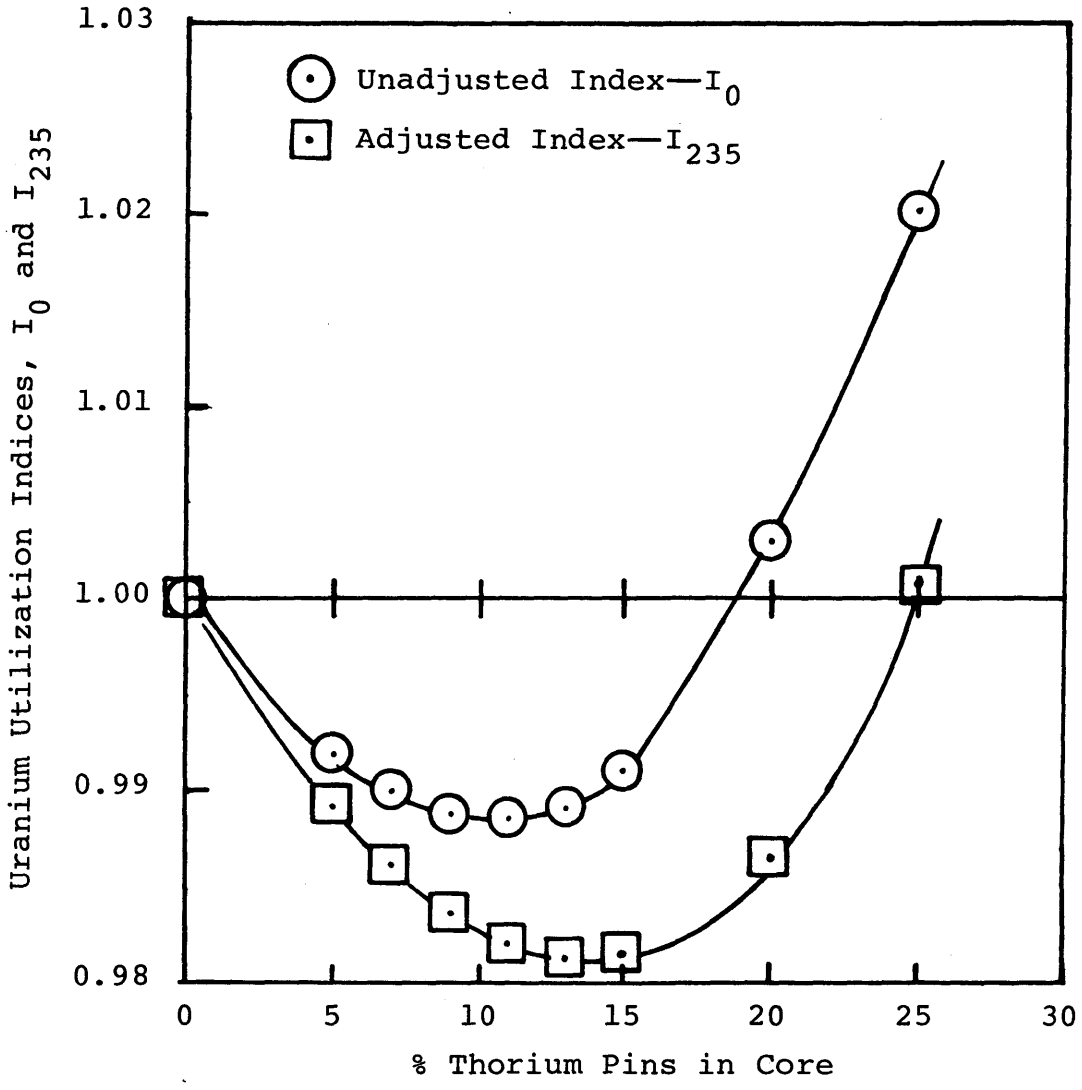

Fig. 4.11 Variation of Uranium Utilization with Fraction of Thorium Pins Dispersed Among Uranium Assemblies in High Burnup PWR Cores.

the variation of the indices I_0 and I_{235} with the fraction of thorium pins per assembly.

Depleted uranium pins were also evaluated in the same mode of operation. These performed worse than the thorium in the current and the high burnup PWRs, with no uranium savings in either case.

4.8 Chapter Summary

In this chapter the first set of thorium evaluations are performed of options considered retrofittable in existing PWRs. The lattices of thorium investigated in this work, having a variety of fuel-to-moderator volume ratios and fuel pin diameters, were described, and the results of LEOPARD burnup evaluations were presented.

A simple model for identifying the more promising of these lattices was developed and applied under thorium-favoring approximations. Results indicated that the drier lattices of thorium performed best in terms of the peak reactivity reached and therefore as potential uranium savers.

Detailed analysis of internal blankets of thorium using the SPILBAC code showed no uranium savings for current burnup

PWRs. For high burnup cores uranium savings of about 3% are possible. The use of spent fuel internal blankets (which in the steady-state corresponds to increasing the number of core batches by one) offered savings comparable to those from the best thorium cases. It was also shown that high (U-235) reload enrichments and the use of fewer batches favor thorium additions in the core.

Radial blankets were evaluated for current and high burnup PWR cores. The results from this analysis show that thorium radial blankets are not useful for current PWR cores (with uranium savings of <1%). Natural uranium radial blankets increased uranium utilization by about 2%, compared to the out-in/scatter reference core. This should be compared to the significantly higher uranium savings from the best low-leakage core (4%), and those from using spent fuel as radial blankets (9%).

In the assessment of the use of radial blankets on high burnup cores, thorium radial blankets performed significantly better. Radially blanketed thorium cores showed uranium savings of about 6% relative to the out-in/scatter reference core for this case. This is, however, only slightly more than the savings from the best low-leakage core (batch 5 on the core periphery). Spent fuel again performed better than any of

the other blanket materials, with uranium savings of about 9% over the reference case.

An evaluation of thorium pins dispersed within uranium fuel assemblies for current PWR cores showed that including any quantity of thorium in this mode worsens uranium utilization. In high burnup cores the inclusion of thorium pins in the core improved uranium utilization by a maximum of 2%.

CHAPTER 5

LESS CONVENTIONAL OPTIONS

5.1 Introduction

The evaluations presented thus far have been of options which can be implemented in existing PWRs. Here, a second set of fuel management strategies are examined, those considered more exotic, and less retrofittable. The distinction is somewhat subjective since the cost of implementing a "retrofittable" option in an existing reactor may be too high compared to the benefits gained from it.

Three options are evaluated in this chapter. The first is the reconstitution of burned thorium assemblies and their reinsertion into the core as radial blankets. The second is spectral shift control (SSC) in PWRs with and without thorium. The last is the option of using smaller assemblies in PWRs. In all cases the focus will be on the quantification of the uranium utilization advantage associated with each strategy. As before, an effort has been made to present the results relative to well defined reference cases, so that meaningful comparisons can be made.

5.2 Reconstitution of Thorium Assemblies

In this section the feasibility of reconstituting burned thorium assemblies at lower fuel-to-moderator volume ratios, V_F/V_M, and their reinsertion into the core as radial blanket assemblies will be assessed as a uranium conservation measure. The scheme considered here is similar to that considered for BWRs, where savings in uranium usage of between 4 and 10 percent have been predicted (W-2).

The basic concept is to breed U-233 in (dry) thorium assemblies, or by selectively placing thorium pins in uranium fuel assemblies. Upon their discharge from the core they are disassembled and reassembled at lower V_F/V_M (wet lattice configurations) for subsequent reinsertion into the core as radial blankets. The reconstitution enables better utilization of the bred U-233 by providing a softer neutron spectrum. The variation of the thorium reactivity and U-233 enrichment as functions of burnup, before and after reconstitution, are shown schematically in Fig. 5.1. The discontinuous increase in the U-233 enrichment upon reconstitution is caused by the decay of protactinium-233, with a half-life of 27 days, to U-233.

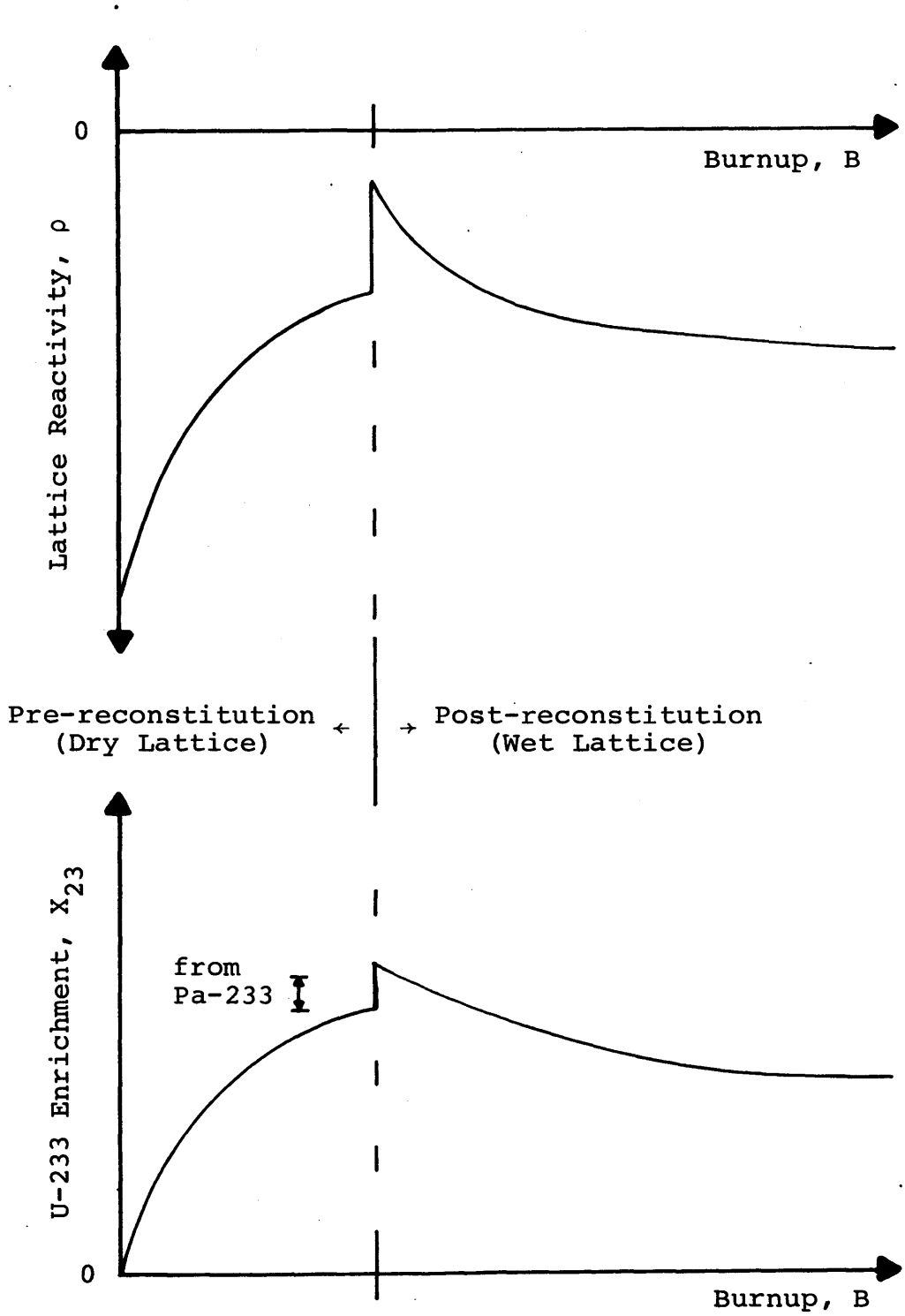

Fig. 5.1 A Schematic Representation of the Reactivity and U-233 Enrichment for a Thorium Lattice Before and After Reconstitution.

Potential disadvantages of reconstituting thorium are the lower asymptotic reactivities of the wet thorium lattices, and the increased worth of fisson product poisons.

The pre-reconstitution burnup accumulated by the thorium pins plays an important role in determining the post-reconstitution reactivity-burnup behavior, and therefore the uranium utilization advantage that can be realized. High pre-reconstitution burnup allows more time for breeding U-233, but also penalizes the reconstituted thorium reactivity via increased fission product concentrations. As the following analysis will show, this trade-off favors a relatively low pre-reconstitution burnup of the thorium pins. Once reconstituted, low burnups are again favorable to uranium utilization since the asymptotic reactivities of wet thorium lattices are substantially lower than for the drier lattices, an effect aggravated by the presence of the pre-reconstitution fission products in the reconstituted thorium assemblies.

In this analysis the reconstitution was performed using (pre-reconstitution) thorium d-t assemblies. The reader is referred to Table 4.2 of Chapter 4 and the accompanying text for the notation used throughout this work. As shown in Table 4.2, lattice d-t has a V_F/V_M of 1.0 and a pin diameter of 0.5 cm.. Table 4.2 also indicates that, with the exception of the effectively homogeneous thorium lattices, thorium lattice d-t

has the highest peak U-233 enrichment. Furthermore, thorium d-t assemblies performed well in the assessment of internal and radial blankets, also analyzed in Chapter 4. The post-reconstitution V_F/V_M of the thorium assemblies was 0.6. Stated differently, thorium lattice d-t assemblies, after a period of residence in the core, were reconstituted as lattice d-s assemblies, and analyzed for their potential as radial blankets. The reconstitution option is considered here for both current and high burnup PWR cores. In each case the reconstitution of thorium d-t assemblies into thorium d-s assemblies was modelled at three different (pre-reconstitution) thorium burnups: 4 GWD/MT, 13 GWD/MT and 19 GWD/MT. In order to compare directly the uranium utilization benefits of reconstituted thorium blankets with the unreconstituted thorium blankets assessed in Chapter 4, it was assumed that an exogenous supply of reconstituted thorium lattices was available. The results are thereby decoupled from the pre-reconstitution phase, making the comparisons consistent in that radial blankets are assessed on a relative basis.

The analysis which follows is therefore designed to provide an upper limit on the savings in uranium usage that reconstituted thorium assemblies can be expected to provide. As mentioned earlier, in the analysis of internal and radial blankets, constraints imposed by thermal-hydraulic consider-

ations may force the adoption of a less than optimal reconstitution scheme.

5.2.1 Reconstitution of Thorium in Current Burnup PWRs

The reference reactor for this assessment was the same as the one used in Chapter 4 for comparing radial blankets and low-leakage refuelling schemes (see section 4.6 of Chapter 4). The reactivity versus burnup traces for the reconstituted assemblies (for subsequent modelling in the SPILBAC code) were generated using the LEOPARD program, with BOL U-233 enrichments and fission product concentrations corresponding to the burnups at which the reconstitution was modelled as having taken place. As stated above, three pre-reconstitution burnups were considered (4, 13, 19 GWD/MT). Figure 5.2 shows the variation of reactivity as a function of both pre- and post-reconstitution burnup for the three cases.

The key results from the SPILBAC code for the reconstituted thorium blanket assemblies in steady-state, current burnup PWR cores is shown in Table 5.1. The reference core results are also included for comparison. These results show that the use of reconstituted thorium radial blankets improves uranium utilization by between 3% and 5%, as measured by the index I_{235}. The 3% savings are predicted for the low

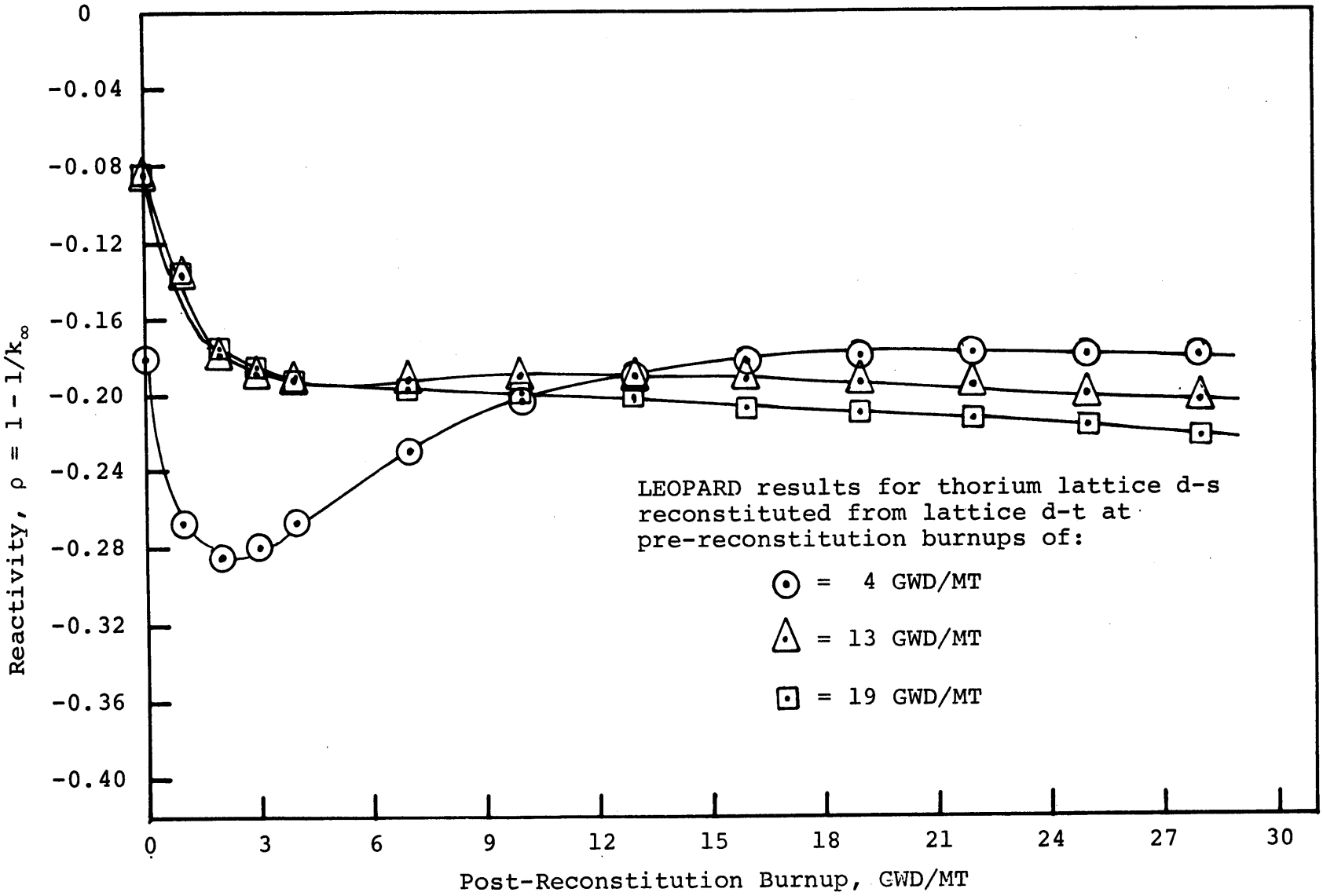

Fig. 5.2 Reactivity versus Burnup Traces for Reconstituted Thorium Assemblies.

TABLE 5.1

Key Results for Reconstituted Thorium Blankets in Current Burnup PWR Cores

	Cycle	Average EOC Burnups GWD/MT		Uranium Utilization Indices		
		Uranium Core	Thorium Blanket[a]	I_0	I_{235}	I_{efph}
Reference Case: All-Uranium, Out-In/ Scatter Loading	1	9.247				
	2	19.327	—	1.0000[b] (0.0%)	1.0000 (0.0%)	1.0000 (0.0%)
	3	28.198[c]				
Reference Case with Thorium Radial Blanket Reconstituted at 4 GWD/MT	1	9.587	4.009			
	2	17.890	8.119	0.9923 (0.7%)	0.9705 (3.0%)	0.9929 (0.7%)
	3	25.316	12.399			
Reference Case with Thorium Radial Blanket Reconstituted at 13 GWD/MT	1	9.746	4.435			
	2	18.169	8.801	0.9724 (2.8%)	0.9511 (4.9%)	0.9744 (2.6%)
	3	25.697	13.205			
Reference Case with Thorium Radial Blanket Reconstituted 19 GWD/MT	1	9.710	4.377			
	2	18.109	8.712	0.9765 (2.4%)	0.9551 (4.5%)	0.9782 (2.2%)
	3	25.614	13.059			

[a] Thorium blanket burnups are post-reconstitution. Reconstitution from lattice d-t to lattice d-s.

[b] Numbers in parentheses indicate percent improvement in uranium utilization relative to reference case.

[c] Since steady-state cores are analyzed, the EOC3 burnup = average discharge burnup (in all cases).

pre-reconstitution burnup case (4 GWD/MT). The cores with radial blankets of thorium reconstituted at 13 and 19 GWD/MT show only a small difference in the uranium savings associated with their use (0.5%), with the 13 GWD/MT core showing the highest uranium savings (5%).

It is interesting that in delaying reconstitution from 13 GWD/MT to 19 GWD/MT the improvement in uranium utilization only decreased by one-half percent. This relative insensitivity to the pre-reconstitution burnup of the reconstituted thorium blankets is useful, since it allows other considerations to determine the point of reconstitution and increases the flexibility of the fuel management scheme.

One option, not evaluated here, is the use of thorium pins, strategically placed in uranium fuel assemblies to act as "poisons", and, after discharging the assemblies, refabrication of the thorium pins into radial blanket assemblies. In the analysis of thorium pins among uranium assemblies in section 4.7 of Chapter 4, the inclusion of thorium pins uniformly distributed in the uranium assemblies resulted in a monotonic increase in the uranium usage as the fraction of thorium pins in these assemblies was increased. However by including thorium pins selectively (e.g. at assembly corners or near water holes) it should be possible to reduce the loss in uranium utilization in the pre-reconstitution phase, and

also gain power shaping advantages. This, basically, is the strategy adopted by GE for BWRs.

It is important to recognize that the merits of the reconstituted radial blankets must be compared to those of other blanket materials, without regard to the means used to produce the reconstituted thorium assemblies. This is because any advantage of the pre-reconstitution phase will not be affected by whether, after being discharged, the thorium is reconstituted or not. The decision to reconstitute would, in turn, be based on the performance of the reconstituted assembly relative to that of other options available to the fuel manager.

Comparing the results for radial blankets of reconstituted thorium assemblies in Table 5.1 with those of the blanket materials assessed in section 4.6.1 (of Chapter 4) shows that while the uranium savings from reconstituted thorium blankets (5%) are much higher than those from unreconstituted thorium blankets (1%) or from natural uranium blankets (2%), they are comparable to the savings from using the oldest batch (batch 3) at the core periphery (4%), and substantially lower than the savings by using spent fuel radial blankets (9%).

To conclude, the reconstitution of thorium for use as radial blanket assemblies in current burnup PWRs does not offer any advantages in uranium utilization that cannot be

derived from other options that appear to be more attractive. For example, the use of reconstituted thorium assemblies as radial blankets offers uranium savings comparable to those obtained from using the oldest batch on the core periphery(i.e. low-leakage fuel management). The use of spent fuel as a radial blanket remains the best option of those evaluated here (the same as increasing the number of in-core batches by one, and using low-leakage fuel management).

5.2.2 Reconstitution of Thorium in High Burnup PWRs

The three reconstituted thorium blankets evaluated in the previous section for use in current burnup PWRs were also evaluated in high burnup cores. The high burnup reference case was the same as that used in Chapter 4 (section 4.6.2) for evaluating low-leakage schemes and radial blankets of unreconstituted thorium, depleted and natural uranium.

The key results from this assessment are shown in Table 5.2. The use of the reconstituted thorium radial blankets results in uranium savings of between 6.5 and 7% in high burnup PWRs, as measured by the uranium utilization index I_{235}. The small spread of the uranium savings indicates that the sensitivity of the blanket performance to the pre-reconstitution burnup is very weak, even less than for

TABLE 5.2

Key Results for Reconstituted Blankets in High Burnup PWR Cores

	CYCLE	Average EOC Burnups GWD/MT		Uranium Utilization Indices		
		Uranium Core	Thorium Blanket[a]	I_0	I_{235}	I_{efph}
Reference Case: All-Uranium, Out-In/ Scatter Loading	1	8.832				
	2	21.072				
	3	31.716	—	1.0000[b] (0.0%)	1.0000 (0.0%)	1.0000 (0.0%)
	4	41.227				
	5	49.912[c]				
Reference Case with Thorium Radial Blanket Reconstituted at 4 GWD/MT	1	11.808	4.472			
	2	21.944	9.081			
	3	30.964	13.833	0.9483 (5.2%)	0.9352 (6.5%)	0.9508 (4.9%)
	4	39.172	18.653			
	5	46.756	23.515[c]			
Reference Case with Thorium Radial Blanket Reconstituted at 13 GWD/MT	1	11.838	4.863			
	2	22.001	9.658			
	3	31.049	14.460	0.9433 (5.7%)	0.9302 (7.0%)	0.9460 (5.4%)
	4	39.286	19.265			
	5	46.893	24.086			
Reference Case with Thorium Radial Blanket Reconstituted at 19 GWD/MT	1	11.798	4.874			
	2	21.919	9.624			
	3	30.932	14.355	0.9475 (5.3%)	0.9344 (6.6%)	0.9500 (5.0%)
	4	39.140	19.078			
	5	46.723	23.810			

[a]Thorium blanket burnups are post-reconstitution. Reconstitution from lattice d-t to lattice d-s.

[b]Numbers in parentheses indicate percent improvement in uranium utilization relative to reference case.

[c]Since steady-state cores have been analyzed, the EOC5 burnup = average discharge burnup (in all cases).

current PWR cores. This is because the initially high reactivities of the reconstituted thorium blankets lasts for a relatively small fraction of the total residence time of the blanket in the core. For most of its stay in the core the blanket is close to its asymptotic reactivity, as dictated by the reconstituted lattice spectrum.

A comparison of these results with those for radial blankets and low-leakage schemes in high burnup PWRs (Tables 4.11 and 4.12 in Chapter 4) shows that the maximum uranium savings from reconstituted thorium radial blankets (7%) are the same as those from using unreconstituted thorium assemblies. Furthermore, using spent fuel as radial blankets still promises the highest improvement (9%), relative to the same reference core.

In conclusion, the use of reconstituted thorium radial blankets in high burnup PWRs offers uranium utilization advantages almost exactly equal to those possible from using unreconstituted thorium blankets. Spent fuel radial blankets still offer the highest uranium savings of all the blanket materials considered.

5.3 Spectral Shift Control

The excess reactivity in PWRs is controlled by the introduction of soluble boron poison into the core. This method of reactivity control is very wasteful of neutrons since essentially no benefit is derived from the excess neutrons. Ideally, all the neutrons not required for maintaining criticality should be used to breed fissile material through fertile absorptions, which in turn would lead to higher discharge burnups and improved uranium utilization.

Conceptually such a scheme would involve continuously changing the effective fuel-to-moderator volume ratio (V_F/V_M) by the introduction of voids or D_2O in the core, or by mechanical movement of the fuel. At beginning of life a "dry" effective V_F/V_M would be chosen, just sufficient to attain criticality, and as the core is depleted the lattice would be made wetter, softening the neutron spectrum, and thus adding reactivity to the reactor. While the spectrum is hard, extra breeding of fissile material would take place, and this bred fuel would then be utilized to extend the cycle length. This scheme would therefore maximize conversion ratios and increase discharge burnups.

Continuous spectral shift control (SSC) is very difficult and expensive to implement in practice. It is assessed here to

provide the upper limit on the possible uranium savings from the use of thorium in discrete spectral shift cores. See reference (M-7) for a recent re-assessment of the use of the well-known H_2O/D_2O spectral shift control for PWRs. In the present analysis we will not deal with the specific means by which spectral shift is to be accomplished.

An exact calculation of this option is very expensive to perform. The problem is further complicated if there is more than one type of fuel in the core. A simple treatment has been developed to provide a measure of the advantage of SSC in cores containing thorium. This treatment is a modification of the model developed by Sefcik (S-4) to analyze continuous spectral shift in PWRs.

5.3.1 The Model for Continuous Spectral Shift

The variation in the unpoisoned reactivity of a uranium fuel sub-batch, ρ_U , as a function of the sub-batch burnup, B can be represented as:

$$\rho_U = \rho_0 - AB \qquad (5.1)$$

where,

ρ_0 = the extrapolated BOL reactivity,

B = the average sub-batch burnup, GWD/MT,

A = the slope of the reactivity versus burnup curve, MT/GWD.

The instantaneous reactivity balance for the sub-batch can be written in the form:

$$\rho_U = \frac{\nu F - a_{FIS} - a_{FER} - a_{FP}}{\nu F} \tag{5.2}$$

where νF is the fission neutron production rate, and a_{FIS}, a_{FER} and a_{FP} are the rates at which neutrons are lost to fissile, fertile and fission product absorptions, respectively. If the fission rate is held constant, then the bundle reactivity can be written as a linear combination of the fuel and fission product reactivities, i.e.

$$\rho_U = \rho_{FUEL} - \rho_{FP} \tag{5.3}$$

The expression for ρ_U in Eq. (5.3) can be further decomposed into an initial (zero-burnup) reactivity, ρ_0, and two burnup dependent components, which account for the changes in the fissile-fertile reactivity and that of the fission products. i.e.

$$\rho_U = \rho_0 - f_{FUEL}(B) - f_{FP}(B) \tag{5.4}$$

The fission product reactivity as a function of burnup is, to a good approximation, proportional to the fission product concentration, which in turn is directly proportional to the accumulated fuel burnup, B. Therefore, $f_{FP}(B)$ in Eq.(5.4) can be approximated as:

$$f_{FP}(B) \approx A_{FP}B \tag{5.5}$$

Substituting for f_{FP} in Eq.(5.4) from Eq.(5.5) and subtracting the result from Eq.(5.1) yields

$$f_{FUEL}(B) = (A - A_{FP})B \tag{5.6}$$

or, with $A_{FUEL} = A - A_{FP}$, in Eq.(5.6)

$$f_{FUEL}(B) = A_{FUEL} \cdot B \tag{5.7}$$

Substituting for the f's from Eq.(5.5) and (5.7) in Eq.(5.4) gives

$$\rho_U = \rho_0 - A_{FUEL}B - A_{FP}B \tag{5.8}$$

Equation (5.8) indicates that the uranium sub-batch reactivity is a linear super-position of a fissile-fertile term and a fission product term. This result is confirmed by calcu-

lations using the LEOPARD code, with and without the inclusion of fission products. The reactivity versus burnup data with fission products has the slope A. With the fission products supressed, the slope of the reactivity versus burnup data gives A_{FUEL}, and the difference of the two slopes yields A_{FP}. Table 5.3 shows the values for these constants, for a PWR core with an initial U-235 enrichment of 3 w/o, and a (fixed) V_F/V_M of 0.6.

For thorium sub-batches, the reactivity increases from a low initial value and attains an almost flat profile as a function of burnup, once the initial buildup has occured (typically in 16 MWD/MT). Due to this flat reactivity versus burnup profile, the thorium sub-batch can be approximated as contributing its peak reactivity, $\hat{\rho}_{Th}$, at all end-of-cycle points. This approximation clearly favors thorium. If, in addition, the equal power sharing approximation is made, and an EOC reactivity balance performed (following closely the approach used in Chapter 2, section 2.4), the average core discharge burnup, B_d, for an infinite reactor is given by the expression :

$$B_d = \frac{M_U(\rho_0 - \hat{\rho}_{Th}) + \hat{\rho}_{Th}}{M_U \{ \frac{n+1}{2n} A_{FP} + \frac{n+1}{2n} A_{FUEL} \}} \qquad (5.9)$$

TABLE 5.3

Key Parameters Used in the Analysis of SSC Cores*

ρ_0 = 0.22045

A = 0.91204×10^{-2}, MT/GWD

A_{FUEL} = 0.34456×10^{-2}, MT/GWD

A_{FP} = 0.56748×10^{-2}, MT/GWD

*From least-squares curve fits to LEOPARD results, as explained in the text.

where,

M_U = the fraction of each batch that is uranium,

($1 - M_U = M_{Th}$, the fraction that is thorium),

n = the number of batches in the core.

Since the equal power sharing approximation has been made, the discharge burnups of the uranium and thorium sub-batches will both be equal to B_d. In deriving Eq.(5.9) it was also assumed up to this point that the reactor was operating at a fixed fuel-to-moderator ratio, V_F/V_M, and that steady-state systems are of interest.

If the reactor were operating with spectral shift control (SSC), at BOC the core will start off dry and the lattice made continuously wetter till, at EOC, the wettest V_F/V_M will be reached. By the analysis of the EOC lattice, the constants in Eq.(5.9) are known, as is explained below.

The fission product concentration in the uranium sub-batch at each EOC state-point depends only on the burnup and the number of staggered reload batches, with A_{FP} evaluated under EOC lattice conditions with regard to V_F/V_M, which also determines the spectrum and the fission product spectrum-averaged cross-section values.

The remaining aspect of concern for the uranium sub-batches is the combined fissile-fertile term. The argument here is more subtle: In both SSC and infinite-number-of-batch operations (i.e. continuous refueling) no neutrons are wasted to control poison. Thus, as postulated by Sefcik, if the A_{FUEL} is computed based on EOC lattice conditions with the limit $n \to \infty$, then the same net fissile history will be traced out, and the same EOC state-point will be reached as in the SSC case. The results from using this methodology are in good agreement with more detailed neutronics calculations (see below).

For the thorium sub-batch the EOC reactivity state-point is a function of only the EOC V_F/V_M, because the reactivity versus burnup trace is approximated as being invariant with burnup.

Therefore in order to assess the continuous spectral shift option the $(n+1)/2n$ factor multiplying A_{FUEL} in Eq.(5.9) should be evaluated at the continuously renewed fuel burnup limit ($n \to \infty$). i.e.

$$\left(\frac{n+1}{2n} A_{FUEL} \right)_{SSC} = \lim_{n \to \infty} \left\{ \frac{n+1}{2n} A_{FUEL} \right\} = \frac{1}{2} A_{FUEL} \qquad (5.10)$$

with A_{FP} evaluated at the EOC V_F/V_M, for the SSC core.

Substituting Eq.(5.10) into Eq. (5.9) yields the expression for the average core discharge burnup under continuous spectral shift operation, $B_{d,SSC}$

$$B_{d,SSC} = \frac{M_U(\rho_0 - \hat{\rho}_{Th}) + \hat{\rho}_{Th}}{M_U \{ \frac{n+1}{2n} A_{FP} + \frac{1}{2} A_{FUEL} \}} \qquad (5.11)$$

As noted previously, by virtue of the equal power sharing approximation the uranium and thorium sub-batch burnups are equal.

5.3.2 Improvements in Uranium Utilization with SSC

Equation (5.11) can be used to evaluate SSC cores with and without thorium additions in an approximate manner. Here these calculations will be performed to quantify the uranium utilization advantages of the SSC cores.

The thorium lattice that reached the highest reactivity over its lifetime, and also had the highest bred U-233 content, namely lattice d-t, was also used in this analysis. As shown in Table 4.2 (of Chapter 4), the peak reactivity reached by this thorium lattice is -0.1567. Using this value for the peak reactivity of the thorium sub-batch and the data

listed in Table 5.3, Eq.(5.11) was used to calculate the discharge burnups for spectral shift reactors with different fractions of thorium in the core, and for both 3 and 4 batch cores. The results from these calculations are presented in Tables 5.4 and 5.5.

The reference case for these comparisons was a three-batch, all-uranium core at a fixed V_F/V_M of 0.6. The discharge burnup for this core was 36.257 GWD/MT, obtained from Eq.(5.9), using the data in Table 5.3.

Compared to the reference case, the all-uranium 3-batch SSC core shows a 8.8% improvement in uranium utilization. Since the two cores contain the same quantity of U-235, the unadjusted index I_0 and the index which adjusts for the U-235 differences in the test and reference cores, I_{235}, are equal. A recent Combustion Engineering assessment of all-uranium PWRs in a SSC mode of operation shows improvements in uranium utilization of 9.6% over a fixed V_F/V_M reference core (M-7).

The results in Table 5.4 also show that the SSC cores with thorium d-t inserts result in uranium savings, up to a maximum of 13.8% (at 20% thorium in the core) relative to the reference case, as measured by the index I_{235}. This corresponds to an improvement of 5.0% relative to the all-uranium SSC core.

TABLE 5.4

Key Results for Three-Batch Spectral Shift Control Cores with Thorium d-t Assemblies

n = 3

M_{Th}[a]	SSC Discharge Burnup $B_{d,ssc}$[b]	Uranium Utilization Indices[c]		
		I_0	I_{235}	I_{efph}
0%	40.038	0.9056	0.9056	0.9120
5%	38.540	0.8937	0.8896	0.9008
10%	36.876	0.8849	0.8763	0.8926
15%	35.016	0.8801	0.8665	0.8880
20%	32.923	0.8810	0.8617[d]	0.8889
25%	30.551	0.8901	0.8639	0.8975
30%	27.841	0.9116	0.8768	0.9177
35%	24.714	0.9536	0.9075	0.9569
40%	21.065	1.0327	0.9704	1.0302

[a]Percentage of thorium d-t assemblies in the spectral shift control (SSC) cores.

[b]Uranium and thorium discharge burnups are equal.

[c]Relative to three-batch all-uranium core at fixed V_F/V_M.

[d]Lowest uranium consumption as measured by index I_{235}.

TABLE 5.5

Key Results for Four-Batch Spectral Shift Control Cores with Thorium d-t Assemblies

n = 4

M_{Th}[a]	SSC Discharge Burnup $B_{d,ssc}$[b]	Uranium Utilization Indices[c]		
		I_0	I_{235}	I_{efph}
0%	41.834	0.8667	0.8667	0.8754
5%	40.269	0.8554	0.8515	0.8647
10%	38.530	0.8469	0.8387	0.8567
15%	36.587	0.8423	0.8293	0.8523
20%	34.400	0.8431	0.8246[d]	0.8531
25%	31.922	0.8519	0.8268	0.8614
30%	29.090	0.8725	0.8392	0.8809
35%	25.823	0.9127	0.8686	0.9187
40%	22.010	0.9884	0.9287	0.9893

[a]Percentage of Thorium d-t assemblies in the spectral shift control (SSC) cores.

[b]Uranium and thorium discharge burnups are equal.

[c]Relative to three-batch all-uranium core at fixed V_F/V_M.

[d]Lowest uranium consumption as measured by index I_{235}.

Increasing the number of batches in the SSC cores from 3 to 4 results in an improvement in uranium utilization of 13.3%, for the all-uranium core, compared to the 3-batch reference core. The maximum uranium savings from employing thorium in these 4-batch SSC cores are 17.5%. (at 20% thorium in the core). This is an improvement of 4.2% over the all-uranium 4 batch SSC core.

The results of this thorium-favoring evaluation indicate that using thorium in PWR cores which employ spectral shift control results in improvements in uranium utilization of about 5% over all-uranium SSC cores. While the savings increase as the number of batches in the core are increased, the incremental savings from thorium (i.e. the gain from adding thorium, compared to the all-uranium SSC core with the same number of batches) is reduced. From the results in Tables 5.4 and 5.5 it can also be inferred that high U-235 enrichments in the uranium sub-batch (for a constant number of batches in the core) favors thorium additions.

5.4 Small Fuel Assemblies in PWRs

The use of small fuel assemblies in PWRs offers, in principle, many advantages in implementing the newer fuel management

strategies and in improving the performance of existing schemes. In low-leakage fuel management schemes, for example, small fuel assemblies can be better deployed to reduce the power peaking in the core interior. This improves thermal margins and reduces the burnable poison loading and residuals, by reducing the quantity of burned fuel that needs to be loaded on the core periphery, making the remainder available for power flattening in the core interior. The power flattening effect is also enhanced by the more intimate mixing of the fuel assemblies that the smaller assemblies facilitate. In passing it is noted that for several decades BWRs have sucessfuly and economically made use of smaller fuel assemblies (8x8 versus 16x16 or 17x17 fuel pin arrays for PWRs).

The reduction in the size of PWR fuel assemblies can also lead to more effective radial blanketing, again because the fraction of blanket material can be reduced by about half (from 20% of the core volume to about 10%). Smaller assemblies can also reduce the amount of fuel prematurely discharged when an assembly must be removed from the core due to leaks or other defects.

A recent study by Combustion Engineering (M-6) assessed the smaller fuel assembly option for PWRs. The small assembly design considered is very much like the one assessed here. An improvement in uranium utilization of between 4 and 5 percent

is reported possible by using the smaller PWR assemblies. This overall improvement is composed of about 1.5% from improved poison residual, between 2 and 3% from radial blankets (the blanket material is not specified), and about 1% from the reinsertion of fuel that has not been irradiated its full lifetime. The CE study also points to the possibility of (small) indirect uranium savings, through reduced power peaking in the core.

In this analysis the small fuel assemblies analyzed were one quarter the size of standard PWR assemblies. The two assembly types are shown in Fig. 5.3. The small assemblies can be clamped together to reduce the impact of increased fuel shuffling that would result if such assemblies (four times as many as standard assemblies) were moved one at a time. The clamped assemblies could be dissociated and recombined in different configurations when required.

As before, the analysis is divided into two parts. The first examines the potential advantages of small assemblies in the core interior, while the second quantifies the effects of employing small assemblies concurrently with low-leakage or radial blanket fuel management.

There were two main steps involved in extending our models for the analysis of this option: calculating a value for the

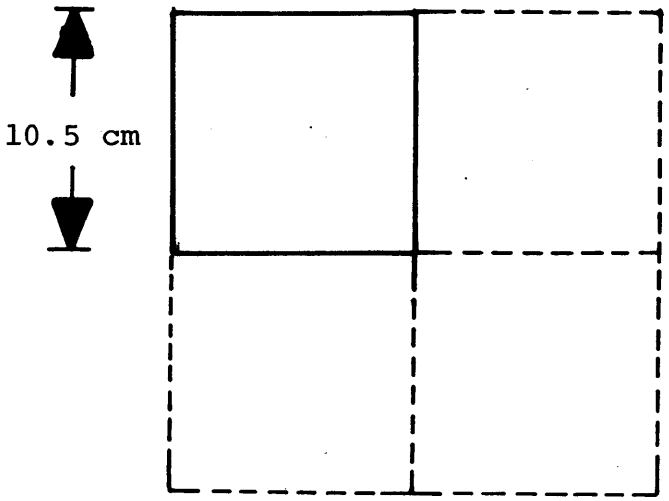

Small Fuel Assembly for PWRs
(8 x 8 = 64 fuel rods/assembly)

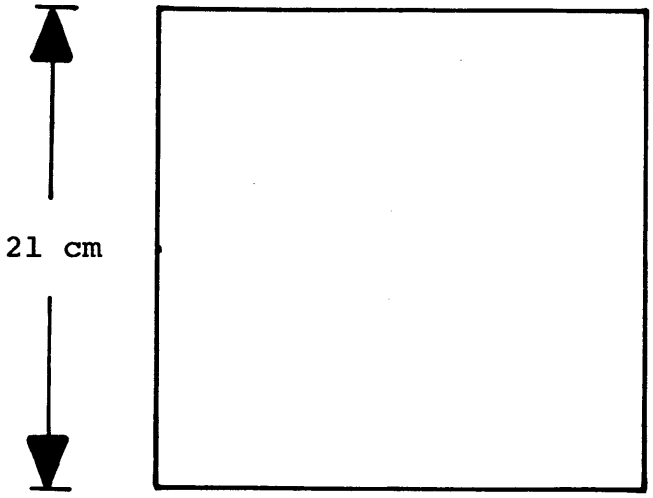

Standard PWR Assembly
(16 x 16 = 256 fuel rods/assembly)

Fig. 5.3 Small and Standard PWR Fuel Assemblies.

theta constant for small assemblies, and determining the correct treatment of radial leakage.

The theoretical estimate for theta for small assemblies is 1.36 (see Appendix C). A series of PWR cores with these small fuel assemblies were modelled in different fuel loading configurations at approximate end-of-cycle conditions, using the PDQ-7 code. From the resulting core maps a set of thirty 3x3 (small) assembly clusters were used to calculate θ, following closely the approach used for the standard fuel assemblies in Chapter 3. The value for θ from this analysis was 1.33, with an average error of 1.8% and a maximum error of 2.4% in the prediction of power sharing.

In employing smaller assemblies, one of the advantages is expected to be from more flexible low-leakage and radial blanket schemes, which retain the advantages that these options offer in cores with standard assemblies but with significantly reduced power peaking. This was further reinforced by the observation that the leakage from the core is dominated by the power being produced in the last 10 cm. or so of fuel at the edge of the core. This characteristic length for neutron leakage corresponds almost exactly to the width of the small fuel assemblies examined here. Appendix C includes evidence to support the assertion that core leakage can be modelled more accurately by using two core leakage constants when dealing

with small assemblies, instead of the one α that was used in the case of standard assemblies. Stated differently, for small assemblies the radial leakage is a function of the power being produced by the (small) assemblies occupying the core periphery and the row of (small) assemblies adjacent to this peripheral fuel. The fuel at the core periphery, termed the "principal peripheral assemblies", dominates the radial neutron leakage, while the "secondary peripheral assemblies" (one row in) also make a small contribution. The core leakage constant for the principal peripheral region, α_1, is in general an order of magnitude more than α_2, the core leakage constant for the secondary peripheral region. The two core leakage constants for the Combustion Engineering System-80^{TM} core used in this analysis were deduced from published data on the System-80^{TM} core and from the PDQ-7 generated results for cores with small assemblies. The values are:

$$\alpha_1 = 0.6690$$

$$\alpha_2 = 0.0326$$

The reader is referred to Appendix C for details.

5.4.1 Small Fuel Assemblies in the Core Interior

In this section the potential of smaller fuel assemblies in the core interior will be assessed. The main aim will be to analyze the effects on discharge burnup and power-sharing from

the deployment of the small assemblies. An infinite reactor is considered for this purpose and the analysis is performed using the SPILBAC code.

Table 5.6 shows the main results from the modelling of current burnup PWR cores with the small fuel assemblies. The previously analyzed current burnup PWR core with standard assemblies (also in an infinite reactor) serves as the reference case. The main point of interest is that while the cycle burnups in the two cores differ substantially, the discharge burnups differ by less than 0.5%, suggesting little or no direct uranium utilization advantage associated with using smaller fuel assemblies in the core interior. However, a comparison of the batch-averaged power densities shows that the small assemblies reduce the BOC maximum batch-averaged power peak by about 2.5%, and have a distinct power flattening effect throughout the core.

It is worth emphasizing that, since the models used here deal exclusively with batch averages, the power flattening effect of the small assemblies would be more pronounced if the hottest pin or assembly from the two cores was compared. A flatter power profile can, of course, lead to small savings in uranium utilization through higher power rating and improved steam-side performance (L-2).

TABLE 5.6

Key Results from the Comparison of Regular and Small PWR Assemblies in the Core Interior (Standard Burnup)

	CYCLE 1	CYCLE 2	CYCLE 3
1. REFERENCE CORE (REGULAR PWR ASSEMBLIES)			
EOC Burnup—GWD/MT, B_{EOC}	14.043	25.720	35.852**
Cycle-Averaged Batch Power Density, q_{CA}*	1.187	0.984	0.859
BOC Batch Power Density, q_{BOC}*	1.229	0.972	0.829
EOC Batch Power Density, q_{EOC}*	1.172	0.989	0.870
2. PWR WITH SMALL ASSEMBLIES			
EOC Burnup—GWD/MT, B_{EOC}	13.818	25.576	35.917**
Cycle-Averaged Batch Power Density, q_{CA}*	1.166	0.989	0.875
BOC Batch Power Density, q_{BOC}*	1.199	0.981	0.851
EOC Batch Power Density, q_{EOC}*	1.154	0.992	0.884

*Fraction of core-averaged power density.

**EOC3 burnup = discharge burnup, since the steady-state is being analyzed.

Table 5.7 compares the results for high burnup PWR cores with standard and small fuel assemblies. Again the increase in discharge burnups due to the small assemblies is negligible. The reduction in the maximum batch-averaged power density from using the small assemblies is 4.5% compared to the reference case.

The insensitivity of the discharge burnup to the improvement in power sharing (through the use of smaller assemblies) is interesting and somewhat counter-intuitive. A closer look at the power densities provides the solution. When the power-sharing is improved the fresher fuel batches burn less than before while the burnup of the older fuel batches is enhanced. This effect, which acts to increase discharge burnups by conserving the higher reactivities of the fresher batches while burning more of the older batches, is undermined by the increased contribution of the older batches (through their higher power fractions) to the system or core reactivity, which is the power-weighted sum of the individual batch reactivities. The net effect is that while the batch burnups can be substantially different, the discharge burnups are not.

To conclude, the deployment of smaller fuel assemblies in the core interior does not have adirect advantage in terms of improved uranium utilization but offers the potential for

TABLE 5.7

Key Results from the Comparison of Regular and Small PWR Assemblies in the Core Interior (High Burnup)

	CYCLE 1	CYCLE 2	CYCLE 3	CYCLE 4	CYCLE 5
1. REFERENCE CORE (REGULAR PWR ASSEMBLIES)					
EOC Burnup—GWD/MT, B_{EOC}	16.143	29.496	41.204	51.753	61.295**
Cycle-Averaged Batch Power Density, q_{CA}*	1.319	1.092	0.952	0.855	0.783
BOC Batch Power Density, q_{BOC}*	1.401	1.099	0.932	0.823	0.745
EOC Batch Power Density, q_{EOC}*	1.292	1.090	0.959	0.865	0.795
2. PWR WITH SMALL ASSEMBLIES					
EOC Burnup—GWD/MT, B_{EOC}	15.671	28.997	40.843	51.620	61.446**
Cycle-Averaged Batch Power Density, q_{CA}*	1.278	1.087	0.966	0.871	0.803
BOC Batch Power Density, q_{BOC}*	1.338	1.095	0.948	0.847	0.773
EOC Batch Power Density, q_{EOC}*	1.276	1.085	0.967	0.879	0.813

*Fraction of core-averaged power density.

**EOC5 burnup = discharge burnup, since steady state is being analyzed.

small (less than 2%) indirect improvements in uranium usage through flatter power profiles and improved thermal margins.

5.4.2 Smaller Fuel Assemblies and Low-leakage Schemes in Current PWR Cores

As mentioned earlier, the main advantage from smaller fuel assemblies can be expected to come from better low-leakage fuel management than is possible using standard PWR assemblies. Here this option is assessed for current burnup PWRs and the advantage quantified.

The results for standard burnup PWRs employing smaller fuel assemblies and low-leakage loadings are shown in Table 5.8. The standard fuel assembly core with out-in/scatter fuel management analyzed in Chapter 4 serves as the reference case. The complete range of low leakage schemes is investigated here, with each of two burned batches as the principal peripheral batch. The results for the out-in/scatter core with small assemblies are also included. In all cases fresh fuel was modelled as the secondary peripheral batch. This was done to minimize power peaking in the core interior.

A comparison of the results in Table 5.8 with those for low-leakage schemes with standard PWR assemblies (Table 4.9 in

TABLE 5.8

Key Results for Small Fuel Assemblies in Current PWRs with Out-In/Scatter and Low Leakage Fuel Loading Schemes

PRINCIPAL PERIPHERAL BATCH	END OF CYCLE BATCH BURNUP (GWD/MT)			URANIUM UTILIZATION INDICES	
	CYCLE 1	CYCLE 2	CYCLE 3[d]	I_{0}, I_{235}	I_{efph}
1 (Fresh Fuel)[a] Reference Case	9.247	19.327	28.198	1.0000	1.0000
1 (Fresh Fuel)[b]	9.206	19.181	28.115	1.0030 (-0.3%)[c]	1.0028 (-0.3%)
2[b]	11.369	19.945	29.024	0.9715 (2.9%)	0.9736 (2.6%)
3[b] (Oldest Fuel)	11.483	21.576	29.377	0.9599 (4.0%)	0.9628 (3.7%)

[a]Reference core with regular-sized PWR assemblies (Out-In/Scatter).

[b]Core has small assemblies. Fresh fuel is secondary peripheral batch.

[c]Percentage savings in uranium, relative to the reference case.

[d]EOC3 burnup = discharge burnup.

Chapter 4) show that the uranium savings from the smaller assemblies are comparable to the savings from the equivalent strategy using standard assemblies. For example, with the oldest fuel on the core periphery the standard assembly core improves uranium utilization by 4.2% while for the small assembly core with the oldest fuel as the principal peripheral batch the uranium savings are 4.0% relative to the same reference case. The uranium saving can be improved further in the small assembly core by using burned fuel in the secondary peripheral region, but the additional gain is expected to be small since the secondary peripheral batch is effectively in the core interior.

While the uranium utilization advantage using small assemblies is comparable to that for standard assemblies, the power peaking in the smaller assembly cores is substantially lower. For example, with batch 3 as the principal peripheral batch, there is a 4% reduction in the maximum batch-averaged BOC power density in the small assembly core relative to the same loading scheme with standard assemblies. As mentioned earlier, the model used here treats batch-averages, and therefore assembly-wise power differences are averaged-out. An analysis of these small fuel assemblies which accounts for individual assemblies can be expected to show much larger power flattening effects, when the hottest assemblies (or pins) are considered.

In order to study the efficacy of radial blankets in PWRs with smaller fuel assemblies, a small assembly radial blanket of thorium lattice d-f (see Chapter 4, section 4.2) was modelled on the SPILBAC code as occupying the principal peripheral region. The key results from this analysis are shown in Table 5.9, with the out-in/scatter core with standard sized assemblies as the reference case. The results for radial blankets with standard assemblies are included for comparison.

In the regular-assembly current-burnup cores the inclusion of a thorium radial blanket resulted in a maximum improvement in uranium utilization of about 1%, as measured by the index I_{235}. For the thorium radial blanket of small assemblies the same index predicts an improvement in uranium utilization of about 5%. The large increase is primarily due to the almost ideal deployment of the radial blanket which the smaller assemblies facilitate. The small assemblies also reduce the batch-averaged maximum power density (BOC) by about 6% compared to the radially blanketed core with standard assemblies.

TABLE 5.9

Key Results for a Thorium Radial Blanket in Current Burnup PWR Cores Employing Small Fuel Assemblies

	CYCLE	Average EOC Burnups GWD/MT		Uranium Utilization Indices		
		Uranium Core	Thorium Blanket	I_0	I_{235}	I_{efph}
Reference Case (Regular-Sized Assemblies, Out-In/Scatter Fuel Loading)	1	9.247	—	1.0000[a] (0.0%)	1.0000 (0.0%)	1.0000 (0.0%)
	2	19.327				
	3	28.198[b]				
Reference Case with Radial Blanket of Thorium (d-f) (Regular-Sized Assemblies)	1	9.449	3.317	1.0135 (-1.4%)	0.9912 (0.9%)	1.0125 (-1.3%)
	2	17.641	7.204			
	3	24.975[b]	11.396			
Core with Radial Blanket of Thorium (d-f), and Small Assemblies	1	10.477	3.376	0.9584 (4.2%)	0.9491 (5.1%)	0.9617 (3.9%)
	2	19.802	7.171			
	3	28.178[b]	11.182			

[a] Numbers in parentheses indicate percent uranium savings over reference case.

[b] EOC3 burnup = discharge burnup.

5.4.3 Smaller Fuel Assemblies and Low-leakage Schemes in High Burnup PWR Cores

The assessment performed above for current burnup PWRs was also done for high burnup PWR cores. Table 5.10 shows the key results for low-leakage schemes with the small assemblies in such cores. The high burnup core with out-in/scatter fuel management serves as the reference case. Each of the 5-batches in the core was modelled as the principal peripheral batch, with fresh fuel as the secondary peripheral batch in all cases.

The results in Table 5.10 indicate that again the direct savings in uranium from low-leakage schemes are almost identical to those obtained from low-leakage schemes with standard PWR assemblies (Table 4.11 in Chapter 4). The power peaking is however significantly reduced by the use of small assemblies. For example, in the core with the oldest batch on the periphery the batch-averaged maximum power density is about 7% lower in the small assembly case, relative to the same case with standard assemblies.

A radial blanket of small thorium (lattice d-f)assemblies was also modelled to assess the efficacy of small assembly radial blankets in high burnup cores. As in the current burnup core, the small assembly radial blanket occupied the

TABLE 5.10

Key Results for Small Fuel Assemblies in High Burnup PWRs with Out-In/Scatter and Low Leakage Fuel Loading Schemes

PRINCIPAL PERIPHERAL BATCH	END OF CYCLE BURNUP (GWD/MT)					URANIUM UTILIZATION INDICES	
	CYCLE 1	CYCLE 2	CYCLE 3	CYCLE 4	CYCLE 5[d]	I_0, I_{235}	I_{efph}
1 (Fresh Fuel)[a] Reference Case	8.832	21.072	31.716	41.227	49.912	1.0000	1.0000
1 (Fresh Fuel)[b]	8.940	20.860	31.429	41.024	49.872	1.0008 (-0.1%)[c]	1.0008 (-0.1%)
2[b]	13.128	21.902	32.634	42.380	51.365	0.9717 (2.8%)	0.9731 (2.7%)
3[b]	13.233	24.998	33.033	42.823	51.864	0.9624 (3.8%)	0.9642 (3.6%)
4[b]	13.319	25.161	35.722	43.204	52.275	0.9548 (4.5%)	0.9570 (4.3%)
5[b] (Oldest Fuel)	13.407	25.308	35.920	45.590	52.624	0.9485 (5.2%)	0.9510 (4.9%)

[a]Regular core with standard PWR assemblies and Out-In/Scatter fuel management.

[b]Core has small assemblies; fresh fuel in secondary peripheral batch.

[c]Percent savings in uranium relative to reference case.

[d]EOC5 burnup = discharge burnup.

principal peripheral region, with fresh (uranium) fuel in the secondary peripheral region. The key results from this assessment are listed in Table 5.11, with the out-in/scatter high burnup core with standard assemblies as the reference core. The results for the thorium (d-f) radially blanketed core with standard assemblies (from Chapter 4) is included for comparison.

In cores with regular PWR assemblies the inclusion of this thorium radial blanket resulted in a uranium saving of 6.1%, as measured by the index I_{235}. In the radially blanketed core with small assemblies the same index shows a saving of 7.7%. This increase of 1.5% in uranium utilization is directly attributable to the increased effectiveness of radial blankets when used concurrently with smaller fuel assemblies. The radially blanketed core with small assemblies also has a batch-averaged maximum power density which is 8% lower than in the radially blanketed core with standard assemblies.

To conclude, the efficacy of radial blankets in high burnup PWRs is increased by the concurrent deployment of small fuel assemblies in the core and power peaking effects are also reduced.

TABLE 5.11

Key Results for Thorium Radial Blanket in High Burnup PWR Cores with Small Fuel Assemblies

	Cycle	Average EOC Burnups GWD/MT		Uranium Utilization Indices		
		Uranium Core	Thorium Blanket	I_0	I_{235}	I_{efph}
Reference Case: (Standard PWR Assemblies, Out-In/ Scatter Loading)	1	8.832				
	2	21.072				
	3	31.716	—	1.0000[a] (0.0%)	1.0000 (0.0%)	1.0000 (0.0%)
	4	41.227				
	5	49.912[b]				
Reference Case with Radial Blanket of Thorium (d-f) and Standard Fuel Assemblies	1	11.791	3.806			
	2	21.910	8.284			
	3	30.914	13.051	0.9527 (4.7%)	0.9395 (6.1%)	0.9550 (4.5%)
	4	39.108	17.922			
	5	46.678[b]	22.846			
Core with Radial Blanket of Thorium (d-f), and Small Fuel Assemblies	1	12.678	3.741			
	2	23.813	7.951			
	3	33.795	12.355	0.9285 (7.2%)	0.9230 (7.7%)	0.9319 (6.8%)
	4	42.922	16.835			
	5	51.385[b]	21.368			

[a] Numbers in parentheses indicate percent uranium savings relative to reference case.

[b] Cycle 5 EOC burnup = discharge burnup.

5.5 Chapter Summary

In this chapter a second set of evaluations were performed, of options considered more difficult to retrofit in existing PWRs. The options examined were; (1) the reconstitution of thorium assemblies and their reinsertion into the core as radial blankets, (2) the concept of spectral shift control in all-uranium cores and those with small quantities of thorium, and, (3) the use of smaller fuel assemblies in PWRs. The focus was on the quantification of the uranium utilization potential of each scheme relative to the reference cases typical of today's PWRs. For the most part, the methods developed and applied previously in this work were also used for these analyses.

For current burnup PWR cores reconstituted thorium blanket assemblies result in uranium savings of about 5% relative to an out-in/scatter all-uranium reference case. These savings are higher than those obtained (see Chapter 4) from using un-reconstituted thorium assemblies (1%), or natural uranium assemblies (2%), as radial blankets. The uranium savings from using reconstituted thorium are comparable to those from using the oldest batch (batch 3) on the core periphery (4%), but much lower than the savings from using spent fuel radial blankets (9%), relative to the same reference case.

In high burnup cores the use of reconstituted thorium resulted in a maximum improvement in uranium utilization of about 7% compared to an out-in/scatter all-uranium reference case. This saving is equal to that obtained (in Chapter 4) from using un-reconstituted thorium radial blankets and lower than that from using spent fuel as a radial blanket (9%).

Thus reconstitution of thorium assemblies does not offer any advantages from a uranium utilization point of view, that cannot be realized by using other options which would be much easier to implement.

A simple model was developed and applied to assess the maximum potential of using spectral shift control (SSC) in PWRs, with particular emphasis on the concurrent use of thorium. The model was based on the prior work of Sefcik (S-4).

The PWR cores employing SSC evaluated here showed uranium savings of about 9% compared to the reference (fixed fuel-to-moderator ratio) cores. The inclusion of the best thorium lattice into the SSC core improved uranium utilization by a further 5%. It was also shown that increasing the number of batches does not favor the addition of thorium to a core.

The use of smaller fuel assemblies in PWRs was also evaluated. The assembly size considered was one quarter that of current PWR assemblies (i.e roughly equivalent to current BWR practice). The smaller assemblies were evaluated for use in the core interior and the on the core periphery. In the interior of the core the use of the smaller fuel assemblies did not result in any uranium utilization advantages. The small assemblies can, however, be expected to lead to indirect uranium savings through flatter power histories, improved thermal margins and lower burnable poison requirements and residuals.

The use of the small assemblies was found to greatly improve the performance of radial blankets. Thorium radial blankets of small assemblies resulted in uranium savings of about 5% in current burnup PWRs. This should be compared to the 1% savings obtained in Chapter 4 by using thorium radial blankets of standard sized PWR assemblies. For high burnup cores, thorium radial blankets of small assemblies improved uranium utilization by 2% compared to the radially blanketed PWR with standard PWR assemblies and the same blanket material. However, these results must be viewed from the perspective of our general finding that blankets of spent fuel generally out-perform thorium blankets.

Apart from any association with thorium utilization, the use of small assemblies in PWRs offers advantages that are especially useful for the newer low-leakage fuel management schemes being deployed or considered. The efficacy of the radial blankets is increased and their unfavorable impact on the power shape in the core interior is reduced when small assemblies are used.

CHAPTER 6

SUMMARY, CONCLUSIONS AND RECOMMENDATIONS

6.1 Introduction

In recent years there has been a growing interest in increasing uranium utilization in light water reactors (LWRs). The conviction of some to defer reprocessing because of concern over the resulting commerce in weapons-usable material, the slower than anticipated progress towards the deployment of fast breeder reactors (FBRs), and a reassessment of the near-term cost-effectiveness of fuel recycle restricted to thermal reactors, have all pointed to the need to make more efficient use of the world's uranium resources. This need is also compatible with the desire of utilities to extend their reactors' burnup cycles and to improve fuel reliability.

The present work was done under the sponsorship of the LWR Technology Assessment Program for Improved Uranium Utilization of the U.S. Department of Energy, and was part of a nation-wide effort to analyze fuel management options which can improve uranium utilization in LWRs.

The primary objective of the research reported here was to investigate the selective use of thorium in pressurized water reactors (PWRs) as a uranium conservation strategy for the once-through fuel-cycle. Thus, the criterion of merit applied was uranium utilization: the energy extracted from a batch of steady-state reload fuel per unit mass of natural uranium required to produce the fuel.

Thorium is potentially an inexpensive and relatively abundant energy resource. It is believed that thorium reserves at least equal, and may well exceed, those of uranium. Thus there has been a long-standing interest in the use of thorium in PWRs and other thermal reactors in the recycle mode. However, prior investigation of thorium in PWRs on the once-through cycle has been very limited. Furthermore, at the conceptual level, the suggested ways in which thorium might be used in the once-through cycle, have increased both in number and complexity. All these factors motivated the present analysis.

A wide spectrum of thorium-related uranium conservation options were investigated in the present work; these are: internal and radial blankets of thorium, thorium pins dispersed within uranium fuel assemblies, the use of thorium in PWRs operating with spectral shift control, the reconstitution and reinsertion of thorium blanket assemblies, and the

use of smaller fuel assemblies for PWRs (in cores with and without thorium). The assessments were performed for both current and high burnup PWR cores in their steady-state.

Particular emphasis was placed on making all assessments of uranium utilization on a consistent and clearly defined basis. Relative comparisons between competing alternatives were also preferred: fuel management options which can be regarded as reasonable substitutes for employing thorium (or those which otherwise facilitate useful comparisons) were analyzed in parallel with the thorium designs.

The sections which follow outline the methods used and summarize the principal findings of this research effort.

6.2 The Methodology and Theoretical Bases

The methods used in these assessments rely, for the most part, on state-of-the-art neutronics computer codes (such as LEOPARD and PDQ-7) coupled with batch-wise core depletion models based on "group-and-one-half" theory. These models were verified using detailed computer analyses on the Combustion Engineering System-80^{TM} and the Maine Yankee reactors.

The essence of the "group-and-one-half" model is the approximation that thermal neutrons are absorbed at the point of their removal from the fast group. Stated differently, in this model the thermal leakage is neglected by setting $\nabla^2\phi = 0$ for the thermal group in the two neutron energy group model. With the additional approximation that the energy released per fission (κ/ν) is constant (with burnup and for fissile species of interest), the basic power sharing algorithms used in this work can be derived merely by introducing approximations, at various levels of sophistication, for the fast neutron leakage term. Many applications for these power sharing prescriptions were investigated.

In studies dealing with uranium utilization, the main quantities of interest are the discharge burnups in the cores being analyzed. To determine the discharge burnup, one must compute the power history of a given fuel batch subjected to a defined in-core environment. The "group-and-one-half" model yields the following relation for the batch-wise power split:

$$f_i \simeq \frac{\bar{f}}{1 - \theta_i \rho_i} \tag{6.1}$$

where,

f_i = the fraction of core power provided by batch i.

$\bar{f}$ = 1/n, the fraction of core power delivered by the core-averaged batch.

ρ_i = the average reactivity of batch i.

θ_i = the reactivity-power coupling factor (RPCF) for the batches in the core; this is a function of the size of the assembly and the neutron migration area.

n = the number of batches in the core.

The importance of this relation lies in the fact that the instantaneous power sharing determines the instantaneous burnup of each batch, and the cumulative power fractions determine where, and how, the end-of-cycle points are reached, and therefore what burnup is accumulated by each batch.

The batch-wise power sharing relation embodied in Eq. (6.1) was verified using detailed PDQ-7 core-maps computed especially for this purpose, and published results for the CE System-80^{TM} and the Maine Yankee reactors. Figures 6.1 and 6.2 show (the inverse of) the batch-averaged power densities as a function of the average batch reactivity, for these two cores. As can be seen, a constant value of θ can be defined which adequately characterizes the fuel in a given core. The empirical values of θ determined from such curve-fits were found to be in good agreement with the theoretical estimates derived using the group-and-one-half model. The power sharing prescription was extended to allow two or more distinct fuel types (sub-batches) to be part of a steady-state reload batch.

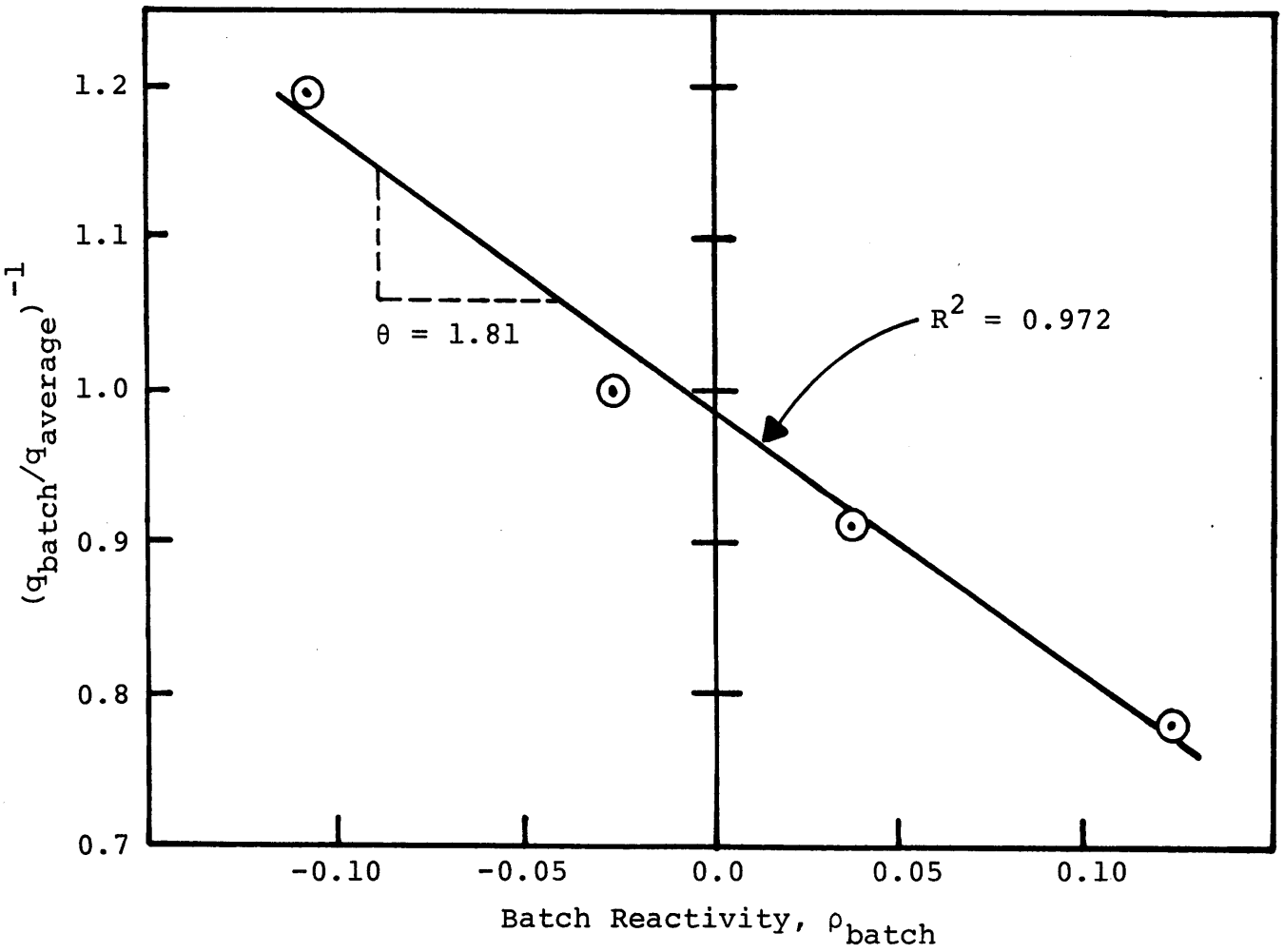

Fig. 6.1 Verification of the Batch Power Sharing Algorithm for the Combustion Engineering System-80™ Core.

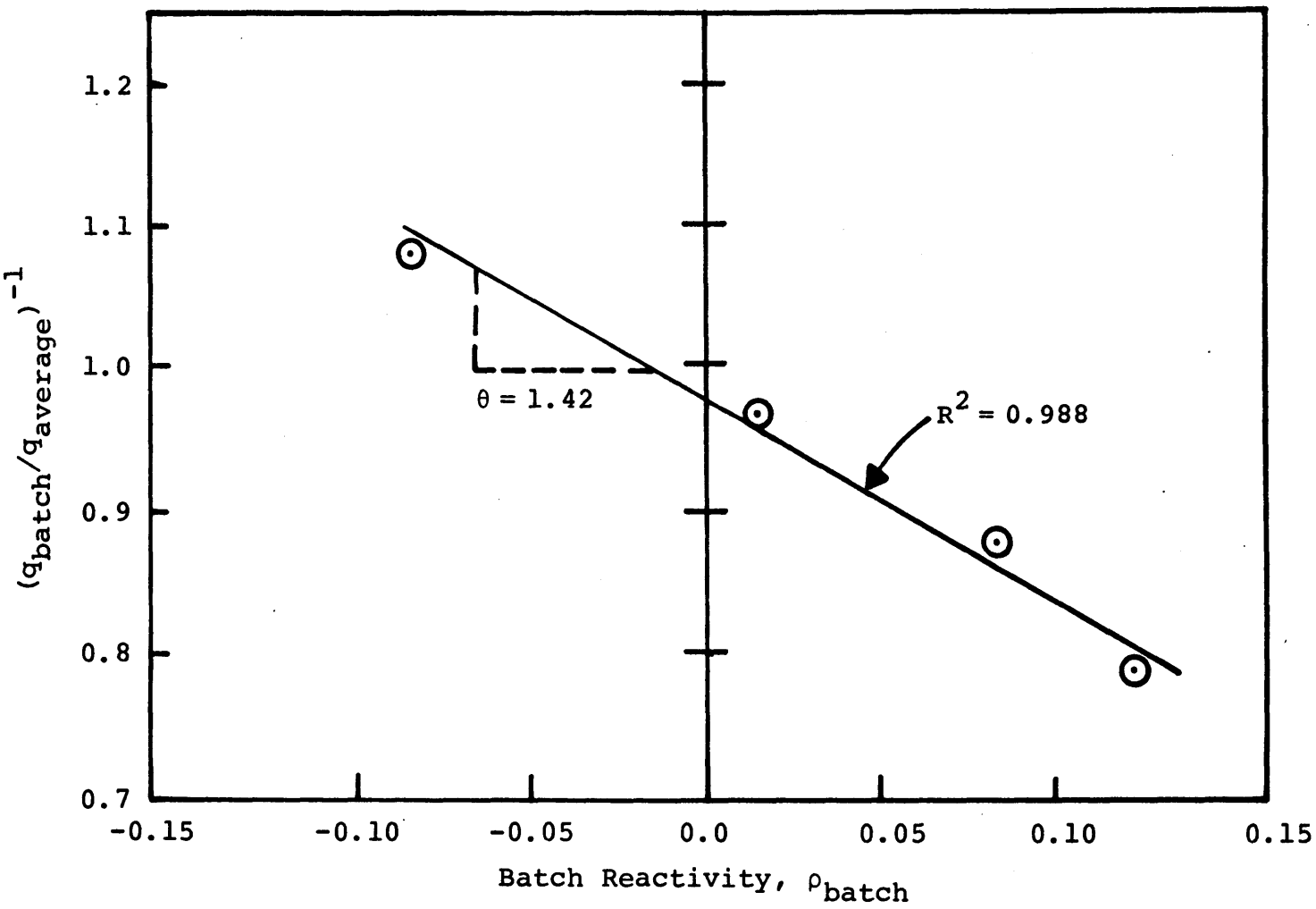

Fig. 6.2 Verification of the Batch Power Sharing Algorithm for the Maine Yankee Cycle 4 Redesign.

Finally the radial neutron leakage from the core was successfully modelled in terms of the power generated at the core periphery and a core leakage constant, α. This relation was also tested against detailed neutronics calculations and incorporated into the model.

6.3 The SPILBAC Code

The generalized methodology for sub-batch power sharing and core depletion was incorporated into a computer program: SPILBAC. The code is designed to calculate reactivity-limited cycle and discharge burnups, and power fractions for the sub-batches of a specified steady-state reload batch.

The input to SPILBAC consists of the number of reload batches in the core, the fraction of each of the two sub-batches in the reload batch, reactivity versus burnup data for the two sub-batches, the RPCF (or θ constants), and the core leakage constant (α). The user also specifies which sub-batch is on the core periphery, and during which cycle. The burnup step-size (after which the sub-batch power fractions are recalculated and the core power renormalized), and the convergence criterion applied to the sub-batch cycle burnups, are also input variables.

The flexibility of the SPILBAC code allows the modelling of many different fuel management strategies of contemporary interest. For example, one of the sub-batches can be uranium fuel and the other thorium or depleted uranium (as a radial or internal blanket).

Figure 6.3 shows the flowchart for the SPILBAC code. The numerical scheme used in the code is unconditionally convergent, and the relative results for uranium utilization are fairly insensitive to the main input variables, namely the RPCFs and the core leakage constant.

6.4 Uranium Utilization Indices

The basic (unadjusted) dimensionless index for uranium utilization, I_0, comparing the uranium utilization of a test case to a reference case, is defined as the ratio:

$$I_0 = \frac{U}{U_R} = \frac{B_R}{(M_U B_U + M_{Th} B_{Th})/M_U} \qquad (6.2)$$

where,

U, U_R = the uranium usage (STU_3O_8/MWD) for the test and the reference cores respectively. It is assumed that the two have the same uranium enrichment.

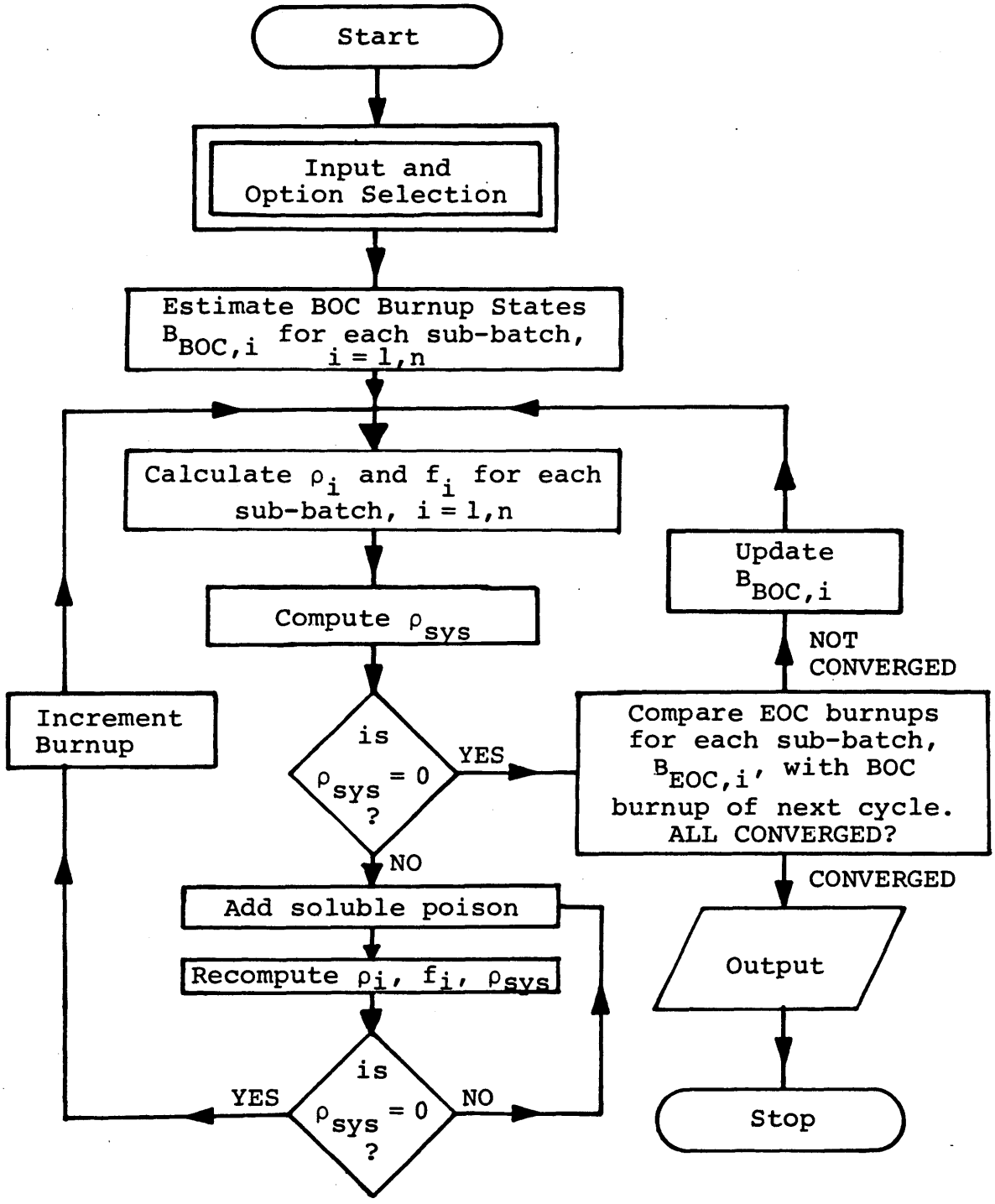

Fig. 6.3 A Flow chart for the SPILBAC Code.

M_U, M_{Th} = the fraction of uranium and thorium (as sub-batches) in the test core. Note that $M_U + M_{Th} = 1.0$.

B_R = the average discharge burnup of the reference (all-uranium) core, GWD/MT.

B_U, B_{Th} = the uranium and thorium average discharge burnups in the test core, GWD/MT.

An important semantic note is in order here. Some investigators compute the energy extracted from a given amount of natural uranium, and others deal with its inverse - as we do here. Thus, I_0 measures relative uranium requirements. If I_0 is 0.98, for example, this indicates a uranium saving in the test core over the reference core of 2 percent; Conversely, an I_0 value of 1.03 indicates a 3 percent loss in uranium utilization. The unadjusted uranium utilization index, I_0, can be analytically adjusted (using prescriptions developed as part of the present study) to give the uranium saving (or loss) for cases when the test and the reference cores are required to have the same U-235 loading (and therefore natural uranium requirement). The index derived under this constraint is termed I_{235}. Similarly, the uranium utilization index derived under the premise that the test and the reference cores deliver equal effective full power hours (efph) is termed I_{efph}.

Of the three indices for measuring uranium utilization (i.e I_0, I_{235}, and I_{efph}), the index I_{235} is particularly important

for studies of the present type. This is because it gives the uranium utilization when the test and the reference cores have the same natural uranium commitment per reload batch. Unless otherwise stated, this index is used for the quantification of the uranium savings in this chapter.

6.5 Thorium Lattices Investigated

A total of 12 thorium oxide lattices were investigated, encompassing a wide-range of fuel-to-moderator ratios (V_F/V_M) and fuel pin diameters, using the LEOPARD code.

The peak thorium reactivity and other information for the 12 lattices is shown in Table 6.1. A two-letter designator was used for identifying the lattices. These designators are also included in the Table.

6.6 The Preliminary Assessment of Thorium

An analytical model was developed to provide a preliminary screening mechanism for assessing the thorium lattices under investigation, such that subsequent detailed analyses could be concentrated on the more promising variations. Since all thorium lattice configurations with uranium-saving potential

TABLE 6.1

Important Characteristics of Thorium Lattices Analyzed Using LEOPARD

Thorium Fuel Pin Diameters, D_f	Fuel-to-Moderator Volume Ratio		
	$V_F/V_M = 1.0$	$V_F/V_M = 0.60$	$V_F/V_M = 0.20$
$D_f = 0.025$ cm			
Lattice[a]	d-h	s-h	w-h
$\hat{\rho}$[b]	-0.1653	-0.1715	-0.3044
$\hat{X}$[c]	2.07	1.81	1.53
$B_{\hat{\rho}}$[d]	25.0	25.0	30.0
$D_f = 0.5$ cm			
Lattice	d-t	s-t	w-t
$\hat{\rho}$	-0.1567	-0.1702	-0.3292
$\hat{X}$	1.69	1.53	1.33
$B_{\hat{\rho}}$	25.0	25.0	25.0
$D_f = 1.0$ cm			
Lattice	d-s	s-s	w-s
$\hat{\rho}$	-0.1676	-0.1874	-0.3761
$\hat{X}$	1.65	1.45	1.28
$B_{\hat{\rho}}$	20.0	20.0	25.0
$D_f = 2.0$ cm			
Lattice	d-f	s-f	w-f
$\hat{\rho}$	-0.1607	-0.1814	-0.4509
$\hat{X}$	1.46	1.34	1.23
$B_{\hat{\rho}}$	15.0	15.0	25.0

[a]The two-letter index for identifying lattices.

[b]Peak reactivity, $\rho = 1 - 1/k_\infty$.

[c]Peak U-233 enrichment (at. %).

[d]Burnup at which peak reactivity occurs, GWD/MT.

needed to be identified, two thorium-favoring approximations were made in the model. These were:

- At all points during the cycle, the thorium sub-batches in the (otherwise uranium-fuelled) core contribute their peak reactivities to the core reactivity, and

- There is equal power sharing within each sub-batch, during all cycles of its residence in the core.

The simple analytical model was used to assess assembly-sized thorium internal blankets, and thorium pins dispersed among uranium-fueled assemblies, for both current and high burnup PWRs.

The analytical assessment of the 12 thorium lattices showed that even under these thorium-favoring assumptions, the potential for using thorium to increase uranium utilization on the once-through cycle is fairly limited. Using the unadjusted index I_0, the maximum uranium savings predicted by the simple analytical model for thorium internal blankets were about 1.5% for current burnup PWRs (with 15% thorium in the core). For high burnup PWRs the maximum (unadjusted) uranium savings were about 5% (at about 28% thorium in the core). The reference reactor in each case was an all-uranium-fueled PWR.

The use of thorium pins uniformly dispersed within uranium fuel assemblies resulted in small (<1%) uranium savings for current burnup PWR cores, and about 2% for high burnup PWRs (using the unadjusted index I_0).

"Dry" thorium latices, namely lattices d-f, d-s, and d-t (see Table 6.1), performed best in the simple model evaluations. By virtue of its thorium-favoring nature the simple model identified these lattices as deserving more detailed analyses, while ruling out others as being unsuitable from the point of view of uranium utilization.

6.7 The Use of Thorium in a Retrofittable Mode

In the assessment of retrofittable fuel management options involving thorium, the current burnup PWR reference core was a 3-batch all-uranium core with a steady-state fuel reload enrichment of 3.0 w/o U-235, and an average discharge burnup of about 36 GWD/MT. The high burnup reference core had 5-batches, a steady-state fuel reload enrichment of 4.34 w/o U-235, and an average discharge burnup of about 61 GWD/MT.

The lattices of thorium identified as the most promising using the simple analytical model were reassessed in greater detail using the SPILBAC code. The key results from this

assessment are presented below. Note that all uranium savings are derived using the uranium utilization index I_{235}.

6.7.1 Thorium Assemblies as Internal Blankets

The analysis of thorium internal blankets in current burnup PWRs using the SPILBAC code showed a maximum uranium savings of less than 0.5%, relative to the all-uranium reference core. Internal blankets of depleted uranium were also evaluated. These did not yield any uranium savings, and were found to be worse than the best thorium blankets.

In high burnup PWRs, the inclusion of thorium internal blankets resulted in a maximum uranium savings of about 3%, at 20% thorium in the core. Depleted uranium blankets again performed worse than the best thorium cases. The use of spent fuel internal blankets in high burnup PWRs was also evaluated. In the steady-state this strategy corresponds to increasing the number of batches in the core by one (in this case from 5 to 6). The uranium savings from this option were about 3% (i.e. equal to those from the best thorium internal blankets).

6.7.2 Thorium Assemblies as Radial Blankets

In the assessment of radial blankets of thorium, the all-uranium reference cases employed the conventional out-in/scatter fuel management strategy.

In current burnup PWRs the introduction of thorium radial blankets showed uranium savings of less than 1%, relative to the out-in/scatter all-uranium reference core. Natural uranium radial blankets, evaluated for comparison, improved uranium utilization by about 2%. These results should be compared to the significantly higher uranium savings (about 4%) from the best low-leakage core (batch-3 on the core periphery), and the 9% uranium savings achieved using radial blankets of spent fuel. In the steady-state, using spent fuel radial blankets corresponds to increasing the number of batches in the core by one, and using the oldest batch on the core periphery as a "radial blanket" - the most extreme form of "low-leakage" fuel management.

Thorium radial blankets performed significantly better in high burnup PWR cores, yielding improvements in uranium utilization of up to 6% relative to the reference core. These uranium savings are comparable to the 5% savings from the best low-leakage scheme (batch-5 on the periphery), but still lower than the 9% savings from using spent fuel as a radial blanket.

It is important to note that using radial blankets (or extreme low-leakage schemes) results in significantly increased power peaking in the interior of the core, which must be counterbalanced by employing burnable poisons. Compromises due to limits imposed by burnable poison performance or reduced thermal margins, especially in the case of thorium blankets with significantly different lattices than the uranium fuel, may force the adoption of less than optimal radial and internal blankets. Experience with the light water breeder reactor (LWBR) core suggests that different lattices can be accommodated within a core without necessarily compromising thermal margins. This aspect of implementing radial or internal blankets needs further study.

6.7.3 Thorium Pins in Uranium Fuel Assemblies

Analysis of thorium pins uniformly dispersed among uranium fuel assemblies, in current burnup PWRs, showed that the inclusion of thorium pins monotonically increases natural uranium requirements as the fraction of thorium in the core is increased.

For high burnup cores the inclusion of thorium pins within uranium fuel assemblies showed uranium savings up to a maximum of about 2% (at 13% thorium in the core).

6.8 Less Conventional Options

A second set of evaluations was performed, of fuel management options considered more exotic and less retrofittable. The reconstitution and reinsertion of thorium assemblies, spectral shift control in both all-uranium and thorium-containing cores, and the deployment of smaller fuel assemblies in PWRs, were all evaluated for their uranium efficiency. The results of these assessments are summarized below.

6.8.1 Reconstitution of Thorium Assemblies

The reconstitution of thorium assemblies and their subsequent use as radial blanket assemblies was evaluated under the assumption that an exogenous supply of reconstituted thorium asemblies at different pre-reconstitution burnups was available. This was done in order to compare directly the uranium utilization advantage from using reconstituted thorium against other radial blanket materials, previously examined.

For current burnup PWRs the use of reconstituted thorium assemblies as radial blankets resulted in (maximum) uranium savings of about 5% relative to the all-uranium out-in/scatter

reference core. These savings are much higher than those from using unreconstituted thorium assemblies as radial blankets (1%), and comparable to those from the best (all-uranium) low leakage core (4%). However, savings from reconstituted thorium assemblies are substantially lower than the 9% improvement in uranium utilization from using spent fuel as a radial blanket.

In high burnup PWRs, reconstituted thorium radial blankets improved uranium utilization by about 7%. This improvement is comparable to the uranium savings from using unreconstituted thorium radial blankets (6%). Again, spent fuel radial blankets offer the highest uranium savings (here about 9%) of all the blanket materials considered in the assessment of high burnup PWRs.

Another important finding of the assessment was that the performance of the reconstituted thorium radial blanket was not very sensitive to the pre-reconstitution burnup of the thorium, especially for the blankets in high burnup PWRs.

6.8.2 Spectral Shift Control

For current-burnup all-uranium PWRs, spectral shift control (SSC) operation was found to improve uranium utilization by

about 9% relative to the same core operating at a fixed fuel-to-moderator ratio (V_F/V_M) typical of PWRs. The inclusion of thorium in SSC cores increased uranium savings to 14%, relative to the all-uranium PWR at fixed V_F/V_M.

Increasing the number of reload batches (at constant uranium fuel enrichment) was found to decrease the incremental uranium savings from introducing thorium in SSC cores.

Since the assessment of SSC was performed under thorium-favoring assumptions, these results should be regarded as the upper limits on the potential usefulness of deploying thorium in SSC cores. It is also important to point out that SSC is a difficult and expensive concept to implement in practice.

6.8.3 Small Fuel Assemblies in PWRs

PWR cores with assemblies one-quarter the size of current PWR assemblies (i.e. similar to current BWR assemblies), were assessed for their uranium utilization characteristics. In the assessment of the concurrent deployment of low-leakage fuel management schemes and small assemblies, the results show no advantage from small assemblies over the standard-sized PWR assemblies, for both current and high burnup PWR cores.

On the other hand, the performance of radial blankets (composed of small assemblies of fertile material) improved greatly, for both current and high burnup cores. For current burnup PWRs with small assemblies, a thorium radial blanket (of small assemblies) improved uranium utilization by about 5%, relative to the all-uranium core with out-in/scatter fuel loading and standard PWR assemblies. This should be compared to the maximum uranium savings of 1% for (thorium) radially blanketed current burnup cores with standard-sized fuel assemblies.

A high burnup PWR with small assemblies and a thorium radial blanket gave uranium savings of 8% relative to the reference (standard assembly) high burnup PWR with out-in/scatter fuel loading. This should be compared to the maximum uranium savings of about 6% for (thorium) radially blanketed high burnup cores with standard-sized fuel assemblies.

The deployment of the smaller assemblies also leads to power flattening in the core interior (about 8% on a batch-average basis), which facilitates the deployment of radial blankets or the more extreme low-leakage schemes.

6.9 Recommendations

Table 6.2 summarizes the potential improvements in uranium utilization available from the various fuel management schemes analyzed in this work. Note that the savings from a composite core, employing some combination of strategies, would, in general, be less than the algebraic sum of the savings from each individual innovation.

On the basis of these results, attention is called to the following points:

The introduction of thorium in PWRs on the once-through fuel cycle offers, for the most part, uranium savings which can be equalled (and frequently exceeded) by the deployment of options that are simpler to implement: re-use of "spent" fuel, in particular. Hence it is strongly recommended that priority attention be given to ways in which "spent" fuel can be reused without reprocessing, including its use as blankets, with or without reconstitution.

This conclusion must be tempered by the observation that in a recycle mode of operation (which is recommended and anticipated by most fuel cycle engineers), the premium U-233 fuel bred in the thorium blankets would be a valuable

TABLE 6.2

Potential Uranium Savings for Selected PWR Fuel Management Strategies Emphasizing the Use of Thorium

Strategy	Uranium Savings[a]	Comments
1. Thorium Internal Blankets	(CB)[b] <0.5% (HB)[c] ∿3%	The use of blanket assemblies having a different V_F/V_M from driver assemblies may be problematic from a thermal-hydraulic standpoint.
2. Spent Fuel Internal Blanket	(HB) 3%	In the steady-state this corresponds to adding one more reload batch in the core, in which case cycle length is shorter, other things being equal.
3. Thorium Radial Blanket[d]	(CB) ∿1% (HB) ∿6%	Power-peaking in the core interior may force less than optimal deployment. (See also comments on strategy #1.)
4. Natural Uranium Radial Blanket[d]	(CB) ∿2% (HB) ∿4%	Should be possible to get somewhat higher savings through blanket lattice optimization.
5. Low-Leakage Fuel Management (using oldest fuel batch)[d]	(CB) ∿4% (HB) ∿5%	Potential power peaking problems in core interior; burnable poison required.
6. Spent Fuel Radial Blankets[d]	(CB) ∿9% (HB) ∿9%	Best radial blanket material. Corresponds to adding one more reload batch to the core and using oldest batch on core periphery.
7. Thorium Pins Uniformly Dispersed within Uranium Fuel Assemblies	(CB) negative (HB) ∿2%	Selective use of thorium pins for power shaping within uranium assemblies should be considered, as has been proposed for BWRs.

TABLE 6.2 (Cont'd.)

Strategy	Uranium Savings[a]	Comments
8. Reconstitution/ Reinsertion of Thorium Assemblies as Radial Blankets	(CB) ∿ 5% (HB) ∿ 7%	Assumes exogenous source of reconstituted assemblies. Uranium utilization is fairly insensitive to pre-reconstitution burnup.
9. Spectral Shift Control for 3-Batch All-Uranium Core[f]	(CB) ∿ 9%	Savings increase as number of reload batches is increased (at fixed fuel enrichment); mechanical or H_2O/D_2O spectral shift is difficult to implement.
10. Spectral Shift Control for Cores Containing Thorium[f]	(CB) ∿ 14%	Spectral shift control is difficult to implement in practice. Quoted savings are an upper limit.
11. Small PWR Fuel Assemblies in Low-Leakage Cores (with oldest batch on periphery)[e]	(CB) ∿ 4% (HB) ∿ 5%	Savings comparable to those in strategy #5. Reduced power peaking.
12. Small Fuel Assemblies with Thorium Radial Blanket[e]	(CB) ∿ 5% (HB) ∿ 8%	Reduced power peaking.

[a]All savings for steady state once-through operation (no recycle).

[b]CB = Current Burnup PWR (3-batch core, discharge burnup ≃ 30 GWD/MT).

[c]HB = High Burnup PWR (5-batch core, discharge burnup ≃ 50 GWD/MT).

[d]Savings relative to Out-In/Scatter all-uranium reference cores.

[e]Compared to reference cores having regular PWR assemblies and Out-In/Scatter fuel management.

[f]Compared to all-uranium PWR at fixed V_F/V_M.

asset. While uranium savings from using thorium are small, it is also true that up to 15 or 20 percent thorium can be introduced into PWR cores without incurring a large penalty in uranium utilization. Thus if a policy decision were made to build up an inventory of U-233 as a prelude to future deployment of the thorium cycle in the recycle mode, this could be done <u>if</u> the resulting core designs met all licensing margins - an issue not addressed in the present work, and an obvious priority area requiring attention.

- Thorium pins strategically placed in uranium fuel assemblies (e.g. at assembly corners and next to water holes) need to be investigated in detail. Such a scheme has the potential to locally improve power peaking, and may be particularly useful in low-leakage schemes. GE researchers have already shown this strategy to be advantageous in BWRs.

- As the ultimate burnup capability of LWR fuel and the fuel management practices of utilities become better defined, the need for extending the present analysis should be re-evaluated. In general the performance of thorium improves as the burnup and cycle-length are increased. Thus, if LWR burnups as high as 70 or 80 GWD/MT could ever

be contemplated, and if cycle-lengths as long as 18 to 24 months gain favor, thorium might find a place in the LWR once-through cycle.

- Regardless of the deployment of thorium, the smaller fuel assembly option (especially with the concurrent deployment of radial blankets) should be evaluated in more detail and other aspects related to its eventual deployment should be investigated: economics, thermal-hydraulics, effect on burnable poison requirements, effect on refueling down-time, etc.

- The use of thorium as an axial blanket deserves investigation, especially for use in high burnup PWRs. Vendors are currently evaluating the use of natural and depleted uranium for this purpose. However, the issue of whether the subsequent reprocessing of fuel pins containing both uranium and thorium would be acceptable needs to be addressed.

Finally, attention is called to the companion effort by Loh (L-2), in which methods similar to those used here have been applied to assess other fuel management strategies of contemporary interest.

APPENDIX A

DESIGN PARAMETERS FOR MAINE YANKEE REACTOR*

*The information contained in this Appendix was obtained from publicly available documentation (S-5). It should not be considered as representing that actual system in its present or projected operating configuration, but as an idealization thereof. It should be noted that the results in this report have not been either reviewed or approved by the Yankee organization.

MECHANICAL DESIGN FEATURES OF CYCLE 4 FUEL

	E and F	G, H, and I
Fuel Assembly		
Overall length	156.718*	156.718
Spacer grid size (max. square)	8.115	8.115
Retention grid	0	0
No. Zircaloy grids	8	8
No. Inconel grids	1	1
Fuel rod growth clearance	1.021	1.021
Fuel Rod		
Active fuel length	136.7	136.7
Plenum length	8.575	8.575
Clad OD	0.440	0.440
Clad ID	0.384	0.384
Clad wall thickness	0.026	0.028
Pellet OD	0.3765	0.3765
Pellet length	0.450	0.450
Dish depth	0.023	0.021
Clad material	Zr-4	Zr-4
Pellet density initial	95%	94.75%
Poison Rods		
Overall rod length	146.513	146.322
Clad OD	0.440	0.440
Clad ID	0.388	0.388
Clad wall thickness	0.026	0.026
Pellet OD	0.376	0.376
Clad material	Zr-4	Zr-4

* All length dimensions are in inches.

MAINE YANKEE CYCLES 3 AND 4
NUCLEAR CHARACTERISTICS

Core Characteristics	Units	Cycle 3	Cycle 4
Core Average Exposure at BOC	MWD/MT	7,000	10,000
Expected Cycle Length at Full Power	MWD/MT	10,000	9,900
Initial U-235 Enrichment of Fuel Types			
Type RF 65 Cycle 3 assemblies	w/o	1.93	--
Type E 12 Cycle 3, 61 Cycle 4 assemblies	w/o	2.52	2.52
Type F 68 Cycle 3, 12 Cycle 4 assemblies	w/o	2.90	2.90
Type G 32 Cycle 3 and 4 assemblies	w/o	2.73	2.73
Type H 40 Cycle 3 and 4 assemblies	w/o	3.03	3.03
Type I 72 Cycle 4 assemblies	w/o	--	3.03
Control Characteristics			
Number of Control Element Assemblies (CEA's)			
Full Length		77	77
Part Length (not used)		8	*
Total CEA Worth			
HFP, BOC	%Δρ	9.18	8.30
HFP, EOC	%Δρ	9.56	9.30
Burnable Poison Rods			
Number (B_4C in Al_2O_3/Borosilicate glass)		756/0	160/16
Worth at HFP, BOC	%Δρ	1.4	0.5
Critical Soluble Boron (ARO) at BOC			
HZP, No Xe, Pk Sm	ppm	1075	1097
HFP, No Xe, Pk Sm	ppm	995	1013
HFP, Equilibrium Xe	ppm	782	797
Reactivity Coefficients (ARO)			
Moderator Temperature Coefficient			
HFP, BOC	$10^{-4}\Delta\rho/^{o}F$	-0.34**	-0.28
HFP, EOC	$10^{-4}\Delta\rho/^{o}F$	-1.98	-2.31

Maine Yankee Cycles 3 and 4
Nuclear Characteristics
(Cont.)

	Units	Cycle 3	Cycle 4
Fuel Temperature Component of Power Coeff.			
HZP, BOC	$10\text{-}5\Delta\rho/^{o}F$	-1.00	-1.53
HFP, BOC	$10\text{-}5\Delta\rho/^{o}F$	-1.00	-1.18
HZP, EOC	$10\text{-}5\Delta\rho/^{o}F$	-1.80	-1.76
HFP, EOC	$10\text{-}5\Delta\rho/^{o}F$	-1.37	-1.37
Total Delayed Neutron Fraction (β_{eff})			
BOC		0.00611	0.00597
EOC		0.00517	0.00525
Prompt Neutron Generation Time			
BOC	10^{-6} sec	29.3	29.6
EOC	10^{-6} sec	32.3	31.7
Inverse Boron Worth			
HZP, BOC	ppm/%$\Delta\rho$	84	87
HFP, BOC	ppm/%$\Delta\rho$	89	93
HZP, EOC	ppm/%$\Delta\rho$	74	76
HFP, EOC	ppm/%$\Delta\rho$	79	81

* Part length CEA's removed for Cycle 4
** Conditions of 2100 psia.

MAINE YANKEE CYCLE 4
GENERAL SYSTEM PARAMETERS

Quality	Value Cycle 3	Cycle 4
Reactor power level (102% of Nominal) (MWT)	2683	2683
Average linear heat rate (102% of Nominal) (kw/ft)	6.29	(6.35)*
Peak linear heat generation rate (PLHGR) (kw/ft)	16.5***	(15.7)[1]
Gap conductance at PLHGR (Btu/hr-ft^2-$^\circ$F)	2000***	(1949)[1] (2000)[2]
Fuel centerline temperature at PLHGR ($^\circ$F)	3788.1***	(3613.5)[1] (3782.2)[2]
Fuel average temperature at PLHGR($^\circ$F)	2304.12***	(2212.9)[1]
Hot rod gas pressure (psi)	1221.4***	(1240.5)[1]
Moderator temperature coefficient at initial density ($\Delta\rho/^\circ$F)	0.0	0.0
System flow rate (lbm/hr)	134.57×10^6	124.57×10^6
Core flow rate (lbm/hr)	130.94×10^6	130.94×10^6
Initial system pressure (psia)	2250	2250
Core inlet temperature ($^\circ$F)	554	554
Core outlet temperature ($^\circ$F)	606.1	606.1
Active core height (feet)	11.39	11.39
Fuel rod OD (inches)	0.440	0.440
Number of cold legs	3	3
Number of hot legs	3	3
Cold leg diameter (inches)	33.5	33.5
Hot leg diameter (inches)	33.5	33.5
Safety injection tank pressure (psia)	219.7	219.7
Safety injection tank gas/water volume (cu. ft.)	2069.7/ 1430.3	2069.7/ 1430.3
Hot rod burnup (MWD/MTU) at the most limiting time for PCT	683*	(3391)[1] (1385)[2]

* Parentheses used to denote change in value from previous Cycle 3 reload analysis.
** Cycle 3 used low density fuel from Core IA which was blowdown limited. Cycle 4 does not include any low density fuel so these parameters have been omitted.
*** For most limiting high density fuel (batch F) in Cycle 3.
1 For batch H fuel, Cycle 4.
2 For batch I fuel, Cycle 4.

MAINE YANKEE CYCLE 4

THERMAL HYDRAULIC PARAMETERS AT FULL POWER

General Characteristics		Cycle 3	Cycle 4
Total Heat Output	10^6MWT 10^6Btu/hr	2630 8976	2630 8976
Fraction of Heat Generated in Fuel Rod		0.975	0.975
Nominal	psig	2235	2235(2085)†
Minimum in Steady State	psig	2185	2185(2035)
Maximum in Steady State		2285	2285(2135)
Design Inlet Temperature (steady state)	^oF	554	554(546)
Total Reactor Coolant Flow (design)	10^6lb/hr	134.5	134.6(136.0)
Coolant Flow Through Core (design)	10^6lb/hr	130.7	130.7(132.1)
Hydraulic Diameter (nominal channel)		0.044	0.044
Average Mass Velocity	10^6lb/hr-ft^2	2.444	2.444(2.47)
Pressure Drop Across Cross (design flow)	psi	9.7	9.7(9.9)
Total Pressure Drop Across Vessel (based on nominal dimensions & design flow)	psi	32.4	32.4(33.1)
Core Average Heat Flux	Btu/hr-ft^2	178,740*	180,575*
Total Heat Transfer Area	ft^2	48,978*	48,480*
Film Coefficient at Average Conditions	Btu/hr-ft^2-^oF	5640	5636
Maximum Clad Surface Temp.	^oF	656	656
Average Film Temperature Difference	^oF	31.7	32
Avg. Linear Heat Rate of Rod	kw/ft	6.03*	6.09*
Average Core Enthalpy Rise	Btu/lb		68.7
Calculational Factors			
Engineering Heat Flux Factor		1.03	1.03
Engineering Factor on Hot Channel Heat Input		1.03	1.07
Flow Factors			
Inlet Plenum Nonuniform Distribution		1.05	1.05
End Pitch, Bowing and Clad Diameter		1.065	1.065

* Allows 0.3 percent axial shrinkage due to fuel densification.

† Numbers in parentheses are provided for conditions at a nominal pressure of 2,085 psig and a design inlet temperature of 546°F.

APPENDIX B

REACTIVITY AS A FUNCTION OF BURNUP FOR U235/UO_2 FUELED ASSEMBLIES

APPENDIX B

B.1 REACTIVITY AS A FUNCTION OF BURNUP FOR U235/UO_2 FUELED ASSEMBLIES

It has long been recognized that the reactivity, ρ, is a linear function of the burnup, B, for U235/UO_2 fuel in a PWR. This variation can be represented as

$$\rho = \rho_0 - AB \qquad (B.1)$$

where ρ = the reactivity, defined as $1 - 1/k_\infty$

ρ_0 = the extrapolated BOL reactivity

B = fuel burnup, GWD/MT

A = slope of the reactivity as a function of burnup determined by a linear curve fit, MT/GWD.

The extrapolated BOL reactivity, ρ_0, is, of course, different from the actual BOL reactivity. This is because there is a rapid saturation of certain fission products, xenon and samarium in particular, at the onset of burnup. Once this saturation is complete (typically in 1.5 GWD/MT), the behavior of the reactivity with burnup is very linear indeed. Any fit to the reactivity as a function of burnup data must, therefore, exclude this period. As shown in Chapter 2, the quantity ρ_0/A is an important parameter in determining the

discharge burnup of fuel assemblies which can be characterized by Eq. (B.1). The same ratio is also required to adjust the uranium utilization results (see Appendix E).

A series of LEOPARD supercell calculations were performed using dimensions and material compositions of a typical PWR (Maine Yankee parameters were used for this purpose). The fuel U-235 enrichment was varied from 2.5 w/0 to 5 w/0 in increments of 0.5 w/0. Least-squares linear regression fits of reactivity as a function of burnup were done on this data for burnup points of 3 GWD/MT and greater.

In all cases the goodness-of-fit criterion, R^2, was greater than 0.998, with a maximum error in the fits of less than 1.5%. The values of the constants, ρ_0 and A, as a function of the reload enrichment, X_p, are shown in Table B.1.

The quantities ρ_0, A, and ρ_0/A were each independently correlated with reload enrichment, X_p, for use elsewhere in this work. The variations of these quantities with x_p are shown in Figs. B.1, B.2, and B.3. The results of the curve fits are as follows:

(a) ρ_0 versus X_p:

$$\rho_0 = 0.363038 - 0.418958/X_p$$

Goodness-of-fit criterion, R^2, = 0.999

Table B.1

Variation of ρ_0, A, and ρ_0/A with BOL Enrichment, x_p

BOL Enrichment x_p, w/0	ρ_0	A ($*10^{-3}$MT/GWD)	ρ_0/A GWD/MT	R^{2*}
2.5	0.19517	9.94355	19.6278	0.9990
3.0	0.22413	9.30478	24.0876	1.0000
3.5	0.24325	8.34412	29.1523	0.9998
4.0	0.25818	7.63104	33.8329	0.9996
4.5	0.26864	6.94730	38.6683	0.9995
5.0	0.28029	6.54404	42.8313	0.9989

*Goodness-of-fit criterion for linear fit to ρ versus B; data from LEOPARD.

•Maine Yankee Assembly Design Parameters. (See Appendix A.)

•Fixed $V_F/V_M = 0.601$

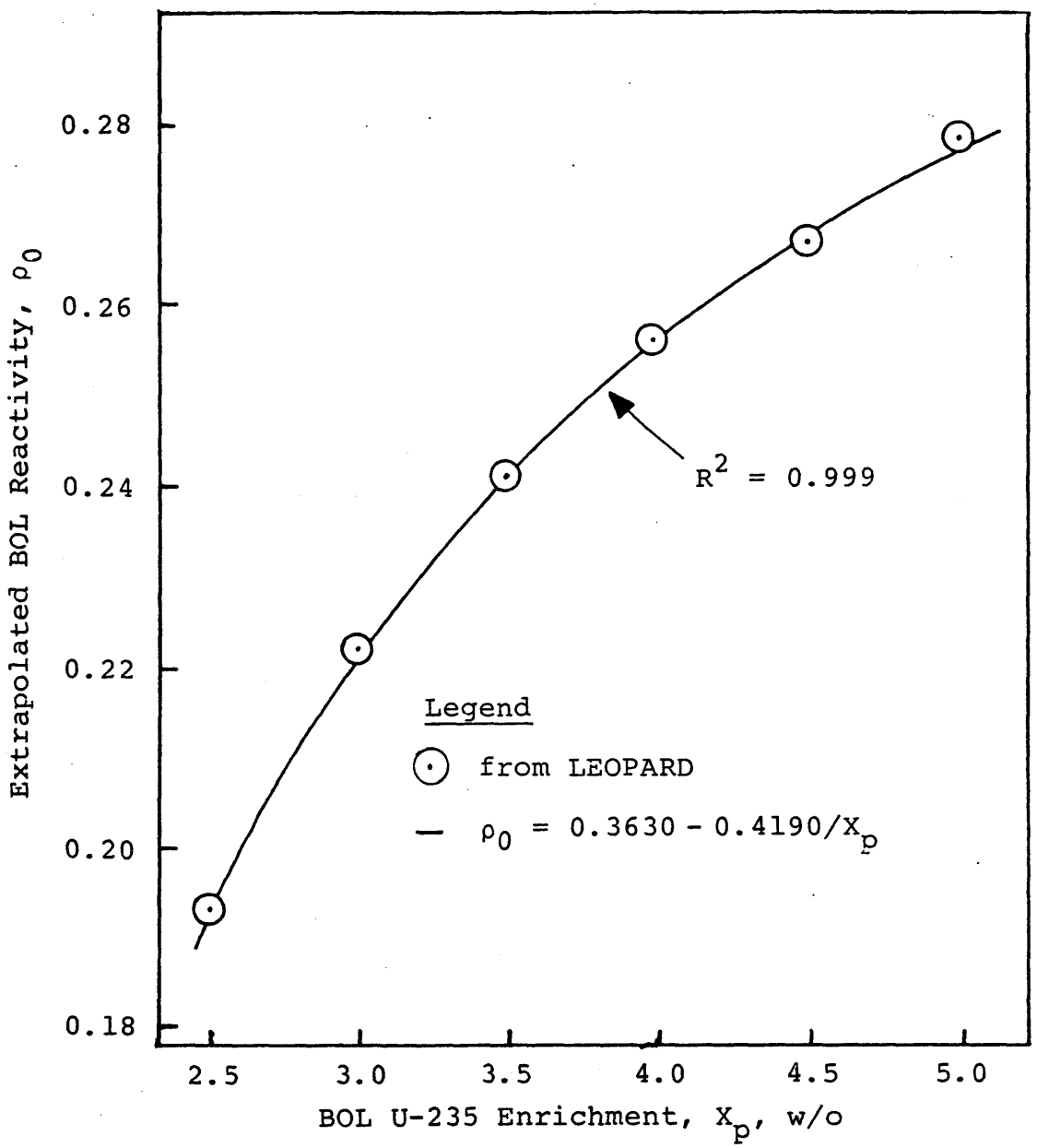

Fig. B.1 Variation of BOL Extrapolated Reactivity with BOL Enrichment

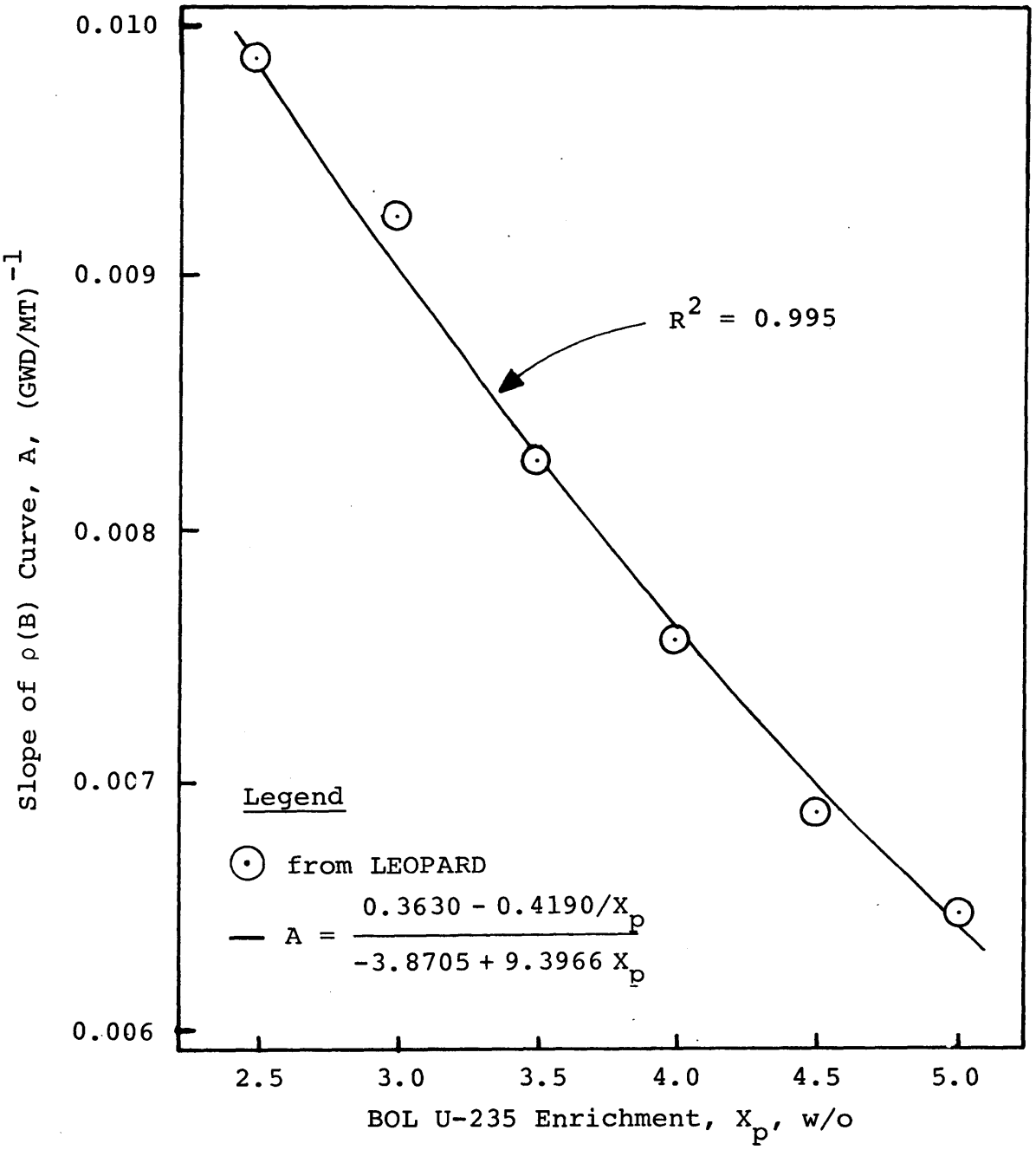

Fig. B.2 Variation of the Slope of ρ(B) with BOL Enrichment.

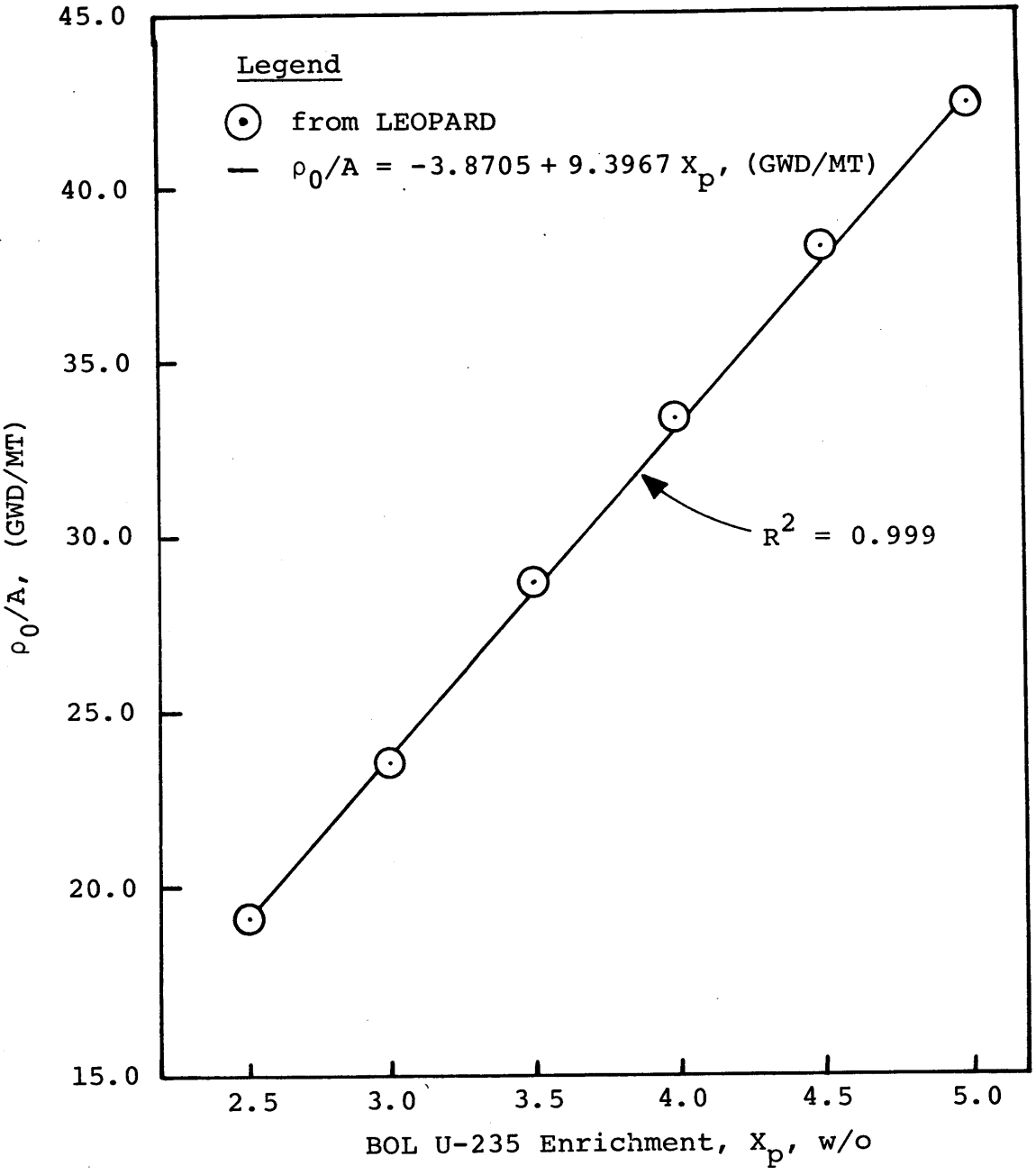

Fig. B.3 Variation of ρ_0/A with BOL Enrichment

(b) ρ_0/A versus X_p:

$$\rho_0/A = -3.87049 + 9.39658X_p \quad , \text{GWD/MT}$$

$$R^2 = 0.999$$

(c) A versus X_p:

$$A = \frac{\rho_0}{\rho_0/A} = \frac{0.363038 - 0.418958/X_p}{-3.87049 + 9.39658X_p} \quad , \text{MT/MWD}$$

These fits are valid over the range $2.5 \leq X_p \leq 5.0$ w/0, and for a constant fuel-to-moderator ratio, V_F/V_M, of 0.601.

Correa [C-4] and Varela [V-1] have also shown that the linearity of reactivity as a function of burnup holds over a wide range of fuel-to-moderator ratios. Table B.2 shows the variation of ρ_0, A, and ρ_0/A, with V_F/V_M. Figures B.4, B.5 and B.6 show the same functional dependence.

(The results in this section are <u>not</u> from a common data set, and therefore lack internal consistency. They are included here merely to show the general form of the functional dependencies in question.)

B.2 VARIATION OF REACTIVITY AS A FUNCTION OF BURNUP FOR THORIUM LATTICES

The variation of the reactivity as a function of burnup (from LEOPARD) for the twelve thorium lattices investigated

Table B.2

Variation of ρ_0, A and ρ_0/A with V_F/V_M*

V_F/V_M	$\rho_0 = 1 - 1/k_\infty$	A ($\times 10^{-3}$ GWD/MT)	ρ_0/A (GWD/MT)
0.3945	0.26287	11.67623	22.5134
0.4452	0.25337	10.84811	23.3561
0.4756	0.24666	10.37193	23.7813
0.5002	0.24164	10.05984	24.0204
0.5272	0.23625	9.75833	24.2104
0.6254	0.21697	8.91130	24.3480
0.6653	0.20927	8.65804	24.1707
0.9558	0.15938	7.65173	20.8294

•Fixed BOL U-235 enrichment (3.04 w/0).

*From Reference (V-1). For Maine Yankee Assembly Design Parameters (see Appendix A).

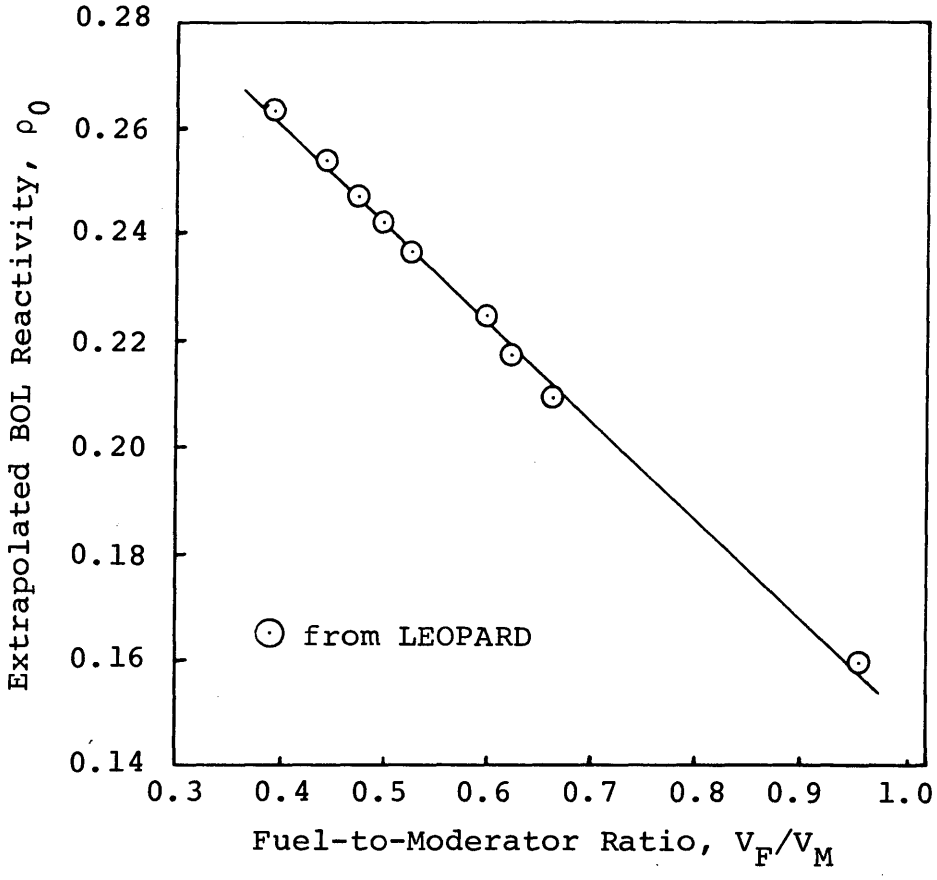

Fig. B.4 Variation of the BOL Extrapolated Reactivity with Fuel-to-Moderator Ratio.

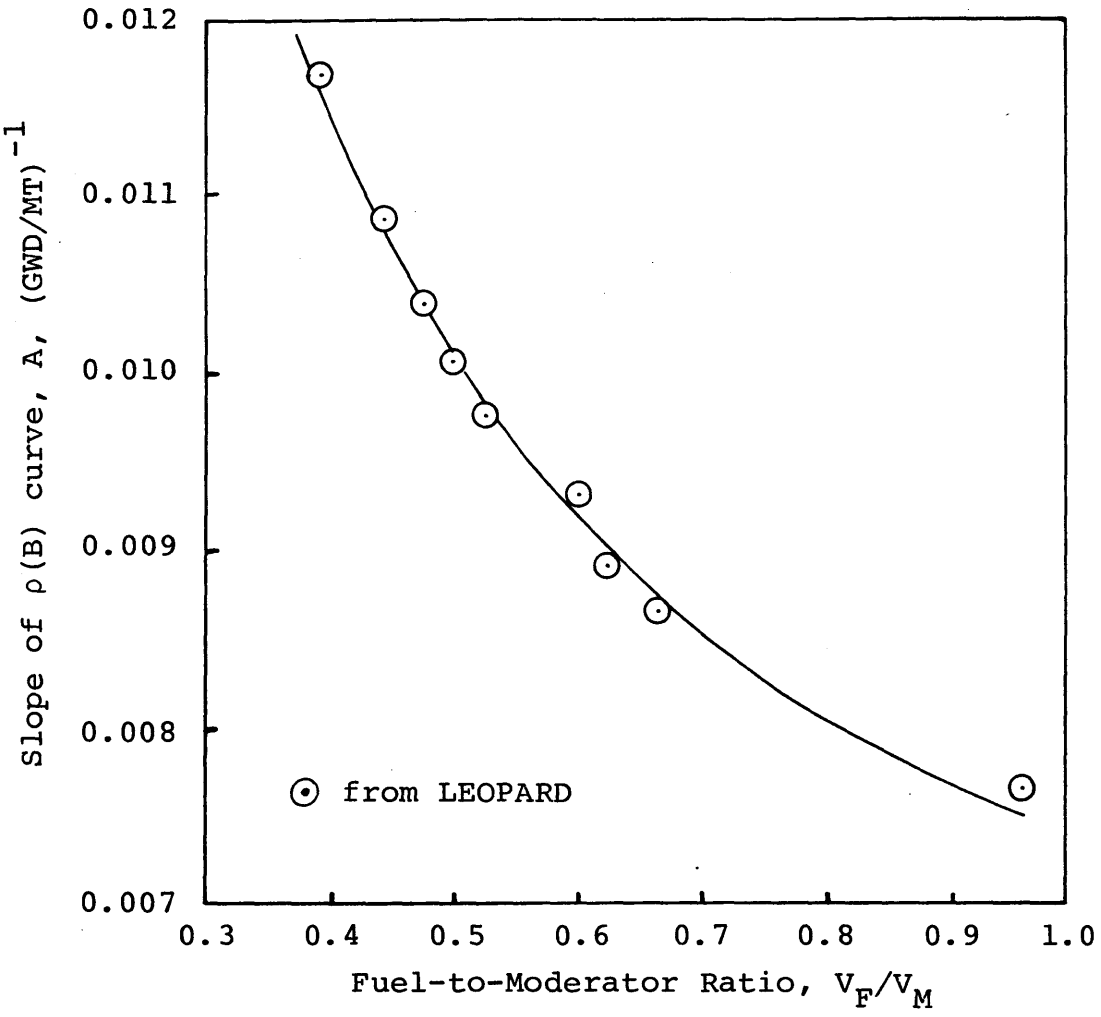

Fig. B.5 Variation of the Slope of ρ(B) with Fuel-to-Moderator Ratio (at Fixed BOL Enrichment).

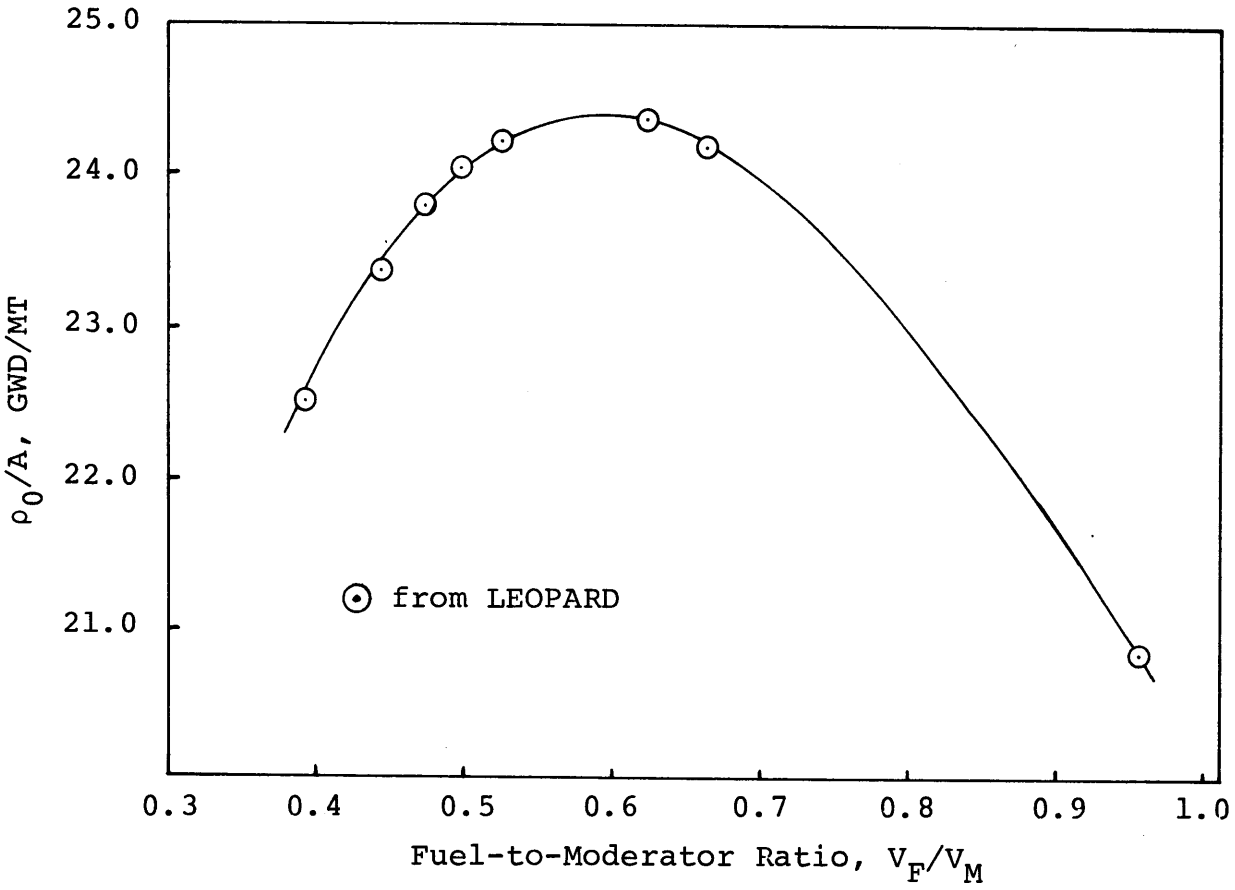

Fig. B.6 Variation of ρ_0/A with Fuel-to-Moderator Ratio (at fixed BOL Enrichment).

in this work is shown in Tables B.3 through B.14. The reader is referred to Section 4.2 of Chapter 4 for details. The relatively high initial reactivities for the thorium are due to the (necessary) inclusion of some fissile material (U-233 in this case) to permit use of the LEOPARD program. However, this initial fissile material does not have any noticeable effect on the reactivity as a function of burnup behavior after a burnup of about 5 GWD/MT.

In Chapter 5 (Section 5.2), the reconstitution of thorium lattice d-t assemblies into lattice d-s assemblies for subsequent use as radial blankets was examined. Three pre-reconstitution burnups were considered. These were: 4 GWD/MT, 13 GWD/MT and 19 GWD/MT. The reactivity as a function of burnup for the three cases after reconstitution is shown in Tables B.15, B.16 and B.17.

Table B.3

Variation of Reactivity with Burnup for Thorium Lattice d-h

Burnup GWD/MT	k_∞	$\rho = 1 - 1/k_\infty$
0.0	0.80984	-0.23481
0.150	0.78293	-0.27725
1.0	0.75424	-0.32587
2.0	0.75341	-0.32730
3.0	0.76476	-0.30760
4.0	0.77906	-0.28360
5.0	0.79268	-0.26154
10.0	0.82995	-0.20489
15.0	0.84830	-0.17883
20.0	0.85577	-0.16854
25.0	0.85815	-0.16530
30.0	0.85746	-0.16624
35.0	0.85520	-0.16932
40.0	0.85181	-0.17397
45.0	0.84810	-0.17911

- $V_F/V_M = 1.0$
- Fuel Pellet Diameter = 0.025 cm. (Simulates a homogeneous assembly.)

Table B.4

Variation of Reactivity with Burnup for Thorium Lattice d-t

Burnup GWD/MT	k_∞	$\rho = 1 - 1/k_\infty$
0.0	0.66688	-0.49952
0.150	0.64347	-0.55407
1.0	0.62571	-0.59818
2.0	0.65509	-0.52651
3.0	0.69573	-0.43734
4.0	0.73188	-0.36634
7.0	0.79467	-0.25839
10.0	0.82847	-0.20704
13.0	0.84618	-0.18178
16.0	0.85586	-0.16842
19.0	0.86113	-0.16126
22.0	0.86368	-0.15784
25.0	0.86456	-0.15666
28.0	0.86409	-0.15729
31.0	0.86270	-0.15915
34.0	0.86076	-0.16176
37.0	0.85816	-0.16528
40.0	0.85549	-0.16892
43.0	0.85258	-0.17291
46.0	0.84962	-0.17700

- $V_F/V_M = 1.0$
- Fuel Pin Diameter = 0.5 cm

Table B.5

Variation of Reactivity with Burnup for Thorium Lattice d-s

Burnup GWD/MT	k_∞	$\rho = 1 - 1/k_\infty$
0.0	0.67521	-0.48102
0.150	0.65159	-0.53471
1.0	0.62934	-0.58897
2.0	0.65363	-0.52992
3.0	0.69174	-0.44563
4.0	0.72726	-0.37502
7.0	0.79032	-0.26531
10.0	0.82448	-0.21289
13.0	0.84149	-0.18837
16.0	0.85042	-0.17589
19.0	0.85472	-0.16997
22.0	0.85643	-0.16764
25.0	0.85639	-0.16769
28.0	0.85515	-0.16940
31.0	0.85293	-0.17243
34.0	0.85026	-0.17611
37.0	0.84721	-0.18034
40.0	0.84381	-0.18510
43.0	0.84034	-0.18999
46.0	0.83690	-0.19489
49.0	0.83362	-0.19959

- $V_F/V_M = 1.0$
- Fuel Pellet Diameter = 1.0 cm

Table B.6

Variation of Reactivity with Burnup for Thorium Lattice d-f

Burnup GWD/MT	k_∞	$\rho = 1 - 1/k_\infty$
0.0	0.70191	-0.42468
0.150	0.67787	-0.47521
1.0	0.65596	-0.52448
2.0	0.68114	-0.46812
3.0	0.71799	-0.39278
4.0	0.75114	-0.33131
7.0	0.80791	-0.23776
10.0	0.83775	-0.19367
13.0	0.85209	-0.17358
16.0	0.85876	-0.16447
19.0	0.86144	-0.16085
22.0	0.86152	-0.16074
25.0	0.86017	-0.16256
28.0	0.85774	-0.16585
31.0	0.85451	-0.17026
34.0	0.85086	-0.17528
37.0	0.84691	-0.18076
40.0	0.84258	-0.18683
43.0	0.83830	-0.19289
46.0	0.83417	-0.19880
49.0	0.83017	-0.20457

- $V_F/V_M = 1.0$
- Fuel Pin Diameter = 2.0 cm

Table B.7

Variation of Reactivity with Burnup for Thorium Lattice s-h

Burnup GWD/MT	k_∞	$\rho = 1 - 1/k_\infty$
0.0	0.80706	-0.23907
0.150	0.78042	-0.28136
1.0	0.74803	-0.33684
2.0	0.74081	-0.34987
3.0	0.74802	-0.33686
4.0	0.76087	-0.31428
5.0	0.77493	-0.29044
10.0	0.81860	-0.22160
15.0	0.84138	-0.18852
20.0	0.85075	-0.17543
25.0	0.85361	-0.17150
30.0	0.85296	-0.17239
35.0	0.85035	-0.17599
40.0	0.84664	-0.18114
45.0	0.84270	-0.18666

- $V_F/V_M = 0.60$
- Fuel Pellet Diameter = 0.025 cm. (Simulates a homogeneous assembly.)

Table B.8

Variation of Reactivity with Burnup for Thorium Lattice s-t

Burnup GWD/MT	k_∞	$\rho = 1 - 1/k_\infty$
0.0	0.65764	-0.52050
0.150	0.63480	-0.57530
1.0	0.60895	-0.64217
2.0	0.62776	-0.60576
3.0	0.66454	-0.50480
4.0	0.70222	-0.42406
7.0	0.77455	-0.29107
10.0	0.81536	-0.22645
13.0	0.83586	-0.19637
16.0	0.84648	-0.18136
19.0	0.85182	-0.17396
22.0	0.85425	-0.17062
25.0	0.85458	-0.17017
28.0	0.85365	-0.17144
31.0	0.85196	-0.17376
34.0	0.84947	-0.17720
37.0	0.84652	-0.18131
40.0	0.84336	-0.18573
43.0	0.84008	-0.19036
46.0	0.83682	-0.19500
49.0	0.83394	-0.19913

- $V_F/V_M = 0.60$
- Fuel Pellet Diameter = 0.5 cm

Table B.9

Variation of Reactivity with Burnup for Thorium Lattice s-s

Burnup GWD/MT	k_∞	$\rho = 1 - 1/k_\infty$
0.0	0.66227	-0.50996
0.150	0.63952	-0.56367
1.0	0.60987	-0.63969
2.0	0.62317	-0.60470
3.0	0.65637	-0.52353
4.0	0.69231	-0.44444
7.0	0.76475	-0.30762
10.0	0.80609	-0.24056
13.0	0.82645	-0.20999
16.0	0.83630	-0.19574
19.0	0.84066	-0.18954
22.0	0.84214	-0.18745
25.0	0.84170	-0.18807
28.0	0.84004	-0.19042
31.0	0.83741	-0.19416
34.0	0.83427	-0.19865
37.0	0.83072	-0.20378
40.0	0.82699	-0.20920
43.0	0.82322	-0.21474
46.0	0.81973	-0.21991

- $V_F/V_M = 0.60$
- Fuel Pellet Diameter = 1.0 cm

(Conventional PWR Lattice Dimensions)

Table B.10

Variation of Reactivity with Burnup for Thorium Lattice s-f

Burnup GWD/MT	k_∞	$\rho = 1 - 1/k_\infty$
0.0	0.87859	-0.13819
0.150	0.85156	-0.17432
1.0	0.81318	-0.22974
2.0	0.80031	-0.24952
3.0	0.80094	-0.24853
4.0	0.80717	-0.23890
5.0	0.81484	-0.22723
10.0	0.83734	-0.19426
15.0	0.84648	-0.18136
20.0	0.84638	-0.18150
25.0	0.84209	-0.18752
30.0	0.83555	-0.19682
35.0	0.82802	-0.20770
40.0	0.82019	-0.21923
45.0	0.81277	-0.23036

- $V_F/V_M = 0.6$
- Fuel Pellet Diameter = 2.00 cm.

Table B.11

Variation of Reactivity with Burnup for Thorium Lattice w-h

Burnup GWD/MT	k_∞	$\rho = 1 - 1/k_\infty$
0.0	0.71555	-0.39753
0.150	0.69380	-0.44134
1.0	0.65582	-0.52481
2.0	0.63145	-0.58366
3.0	0.62129	-0.60955
4.0	0.62147	-0.60909
5.0	0.62840	-0.59134
10.0	0.68340	-0.46327
15.0	0.73017	-0.36954
20.0	0.75468	-0.32506
25.0	0.76454	-0.30798
30.0	0.76661	-0.30444
35.0	0.76503	-0.30714
40.0	0.76194	-0.31244
45.0	0.75828	-0.31877

- $V_F/V_M = 0.2$
- Fuel Pellet Diameter = 0.025 cm. (Simulates a homogeneous assembly.)

Table B.12

Variation of Reactivity with Burnup for Thorium Lattice w-t

Burnup GWD/MT	k_∞	$\rho = 1 - 1/k_\infty$
0.0	0.56009	-0.78543
0.150	0.54211	-0.84464
1.0	0.50292	-0.98839
2.0	0.48927	-1.04386
3.0	0.49880	-1.00481
4.0	0.52211	-0.91513
7.0	0.60325	-0.65769
10.0	0.67268	-0.48659
13.0	0.71526	-0.39809
16.0	0.73780	-0.35538
19.0	0.74831	-0.33634
22.0	0.75204	-0.32972
25.0	0.75231	-0.32924
28.0	0.75041	-0.33260
31.0	0.74758	-0.33765
34.0	0.74429	-0.34356
37.0	0.74069	-0.35009
40.0	0.73705	-0.35676
43.0	0.73355	-0.36323
46.0	0.73032	-0.36926
49.0	0.72749	-0.37459

- $V_F/V_M = 0.20$
- Fuel Pellet Diameter = 0.5 cm

Table B.13

Variation of Reactivity with Burnup for Thorium Lattice w-s

Burnup GWD/MT	k_∞	$\rho = 1 - 1/k_\infty$
0.0	0.74138	-0.34884
0.150	0.71994	-0.38900
1.0	0.67859	-0.47364
2.0	0.65045	-0.53740
3.0	0.63569	-0.57309
4.0	0.63076	-0.58539
5.0	0.63271	-0.58050
10.0	0.67011	-0.49229
15.0	0.70524	-0.41796
20.0	0.72222	-0.38462
25.0	0.72668	-0.37612
30.0	0.72449	-0.38028
35.0	0.71956	-0.38974
40.0	0.71379	-0.40097
45.0	0.70803	-0.41237

- $V_F/V_M = 0.2$
- Fuel Pellet Diameter = 1.00 cm.

Table B.14

Variation of Reactivity with Burnup for Thorium Lattice w-f

Burnup GWD/MT	k_∞	$\rho = 1 - 1/k_\infty$
0.0	0.71782	-0.39311
0.150	0.69857	-0.43150
1.0	0.65699	-0.52209
2.0	0.62949	-0.58859
3.0	0.61456	-0.62718
4.0	0.60891	-0.64228
5.0	0.60981	-0.63986
10.0	0.64153	-0.55877
15.0	0.67211	-0.48785
20.0	0.68629	-0.45711
25.0	0.68923	-0.45089
30.0	0.68633	-0.45703
35.0	0.68103	-0.46836
40.0	0.67509	-0.48128
45.0	0.66933	-0.49403

- $V_F/V_M = 0.2$
- Fuel Pellet Diameter = 2.00 cm.

Table B.15

Variation of Reactivity with Burnup* for Thorium d-t Assemblies Reconstituted (at 4 GWD/MT) into Thorium d-s Assemblies

Burnup* GWD/MT	k_∞	$\rho = 1 - 1/k_\infty$
0.0	0.84878	-0.17816
0.150	0.82189	-0.21671
1.0	0.78876	-0.26781
2.0	0.77869	-0.28421
3.0	0.78151	-0.27957
4.0	0.78940	-0.26678
7.0	0.81300	-0.23001
10.0	0.83027	-0.20443
13.0	0.84039	-0.18992
16.0	0.84594	-0.18212
19.0	0.84855	-0.17848
22.0	0.84923	-0.17754
25.0	0.84850	-0.17855
28.0	0.84689	-0.18079
31.0	0.84460	-0.18399

- Fuel Pellet Diameter = 0.5 cm.
- Pre-Reconstitution $V_F/V_M = 1.0$
- Post-Reconstitution $V_F/V_M = 0.6$

*Post-Reconstitution Burnups.

Table B.16

Variation of Reactivity with Burnup* for Thorium d-t Assemblies Reconstituted (at 13 GWD/MT) into Thorium d-s Assemblies

Burnup* GWD/MT	k_∞	$\rho = 1 - 1/k_\infty$
0.0	0.92261	-0.08388
0.150	0.89524	-0.11702
1.0	0.86445	-0.15680
2.0	0.84919	-0.17759
3.0	0.84261	-0.18679
4.0	0.84022	-0.19016
7.0	0.83947	-0.19123
10.0	0.84008	-0.19036
13.0	0.83996	-0.19053
16.0	0.83909	-0.19177
19.0	0.83761	-0.19387
22.0	0.83543	-0.19699
25.0	0.83299	-0.20049
28.0	0.83014	-0.20462
31.0	0.82705	-0.20912

- Fuel Pellet Diameter = 0.5 cm.
- Pre-Reconstitution $V_F/V_M = 1.0$
- Post-Reconstitution $V_F/V_M = 0.6$

*Post-Reconstitution Burnups.

Table B.17

Variation of Reactivity with Burnup* for Thorium d-t Assemblies Reconstituted (at 19 GWD/MT) into Thorium d-s Assemblies

Burnup* GWD/MT	k_∞	$\rho = 1 - 1/k_\infty$
0.0	0.92191	-0.08470
0.150	0.89545	-0.11676
1.0	0.86628	-0.15436
2.0	0.85120	-0.17481
3.0	0.84377	-0.18516
4.0	0.84004	-0.19042
7.0	0.83567	-0.19664
10.0	0.83343	-0.19986
13.0	0.83119	-0.20309
16.0	0.82907	-0.20617
19.0	0.82656	-0.20983
22.0	0.82380	-0.21389
25.0	0.82104	-0.21797
28.0	0.81788	-0.22267
31.0	0.81473	-0.22740
34.0	0.81147	-0.23233
37.0	0.80826	-0.23723
40.0	0.80493	-0.24234
43.0	0.80197	-0.24693

- Fuel Pellet Diameter = 0.5 cm.
- Pre-Reconstitution $V_F/V_M = 1.0$
- Post-Reconstitution $V_F/V_M = 0.6$

*Post-Reconstitution Burnups.

APPENDIX C

THE POWER SHARING EQUATION

AND THEORETICAL ESTIMATES FOR THETA

APPENDIX C

The Power Sharing Equation and Theoretical Estimates for Theta

C.1 Power Sharing Among Assemblies and Batches

The one-and-one-half group theory, which has been used extensively in this work, will be applied to situations of interest in order to obtain theoretical estimates for θ, the reactivity-power coupling factor (RPCF).

The basic relation for the spatial power variation for a critical system, using the one-and-one-half group model from Chapter 3 (Eq. (3.9)) is:

$$\nabla^2\{q(1-\rho)\} + \frac{\rho q}{M^2} = 0 \qquad \text{(C.1)}$$

where q = the local power density

ρ = the reactivity, defined as $\rho = 1 - 1/k_\infty$, and

M^2 = the migration area, defined by Eq. (3.6) in Chapter 3.

The Laplacian in Eq. (C.1) can be expressed in terms of difference equations involving the local and surrounding regions' reactivity, ρ, and power density, q.

Approximations of the Laplacian can be very complex at one extreme, or, at the other, simple difference relations can be used. In the present work, the primary use of Eq. (C.1) was to arrive at the general form of the power split relations, and then turn to detailed computer calculations to test their

validity, quantify their accuracy, and extract empirical constants for use in subsequent analyses.

Consider the 3 x 3 fuel assembly cluster and its equivalent cylindricized configuration shown in Fig. C.1. The assembly width is 'h'. The cylindricization is a convenient (but not necessary) approximation which greatly simplifies the subsequent analysis and makes the solution more transparent.

For the equivalent cylindrical fuel assembly cluster, as with the 3 x 3 cluster, two regions are of interest. One is the 'interior' assembly, region i, at the center of the cluster. The second region is composed of the 8 surrounding assemblies, region s. Region-wise averages of the power density q and reactivity ρ will be considered. Note that in the case of the surrounding region, the region-wise averaging of the reactivity implies a power-weighted sum, as explained in Chapter 2 (see Section 2.4).

The point-wise fast flux in the cluster, $\phi_1(r)$, can be written in a series expansion as:

$$\phi_1(r) = \sum_{n=-\infty}^{\infty} a_n r^n \qquad (C.2)$$

where the radial distance 'r' is measured from the center of the central assembly (region i).

Requiring that:

(a) $\phi_1(0)$ be finite, and

(b) $\left.\frac{d\phi_1}{dr}\right|_{r=0} = 0$, (symmetry)

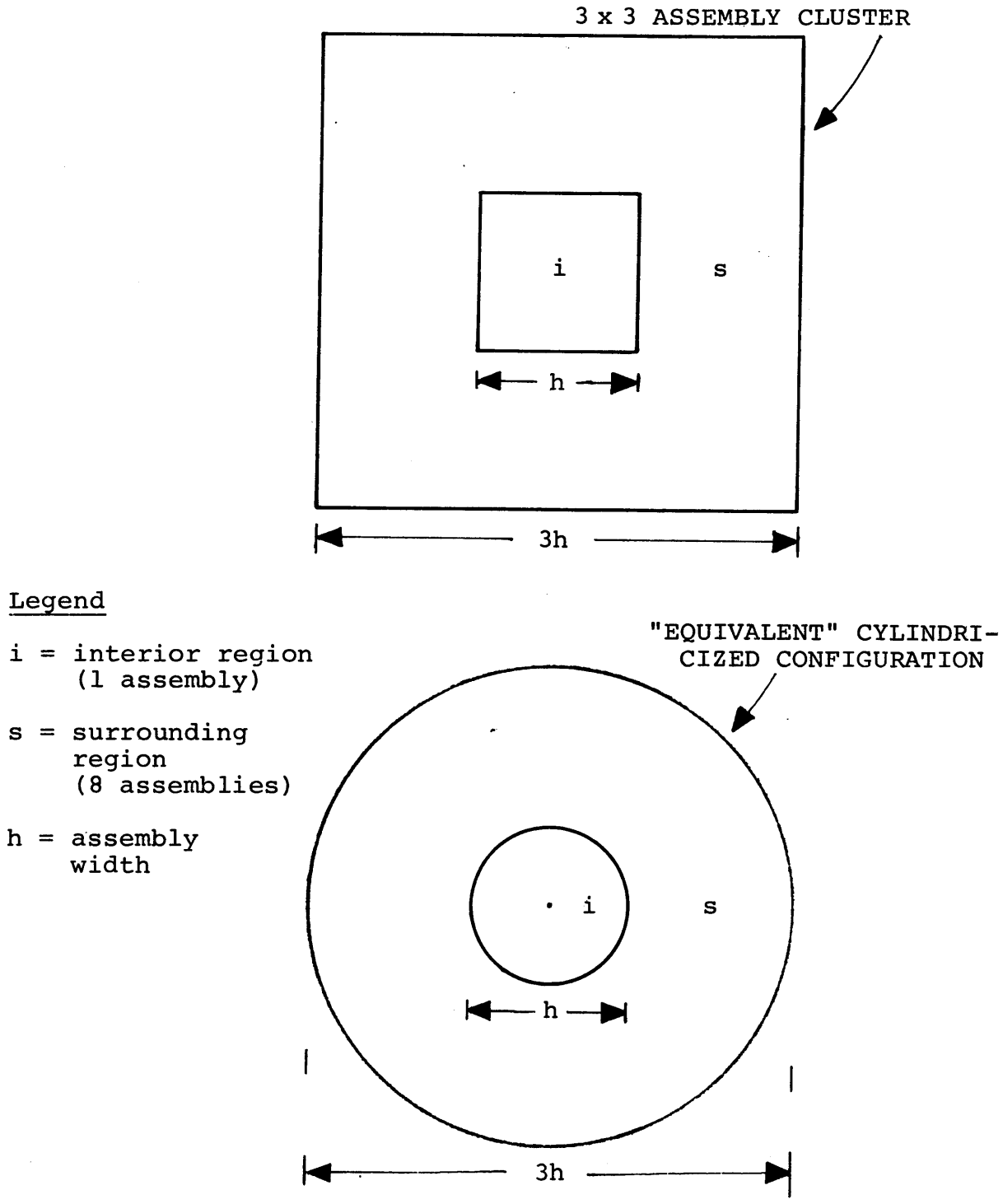

Fig. C.1 3 x 3 Fuel Assembly Cluster and an Equivalent Cylindricized Configuration.

reduces the series in Eq. (C.2) to

$$\phi_1(r) = a_0 + a_2 r^2 + a_3 r^3 + \ldots . \qquad (C.3)$$

From Eqs. (3.5) and (3.9) in Chapter 3, it follows that

$$\phi_1 = q(1 - \rho) \qquad (C.4)$$

Combining Eq. (C.3) and (C.4),

$$q(r)[1 - \rho(r)] = a_0 + a_2 r^2 + a_3 r^3 + \ldots . \qquad (C.5)$$

The next step is to apply Green's Theorem to the integral of Eq. (C.1) over volume to convert the first term to an integral of the gradient over the surface.

At the periphery of region 'i' this transformation gives

$$4h \frac{d}{dr}[q(1 - \rho)]\Big|_{r = h/2} + \frac{h^2}{M^2} \bar{q}_i \bar{\rho}_i = 0 \qquad (C.6)$$

and at the outer periphery of region 's':

$$12h \frac{d}{dr}[q(1 - \rho)]\Big|_{r = 3h/2} + \frac{h^2}{M^2} [\bar{q}_i \bar{\rho}_i + 8\bar{q}_s \bar{\rho}_s] = 0 \qquad (C.7)$$

Equation (C.5) yields upon differentiation:

$$\frac{d\phi_1}{dr} = \frac{d}{dr}\{q(1 - \rho)\} = 2a_2 r + 3a_3 r^2 \qquad (C.8)$$

where only the second order terms have been retained. At $r = h/2$, Eq. (C.8) gives

$$\left.\frac{d\phi_1}{dr}\right|_{r = h/2} = \left.\frac{d}{dr}\{q(1 - \rho)\}\right|_{r = h/2}$$

$$= a_2 h + 3a_3 \frac{h^2}{4} \qquad \text{(C.9)}$$

and similarly at $r = 3h/2$

$$\left.\frac{d\phi_1}{dr}\right|_{r = 3h/2} = \left.\frac{d}{dr}\{q(1 - \rho)\}\right|_{r = 3h/2}$$

$$= 3a_2 h + \frac{27}{4} a_3 h^2 \qquad \text{(C.10)}$$

The slopes of the fast fluxes, $d\phi_1/dr$, at the periphery of the two regions given by Eqs. (C.9) and (C.10) can be used in Eqs. (C.6) and (C.7). This substitution yields, at $r = h/2$:

$$4a_2 h^2 + 3a_3 h^3 + \frac{h^2}{M^2} \bar{q}_i \bar{\rho}_i = 0 \qquad \text{(C.11)}$$

and at $r = 3h/2$:

$$36a_2 h^2 + 81a_3 h^3 + \frac{h^2}{M^2} [\bar{q}_i \bar{\rho}_i + \bar{q}_s \bar{\rho}_s] = 0 \qquad \text{(C.12)}$$

Equation (C.3), which describes the radial variation in the fast neutron flux, can be used to define the region-wise average fluxes. Using Eq. (C.3), the average fast flux in region

'i' can be written as:

$$\bar{\phi}_{1,i} = \int_0^{h/2} \phi_1(r)\, r\, dr \Big/ \int_0^{h/2} r\, dr \tag{C.13}$$

Hence

$$\bar{\phi}_{1,i} = \frac{h^2}{8} \int_0^{h/2} (a_0 + a_2 r^2 + a_3 r^3)\, r\, dr$$

or

$$\bar{\phi}_{1,i} = a_0 + \frac{1}{8} h^2 a_2 + \frac{1}{20} h^3 a_3 \tag{C.14}$$

Substituting for ϕ_1 from Eq. (C.4) in Eq. (C.14) gives:

$$\bar{q}_i (1 - \bar{\rho}_i) = a_0 + \frac{1}{8} h^2 a_2 + \frac{1}{20} h^3 a_3 \tag{C.15}$$

Similarly for region 's' (from $r = h/2$ to $3h/2$), this treatment gives:

$$\bar{q}_s (1 - \bar{\rho}_s) = a_0 + \frac{5}{4} h^2 a_2 + \frac{121}{80} h^3 a_3 \tag{C.16}$$

Subtracting Eq. (C.15) from (C.16) yields:

$$\bar{q}_s (1 - \bar{\rho}_s) - \bar{q}_i (1 - \bar{\rho}_i) = \frac{9}{8} h^2 a_2 + \frac{117}{80} h^3 a_3 \tag{C.17}$$

Eliminating the constants a_2 and a_3, using Eqs. (C.11), (C.12),

and (C.17), yields after considerable algebra:

$$\frac{q_i}{q_s} = \frac{\{1 - (1 - \frac{11}{120}\frac{h^2}{M^2})\rho_s\}}{\{1 - (1 + \frac{91}{480}\frac{h^2}{M^2})\rho_i\}} \qquad (C.18)$$

or

$$\frac{q_i}{q_s} = \frac{1 - \theta_s\rho_s}{1 - \theta_i\rho_i} \qquad (C.19)$$

Equation (C.19) constitutes the power sharing relation, with θ_i and θ_s defined as:

$$\theta_i = 1 + \frac{91}{480}\frac{h^2}{M^2} \qquad (C.20)$$

and

$$\theta_s = 1 - \frac{11}{120}\frac{h^2}{M^2} = \frac{135 - 44\theta_i}{91} \approx \frac{3 - \theta_i}{2} \qquad (C.21)$$

With h = 21 cm and M^2 = 58 cm^2, Eqs. (3.19) and (3.20) yield:

$$\theta_i = 2.4$$
$$\theta_s = 0.30$$

These values are theoretical estimates of the θ constants. In practice, theoretical values are not used if sufficient data on a particular core is available, since that data can be used to

empirically obtain values for the thetas which best model the core.

For batches in a core, each assembly in the batch is, on the average, surrounded by critical neighbors, i.e., $\rho_s \cong 0$. With this approximation the batch-wise power split can be predicted by Eq. (C.19), with $\rho_s = 0$.

$$q_i = \frac{q_s}{1 - \theta_i \rho_i} \tag{C.22}$$

or in terms of the power fractions of each batch, f_i,

$$f_i = \frac{\bar{f}}{1 - \theta\rho_i} = \frac{1/n}{1 - \theta\rho_i} \tag{C.23}$$

where $\bar{f} = 1/n$, the average power fraction of the batches in the n-batch core,

and $$\theta = \theta_i = 1 + \frac{91}{480}\frac{h^2}{M^2} \tag{C.24}$$

C.2 Isolated 3 x 3 Assembly Clusters

In this section the power split relation appropriate for use on "isolated" 3 x 3 assembly clusters will be derived. The "isolated" configuration is shown in Chapter 3 as Fig. 3.1.

Compared to the analysis of 3 x 3 clusters in cores, the additional constraint is that the net neutron current at the mid-plane of the 8 surrounding assemblies, i.e., at r = h, is zero. Thus, using Eq. (C.3),

$$\left.\frac{d\phi_1}{dr}\right|_{r=h} = 0 = \left. 2a_2 r + 3a_3 r^2 \right|_{r=h} \qquad (C.25)$$

or

$$2a_2 h + 3a_3 h^2 = 0 \qquad (C.26)$$

Equations (C.11) and (C.17) are still valid for the isolated clusters, and can be used along with Eq. (C.26) to eliminate a_2 and a_3. This results in:

$$\bar{q}_s(1-\bar{\rho}_s) - \bar{q}_i(1-\bar{\rho}_i) + \frac{3}{40}\frac{h^2}{M^2}\bar{q}_i\bar{\rho}_i = 0$$

which gives upon rearrangement

$$q_i = \frac{q_s(1-\rho_s)}{(1-\theta\rho_i)} \qquad (C.27)$$

where $\theta = 1 + \frac{3}{40}\frac{h^2}{M^2}$

Equation (C.27) is the power split relation appropriate for isolated 3 x 3 clusters which are exactly critical. If the clusters are not critical, the effects of the non-criticality can be included in the algorithm. Supposing the cluster has excess reactivity ρ_x and following closely the treatment in Chapter 3 (Section 3.6), the power sharing algorithm for such a system can be written as:

$$q_i = \frac{q_s[1 - (\rho_s - \rho_x)]}{1 - \theta(\rho_i - \rho_x)} \qquad (C.28)$$

The reactivity of the cluster, ρ_x, is to a first approximation equal to the surrounding region reactivity ρ_s. With this approximation, Eq. (C.28) yields, after successive first order expansions:

$$q_i \approx \frac{q_s}{(1 - \theta_i\rho_i)(1 + \theta_i\rho_s)} \approx \frac{q_s(1 - \theta_s\rho_s)}{(1 - \theta_i\rho_i)} \qquad (C.29)$$

where $$\theta_i \approx \theta_s \approx 1 + \frac{3}{40}\frac{h^2}{M^2} \qquad (C.30)$$

For h = 21 cm, M^2 = 58 cm^2,

$$\theta_i \approx \theta_s \approx 1.6$$

which is again a theoretical estimate for θ.

An analysis of "isolated" 3 x 3 clusters is reported in Chapter 3. The PDQ-7 generated data for this case is included as Table C.1.

C.3 Smaller PWR Assemblies

In Chapter 5, small fuel assemblies for PWRs were examined. Equation (C.24) can be used to obtain a theoretical estimate for the theta constant for the smaller assemblies. The small assemblies considered are one quarter of current PWR assemblies, i.e., the assembly width, h = 10.5 cm, with M^2 = 58 cm^2,

TABLE C.1

PDQ-7 Generated Data for the
3 x 3 "Isolated" Fuel Assembly Clusters

ρ_i	q_i/q_s at		
	$\rho_s = 0.16028$	$\rho_s = 0.06652$	$\rho_s = -0.02715$
0.19756	1.06369	1.24380	1.44940
0.17914	1.03166	1.20570	1.40442
0.16028	1.00000	1.16801	1.35990
0.14135	0.96936	1.13153	1.31677
0.12248	0.93990	1.09646	1.27531
0.10378	0.91183	1.06306	1.23581
0.08510	0.88482	1.03091	1.19782
0.06652	0.85883	1.00000	1.16124
0.04790	0.83395	0.97042	1.12625
0.02927	0.81010	0.94206	1.09273
0.01063	0.78721	0.91487	1.06058
0.00823	0.76516	0.88871	1.02970
-0.02715	0.74388	0.86351	1.00000
-0.04617	0.72353	0.83943	0.97161
-0.06525	0.70408	0.81641	0.94450
-0.08422	0.68563	0.79460	0.91880
-0.10316	0.66810	0.77387	0.89438

ρ_i = interior region reactivity

ρ_s = surrounding region reactivity

q_i/q_s = ratio of the interior and exterior region's power densities

Eq. (C.24) gives:

$$\theta \approx 1.36 \quad \text{for smaller PWR assemblies.}$$

C.4 Internal Consistency of the Power Sharing Algorithm

An important constraint that the power split relation must comply to is given by Eq. (2.6), of Chapter 2, as

$$\sum_{i=1}^{n} f_i = 1.0 \tag{2.6}$$

or

$$\sum_{i=1}^{n} (f_i - \bar{f}) = \sum_{i=1}^{n} (f_i - \frac{1}{n}) = 0 \tag{C.31}$$

Substituting for f_i from Eq. (C.23) yields:

$$\sum_{i=1}^{n} \left\{ \frac{1/n}{1 - \theta\rho_i} - \frac{1}{n} \right\} = \sum_{i=1}^{n} \left\{ \frac{1 - (1 - \theta\rho_i)}{1 - \theta\rho_i} \right\}$$

$$= \sum_{i=1}^{n} \theta \left\{ \left(\frac{1/n}{1 - \theta\rho_i} \right) \rho_i \right\}$$

$$= \theta \sum_{i=1}^{n} f_i\rho_i = 0 \tag{C.32}$$

Since 'θ' is a constant, we get:

$$\sum_{i=1}^{n} f_i\rho_i = 0 \tag{C.33}$$

Equation (C.33) is the power-weighted prescription for core reactivity averaging (which was independently derived as Eq. (2.12) using the definition of reactivity) for a reactor with no leakage (i.e., $\rho_{sys} = 0$).

A similar but more laborious proof of consistency can be obtained with leakage and soluble poison reactivities included in the formulation.

C.5 Relation of the Power Split Relation to Perturbation Theory Methods

To see the effect on the system reactivity, $\Delta\rho_{sys}$, of a local change in reactivity, $\Delta\rho_i$ can be written using a Taylor series expansion as:

$$\Delta\rho_{sys} \simeq \sum \left(\frac{\partial \rho_{sys}}{\partial \rho_i} \right) \cdot \Delta\rho_i \qquad (C.34)$$

Using Eq. (2.12), the contribution of the region "i" reactivity to the system reactivity is $f_i\rho_i$. With this substitution for ρ_{sys}, Eq. (C.34) gives:

$$\Delta\rho_{sys} \simeq \sum \frac{\partial}{\partial \rho_i} (f_i \rho_i) \cdot \Delta\rho_i$$

Substituting for f_i from Eq. (C.23) gives:

$$\Delta\rho_{sys} \simeq \sum \frac{\partial}{\partial \rho_i} \left(\frac{1/n}{1 - \theta\rho_i} \cdot \rho_i \right) \Delta\rho_i$$

or

$$\Delta\rho_{sys} \simeq n \sum f_i^2 \cdot \Delta\rho_i \qquad (C.35)$$

Note that the power split relation (Eq. (C.23)) gives the familiar source-squared weighting characteristic of perturbation theory methods.

Loh [L-2] has discussed these aspects of the power sharing algorithms as well as their relation to nodal methods.

C.6 Core Leakage Constants for PWRs Employing Smaller Fuel Assemblies

In this section the results from PDQ-7 core-maps are used to obtain values for the two core leakage constants α_1 and α_2 used in the analysis of PWR cores with smaller fuel assemblies in Chapter 5. The reader is referred to Section 5.4 of Chapter 5 for details of the smaller assemblies considered in this work.

In the case of the smaller assemblies the leakage reactivity, ρ_2, defined by Eq. (2.14) of Chapter 2, can be written as:

$$\rho_L = \alpha_1 f_{per\ 1} + \alpha_2 f_{per\ 2} \qquad (C.36)$$

where α_1, α_2 = the core leakage constants for the principal peripheral region and the secondary peripheral region, respectively.

$f_{per\ 1}$, $f_{per\ 2}$ = the fractions of total core power being produced in the principal and

secondary peripheral regions, respectively.

It is important to emphasize that by Eq. (3.16) of Chapter 3, the following relation also holds:

$$\rho_L = \alpha f_{per} = \alpha(f_{per\,1} + f_{per\,2}) \qquad (C.37)$$

where α = the core leakage constant when the principal and secondary peripheral regions are taken to be one region (as for the analysis of PWR cores with standard-sized assemblies).

$f_{per} = f_{per\,1} + f_{per\,2}$. The fraction of the total core power produced in the two peripheral regions.

Combining Eqs. (C.36) and (C.37) yields, after some rearrangement:

$$\alpha = \frac{\alpha_1 + \alpha_2 f_{per\,2}/f_{per\,1}}{1 + f_{per\,2}/f_{per\,1}} \qquad (C.38)$$

Table C.2 shows the key parameters obtained from the seven PDQ-7 core maps. A least-squares fit to ρ_L as a function of f_{per} gave:

$$\rho_L = 0.0983\ f_{per} \qquad (C.39)$$

TABLE C.2

Principal and Secondary Peripheral Region Power Fractions and Core Leakage Reactivities from PDQ-7 Core Maps

Core Map #	Fractions of Total Core Power[a]			Leakage Reactivity
	f_{per}	$f_{per\ 1}$	$f_{per\ 2}$	ρ_L[b]
1	0.18099	0.06145	0.11954	0.01668
2[c]	0.19626	0.07731	0.11895	0.01960
3	0.23867	0.08816	0.15051	0.02268
4	0.24161	0.08755	0.15406	0.02282
5	0.29262	0.11133	0.18129	0.02858
6[c]	0.29617	0.11773	0.17844	0.02992
7[c]	0.36147	0.14422	0.21725	0.03650

[a] See accompanying text for definitions. Note that $f_{per} = f_{per\ 1} + f_{per\ 2}$.

[b] ρ_L defined by Eq. (2.14) of Chapter 2.

[c] These 3 cores had the same fuel in the principal and secondary fuel regions.

with $R^2 = 0.984$. The data from Table C.2 and the plot of Eq. (C.39) are shown as Fig. 3.8, of Chapter 3.

A least-squares multiple regression fit to ρ_L as a function of $f_{per\ 1}$, and $f_{per\ 2}$, from Table C.2, yields an excellent fit, with

$$\rho_L = 0.00025 + 0.23476\, f_{per\ 1} + 0.01146\, f_{per\ 2} \qquad (C.40)$$

with an R^2 of 0.9996.

From Eqs. (C.39) and (C.40)

$$\left.\begin{aligned} \alpha &= 0.0983 \\ \alpha_1 &= 0.2348 \\ \alpha_2 &= 0.0115 \end{aligned}\right\} \text{ for the core modelled on PDQ-7} \qquad (C.41)$$

Note that $\alpha_2 << \alpha_1$, which illustrates that core leakage is primarily from the outer half of the assembly, even when the power tilt is accounted for (i.e., $f_{per\ 2}/f_{per\ 1} \approx 2$).

These values of α_1 and α_2 can be used in the analysis of smaller fuel assemblies of the type studied here. However, in order to be consistent with the prior assessment of radial blankets and low-leakage fuel management schemes, it is necessary to deduce the appropriate values of α_1 and α_2 for the Combustion Engineering System-80™ core.

From published data on the CE System-80™ core, Loh [L-2] obtained a value for α of 0.285. This value has been used

throughout the present work to characterize radial neutron leakage.

As noted in Table C.2, three of the seven cores modelled on PDQ-7 had the same fuel loaded in the principal and secondary peripheral regions (i.e., equivalent to using standard PWR assemblies of the same reload batch on the core periphery). The data used by Loh to obtain the α for the CE System-80™ core was also for such fuel loading schemes. Two approximations are now required. The first is that given the same fuel loaded in the two peripheral regions, the ratio $f_{per\ 1}/f_{per\ 2}$ from the PDQ-7 core-map is equal to that for the CE System-80™ core with the same peripheral fuel. The second is that the ratio α_1/α_2 is also equal for the two cores.

With these approximations, Eq. (C.38) can be used with $\alpha = 0.285$, $f_{per\ 1}/f_{per\ 2}$ from Table C.2 and the α_1/α_2 ratio from Eq. (C.41), to obtain three sets of α_1 and α_2 values. The averages of these results (which differ from the individual values by less than 1%) are given below:

$$\left.\begin{aligned} \alpha_1 &\approx 0.6687 \\ \alpha_2 &\approx 0.0326 \end{aligned}\right\} \text{ Estimates for the CE System-80™ Core}$$

Given the similarity of the core modelled on PDQ-7 and the CE System-80™ core, the approximations are reasonable. Also note that the use of two different core leakage constants (α_1 and α_2) for the case of smaller PWR assemblies results in

a very accurate characterization of the radial leakage from the core (R^2 is very nearly exactly 1.0).

APPENDIX D

THE "SPILBAC" CODE

APPENDIX D

THE "SPILBAC" CODE

The SPILBAC program was used extensively in this work to calculate cycle and discharge burnups on a batch-average basis, for assessing a variety of fuel management schemes. The main features of SPILBAC and the calculational methodology used in it have been previously discussed in Chapter 3 (Section 3.7). In this appendix, the sensitivity of the code to the two main variables, the RPCF (or theta constant) and the core leakage constant (α) will be assessed. The input instructions for the program, a program listing, and a sample problem are also included.

D.1 The Sensitivity of SPILBAC to θ and α

The two main variables used in SPILBAC to determine the batch-wise power sharing and core depletion characteristics are the reactivity power coupling factor (RPCF, or θ), and the core leakage constant α (see Chapter 3). In order to quantify the sensitivity of the results to variations in these two parameters, the following investigation was carried out.

Three high-burnup PWR cores were chosen, representative of the largest contrasts in fuel management strategies investigated in this work. The three strategies are: conventional fuel loading (out-in/scatter), extreme low-leakage (batch-5 on periphery) and radial blankets of thorium type d-f assem-

blies. For these three cores, the values of θ and α in SPILBAC were varied from their nominal values ($\theta = 1.5$ and $\alpha = 0.285$).

The SPILBAC results for the key quantities of interest (i.e., discharge burnups and the uranium utilization index) as θ and α were each varied (with the other held constant) are shown in Tables D.1 and D.2.

The relative uranium utilization results are of primary interest in the present work, as measured by the uranium utilization index for a test core—the ratio of U_3O_8 consumption per unit of energy delivered—relative to that of a reference core with the same set of α and θ values as the test core. The results in Tables D.1 and D.2 show the relative insensitivity of the uranium utilization results to variations in either variable. Note, however, that the discharge burnups can vary substantially with θ and α.

Attention is also called to the benchmarking of the "group-and-one-half" model by Loh [L-2], who has shown that, given the complexity of the problem involved, the model produces satisfactory agreement with detailed state of the art physics analyses.

D.2 Code Listing, Input Specification and Sample Problem

The SPILBAC program is written in FORTRAN-IV. The code listing is included as Table D.3. The reader is also referred to the code description in Chapter 3 (Section 3.4).

Table D.1

Sensitivity of SPILBAC Results to Variation in θ (at constant α)

		α = 0.285		
		θ = 1.65	θ = 1.50	θ = 1.35
Reference Case[a] (Out-In/Scatter, i.e., Batch-1 on Periphery)	B_U[b]	49.980	49.912	49.809
	I_0[c]	1.0000	1.0000	1.0000
Reference Core with Batch-5 on Periphery (Low-Leakage)	B_U	52.974	52.845	52.563
	I_0	0.9434 (5.7%)[d]	0.9445 (5.6%)	0.9476 (5.2%)
Reference Core with Thorium d-f Radial Blanket	B_U	47.192	46.678	46.083
	B_{Th}[e]	21.910	22.846	23.931
	I_0	0.9489 (5.1%)	0.9527 (4.7%)	0.9567 (4.3%)

[a] High-Burnup Core, 5-batches.

[b] Uranium (steady-state) average discharge burnup, (GWD/MT).

[c] Unadjusted Index I_0, (see Eq. 4.1 of Chapter 4).

[d] Numbers in parentheses indicate uranium savings in percent (using I_0).

[e] Thorium blanket (steady-state) average discharge burnup, (GWD/MT).

Table D.2

Sensitivity of SPILBAC Results to Variation in α (at constant θ)

		$\theta = 1.50$		
		$\alpha = 0.314$	$\alpha = 0.285$	$\alpha = 0.257$
Reference Case[a] (Out-In/Scatter, i.e., Batch-1 on Periphery)	B_U[b]	49.118	49.912	50.719
	I_0[c]	1.0000	1.0000	1.0000
Reference Core with Batch-5 on Periphery (Low-Leakage)	B_U	52.084	52.845	53.436
	I_0	0.9431 (5.7%)[d]	0.9445 (5.6%)	0.9492 (5.1%)
Reference Core with Thorium d-f Radial Blanket	B_U	46.203	46.678	47.169
	B_{Th}[e]	22.049	22.846	23.835
	I_0	0.9498 (5.0%)	0.9527 (4.7%)	0.9547 (4.5%)

[a] High-Burnup Core, 5-batches.

[b] Uranium (steady-state) average discharge burnup, (GWD/MT).

[c] Unadjusted Index I_0, (see Eq. 4.1 of Chapter 4).

[d] Numbers in parentheses indicate uranium savings in percent (using I_0).

[e] Thorium blanket (steady-state) average discharge burnup, (GWD/MT).

Table D.3

Listing of the SPILBAC Code

```
FILE: SPRINT   CMSUT1   A                VM/SP CONVERSATIONAL MONITOR SYSTEM

C                                                                       SPI00010
C           ****************************                                SPI00020
C           *      THE SPILBAC CODE    *                                SPI00030
C           ****************************                                SPI00040
C                                                                       SPI00050
      IMPLICIT  REAL*8(A-H,M, O-Z) , REAL*8(K)                          SPI00060
      DIMENSION DONE1(20), B1(20), F1(20), RHO1(20), FA1(20),FAVG1(20)  SPI00070
      DIMENSION DONE2(20),B2(20),F2(20),RHO2(20),FA2(20),FAVG2(20)      SPI00080
      DIMENSION X(100),Y(100),G(100),SHIM1(20),SHIM2(20)                SPI00090
      DIMENSION FBOL1(20),FBOL2(20)                                     SPI00100
      REAL*8 TITLE(10)                                                  SPI00110
C                                                                       SPI00120
C                                                                       SPI00130
C                                                                       SPI00140
C       J     NUMBER OF BATCHES                                         SPI00150
C CONVRG    CONVERGENCE CRITERION IN MWD/MT                           SPI00160
C  TSTEP    TIME STEP OR BURNUP INCREMENT IN MWD/MT                   SPI00170
C   IDEG    DEGREE OF LARANGIAN INTERPOLATION                         SPI00180
C RHOINT    EXTRAPOLATED BOL REACTIVITY                               SPI00190
C RHOBOL    BOL REACTIVITY VALUE                                      SPI00200
C       A   SLOPE OF THE LINEAR REACTIVITY-BURNUP TRACE, MT/MWD       SPI00210
C THETA1    THETA VALUE FOR URANIUM FUEL BATCHES                      SPI00220
C THETA2    THETA VALUE FOR THORIUM FUEL BATCHES                      SPI00230
C   SHIM    LEAKAGE OR FIXED POISON REACTIVITY PENALTY                SPI00240
C      M1   MASS FRACTION OF URANIUM SUB-BATCH IN A BATCH             SPI00250
C      M2   MASS FRACTION OF THORIUM SUB-BATCH IN A BATCH             SPI00260
C                                                                       SPI00270
C                                                                       SPI00280
C                                                                       SPI00290
 6501 READ(5,6002)NCASE                                                 SPI00300
      IF(NCASE.GE.50)GOTO 919                                           SPI00310
      READ(5,6000) TITLE                                                SPI00320
      READ(5,6002) J,THETA1,THETA2,TSTEP,CONVRG                         SPI00330
      READ(5,2010) RHINT1,A1                                            SPI00340
      READ(5,6004)M2,M2INC,M2MAX                                        SPI00350
      ITM=0                                                             SPI00360
      IF(M2.NE.0)ITM=1                                                  SPI00370
      ITN=0                                                             SPI00380
      M2=M2-M2INC                                                       SPI00390
      READ(5,6003) NO,IDEG                                              SPI00400
C     READ NO BURNUP VALUES , X(I)                                      SPI00410
      READ(5,6004) (X(I),I=1,NO)                                        SPI00420
C     READ NO K-INFINITY VALUES G(I)                                    SPI00430
      READ(5,6004) (G(I),I=1,NO)                                        SPI00440
C                                                                       SPI00450
C                                                                       SPI00460
C                                                                       SPI00470
      DO 2344 I=1,J                                                     SPI00480
      B1(I)=0.0                                                         SPI00490
 2344 B2(I)=0.0                                                         SPI00500
C                                                                       SPI00510
C                                                                       SPI00520
      DO 2345 I=1,NO                                                    SPI00530
      Y(I)=1.0-(1.0/G(I))                                               SPI00540
 2345 CONTINUE                                                          SPI00550
```

Table D.3 (Cont'd.)

```
FILE: SPRINT   CMSUT1   A                VM/SP CONVERSATIONAL MONITOR SYSTEM

C                                                                       SPI00560
       STORE = TSTEP                                                    SPI00570
C                                                                       SPI00580
      RHBOL1=RHINT1                                                     SPI00590
      RHBOL2=Y(1)                                                       SPI00600
      BI=1000.0                                                         SPI00610
C                                                                       SPI00620
      READ(5,2040) (SHIM1(I),I=1,J)                                     SPI00630
      READ(5,2040) (SHIM2(I),I=1,J)                                     SPI00640
      WRITE(6,6001)TITLE                                                SPI00650
      WRITE(6,6007)RHINT1,A1                                            SPI00660
      WRITE(6,6008)(X(I),I=1,NO)                                        SPI00670
      WRITE(6,6009)(Y(I),I=1,NO)                                        SPI00680
      WRITE(6,6011)IDEG                                                 SPI00690
      WRITE(6,6005)J,THETA1,THETA2,TSTEP,CONVRG                         SPI00700
 6500 M2=M2+M2INC                                                       SPI00710
      M1=1.0-M2                                                         SPI00720
      WRITE(6,6006)M1,M2                                                SPI00730
      WRITE(6,5995)                                                     SPI00740
      WRITE(6,5996) (SHIM1(I),I=1,J)                                    SPI00750
      WRITE(6,5996) (SHIM2(I),I=1,J)                                    SPI00760
C                                                                       SPI00770
      IF. (M1.EQ.1.0) WRITE(6,3000)                                     SPI00780
C                                                                       SPI00790
      NUMB=0                                                            SPI00800
C                                                                       SPI00810
   11 DO 13 I=1,J                                                       SPI00820
      FA1(I)=0.0                                                        SPI00830
      FA2(I)=0.0                                                        SPI00840
   13 CONTINUE                                                          SPI00850
       TSTEP = STORE                                                    SPI00860
      ADD=0.0                                                           SPI00870
C                                                                       SPI00880
C                                                                       SPI00890
C                                                                       SPI00900
      JLESS=J-1                                                         SPI00910
      V=J                                                               SPI00920
      DONE1(1)=0.0                                                      SPI00930
      DONE2(1)=0.0                                                      SPI00940
C                                                                       SPI00950
C     ESTIMATE CYCLE BURNUP                                             SPI00960
C                                                                       SPI00970
      BEST1=2.0*RHINT1/((J+1)*A1)                                       SPI00980
      BEST2=1.5*RHINT1/((J+1)*A1)                                       SPI00990
C                                                                       SPI01000
C                                                                       SPI01010
      DO 120 I=1,J                                                      SPI01020
      L=I-1                                                             SPI01030
      W=L                                                               SPI01040
      DONE1(I)=W*BEST1                                                  SPI01050
      IF(M1.EQ.1.0)GOTO 120                                             SPI01060
      DONE2(I)=W*BEST2                                                  SPI01070
  120 CONTINUE                                                          SPI01080
C                                                                       SPI01090
C                                                                       SPI01100
```

Table D.3 (Cont'd-3)

```
FILE: SPRINT   CMSUT1   A                VM/SP CONVERSATIONAL MONITOR SYSTEM

   190 DO 200  I=1,J                                                    SPIO1110
       B1(I)=DONE1(I)                                                   SPIO1120
       IF(M1.EQ.1.0)GOTO 200                                            SPIO1130
       B2(I)=DONE2(I)                                                   SPIO1140
   200 CONTINUE                                                         SPIO1150
       GO TO 330                                                        SPIO1160
C                                                                       SPIO1170
C                                                                       SPIO1180
   210 CONTINUE                                                         SPIO1190
       FAVGS1=0.0                                                       SPIO1200
       FAVGS2=0.0                                                       SPIO1210
       DO 211 I=1,J                                                     SPIO1220
       FAVG1(I)=FA1(I)/ADD                                              SPIO1230
       FAVG2(I)=FA2(I)/ADD                                              SPIO1240
       FAVGS1=FAVGS1+FAVG1(I)                                           SPIO1250
       FAVGS2=FAVGS2+FAVG2(I)                                           SPIO1260
   211 CONTINUE                                                         SPIO1270
       DO 2110 I=1,J                                                    SPIO1280
       FAVG1(I)=M1*FAVG1(I)/((FAVGS1*M1)+(FAVGS2*M2))                   SPIO1290
       FAVG2(I)=M2*FAVG2(I)/((FAVGS1*M1)+(FAVGS2*M2))                   SPIO1300
  2110 CONTINUE                                                         SPIO1310
       NUMB = NUMB + 1                                                  SPIO1320
   212 IF(DABS(TELL1).LE.CONVRG.AND.DABS(TELL2).LE.CONVRG) GOTO 990     SPIO1330
       IF(NUMB.GT.40) GOTO 991                                          SPIO1340
C                                                                       SPIO1350
       DO 213 I=1,J                                                     SPIO1360
       FA1(I)=0.0                                                       SPIO1370
       FA2(I)=0.0                                                       SPIO1380
   213 CONTINUE                                                         SPIO1390
       ADD=0.0                                                          SPIO1400
       TSTEP = STORE                                                    SPIO1410
       S=0.0                                                            SPIO1420
   220 DO 230  I=1,J                                                    SPIO1430
       L=I-1                                                            SPIO1440
       IF (I.NE.1)  DONE1(I)=(B1(L)+DONE1(I))/2.0                       SPIO1450
       IF(M1.EQ.1.0)GOTO 230                                            SPIO1460
       IF (I.NE.1)  DONE2(I)=(B2(L)+DONE2(I))/2.0                       SPIO1470
   230 CONTINUE                                                         SPIO1480
       ITN=1                                                            SPIO1490
       GO TO 190                                                        SPIO1500
C                                                                       SPIO1510
C                                                                       SPIO1520
   330 DO 370 I=1,J                                                     SPIO1530
       RHO1(I)=RHINT1-A1*B1(I)                                          SPIO1540
       RHO1(I)=RHO1(I)-SHIM1(I)                                         SPIO1550
       IF(M1.EQ.1.0)GOTO 370                                            SPIO1560
       XARG=B2(I)                                                       SPIO1570
   340 DO 350 L=1,NO                                                    SPIO1580
       IF(L.EQ.NO.OR.XARG.LE.X(L)) GOTO 360                             SPIO1590
   350 CONTINUE                                                         SPIO1600
   360 LMAX= L+IDEG/2                                                   SPIO1610
       IF (LMAX.LE.IDEG) LMAX=IDEG+1                                    SPIO1620
       IF (LMAX.GT.NO) LMAX=NO                                          SPIO1630
       LMIN= LMAX-IDEG                                                  SPIO1640
       YINTER=FLAGR (X,Y,XARG,IDEG,LMIN,NO)                             SPIO1650
```

Table D.3 (Cont'd-4)

```
FILE: SPRINT   CMSUT1   A                VM/SP CONVERSATIONAL MONITOR SYSTEM

      RHO2(I)=YINTER                                                    SPIO1660
      RHO2(I)=RHO2(I)-SHIM2(I)                                          SPIO1670
  370 CONTINUE                                                          SPIO1680
C                                                                       SPIO1690
C                                                                       SPIO1700
C                                                                       SPIO1710
C                                                                       SPIO1720
      FSUM1=0.0                                                         SPIO1730
      FSUM2=0.0                                                         SPIO1740
      DO 371 I=1,J                                                      SPIO1750
      F1(I)=M1/(1.0-THETA1*RHO1(I))                                     SPIO1760
      F2(I)=M2/(1.0-THETA2*RHO2(I))                                     SPIO1770
      FSUM2=FSUM2+F2(I)                                                 SPIO1780
      FSUM1=FSUM1+F1(I)                                                 SPIO1790
  371 CONTINUE                                                          SPIO1800
C                                                                       SPIO1810
      RHOSYS=0.0                                                        SPIO1820
  380 DO 390  I=1,J                                                     SPIO1830
      F1(I)=F1(I)/(FSUM1+FSUM2)                                         SPIO1840
      F2(I)=F2(I)/(FSUM1+FSUM2)                                         SPIO1850
      RHOSYS=RHOSYS+((F1(I)*RHO1(I))+(F2(I)*RHO2(I)))                   SPIO1860
  390 CONTINUE                                                          SPIO1870
C                                                                       SPIO1880
C                                                                       SPIO1890
      POISON=0.0                                                        SPIO1900
C                                                                       SPIO1910
C                                                                       SPIO1920
      IF (RHOSYS.GE.0.0) GOTO 3902                                      SPIO1930
      IF (RHOSYS.LT.0.0) GOTO 410                                       SPIO1940
 3902 IF (RHOSYS.LE.0.0001) GOTO 460                                    SPIO1950
      IF (RHOSYS.GT.0.0001) GOTO 392                                    SPIO1960
C                                                                       SPIO1970
C                                                                       SPIO1980
  392 DELTA=RHOSYS                                                      SPIO1990
      POISON=POISON+DELTA                                               SPIO2000
      FSUMM1=0.0                                                        SPIO2010
      FSUMM2=0.0                                                        SPIO2020
      DO 395 I=1,J                                                      SPIO2030
      RHO1(I)=RHO1(I)-DELTA/J                                           SPIO2040
      RHO2(I)=RHO2(I)-DELTA/J                                           SPIO2050
      F1(I)=M1/(1.0-THETA1*RHO1(I))                                     SPIO2060
      F2(I)=M2/(1.0-THETA2*RHO2(I))                                     SPIO2070
      FSUMM1=FSUMM1+F1(I)                                               SPIO2080
      FSUMM2=FSUMM2+F2(I)                                               SPIO2090
  395 CONTINUE                                                          SPIO2100
C                                                                       SPIO2110
C                                                                       SPIO2120
      RHOSYS=0.0                                                        SPIO2130
      DO 397 I=1,J                                                      SPIO2140
      F1(I)=F1(I)/(FSUMM1+FSUMM2)                                       SPIO2150
      F2(I)=F2(I)/(FSUMM1+FSUMM2)                                       SPIO2160
      IF(ITN.EQ.1) FBOL1(I)=F1(I)                                       SPIO2170
      IF(ITN.EQ.1) FBOL2(I)=F2(I)                                       SPIO2180
      RHOSYS=RHOSYS+((F1(I)*RHO1(I))+(F2(I)*RHO2(I)))                   SPIO2190
  397 CONTINUE                                                          SPIO2200
```

Table D.3 (Cont'd-5)

```
FILE: SPRINT   CMSUT1   A                VM/SP CONVERSATIONAL MONITOR SYSTEM

      ITN=0                                                              SPI02210
C                                                                        SPI02220
C                                                                        SPI02230
      IF (RHOSYS.LE.0.0001) GOTO 417                                     SPI02240
      IF (RHOSYS.GT.0.0001) GOTO 392                                     SPI02250
C                                                                        SPI02260
C                                                                        SPI02270
C                                                                        SPI02280
C                                                                        SPI02290
C                                                                        SPI02300
  410 DO 415 I=1,J                                                       SPI02310
      B1(I)=B1(I)-F1(I)*TSTEP/M1                                         SPI02320
      FA1(I)=FA1(I)-F1(I)*TSTEP/M1                                       SPI02330
      IF(M1.EQ.1.0)GOTO 415                                              SPI02340
      B2(I)=B2(I)-F2(I)*TSTEP/M2                                         SPI02350
      FA2(I)=FA2(I)-F2(I)*TSTEP/M2                                       SPI02360
  415 CONTINUE                                                           SPI02370
C                                                                        SPI02380
      ADD=ADD-TSTEP                                                      SPI02390
      TSTEP=TSTEP/2.0                                                    SPI02400
C                                                                        SPI02410
C                                                                        SPI02420
  417 DO 420 I=1,J                                                       SPI02430
      B1(I)=B1(I)+F1(I)*TSTEP/M1                                         SPI02440
      FA1(I)=FA1(I)+F1(I)*TSTEP/M1                                       SPI02450
      IF(M1.EQ.1.0)GOTO 420                                              SPI02460
      B2(I)=B2(I)+F2(I)*TSTEP/M2                                         SPI02470
      FA2(I)=FA2(I)+F2(I)*TSTEP/M2                                       SPI02480
  420 CONTINUE                                                           SPI02490
C                                                                        SPI02500
      ADD=ADD+TSTEP                                                      SPI02510
C                                                                        SPI02520
      GOTO 330                                                           SPI02530
C                                                                        SPI02540
C                                                                        SPI02550
  460  CONTINUE                                                          SPI02560
  540 IF (J.EQ.1)  GO TO 560                                             SPI02570
C                                                                        SPI02580
C     CHECK FOR CONVERGENCE AT CYCLE END-POINTS                          SPI02590
C                                                                        SPI02600
  550 DO 560 I=1,JLESS                                                   SPI02610
      IM=I+1                                                             SPI02620
      TELL1=B1(I)-DONE1(IM)                                              SPI02630
      TELL2=B2(I)-DONE2(IM)                                              SPI02640
      IF (DABS(TELL1).GT.CONVRG) GOTO 210                                SPI02650
      IF (DABS(TELL2).GT.CONVRG) GOTO 210                                SPI02660
  560 CONTINUE                                                           SPI02670
      GO TO 210                                                          SPI02680
  991 WRITE(6,6013)                                                      SPI02690
  990 IF (M1.EQ.1.0) BREF=B1(J)                                          SPI02700
      WRITE(6,3070)NUMB                                                  SPI02710
      WRITE(6,3090) (B1(I),I=1,J)                                        SPI02720
      WRITE(6,3100) (FAVG1(I),I=1,J)                                     SPI02730
      WRITE(6,3100) (FBOL1(I),I=1,J)                                     SPI02740
      WRITE(6,3100) (F1(I),I=1,J)                                        SPI02750
```

Table D.3 (Cont'd-6)

```
FILE: SPRINT   CMSUT1   A              VM/SP CONVERSATIONAL MONITOR SYSTEM

      WRITE(6,3091) (B2(I),I=1,J)                                          SPI02760
      WRITE(6,3100) (FAVG2(I),I=1,J)                                       SPI02770
      WRITE(6,3100) (FBOL2(I),I=1,J)                                       SPI02780
      WRITE(6,3100) (F2(I),I=1,J)                                          SPI02790
      IF(ITM.EQ.1) GOTO 999                                                SPI02800
      UTIL=(M1*B1(J)+M2*B2(J))/(BREF*M1)                                   SPI02810
      WRITE(6,6012)UTIL                                                    SPI02820
  999 WRITE(6,4060)                                                        SPI02830
      IF (M2.GE.M2MAX) GOTO 6501                                           SPI02840
      GOTO 6500                                                            SPI02850
  919 STOP                                                                 SPI02860
C                                                                          SPI02870
C       FORMATS FOR INPUT AND OUTPUT STATEMENTS                            SPI02880
C                                                                          SPI02890
 6000 FORMAT(10A8)                                                         SPI02900
 6001 FORMAT(1H1,1X,10A8)                                                  SPI02910
                                                                           SPI02920
 6002 FORMAT(8X,I2,4F10.5)                                                 SPI02930
 6003 FORMAT(8X,I2,8X,I2)                                                  SPI02940
 6004 FORMAT(8F10.4)                                                       SPI02950
 6005 FORMAT(1X//' NUMBER OF BATCHES=',I2,12X,'THETA FOR URANIUM  ='       SPI02960
     C,F6.4,'.       THAETA FOR THORIUM  =',F6.4,'. '/                     SPI02970
     C' BURNUP STEP,MWD/MT=',F7.0,6X,'CONVERGENCE CRITERON (MWD/MT) = ',SPI02980
     CF5.1/)                                                               SPI02990
 2010 FORMAT(F10.5,E10.5)                                                  SPI03000
 6006 FORMAT(1X/' FRACTION OF URANIUM IN CORE=',F6.3/' FRACTION OF THORISPI03010
     $UM IN CORE=',F6.3)                                                   SPI03020
 6007 FORMAT(1X/' FOR URANIUM;  BOL REACTIVITY=',F8.6/                     SPI03030
     C           '               SLOPE OF FIT (MT/MWD)=',E10.5)            SPI03040
 6008 FORMAT(1X/' FOR THORIUM; REACTIVITY/BURNUP TRACE USED FOR INTERPOLSPI03050
     $ATION;'//                                                            SPI03060
     $' BURNUP'/10(2X,F8.2))                                               SPI03070
 6009 FORMAT(1X/' REACTIVITY'/10(2X,F8.5))                                 SPI03080
 5995 FORMAT(1X/' SHIM OR LEAKAGE IN EACH SUB-BATCH'/)                     SPI03090
 5996 FORMAT(1X/7(3X,F7.5))                                                SPI03100
 6011 FORMAT(1X,' ORDER OF FIT=',I3)                                       SPI03110
 6012 FORMAT(1X//' ***URANIUM UTILIZATION AS A FRACTION OF NO THORIUM CASPI03120
     $SE=',F7.4)                                                           SPI03130
 6013 FORMAT(1X,' &&& DID NOT CONVERGE AFTER 40 ITTERATIONS &&&&'/         SPI03140
     $           '&&&&&&&&&&&&&&&&&&&&&&&&&&&&&&&&&&&&&&&&&&&&&&&')        SPI03150
 2040 FORMAT(8F10.7)                                                       SPI03160
 3000 FORMAT(1X///4X,' THE VALUES OF BATCH BURNUP B(I) IN MWD/MT,'/        SPI03170
     $       4X,' FOR URANIUM AND THORIUM BATCHES RESPECTIVELY AND'/       SPI03180
     $        4X,' THE SUB BATCH POWER FRACTIONS ARE ARRANGED IN'/         SPI03190
     $        4X,' THE FOLLOWING ORDER '///                                SPI03200
     $        13X,4HB(1),9X,4HB(2),9X,4HB(3),9X,4HB(4),9X,4HB(5),          SPI03210
     $        6X,3HETC/13X,4HF(1),9X,4HF(2),9X,4HF(3),9X,                  SPI03220
     $        4HF(4),9X,4HF(5),6X,3HETC,'  (CYCLE AVERAGED)'/13X,          SPI03230
     $        4HF(1),9X,4HF(2),45X,3HETC,'  (BOC)'/13X,                    SPI03240
     $        4HF(1),9X,4HF(2),45X,3HETC,'  (EOC)'///)                     SPI03250
                                                                           SPI03260
C                                                                          SPI03270
 4060 FORMAT(1X//'******** END OF COMPUTATION**********',1H1)              SPI03280
 3070 FORMAT(//3X,'NUMBER OF ITERATIONS=',I3)                              SPI03290
 3090  FORMAT (/5X,'URANIUM',6(3X,F10.1),'BURNUP IN MWD/MT')               SPI03300
```

Table D.3 (Cont'd-7)

```
FILE: SPRINT   CMSUT1   A                VM/SP CONVERSATIONAL MONITOR SYSTEM

 3091  FORMAT (/5X,'THORIUM',6(3X,F10.1),'BURNUP IN MWD/MT')          SPI03310
 3100  FORMAT (12X,6(3X,F10.4),'FRACTION OF CORE POWER')              SPI03320
C                                                                    SPI03330
C                                                                    SPI03340
      END                                                            SPI03350
C                                                                    SPI03360
C     ******* INTERPOLATION ROUTINE                                  SPI03370
C                                                                    SPI03380
      FUNCTION FLAGR(X,Y,XARG,IDEG,LMIN,NO)                          SPI03390
      IMPLICIT REAL*8(A-H,O-Z)                                       SPI03400
      REAL*8 X,Y,XARG,FLAGR                                          SPI03410
      DIMENSION X(NO),Y(NO)                                          SPI03420
      FACTOR=1.0                                                     SPI03430
      LMAX=LMIN+IDEG                                                 SPI03440
      DO 3002 J=LMIN,LMAX                                            SPI03450
      IF (XARG.NE.X(J)) GOTO 3002                                    SPI03460
      FLAGR= Y(J)                                                    SPI03470
      RETURN                                                         SPI03480
 3002 FACTOR=FACTOR*(XARG-X(J))                                      SPI03490
      YEST=0.0                                                       SPI03500
      DO 3005 I=LMIN,LMAX                                            SPI03510
      TERM= Y(I)*FACTOR/(XARG-X(I))                                  SPI03520
      DO 3004 J= LMIN,LMAX                                           SPI03530
 3004 IF(I.NE.J) TERM=TERM/(X(I)-X(J))                               SPI03540
 3005 YEST=YEST+TERM                                                 SPI03550
      FLAGR=YEST                                                     SPI03560
      RETURN                                                         SPI03570
      END                                                            SPI03580
```

Table D.4 presents the input specifications for the code, and Tables D.5 and D.6 show the input to and output from a sample problem, respectively. The Sample Problem is the case of thorium d-f assemblies as radial blanket assemblies in a high burnup PWR (see Section 4.6.2 and Table 4.10 of Chapter 4).

Table D.4

Input Specification for SPILBAC

Card Set 1 (one card)

NCASE: IF 'NCASE' is greater than 49, program terminates.

FORMAT (8X,I2)

Card Set 2 (one card)

TITLE: Title of case.

FORMAT (10A8)

Card Set 3 (one card)

J: Number of batches.

THETA1: The theta constant for sub-batch 1 (labeled 'uranium').

THETA2: The theta constant for sub-batch 2 (labeled 'thorium').

TSTEP: Burnup-step size (MWD/MT).

CONVRG: Converge criterion (MWD/MT).

FORMAT: (8X,I2,4F10.5)

Card Set 4 (one card)

RHINT1: Extrapolated BOL reactivity, ρ_0, for 'uranium' sub-batch.

A1: Slope of linear $\rho(B)$ curve for 'uranium' sub-batch, $(MWD/MT)^{-1}$.

FORMAT (F10.5,E10.5)

Table D.4 (Cont'd.)

Card Set 5	(one card)
M2:	Mass fraction of sub-batch 2 (labeled 'thorium') in the core ($\leq$1.0).
M2INC:	The increment to M2 (for multiple cases).
M2MAX:	The maximum value of M2.
FORMAT	(2F10.4)
Card Set 6	(one card)
NO:	Number of burnup and k_∞ sets of data for the 'thorium' sub-batch.
IDEG:	Order of Lagrangian interpolation.
FORMAT	(2(8X,I2))
Card Set 7	(one or more cards)
X(I):	'Thorium' sub-batch burnup values (MWD/MT); NO entries.
FORMAT	(8F10.4)
Card Set 8	(one or more cards)
G(I):	'Thorium' sub-batch k_∞ values; NO entries.
FORMAT	(8F10.4)
Card Set 9	(one card)
SHIM1(I):	Leakage coefficients (α), or shim poison $\Delta\rho$, for 'uranium' sub-batch over each cycle; J entries.
FORMAT	(8(F10.7))

Table D.4 (Cont'd-3)

Card Set 10 (one card)

SHIM2: Leakage coefficient (α), or shim poison $\Delta\rho$, for 'thorium' sub-batch; J entries.

FORMAT (8(F10.7))

Table D.5

Sample Problem Input

```
FILE: SPRINT   CMSUT1   A                VM/SP CONVERSATIONAL MONITOR SYSTEM

001
THORIUM D-F RADIAL BLANKET IN HIGH-BURNUP PWR -
         5       1.50       1.50      200.0      50.00
   0.26610 0.7154E-5
      0.20      0.020       0.00
        15          4
      0.00     2000.0     4000.0     7000.0     10000.0    13000.0    16000.0    19000.0
   22000.0    25000.0    28000.0    31000.0    34000.0    37000.0    52000.0
   0.60000    0.68114    0.75114    0.80791    0.83775    0.85209    0.85876    0.86144
   0.86152    0.86017    0.85774    0.85451    0.85086    0.84691    0.82658
    0.0000     0.0000     0.0000     0.0000     0.0000
    0.2850     0.2850     0.2850     0.2850     0.2850
9999999999 LAST
```

```
 1 THORIUM D-F RADIAL BLANKET IN HIGH-BURNUP PWR -

  FOR URANIUM;  BOL REACTIVITY=0.266100
                SLOPE OF FIT (MT/MWD)=.71540D-05

  FOR THORIUM; REACTIVITY/BURNUP TRACE USED FOR INTERPOLATION;

  BURNUP
       0.0    2000.00   4000.00   7000.00  10000.00  13000.00  16000.00  19000.00  22000.00  25000.00
   28000.00  31000.00  34000.00  37000.00  52000.00

  REACTIVITY
   -0.66667  -0.46813  -0.33131  -0.23776  -0.19367  -0.17358  -0.16447  -0.16085  -0.16074  -0.16256
   -0.16585  -0.17026  -0.17528  -0.18076  -0.20980
   ORDER OF FIT=  4


  NUMBER OF BATCHES= 5              THETAS FOR POWER SPLIT=1.5000 FOR UARNIUM AND =1.5000 FOR THORIUM.
  BURNUP STEP,MWD/MT=   200.        CONVERGENCE CRITERON (MWD/MT) =  50.0


  FRACTION OF URANIUM IN CORE= 0.800
  FRACTION OF THORIUM IN CORE= 0.200

  SHIM OR LEAKAGE IN EACH SUB-BATCH


    0.0        0.0        0.0        0.0        0.0

    0.28500    0.28500    0.28500    0.28500    0.28500


    NUMBER OF ITERATIONS= 18

      URANIUM       11791.1      21910.3      30914.1      39107.7      46678.0
                     0.2251       0.1932       0.1719       0.1564       0.1445
                     0.2371       0.1970       0.1720       0.1545       0.1415
                     0.2200       0.1914       0.1716       0.1568       0.1452

      THORIUM        3805.6       8284.2      13050.6      17921.9      22846.2
                     0.0182       0.0214       0.0227       0.0232       0.0233
                     0.0150       0.0188       0.0208       0.0216       0.0218
                     0.0206       0.0229       0.0237       0.0240       0.0240

******** END OF COMPUTATION***********1
```

Table D.6
Sample Problem Output

APPENDIX E

THE MODEL FOR URANIUM UTILIZATION

APPENDIX E

THE MODEL FOR URANIUM UTILIZATION

E.1 Introduction

The assessment of the comparative uranium utilization of various fuel management strategies is central to the present work. A number of complications are inherent in making such comparisons in a consistent manner. Here we will present a model for assessing uranium utilization on an "all-else-being-equal" basis, under strictly defined criteria.

The comparison of the uranium utilization of two cores, one of which is often a 'reference' core design, can be made in a number of ways. Four important bases are:

(i) the test case and the reference case use the same quantity of natural uranium per reload batch, or

(ii) the two have the same U-235 commitment per reload batch, or

(iii) they deliver the same effective full power hours, efph, or

(iv) they incur the same fuel discharge burnup.

Often investigators choose one of these bases of comparison, neglecting the others. We will show in the following pages that the constraints give rise to different expressions for the uranium utilization. Examples in the main text illustrate that, depending on the particular fuel management strategy being employed, there can be substantial differences in the numerical results yielded by these relations. In what

follows, a methodology will be presented to convert the results appropriate to any one of these criteria into results corresponding to any of the others.

The basic, unadjusted, index for uranium utilization, I_0, for a test case relative to a reference case (subscript R) is defined as:

$$I_0 = \frac{U}{U_R} = \frac{F / BP}{F_R / B_R P_R} \qquad \text{(E.1)}$$

where U = Uranium yellowcake usage, $STU_3O_8 / (MWD)_{BATCH}$

$= F / BP$

F = U_3O_8 required per reload batch, STU_3O_8

B = The 'effective' batch discharge burnup,

$(MWD)_{BATCH} / MT$

P = Batch Uranium loading, MT

The 'effective' batch discharge burnup, B, is the total energy extracted from the batch (which may have two or more sub-batches), divided by the mass of uranium heavy metal in that batch. The sub-batch concept is important because if one of the sub-batches is composed of enriched uranium and the other of thorium, the energy generated by the thorium sub-batch is "free", as far as natural uranium requirements are concerned. Therefore, if the two sub-batches comprise the mass fractions M_U and M_{Th} in the total batch, then the 'effective' burnup, B, appropriate for use in uranium utilization calculations is:

$$B = \frac{M_U B_U + M_{Th} B_{Th}}{M_U} \quad , \quad \text{MWD/MT} \qquad \text{(E.2)}$$

where M_U, M_{Th} = the fractions of uranium and thorium in the batch, respectively ($M_U + M_{Th} = 1.0$), and

B_U, B_{Th} = the actual discharge burnups of the uranium and thorium sub-batches, respectively, MWD/MT.

Furthermore, the ratio F/P, in Eq. (E.1) is

$$\frac{F}{P} = \frac{\bar{X} - X_W}{X_F - X_W} \qquad \text{(E.3)}$$

where $\bar{X}$ = the average BOL fuel enrichment of the all-uranium batch (or the all-uranium sub-batch)

X_W = the tails enrichment

X_F = the feed enrichment

Substituting for B from Eq. (E.2) and F/P from Eq. (E.3), in Eq. (E.1) yields:

$$I_0 = \frac{U}{U_R} = \left(\frac{\bar{X} - X_W}{\bar{X}_R - X_W}\right) \cdot \frac{B_R \, M_U}{(M_U B_U + M_{Th} B_{Th})} \qquad \text{(E.4)}$$

Here it was assumed that the reference reactor is composed of all-uranium fuel, with average enrichment $\bar{X}_R$ and average dis-

charge burnup B_R.

The adjustment of the uranium utilization index I_0 to match one of the four criteria mentioned above can be accomplished by adjusting either the test case results or the reference case results. It has been shown that the two approaches give essentially identical results [K-2]. We will adjust the reference case results, since for the applications considered here it is considerably easier to do so in an accurate and unambiguous manner.

E.2 The Adjusted Reference Case Model

As stated above, in the adjusted reference case model the reference case parameters are adjusted so that the test and reference cases conform to one of the four constraints above.

If the uranium sub-batches in the test case and the uranium batches in the reference case have the same quantity of uranium per pincell, the four conditions are reduced to two. This is because if the uranium pincells are identical in the test and the reference cases (same fuel-to-moderator ratio, fuel pellet radius and fuel density, etc.), then the requirement that the two use the same quantity of natural uranium per reload batch automatically requires that the same quantity of U-235 be loaded into both, through Eq. (E.3). The conditions of equal discharge burnup and equal efph are similarly identical. The four criteria differ, however, for cases (not considered here) in which pincell uranium mass is

not conserved—as when annular fuel is used; reference [K-2] considers comparisons of this type.

The set of four initial constraints are therefore reduced to two. These are restated below.

Constraint a: The test and reference cases use the same quantity of uranium yellowcake (and therefore the same quantity of U-235). The adjusted uranium utilization index derived under this constraint will be termed I_{235}.

Constraint b: The test and reference cases produce equal effective full power hours in the reactor. This condition is identical to requiring that the effective discharge burnups of the test case and of the reference case be equal. The uranium utilization index derived under this constraint will be termed I_{efph}.

Denoting the adjusted reference parameters by a superscript '*', we can write I_{235} and I_{efph} using Eq. (E.1) as:

$$I_{235} = \frac{F / BP}{(F^*_R / B^*_R P^*_R)_{235}} \qquad \text{(E.5)}$$

and

$$I_{efph} = \frac{F / BP}{(F^*_R / B^*_R P^*_R)_{efph}}$$

Substituting for B from Eq. (E.4) yields

$$I_{235} = \left(\frac{U}{U_R^*}\right)_{235}$$

$$= \left[\left(\frac{\bar{X} - X_W}{\bar{X}_R^* - X_W}\right) \cdot \frac{B_R^* M_U}{(M_U B_U + M_{Th} B_{Th})}\right]_{235} \qquad (E.7)$$

and $$I_{efph} = \left(\frac{U}{U_R^*}\right)_{efph}$$

$$= \left[\left(\frac{\bar{X} - X_W}{\bar{X}_R^* - X_W}\right) \cdot \frac{B_B^* M_U}{(M_U B_U + M_{Th} B_{Th})}\right]_{efph} \qquad (E.8)$$

In general, the adjusted reference case burnups, B_R^*, in Eqs. (E.7) and (E.8) will be unequal. The same is true for the adjusted reference case enrichments, $\bar{X}_R^*$ in the two equations.

All reference cases in our comparison are uranium fuel enriched to between 2 and 5 w/0 in U-235. As illustrated in Chapter 2, in this range the reactivity, ρ, is a linear function of burnup, B, the two being related by Eq. (2.2) as

$$\rho = \rho_0 - AB \qquad (E.9)$$

where A = the slope of the ρ versus B linear fit,

MT/MWD

ρ_0 = the extrapolated BOL reactivity

The constants ρ_0 and A are functions of enrichment as well as the design of the lattice.

For such cases, the steady state discharge burnup, B_R, employing the equal power sharing approximation and neglecting leakage, is given by Eq. (2.18) as

$$B_R = \frac{2n}{n+1} \frac{\rho_0}{A} \tag{E.10}$$

where n is the number of batches in the core.

As shown in Appendix B, for a fixed assembly design, the quantity ρ_0/A is a linear function of the reload enrichment, X, over the range of enrichments of interest

$$\left(\frac{\rho_0}{A}\right) = a + b\bar{X} \tag{E.11}$$

where a and b are constants. Using Eqs. (E.10) and (E.11) for the ratio B_R^*/B_R leads to

$$\frac{B_R^*}{B_R} = \frac{a + b\bar{X}_R^*}{a + b\bar{X}_R} \tag{E.12}$$

Using Eq. (E.3) for the ratio F_R^*/F_R yields

$$\frac{F_R^*}{F_R} = \frac{\bar{X}_R^* - X_W}{\bar{X}_R - X_W} \quad , \tag{E.13}$$

since $P_R = P_R^*$, i.e., the actual and adjusted reference cases have the same uranium loading.

For Constraint (a): equal U-235 and uranium yellowcake

In this condition we require that the test and adjusted reference cases require the same quantity of ore, i.e.,

$$\bar{X}_R^* P_R = \bar{X} P \tag{E.14}$$

In our test cases the enrichment of the uranium sub-batch, $\bar{X}$, was equal to the reference case enrichment, $\bar{X}_R$. Also, the uranium content in the test case is equal to the product of the reference case uranium mass and the fraction of uranium in the test case, M_U. Making these substitutions in Eq. (E.14), one obtains

$$\bar{X}_R^* = \bar{X}_R \cdot M_U \tag{E.15}$$

Substituting for $\bar{X}_R^*$ from Eq. (E.15) into Eq. (E.12) yields:

$$B_R^* = \left(\frac{a + b\bar{X}_R M_U}{a + b\bar{X}_R} \right) B_R \tag{E.16}$$

And, finally, substituting for $\bar{X}_R^*$ and B_R^* from Eqs. (E.15) and (E.16) respectively, in Eq. (E.7), and with $\bar{X} = \bar{X}_R$, there results:

$$I_{235} = \left(\frac{\bar{X}_R - X_W}{X_R M_U - X_W} \right) \cdot \frac{M_U B_R (a + b\bar{X}_R M_U)}{(a + b\bar{X}_R)(M_U B_U + M_{Th} B_{Th})} \tag{E.17}$$

For Constraint (b): equal efph and burnup

Under this condition, we require that the test case and the adjusted cases deliver the same effective full power hours, i.e.,

$$B_R^* = B = \frac{M_U B_U + M_{Th} B_{Th}}{M_U} \tag{E.18}$$

where we have used the expression for B given by Eq. (E.2). Rearrangement of Eq. (E.12) yields:

$$\bar{X}_R^* = \frac{B_R^*}{B_R} \left(\frac{a}{b} + \bar{X}_R \right) - \frac{a}{b} \tag{E.19}$$

Substituting from Eq. (E.18) for B_R^* into Eq. (E.19),

$$X_R^* = \left(\frac{B_U + M_{Th} B_{Th}/M_U}{B_R} \right) \left(\frac{a}{b} + \bar{X}_R \right) - \frac{a}{b} \tag{E.20}$$

Substituting for X_R^* from Eq. (E.20) and for B_R^* from Eq. (E.18), in Eq. (E.8), with $\overline{X} = \overline{X}_R$, gives

$$I_{efph} = \frac{(\overline{X}_R - X_W)}{\left[\left\{\frac{B_U + B_{Th}(M_{Th}/M_U)}{B_R}\left(\frac{a}{b} + \overline{X}_R\right) - \frac{a}{b}\right\} - X_W\right]} \qquad \text{(E.21)}$$

Equations (E.17) and (E.21) are the expressions for the two adjusted uranium utilization indices used in this work. As explained in the main text, this treatment is necessary if the final results are to be compared on a consistent basis.

REFERENCES

REFERENCES

A-1 L.S. Abbot, D.E. Bartine and T.J. Burns,(Editors), "Interim Assessment of the Denatured U-233 Fuel Cycle: Feasibility and Non Proliferation Characteristics," Oak Ridge National Laboratory, ORNL-5338, (December 1979).

A-2 H. Amster and R. Suarez, "The Calculation of Thermal Constants Averaged Over a Wigner-Wilkins Flux Spectrum: A Description of the SOFOCATE Code," WAPD-TM-39, (1957).

B-1 Bettis Atomic Power Laboratory, "Three Core Concepts for Producing Uranium-233 in Commercial Pressurized Light Water Reactors for Possible Use in Water-Cooled Breeder Reactors," WAPD-TM-1310, (December 1979).

B-2 R.F. Barry, "LEOPARD - A Spectrum Dependent Non-Spatial Depletion Code," WCAP-3269-26, (September 1973).

B-3 H. Bohl, E. Gelbard and G.Ryan, "MUFT-4 - Fast Neutron Spectrum Code for the IBM-704," WAPD-TM-72, (July 1957).

C-1 G.W. Cunningham, "Optimized Once-Through Cycle and International Non-Proliferation Objectives," Trans. Am. Nucl. Soc.,30,274, (1978)

C-2 R.L. Crowther, et. al., "BWR Thorium Cycles with Improved Performance," Trans. Am. Nucl. Soc., 28, 337, (1978).

C-3 Y.I. Chang, et. al., "Alternative Fuel Cycle Options: Performance Characteristics and Impact on Nuclear Power Growth Potential," RSS-TM-4, Argonne National Laboratory, (January 1979).

C-4 F. Correa, M.J. Driscoll and D.D Lanning, "An Evaluation of Tight-Pitch PWR Cores", MIT Energy Laboratory Report No. MIT-EL 79-022, (August 1979).

C-5 W.R. Cadwell, "PDQ-7 Reference Manual," Bettis Atomic Power Laboratory, WAPD-TM-678, (1967).

D-1 M.J. Driscoll, E.K. Fujita and D.D. Lanning, "Improvements of PWRs on the Once-Through Fuel Cycle," Trans. Am. Nucl. Soc., 30, 280, (1978).

D-2 M.J. Driscoll, E.E. Pilat and F. Correa, "Routine Coastdown in LWRs as an Ore Conservation Measure," Trans. Am. Nucl. Soc., 33, 399, (1979).

E-1 E.A. Eschbach, E.T. Merrill and A.W. Prichard, "An Analysis of Thorium-Salted Fuels to Improve Uranium Utilization in the Once-Through Fuel Cycles," Battelle Memorial Institute (Northwest Laboratory), PNL-3977, (September 1981).

F-1 E.K. Fujita, M.J. Driscoll and D.D. Lanning, "Design and Fuel Management of PWR Cores to Optimize The Once-Through Fuel Cycle," M.I.T. Energy Laboratory Report No. MIT-EL-78-017, (1978).

G-1 K.C. Garel, et. al., "A Comparitive Assessment of the PWR, SSCR and PHWR Concepts,"Trans. Am. Nucl. Soc., 31, 301, (1978).

G-2 K.C. Garel, and M.J. Driscoll,"Fuel Cycle Optimization of Thorium and Uranium Fueled PWR Systems," M.I.T. Energy Laboratory Report No. MIT-EL-77-018, (1977).

H-1 A.F. Henry, "Nuclear-Reactor Analysis," MIT Press, Cambridge MA, (1975).

H-2 L.A. Hageman, "Numerical Methods and Techniques Used in the Two-Dimensional Neutron Diffusion Program PDQ-5," WAPD-TM-364, (1963).

I-1 M. Izenson, "Revisions to SONUFA/B," Special Problem (22.901), MIT Dept. of Nuclaer Engineering, (May 1982).

I-2 "INFCE Report of the International Fuel Cycle Evaluation," The International Atomic Energy Agency, Vienna, (1980).

K-1 P.R. Kasten, et. al., "Assessment of the Thorium Fuel Cycle in Power Reactors," Oak Ridge National Laboratory, ORNL/TM-5565, (January 1978).

K-2 A. Kamal, "The Effect of Axial Power Shaping on Ore Utilization in Pressurized Water Reactors," S.M. Thesis, Department of Nuclear Engineering, M.I.T., (January 1980).

L-1 P.M. Lang, "Future Trends in LWR Fuel to Improve Uranium Utilization," Trans. Am. Nucl. Soc.,30,274, (1978).

L-2 W.T. Loh, M.J. Driscoll and D.D. Lanning, "The Use of Burnable Poison to Improve Uranium Utilization in PWRs," M.I.T. Energy Laboratory Report No. MIT-EL-82-014, (May 1982).

L-3 J.S. Lan, "Assessment of the Prevailing Physics Codes: LEOPARD, LASER, and EPRI-CELL," Trans. Am. Nucl. Soc., 38, 685, (June 1981)

M-1 R.A. Matzie and J.R. Rec, "Assessment of Thorium Fuel Cycles in Pressurized Water Reactors," Combustion Engineering Power Systems, EPRI NP-359, (February 1977).

M-2 R.A. Matzie and J.R. Rec, "Practical Considerations in the Use of a Thorium Cycle in PWRs," Trans. Am. Nucl. Soc., 24, 220, (1976).

M-3 R.A. Matzie, et. al., "Uranium Resource Utilization Improvements in the Once-Through PWR Fuel Cycle," Combustion Engineering Power Systems, CEND-380, (April 1980).

M-4 W.V. Macnabb, "Two Near-Term Alternatives for Improved Nuclear Fuel Utilization," Trans. Am. Nucl. Soc., 33, 398, (1979).

M-5 M.A. Malik, et. al., "Optimization of the Axial Power Shape in Pressurized Water Reactors," M.I.T. Energy Laboratory Report No. MIT-EL-81-037, (November 1981).

M-6 R.A. Matzie, et. al., "Industrial Assessment of Nonbackfittable PWR Design Modifications," Combustion Engineering Power Systems, CEND-385, (November 1980).

M-7 R.A. Matzie and G.P. Menzel, "Conceptual Design of a Large Spectral Shift Controlled Reactor," Combustion Engineering Power Systems, CEND-377, (August 1979).

N-1 Nuclear News, "Data on World Nuclear Reactors," 24 (10),85, (August 1981).

N-2 R.D. Nininger and S.H.U. Bowie, "Technological Status of Nuclear Fuel Resources," Trans. Am. Nucl. Soc., 25, 35, (1976).

O-1 Oak Ridge National Laboratory, "The Economics and Utilization of Thorium in Nuclear Reactors", ORNL/TM-6331, (May 1978).

P-1 S. Peterson, et. al., "Utilization of Thorium in Power Reactors," Technical Report Series No. 52, International Atomic Energy Agency, Vienna, (1966).

R-1 T. Robbins, "Preliminary Evaluation of a Variable Lattice Fuel Assembly and Reactor Design Concept," Pickard, Lowe and Garrick, Inc., Washington, D.C., (February 1979).

S-1 Stockholm International Peace Research Institute, "Nuclear Power and Nuclear Weapons Proliferation," 91, Taylor and Francis (London), (1979).

S-2 F.M. Sider, "An Improved Once-Through Cycle for Pressurized Water Reactors," Combustion Engineering Power Systems, TIS-6529, (June 1980).

S-3 M.L. Smith, et. al., "Extended Burnup and Extended Cycle Design," Trans. Am. Nucl. Soc., 34, 389, (1980).

S-4 J.A. Sefcik, M.J. Driscoll and D.D. Lanning, "Analysis of Stratergies for Improving Uranium Utilization in Pressurized Water Reactors," M.I.T. Energy Laboratory Report No. MIT-EL-80-032, (January 1980).

S-5 G.M. Solan, J.A. Handschuh, and P.A. Bergeron, "Maine Yankee Cycle 4 Design Report," YAEC-1171, (January 1979).

T-1 D.B. Townsend, R.L. Crowther and R.A. Wolters, "A Once-Through Thorium Cycle for BWRs," Trans. Am. Nucl. Soc., 32, 354, (1979).

U-1 U.S. Department of Energy, "Nuclear Proliferation and Civilian Nuclear Power," DOE/NE-0001/9, 9, (June 1980).

V-1 J. Varela, "Correlation of Reload Enrichment Versus Fissile Consumption," Nuclear Fuel Management (22.35) Term Project, MIT Dept. of Nuclear Engineering, (May 1982).

W-1 H.E. Williamson, "Assessment of Utilization of Thorium in BWRs," Oak Ridge National Laboratory, ORNL/SUB-4380-5, (January1978).

W-2 P. Wei, et. al., "BWR Uranium Utilization Improvement Potential," Oak Ridge National Laboratory, ORNL/SUB/7537/15, (June 1980).

Z-1 G.B. Zorzoli, "Use of Metallic Thorium for LWBRs and LWRs, Nuclear Technology, 20 (2), 109, (November 1973).